

**CYTOSKELETAL MECHANISMS OF SYNAPTIC CARGO
TRAFFICKING**

ISBN: 978-90-393-6756-8

Copyright © Marta Esteves da Silva 2017
All rights reserved.

The studies described in this thesis were performed at the division of Cell Biology at the Faculty of Science of Utrecht University, The Netherlands.

This thesis was partly accomplished with financial supported from Fundação para a Ciência e Tecnologia (FCT-Portugal, grant SFRH/BD/68642/2010). Printing of this thesis was kindly supported by Charles River Laboratories.

Cover by © Daniel João Duarte.
Design and layout by Daniel João Duarte.

Printed in the Netherlands by Gildeprint with certified paper.



CYTOSKELETAL MECHANISMS OF SYNAPTIC CARGO TRAFFICKING

De rol van het cytoskeleton van en naar synapsen
(met een samenvatting in het Nederlands)

Mecanismos do citosqueleto no transporte de carga sináptica
(com sumário em Português)

Proefschrift

ter verkrijging van de graad van doctor aan de Universiteit Utrecht op gezag van de rector magnificus, prof.dr. G.J. van der Zwaan, ingevolge het besluit van het college voor promoties in het openbaar te verdedigen op maandag 22 mei 2017 des middags te 4.15 uur

door

Marta Santos Esteves da Silva

geboren op 3 mei 1986 te Almada, Portugal

Promotor: Prof. dr. Casper C. Hoogenraad

Copromotor: Dr. Corette J. Wierenga

Para os meus pais

TABLE OF CONTENTS

Chapter 1	General Introduction	9
Chapter 2	Positioning of AMPA receptor-containing endosomes regulates synapse architecture	31
Chapter 3	Activity-dependent actin remodeling at the base of dendritic spines promotes microtubule entry	65
Chapter 4	Three-step model for polarized sorting of KIF17 into dendrites	93
Chapter 5	Spire proteins reorganize a pool of axonal actin and target cargo to the presynapse	115
Chapter 6	DeActs: genetically encoded tools for perturbing the actin cytoskeleton in single cells	145
Chapter 7	General Discussion	169
Addendum	Summary	184
	Samenvatting	186
	Sumário	188
	Curriculum vitae	190
	Publications	191
	Acknowledgements	192

General Introduction

Marta Esteves da Silva

Cell Biology, Faculty of Science, Utrecht University, Utrecht, The Netherlands

BRAIN FUNCTION AND NEURONAL CELLS

The mammalian brain is a fascinating organ formed by hundreds of billions of cells that work together to ultimately perform a wide range of tasks, be it very simple or highly complex, such as learning how to walk or solving mathematical equations. The brain is organized in several functional circuits that process information, ultimately resulting in sensorial, motor, emotional and rational behaviors. Our current knowledge about brain function is still very limited. For example, we do not fully understand how information is stored in the brain or how different brain regions execute specific tasks. Answering these questions requires the integration of different approaches where cellular, molecular, behavioral, or cognitive aspects need to be considered. The brain is composed by different types of cells, of which neuronal cells have a central role. Studying brain function at the cellular level implies learning more about neuronal development, organization and function.

Neurons: axon, dendrites and communication

Already at the single cell level, neurons are highly specialized. They have two distinct morphological and functional compartments - the axon, a very long and often myelinated neurite that propagates information, and the dendrites, smaller and highly branched neurites that receive and process electrochemical inputs from different neurons (Barnes and Polleux, 2009; Takano *et al.*, 2015). Most communication between neurons occurs from axon to dendrite through highly specialized junctions called synapses. A synapse is made by the presynaptic axon of one neuron contacting the postsynaptic dendrite of another neuron, transmitting an electrical and chemical signal. Synapses need to be accurately assembled and maintained in order to guarantee the correct response to a specific stimulus.

Neuronal polarization and development

Both axons and dendrites extend from the cell body of the neuron, generating an intricate network of communicating cells. Neuronal polarization occurs early in development: as immature, postmitotic neurons migrate to reach their final destination, polarization ensues with the formation of a leading and a trailing process that will become axon and dendrite, respectively. From an extensive *in vitro* and *in vivo* body of work, it is now evident that polarization is a complex process regulated by extracellular cues and intracellular signaling mechanisms involving rearrangement of the neuronal cytoskeleton (Kuijpers and Hoogenraad, 2011). Ultimately, neuronal polarization is fundamental for the axon-to-dendrite propagation of information along the central nervous system (Barnes and Polleux, 2009; Takano *et al.*, 2015; Witte and Bradke, 2008). Upon establishment of polarization, both axon and dendrites undergo expansion and outgrowth. After that, synapse formation ensues.

The presynaptic terminals are the location of neurotransmitter release and contact with the postsynapse (Sudhof, 2004). At the presynaptic active zone (AZ), synaptic vesicles (SVs) filled with neurotransmitters are exocytosed to the synaptic cleft upon the arrival of an action potential. Once in the cleft, neurotransmitters are recognized by transmembrane

receptors located in the postsynaptic membrane. Synaptic vesicles are then endocytosed and later reutilized on a new cycle of neurotransmitter transport and release (Gundelfinger and Fejtova, 2012; Sudhof, 2012). In the hippocampus, an important area of the brain where learning and memory events occur (Kandel, 2001), the postsynapse is located in dendritic spines. Dendritic spines are formed by a bulbous head where the postsynaptic components are localized, many of them transmembrane proteins that are in contact with the dendritic shaft and the presynapse. The spine neck physically constricts the spine head from the dendritic shaft providing compartmentalization, important for the generation and integration of response to stimulus (Sheng and Hoogenraad, 2007). Spines undergo dynamic morphological changes, ranging from long, immature structures called filopodia, to mushroom spines, with larger heads and a defined neck. Larger spines can harbor larger postsynaptic densities (PSDs), being more stable and likely to contain a diverse array of membrane-bound organelles, which overall contribute to stronger synaptic connections (Bourne and Harris, 2008; Sheng and Hoogenraad, 2007).

Synaptogenesis and further synapse maturation requires local availability of many molecular components, from receptors to signaling proteins and synapse-associated proteins. Most of these have to be transported from the soma to the synapse. The most efficient way to target axonal and dendritic components is through intracellular trafficking along the cytoskeleton network, where they can be transported as cargo by motor proteins (Kapitein and Hoogenraad, 2011).

THE CYTOSKELETON

As in other eukaryotic cells, the neuronal cytoskeleton is a flexible structure, constantly changing in response to the surrounding environment. The cytoskeleton is important for cell morphology, division, growth and migration, organelle positioning and intracellular transport of cargo. Microtubule and actin filaments are the major components of the cytoskeleton. Both cytoskeleton structures are polarized polymers, with one end having a greater rate of polymerization than the other (Figure 1A). The cytoskeleton is highly dynamic, as filaments can be polymerized or depolymerized by addition or removal of monomers of actin or tubulin (Desai and Mitchison, 1997; Pacheco and Gallo, 2016).

Microtubules

Microtubules (MTs) are key structural constituents of the mitotic spindle ensuring fidelity in cell division, organization of the cytoplasm, positioning of the nucleus and transport of cargo over long distances in the cell. Microtubules are hollow cylinders, composed by a circular array of protofilaments, made of heterodimers of α - and β -tubulin (Figure 1A). A new protofilament is initiated by the nucleation of tubulin monomers and further elongated by the addition of GTP-bound tubulin monomers. The polymer can also shrink by loss of tubulin monomers from the tip. Microtubules have a fast growing plus-end, and a slowly growing, more stable minus-end (de Forges *et al.*, 2012), and undergo several polymerization and depolymerization

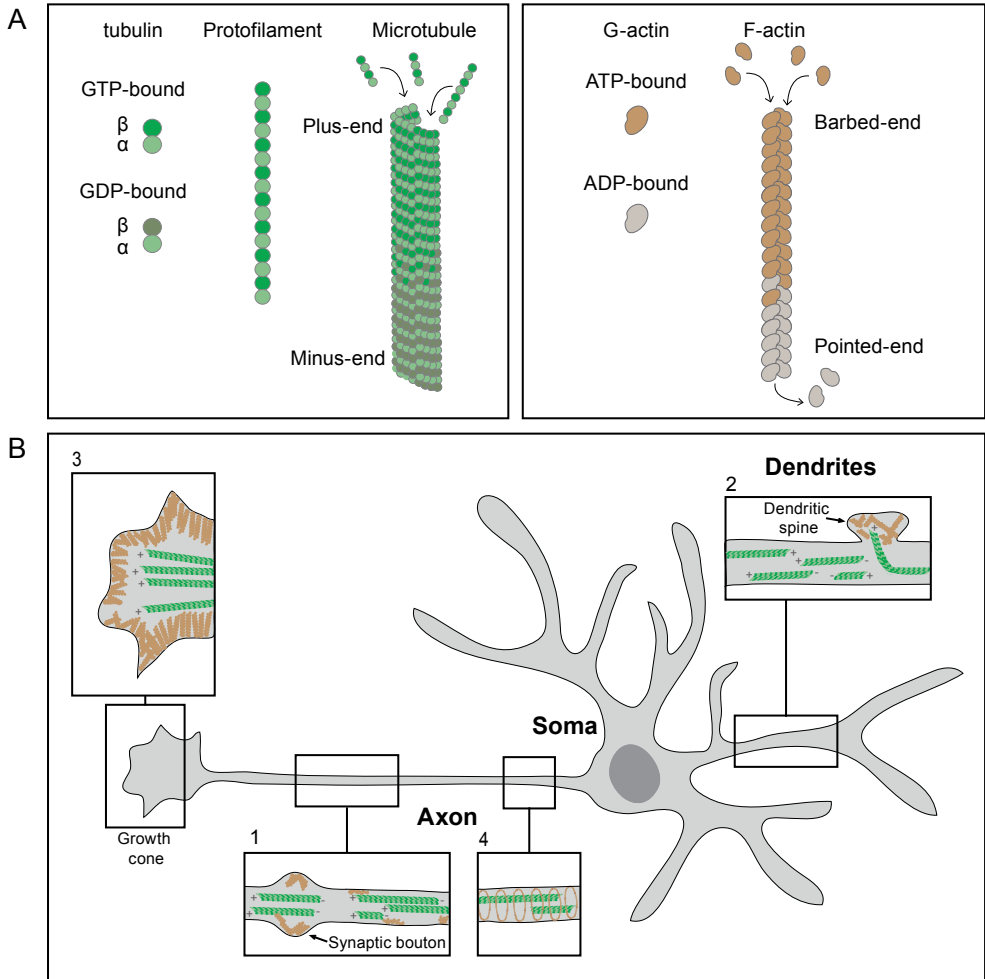


Figure 1. Microtubules and actin filaments are the major components of the neuronal cytoskeleton

A. Microtubules and actin filaments are cytoskeletal components of all eukaryotic cells. Left: Stable α - and β -tubulin heterodimers are nucleated, generating protofilaments. Protofilaments are organized in a circular array generating the microtubule. Microtubules are dynamic structures, undergoing repetitive cycles of growth and catastrophe. Microtubule polymerization preferentially occurs in the plus-end (+), whereas the minus-end (-) is more stabilized. Microtubule growth occurs by addition of GTP-bound tubulin dimers that are later hydrolyzed to GDP-tubulin as the polymer elongates. Right: Actin filaments are composed of two helical strands of actin filaments (F-actin). F-actin is formed by polymerization of ATP-actin monomers (G-actin) that undergo hydrolysis after forming the filament. Like microtubules, actin filaments are dynamic structures. Most polymerization occurs at the barbed end, whereas depolymerization happens preferentially at the pointed end. **B.** The neuronal cytoskeleton. Microtubules are distributed along axonal and dendritic shaft. 1) In the axon, microtubule orientation is mostly unidirectional, with plus-ends facing the tip of the neurite. 2) In dendrites, microtubules have mixed orientation. Most microtubules plus-ends are oriented to the tip of the neurite but a substantial fraction of dendritic microtubules has the opposite orientation. Growing microtubules can also target dendritic spines. 3) Actin filaments are enriched at growth cones, where actin dynamics is important for the elongation of the neurite. Actin is also enriched at pre- and postsynapses (1 and 2). Different actin structures have been identified in the axonal shaft, such as actin rings (4), actin patches and hotspots (1). The role of these actin structures is at the moment unclear.

events, in a process called dynamic instability (Mitchison and Kirschner, 1984), which allows quick reorganization of the cytoskeleton (Desai and Mitchison, 1997). The microtubule organization and dynamics is orchestrated by the turnover of GTP-tubulin, post-translational tubulin modifications, and several regulatory proteins such as Microtubule-Associated Proteins (MAPs), microtubule plus-end tracking proteins, and motor proteins (kinesin and dynein).

Actin filaments

The actin cytoskeleton plays a critical role during cell division, adhesion, motility and transport. Much like microtubules, actin filaments (F-actin) are formed by polymerization of ATP-bound G-actin monomers (β and γ -actin isoforms), creating a two-stranded helical structure with two polarized ends, the barbed (plus) end, and the pointed (minus) end (Figure 1A). Actin polymerization occurs mostly on the barbed end, whereas depolymerization happens at the pointed end (Coles and Bradke, 2015). As spontaneous nucleation of filamentous actin is not a kinetically favorable event in cells, nucleation complexes are involved to initiate filament formation and polymerization. To date, different actin nucleation and elongation families of proteins have been identified: the Arp2/3 complex, Formins and Spire (Disanza and Scita, 2008). As is the case with microtubules, actin filaments are highly dynamic and the stability of these filaments is regulated by several different Actin-Binding Proteins (ABPs).

The neuronal cytoskeleton

Microtubules and actin filaments have additional roles that are specific to neuronal cells. Both these filaments are instrumental for neuronal development and polarization, long-range organelle transport along the axon and the setting up of local trafficking routes to pre- and post-synaptic locations or extending growth cones (Lowery and Van Vactor, 2009). Microtubule and actin-based transport is fundamental for neuronal development and function as defects arising from missorted cargo ultimately result in pathology and neurodegeneration (Franker and Hoogenraad, 2013).

Microtubule organization and function in neurons. In mature hippocampal neurons, microtubules are distributed along the axonal shaft and the somato-dendritic compartment (Conde and Caceres, 2009) (Figure 1B). In the axon, the majority of microtubules have their plus-end facing the growth cone, whereas in dendrites microtubules are present along the dendritic shaft with mixed orientation, with some microtubules having their plus-end facing the tip of the neurite while others are minus-end oriented that way (Baas *et al.*, 1988; Burton, 1988). This mixed orientation is acquired later in development than the axonal microtubule orientation, as dendritogenesis begins, and prior to synapse formation (Baas *et al.*, 1989; Kapitein *et al.*, 2010). In mature hippocampal neurons, dendritic spines are highly enriched in actin and until recently it was believed that microtubules were absent from spines. Surprisingly, recent studies using live-cell imaging have shown that microtubules can invade dendritic spines (Hu *et al.*, 2008; Jaworski *et al.*, 2009). However, the role of these invasions remains to be elucidated. In

Chapter 2, we describe the involvement of actin and microtubules in the transport of recycling endosomes in and out of dendritic spines. Moreover, in Chapter 3 we discuss recent data on the regulation of microtubule dynamics in dendritic spines by synaptic activity.

Neuronal microtubules can undergo post-translational modifications that make them either more or less stable (Ikegami and Setou, 2010; Verhey and Hammond, 2009; Westermann and Weber, 2003). For example, microtubule detyrosination stabilizes the lattice of microtubules, as it reduces microtubule disassembly by the Microtubule Polymerase Mitotic Centromere-Associated Kinesin (MCAK). Detyrosinated microtubules are often present along the axonal shaft, suggesting that axons have more stable microtubules than dendrites do. Moreover, axons have a higher fraction of stable, acetylated microtubules as opposed to dendrites, that in turn have more deacetylated microtubules, suggesting a polarized distribution or differential activation of microtubule-modifying enzymes as a way to provide functional diversity to the microtubule cytoskeleton in specific compartments (Hammond *et al.*, 2010; Witte *et al.*, 2008). Many different Microtubule-Associated Proteins (MAPs) can bind to microtubules and affect microtubule stability and function. The most widely studied neuronal MAPs are MAP2 and Tau. MAP2 is exclusively located in the dendrite, and Tau is enriched in the axon. Both are involved in microtubule stabilization and bundling (Chen *et al.*, 1992) and it has also been suggested that MAP2 is involved in neuronal plasticity (Fanara *et al.*, 2010; Quinlan and Halpain, 1996). Microtubule plus-end tracking proteins (+TIPs) are a class of MAPs that bind specifically to the growing ends of microtubules, and are able to interact with several other proteins, providing an additional layer of regulation on the microtubule cytoskeleton (Akhmanova and Steinmetz, 2010; Morrison *et al.*, 1998).

Neuronal microtubules are typically used for long-range cargo transport, with the help of molecular motor proteins (Figure 2). Motor proteins are typically formed by motor domains that binds and walks along the cytoskeleton at the expense of ATP hydrolysis, a stalk domain required for motor dimerization and a tail domain that binds and accommodates the cargo to be transported (Vale, 2003). There are two types of microtubule-motor proteins: kinesins that transport cargo to the plus-end of the microtubules, and dynein that moves cargo to the minus-end (Hirokawa *et al.*, 2010). As axons have a uniform, plus-end out microtubule orientation, kinesins are involved in anterograde transport of cargo from the soma to the distal tip and dynein is responsible for retrograde transport in the opposite direction (Kapitein and Hoogenraad, 2011). The heterogeneous microtubule orientation found in dendrites is crucial to establish dendritic selective transport, as dynein is the only motor to drive cargo from the soma to the dendrite via the minus-end directed microtubule population (Black and Baas, 1989). It has been shown that only cytoplasmic dynein can transport cargo exclusively to the dendrite, whereas most kinesins target cargos to the axon (Huang and Banker, 2012; Lipka *et al.*, 2016). In addition, the axon initial segment (AIS) works as a sorting filter, as it prevents dendritic cargo from entering the axon (Kuijpers *et al.*, 2016; Song *et al.*, 2009; Watanabe *et al.*, 2012). In Chapter 4 we describe a three-step model for polarized sorting of KIF17 into dendrites.

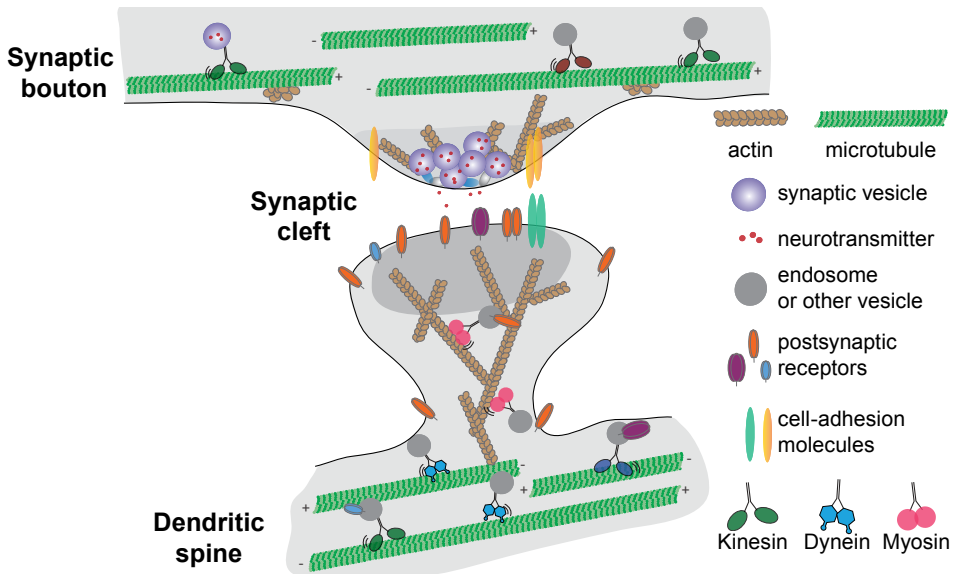


Figure 2. Cytoskeleton involvement in synaptic structure

Neuronal cells communicate via synapses, where the axon of one neuron contacts the dendrite of another neuron. In the axon, the presynapse is localized in synaptic boutons. Synaptic vesicles are transported to the active zone and exocytosed, resulting in the release of neurotransmitter to the synaptic cleft. Neurotransmitters bind to postsynaptic receptors in dendritic spines, generating an electrical change in the postsynaptic neuron. Most synaptic proteins need to reach the synapse from the soma. The neuronal cytoskeleton provides the tracks for intracellular transport of synaptic cargo. Microtubules serve as tracks for long-range transport of synaptic cargo. Kinesins anterogradely transport cargo along the axon. For example, presynaptic proteins syntaxin and SNAP 25 are transported by KIF5. KIF1A and KIF1 β move Rab3-vesicles in the axonal shaft (Goldstein *et al.*, 2008; Morton *et al.*, 2010; Niwa *et al.*, 2008). Kinesins are also involved in the transport of other cargo in axons. Dynein transports cargo exclusively to dendrites, however some kinesins can also move dendritic cargo, as is the case of KIF5 and KIF1A that transport AMPA receptor subunits and KIF17 that carries NMDA receptor subunits in the dendrite (Guillaud *et al.*, 2003; Kapitein and Hoogenraad, 2011; Setou *et al.*, 2000; Setou *et al.*, 2002). Actin filaments are enriched in the pre- and postsynapse, where they function as scaffolding for recruitment and stabilization of synaptic components. Moreover, synaptic actin dynamics can dramatically change upon synaptic activity. Actin is also involved in transport of synaptic cargo, as AMPA receptors are transported to dendritic spines by Myosin V.

Actin organization and function in neurons. As nascent neurites emerge from the soma during neuronal polarization, actin dynamics shape the morphological rearrangements that occur at this stage. It is well known that axonal growth cones are highly enriched in actin cytoskeleton (Figure 1B). Several *in vitro* studies demonstrated that actin filaments are particularly unstable at the growth cone (Bradke and Dotti, 1999; Witte and Bradke, 2008). Actin function at growth cones is explained by activation of particular signaling pathways and a coordinated interplay between the actin and microtubule cytoskeleton. It has been suggested that in the axonal growth cone, actin filaments are destabilized by the severing activity of cofilin, which allows microtubules to enter the growth cone and extend the neurite (Bradke and Dotti, 1999; Flynn *et al.*, 2012). At dendritic growth cones, microtubule entry is prevented by

1

the combined action of Myosin II and profilin IIa that stabilize the actin filaments (Da Silva *et al.*, 2003; Kollins *et al.*, 2009). So far, many other molecules have been identified as regulators of axon outgrowth, through their action on the actin cytoskeleton, including members of the Rho family of small GTPases, Rac- and Par-complex specific GEFs, and Cdc42 (Arimura and Kaibuchi, 2007; Takano *et al.*, 2015). In addition, F-actin is located at the plasma membrane, working as an organizer and a cortical scaffold for the localization of many different protein complexes (Letourneau, 2009). As so, even though actin is not the only cytoskeleton element required for axon elongation, it is essential for growth cone exploration (Lowery and Van Vactor, 2009).

In mature neurons, actin is enriched at synapses, where its scaffolding role is important to stabilize pre- or postsynaptic structures (Figure 1B, Figure2). Rapid actin dynamics is fundamental for remodeling of the synaptic structure in response to plasticity (Cingolani and Goda, 2008; Hotulainen and Hoogenraad, 2010). In dendritic spines, a network of branched F-actin forms the major cytoskeletal component of excitatory synapses (Landis and Reese, 1983). Here, actin is found underneath the postsynaptic density (PSD), where it stabilizes postsynaptic proteins and modulates the response of the postsynapse to stimulation (Hotulainen and Hoogenraad, 2010). Many ABPs are present in the spine head, where they can bind to actin and be involved in different signaling pathways or either promote nucleation, bind to the filament ends to facilitate polymerization or depolymerization, crosslink, stabilize or sever actin filaments (Letourneau, 2009; Sheng and Hoogenraad, 2007). The involvement of ABPs in the postsynaptic structure has been depicted in several studies, where downregulation of these proteins results in defects on spine formation and maturation (Hering and Sheng, 2003; Ivanov *et al.*, 2009; Okamoto *et al.*, 2007; Terry-Lorenzo *et al.*, 2005) with negative effects on synaptic plasticity and memory assembly (Kojima *et al.*, 2010; van Woerden *et al.*, 2009; Wu *et al.*, 2008).

In dendritic spines, the highly enriched F-actin cytoskeleton facilitates rapid changes in spine shape, size, motility and stability of the entire structure (Figure 2). Electron microscopy studies show that actin in spines consists of a network of branched and long, linear actin filaments (Korobova and Svitkina, 2010). The Arp2/3 complex is highly enriched in spines (Racz and Weinberg, 2008) where it is believed to be the main actin nucleator. The complex binds to existing actin filaments and nucleates a new filament, thus generating a branched structure of actin filaments (Goley and Welch, 2006). Activators of the Arp2/3 complex and other actin-binding proteins such as profilins are also very important for the correct assembly and localization of branched actin structures found in dendritic spines (Hotulainen and Hoogenraad, 2010).

Actin is very dynamic in the spine head at basal conditions and upon synaptic stimulation (Honkura *et al.*, 2008; Star *et al.*, 2002). Long-term potentiation (LTP) alters the equilibrium between G-actin and F-actin towards F-actin, increasing spine volume. On the other hand, long-term depression (LTD) shifts the ratio to G-actin, resulting in spine shrinkage (Cingolani and Goda, 2008; Okamoto *et al.*, 2004). Moreover, application of Latrunculin A, an actin

destabilizing drug, blocks LTP expression, suggesting actin polymerization is required for LTP (Chen *et al.*, 2007; Fukazawa *et al.*, 2003; Okamoto *et al.*, 2004; Ramachandran and Frey, 2009) and processing of memories upon learning stimuli (Lamprecht and LeDoux, 2004). There is a growing body of evidence linking spine actin with neurological disorders (Blanpied and Ehlers, 2004). For example, DISC1, a Schizophrenia risk factor, regulates spine morphology via Rac1 (Hayashi-Takagi *et al.*, 2010). Moreover, mutation in the cofilin kinase PAK3 gene leads to X-linked mental retardation (Allen *et al.*, 1998) and decreased levels of PAK3 correlate with synaptic impairment in Alzheimer's disease (Kreis and Barnier, 2009).

Actin is also highly enriched at the presynapse, where it is essential for synaptogenesis (Chia *et al.*, 2012; Koch *et al.*, 2014; Ozkan *et al.*, 2014). Recent studies point to an important role of cell-adhesion molecules in determining the location of the subcellular rearrangement of F-actin, that result in trapping of synaptic vesicles components and trigger the formation of the presynapse (Bury and Sabo, 2014; Chia *et al.*, 2014; Chia *et al.*, 2012; Chua, 2014; Nelson *et al.*, 2013). In analogy to actin in spines, actin is highly dynamic at the presynapse and organized by the Arp2/3 complex, generating a branched network (Korobova and Svitkina, 2010). Additionally, synaptic activity increases actin polymerization at the presynapse (Sankaranarayanan *et al.*, 2003). Even though many studies have been conducted to unravel the role of actin at the presynapse, our current understanding is incomplete. There is evidence of a structural function for presynaptic actin, important for the correct synaptic vesicle cycle at the active zone (Halpain, 2003; Rust and Maritzen, 2015) or a scaffolding function, by recruiting and stalling synaptic vesicles in the presynapse (Wolf *et al.*, 2015). Actin might also be important for transport of synaptic vesicles by actin-based motor proteins (Cingolani and Goda, 2008; Dillon and Goda, 2005; Rust and Maritzen, 2015). Several studies have associated defective actin function at synapses with mental disorders, such as Fragile X syndrome or Parkinson's disease (Klemmer *et al.*, 2011; Letourneau, 2009; Sousa *et al.*, 2009).

The development of new visualization techniques, such as super-resolution microscopy allowed for new studies and a deeper understanding on the precise organization of the actin cytoskeleton in neurons (Figure 1B). The Zhuang lab was the first to describe that along the axon, sub-cortical actin is organized in rings which are regularly spaced (180-190nm apart) and interspaced with rings of spectrin (Leterrier *et al.*, 2015; Xu *et al.*, 2013). The same type of organization was later described in a subset of dendrites and spines necks and in other neuronal types (Bar *et al.*, 2016; D'Este *et al.*, 2015; He *et al.*, 2016; Sidenstein *et al.*, 2016). The function behind such actin rearrangements in neurons is at the moment unclear. One hypothesis suggests that the actin-spectrin organization is required to protect axons from mechanical damage (Arnold and Gallo, 2014; Xu *et al.*, 2013). In *C. elegans* spectrin mutants, axons are particularly fragile and prone to break during the normal movement of the animal (Hammarlund *et al.*, 2007). Another model suggests that periodical actin-spectrin rings may play a role in the organization of the axonal plasma membrane, as sodium channels present in the AIS are regularly spaced in a coordinated manner with this structure (Xu *et al.*, 2013). Future studies will expand our knowledge on the function of the periodic actin-spectrin rings

in axonal structure and function.

Actin is also organized in patches in neurons. These patches are found both in axons and dendrites as meshworks, resembling the actin organization found in lamellipodia (Korobova and Svitkina, 2010; Spillane *et al.*, 2011; Watanabe *et al.*, 2012). Actin patches at the AIS trap cargo, preventing its transport along the axon (Watanabe *et al.*, 2012). Both in the distal axon and dendrites, actin patches act as precursors of filopodia, which later may develop into axon collateral branches or dendritic spines (Andersen *et al.*, 2005; Gallo, 2011, 2013; Korobova and Svitkina, 2010). The Arp2/3 complex is most likely responsible in the generation and assembly of these patches (Spillane *et al.*, 2011). However, other actin nucleators such as Formins or cordon-bleu may also be involved (Kessels *et al.*, 2011).

In a recent study using F-actin binding probes in live-cell imaging and super resolution microscopy, a new axonal actin network has been described (Ganguly *et al.*, 2015). In young neurons, hotspots of F-actin are found regularly distributed along the axon from where continuous actin polymerization and depolymerization occurs, generating bidirectional actin trails. Even though actin trails are highly dynamic and its assembly is Formin-dependent, the generation of hotspots and trails is Formin-independent, suggesting an alternative mechanism behind the nucleation step. These hotspots often colocalize with stationary endosomes, and previous studies show that F-actin nucleates on the surface of endosomes in non-neuronal cells (Ganguly *et al.*, 2015; Hong *et al.*, 2015). As so, a model is proposed where actin hotspots could be nucleated on the surface of vesicles and further elongated by members of the Formin family to generate actin trails (Ganguly *et al.*, 2015; Roy, 2016). In fact, Spire proteins have been recently identified as a new family of actin nucleators (Quinlan *et al.*, 2005) that nucleate actin filaments and generate an extensive actin network from the membrane of vesicles (Schuh, 2011). In chapter 6 the results on the role of Spire proteins in the axonal actin cytoskeleton are discussed.

To better understand the role of the actin cytoskeleton in neurons, we must focus with detail in the actin structure and organization. Manipulation of actin is still challenging in various model systems as most approaches rely on the use of pharmacological drugs that either affect the actin structure (MacLean-Fletcher and Pollard, 1980; Spector *et al.*, 1983) or specific downstream or upstream pathways (Hetrick *et al.*, 2013; Rizvi *et al.*, 2009). In Chapter 6 we describe a new set of genetically-encoded tools that directly disturb the actin cytoskeleton in a single-cell manner that can be applied in different model systems.

SYNAPTIC CARGO TRANSPORT: THE ROLE OF THE NEURONAL CYTOSKELETON

As synapses are formed, assembled and modified in response to plasticity, an assortment of synaptic components that are synthesized in the cell body needs to be accurately distributed to their site of action. Synaptic vesicle precursors need to be targeted to the presynaptic terminal, whereas neurotransmitter receptors have to reach the postsynapse, as well as other components like mitochondria and signaling proteins (Figure 2). Moreover, the recruitment and assembly

of a particular set of receptors and associated proteins will be determinant to synaptic function. For example, α -amino-3-hydroxy-5-methyl-4-isoxazole propionate (AMPA) receptors and N-methyl D-aspartate (NMDA) receptors are located in excitatory synapses at dendritic spines, while inhibitory synapses are distributed at dendritic shafts and contain glycine receptors and γ -aminobutyric acid type A (GABA_A) receptors (Jacob *et al.*, 2008; Sheng and Hoogenraad, 2007). Effective transport mechanisms have to be in place to correctly distribute synaptic receptors to their final destination (Schlager and Hoogenraad, 2009).

Mechanisms controlling cargo trafficking

Intracellular trafficking of cargo predominantly occurs through active transport along the neuronal cytoskeleton. Microtubule-based motors (kinesins and dynein), or actin-based motors (myosins) bind and transport cargo along the cytoskeleton tracks. Given the organization of the neuronal cytoskeleton discussed above, selective transport of axonal or dendritic cargo is not trivial.

Synaptic cargo can move bidirectionally along the same cytoskeletal tracks or switch between actin filaments and microtubules (Karcher *et al.*, 2002) (Figure 3). Additionally, and as mentioned above, post-translational modifications and microtubule- or actin-associated proteins generate functional diversity of the cytoskeletal structure and binding affinity to motor proteins (Schlager and Hoogenraad, 2009). A single synaptic cargo may use multiple motors resulting in bidirectional transport that is illustrated on a ‘tug-of-war’ model. In this model, motors of opposite orientation compete to move the cargo, and motor loss or changes in their activity determine the directionality of transport (Muller *et al.*, 2008). Synaptic cargo movement may also be illustrated on a ‘coordination’ model, where one motor is actively transporting cargo while the opposing motor is not engaged (Gross *et al.*, 2002). The selective activation-inactivation of motors would be regulated by complexes of signaling and scaffolding proteins, phospholipids, membrane receptors, and Rab GTPases and their effector proteins (Kapitein and Hoogenraad, 2011; Karcher *et al.*, 2002; Welte, 2004) (Figure 3). The tail domains of motor proteins are very heterogeneous, providing another layer of specificity, as cargo adaptors can directly interact with the tail to either promote or interfere with motor protein function in time and space (Akhmanova and Hammer, 2010; Hirokawa and Takemura, 2005; Kardon and Vale, 2009). Finally, the motor protein can also be auto-regulated. As it has been shown, in the absence of bound cargo, the tail domain interacts and auto-inhibits the motor domain (Coy *et al.*, 1999; Thirumurugan *et al.*, 2006). A recent study describes that Kinesin-Binding Protein (KBP) inhibits kinesin movement upon binding to the motor domain, thus regulating the bidirectional movement of axonal cargos (Kevenaar *et al.*, 2016).

Motor-cargo adaptors

The complex and redundant contribution of individual factors controlling synaptic cargo transport makes this a challenging process to investigate in great detail. Nevertheless, over the years, work has been published unraveling some of the molecular mechanisms of pre- and

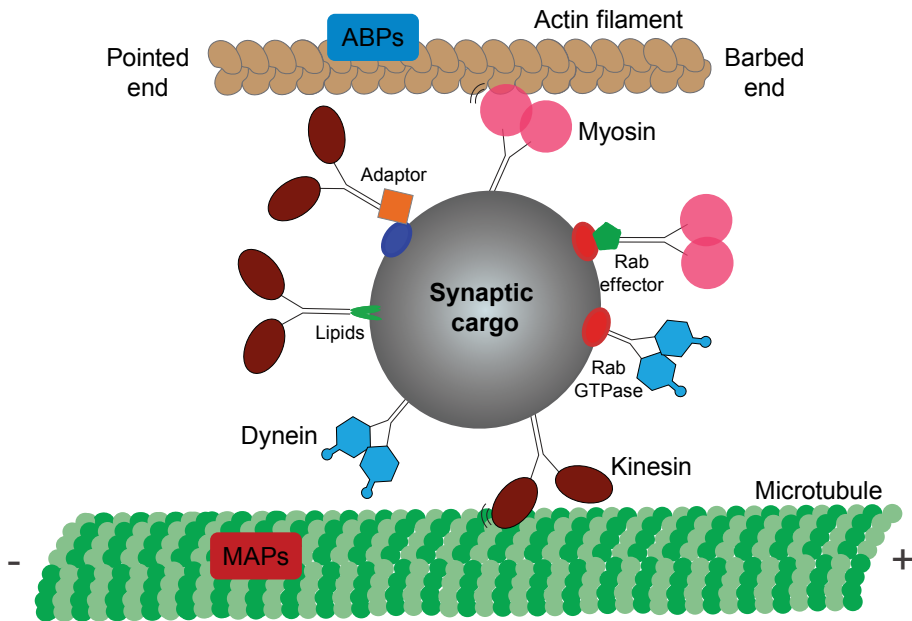


Figure 3. Mechanisms controlling synaptic cargo transport

Some examples of regulation of the cytoskeleton in intracellular transport of synaptic cargo. Proper sorting and delivery of synaptic cargo by the cytoskeleton involves different sets of proteins and mechanisms. The polarized structure of microtubules and actin filaments allows for bidirectional transport in the same track, and cargo can frequently switch from microtubule- to actin-based motors. As one single cargo can simultaneously bind different motor proteins, the result could be either competition from the different motors proteins or coordination of motor activity. Additional layers of transport specificity are in place, as binding of microtubule- or actin-associated proteins (MAPs and ABPs, respectively) to the cytoskeleton makes it more or less available for transport by motor proteins. Motor protein activity is also regulated, either by backfolding of the motor protein or by adaptor proteins, or with the involvement of signaling complexes, phospholipids or GTPases and their effectors localized at the cargo membrane.

postsynaptic cargo trafficking. For example, it was shown that anterograde transport of Rab3-positive vesicles, precursors of synaptic vesicles, along the axon is dependent on the kinesin-3 family member, KIF1A and KIF1 β via a Rab3-effector protein DENN/MADD or liprin- α (Hall and Hedgecock, 1991; Kondo *et al.*, 2012; Miller *et al.*, 2005; Niwa *et al.*, 2008; Okada *et al.*, 1995; Shin *et al.*, 2003). Moreover, KIF5, a member of the Kinesin-1 family, targets different cargos to the axon, such as the presynaptic molecules syntaxin (together with the adaptor syntabulin) and SNAP25 (Cai *et al.*, 2007; Diefenbach *et al.*, 2002; Goldstein *et al.*, 2008; Morton *et al.*, 2010; Niwa *et al.*, 2008; Su *et al.*, 2004) (Figure 2), but also other proteins and organelles, such as dense core vesicles, amyloid precursor protein (APP) vesicles, or mitochondria, with the help of different sets of adaptors (Babic *et al.*, 2015; Brickley and Stephenson, 2011; Cai *et al.*, 2005; Campbell *et al.*, 2014; Colin *et al.*, 2008; Fransson *et al.*, 2006; Fu and Holzbaaur, 2013; Fujita *et al.*, 2007; Kamal *et al.*, 2000; Lo *et al.*, 2011; Patil

et al., 2013; Tanaka *et al.*, 1998; van Spronsen *et al.*, 2013). Another example is the NMDA receptor subunit NR2B, which is transported along the dendritic shaft by KIF17, through interaction with the scaffolding proteins Lin2/CASK, Lin7/MALS/Velis and Lin10/Mint1 (Guillaud *et al.*, 2003; Setou *et al.*, 2000). AMPA receptor subunits GluA2/A3 can be targeted to the dendrite by KIF5 through GRIP/ABP (Setou *et al.*, 2002), or by KIF1A through GRIP interacting protein liprin- α (Shin *et al.*, 2003) (Figure 2). Another example are recycling endosomes containing AMPA receptors that are transported into dendritic spines by Myosin Vb upon binding to a Rab11-effector protein, Rab11-FIP2 (Wang *et al.*, 2008). These and many other motor-adaptor interactions important for the transport of synaptic cargos are reviewed in Schlager and Hoogenraad 2009.

Over the last years much effort has been put into unravelling more about synaptic cargo transport. The development of innovative imaging and genetic techniques allowed for a better understanding of cargo trafficking in axons and dendrites, but much is still to be discovered. Further understanding of the cytoskeletal organization and regulation, the role of multiple motor complexes, specific motor-cargo interactions, and the signaling mechanisms involved in polarized transport will be fundamental to broaden our knowledge on transport, delivery, assembly or removal of synaptic components in health and disease.

SCOPE OF THIS THESIS

Transport of synaptic components to the synapse is a complex and highly regulated event. Cargo needs to be properly translocated from the cell body or any other location in the neuron to the pre- or postsynapse either in basal conditions or in response to a stimulus. Even though the involvement of the cytoskeleton in transporting cargo along neuronal cells is indisputable, many important aspects of such process are still to be explored. In this thesis the involvement of the cytoskeleton machinery in the trafficking of synaptic cargo was investigated. In **Chapter 2** we described the intracellular trafficking of postsynaptic AMPA receptors to dendritic spines via recycling endosomes, examining in detail the contribution of the microtubule and actin cytoskeleton in dendrites and dendritic spines. Using a chemically-induced dimerization assay it was possible to control the translocation of recycling endosomes to or from the postsynapse after coupling them to different motor proteins, and explored the consequences of such manipulation in the postsynapse. In **Chapter 3**, we investigated the role of dynamic microtubules at the postsynapse. Microtubule invasions of dendritic spines were explored in great detail, as well as its functional implications in basal conditions or upon synaptic plasticity. The role of motor proteins in synaptic cargo transport is also examined in **Chapter 4**. We focused particularly on the dendritic kinesin KIF17 and its regulation and polarized sorting to dendrites, which occurs in three steps: 1) auto-inhibition by its tail domain that is relieved upon cargo binding, 2) exclusion from the axonal compartment by anchoring at the AIS, and 3) dynein-based sorting to dendrites. In **Chapter 5**, presynaptic cargo transport along the axon is explored. We studied the role of a new family of actin nucleators - Spire proteins - in hippocampal neurons and found that Spire proteins are distributed along the axonal shaft and contribute to the organization

and maintenance of actin structures along the axon which might be important in the targeting of cargo to the presynapse. Finally, in **Chapter 6** we focused our efforts in developing novel tools to manipulate the actin cytoskeleton. We characterized DeActs (Disassembly-promoting, encodable Actin tools) in different model systems to highlight its robustness and wide applicability, which will prove a useful tool to better understand the role of actin dynamics in health and disease.

REFERENCES

- Akhmanova, A., and Hammer, J.A., 3rd (2010). Linking molecular motors to membrane cargo. *Current opinion in cell biology* 22, 479-487.
- Akhmanova, A., and Steinmetz, M.O. (2010). Microtubule +TIPs at a glance. *Journal of cell science* 123, 3415-3419.
- Allen, K.M., Gleeson, J.G., Bagrodia, S., Partington, M.W., MacMillan, J.C., Cerione, R.A., Mulley, J.C., and Walsh, C.A. (1998). PAK3 mutation in nonsyndromic X-linked mental retardation. *Nature genetics* 20, 25-30.
- Andersen, R., Li, Y., Resseguie, M., and Brenman, J.E. (2005). Calcium/calmodulin-dependent protein kinase II alters structural plasticity and cytoskeletal dynamics in *Drosophila*. *The Journal of neuroscience : the official journal of the Society for Neuroscience* 25, 8878-8888.
- Arimura, N., and Kaibuchi, K. (2007). Neuronal polarity: from extracellular signals to intracellular mechanisms. *Nature reviews Neuroscience* 8, 194-205.
- Arnold, D.B., and Gallo, G. (2014). Structure meets function: actin filaments and myosin motors in the axon. *Journal of neurochemistry* 129, 213-220.
- Baas, P.W., Black, M.M., and Banker, G.A. (1989). Changes in microtubule polarity orientation during the development of hippocampal neurons in culture. *The Journal of cell biology* 109, 3085-3094.
- Baas, P.W., Deitch, J.S., Black, M.M., and Banker, G.A. (1988). Polarity orientation of microtubules in hippocampal neurons: uniformity in the axon and nonuniformity in the dendrite. *Proceedings of the National Academy of Sciences of the United States of America* 85, 8335-8339.
- Babic, M., Russo, G.J., Wellington, A.J., Sangston, R.M., Gonzalez, M., and Zinsmaier, K.E. (2015). Miro's N-terminal GTPase domain is required for transport of mitochondria into axons and dendrites. *The Journal of neuroscience : the official journal of the Society for Neuroscience* 35, 5754-5771.
- Bar, J., Kobler, O., van Bommel, B., and Mikhaylova, M. (2016). Periodic F-actin structures shape the neck of dendritic spines. *Scientific reports* 6, 37136.
- Barnes, A.P., and Polleux, F. (2009). Establishment of axon-dendrite polarity in developing neurons. *Annual review of neuroscience* 32, 347-381.
- Black, M.M., and Baas, P.W. (1989). The basis of polarity in neurons. *Trends in neurosciences* 12, 211-214.
- Blanpied, T.A., and Ehlers, M.D. (2004). Microanatomy of dendritic spines: emerging principles of synaptic pathology in psychiatric and neurological disease. *Biological psychiatry* 55, 1121-1127.
- Bourne, J.N., and Harris, K.M. (2008). Balancing structure and function at hippocampal dendritic spines. *Annual review of neuroscience* 31, 47-67.
- Bradke, F., and Dotti, C.G. (1999). The role of local actin instability in axon formation. *Science* 283, 1931-1934.
- Brickley, K., and Stephenson, F.A. (2011). Trafficking kinesin protein (TRAK)-mediated transport of mitochondria in axons of hippocampal neurons. *The Journal of biological chemistry* 286, 18079-18092.
- Burton, P.R. (1988). Dendrites of mitral cell neurons contain microtubules of opposite polarity. *Brain research* 473, 107-115.
- Bury, L.A., and Sabo, S.L. (2014). Dynamic mechanisms of neuroligin-dependent presynaptic terminal assembly in living cortical neurons. *Neural development* 9, 13.
- Cai, Q., Gerwin, C., and Sheng, Z.H. (2005). Syntabulin-mediated anterograde transport of mitochondria along neuronal processes. *The Journal of cell biology* 170, 959-969.
- Cai, Q., Pan, P.Y., and Sheng, Z.H. (2007). Syntabulin-kinesin-1 family member 5B-mediated axonal transport contributes to activity-dependent presynaptic assembly. *The Journal of neuroscience : the official journal of the Society for Neuroscience* 27, 7284-7296.

- Campbell, P.D., Shen, K., Sapio, M.R., Glenn, T.D., Talbot, W.S., and Marlow, F.L. (2014). Unique function of Kinesin Kif5A in localization of mitochondria in axons. *The Journal of neuroscience : the official journal of the Society for Neuroscience* 34, 14717-14732.
- Chen, J., Kanai, Y., Cowan, N.J., and Hirokawa, N. (1992). Projection domains of MAP2 and tau determine spacings between microtubules in dendrites and axons. *Nature* 360, 674-677.
- Chen, L.Y., Rex, C.S., Casale, M.S., Gall, C.M., and Lynch, G. (2007). Changes in synaptic morphology accompany actin signaling during LTP. *The Journal of neuroscience : the official journal of the Society for Neuroscience* 27, 5363-5372.
- Chia, P.H., Chen, B., Li, P., Rosen, M.K., and Shen, K. (2014). Local F-actin network links synapse formation and axon branching. *Cell* 156, 208-220.
- Chia, P.H., Patel, M.R., and Shen, K. (2012). NAB-1 instructs synapse assembly by linking adhesion molecules and F-actin to active zone proteins. *Nature neuroscience* 15, 234-242.
- Chua, J.J. (2014). Macromolecular complexes at active zones: integrated nano-machineries for neurotransmitter release. *Cellular and molecular life sciences : CMLS* 71, 3903-3916.
- Cingolani, L.A., and Goda, Y. (2008). Actin in action: the interplay between the actin cytoskeleton and synaptic efficacy. *Nature reviews Neuroscience* 9, 344-356.
- Coles, C.H., and Bradke, F. (2015). Coordinating neuronal actin-microtubule dynamics. *Current biology : CB* 25, R677-691.
- Colin, E., Zala, D., Liot, G., Rangone, H., Borrell-Pages, M., Li, X.J., Saudou, F., and Humbert, S. (2008). Huntingtin phosphorylation acts as a molecular switch for anterograde/retrograde transport in neurons. *The EMBO journal* 27, 2124-2134.
- Conde, C., and Caceres, A. (2009). Microtubule assembly, organization and dynamics in axons and dendrites. *Nature reviews Neuroscience* 10, 319-332.
- Coy, D.L., Hancock, W.O., Wagenbach, M., and Howard, J. (1999). Kinesin's tail domain is an inhibitory regulator of the motor domain. *Nature cell biology* 1, 288-292.
- D'Este, E., Kamin, D., Gottfert, F., El-Hady, A., and Hell, S.W. (2015). STED nanoscopy reveals the ubiquity of subcortical cytoskeleton periodicity in living neurons. *Cell reports* 10, 1246-1251.
- Da Silva, J.S., Medina, M., Zuliani, C., Di Nardo, A., Witke, W., and Dotti, C.G. (2003). RhoA/ROCK regulation of neurogenesis via profilin IIa-mediated control of actin stability. *The Journal of cell biology* 162, 1267-1279.
- de Forges, H., Bouissou, A., and Perez, F. (2012). Interplay between microtubule dynamics and intracellular organization. *The international journal of biochemistry & cell biology* 44, 266-274.
- Desai, A., and Mitchison, T.J. (1997). Microtubule polymerization dynamics. *Annual review of cell and developmental biology* 13, 83-117.
- Diefenbach, T.J., Latham, V.M., Yimlamai, D., Liu, C.A., Herman, I.M., and Jay, D.G. (2002). Myosin 1c and myosin IIB serve opposing roles in lamellipodial dynamics of the neuronal growth cone. *The Journal of cell biology* 158, 1207-1217.
- Dillon, C., and Goda, Y. (2005). The actin cytoskeleton: integrating form and function at the synapse. *Annual review of neuroscience* 28, 25-55.
- Disanza, A., and Scita, G. (2008). Cytoskeletal regulation: coordinating actin and microtubule dynamics in membrane trafficking. *Current biology : CB* 18, R873-875.
- Fanara, P., Husted, K.H., Selle, K., Wong, P.Y., Banerjee, J., Brandt, R., and Hellerstein, M.K. (2010). Changes in microtubule turnover accompany synaptic plasticity and memory formation in response to contextual fear conditioning in mice. *Neuroscience* 168, 167-178.
- Flynn, K.C., Hellal, F., Neukirchen, D., Jacob, S., Tahirovic, S., Dupraz, S., Stern, S., Garvalov, B.K., Gurniak, C., Shaw, A.E., et al. (2012). ADF/cofilin-mediated actin retrograde flow directs neurite formation in the developing brain. *Neuron* 76, 1091-1107.
- Franker, M.A., and Hoogenraad, C.C. (2013). Microtubule-based transport - basic mechanisms, traffic rules and role in neurological pathogenesis. *Journal of cell science* 126, 2319-2329.
- Fransson, S., Ruusala, A., and Aspenstrom, P. (2006). The atypical Rho GTPases Miro-1 and Miro-2 have essential roles in mitochondrial trafficking. *Biochemical and biophysical research communications* 344, 500-510.
- Fu, M.M., and Holzbaur, E.L. (2013). JIP1 regulates the directionality of APP axonal transport by coordinating kinesin and dynein motors. *The Journal of cell biology* 202, 495-508.
- Fujita, T., Maturana, A.D., Ikuta, J., Hamada, J., Walchli, S., Suzuki, T., Sawa, H., Wooten, M.W., Okajima, T., Tatematsu, K., et al. (2007). Axonal guidance protein FEZ1 associates with tubulin and

- kinesin motor protein to transport mitochondria in neurites of NGF-stimulated PC12 cells. *Biochemical and biophysical research communications* 361, 605-610.
- Fukazawa, Y., Saitoh, Y., Ozawa, F., Ohta, Y., Mizuno, K., and Inokuchi, K. (2003). Hippocampal LTP is accompanied by enhanced F-actin content within the dendritic spine that is essential for late LTP maintenance *in vivo*. *Neuron* 38, 447-460.
- Gallo, G. (2011). The cytoskeletal and signaling mechanisms of axon collateral branching. *Developmental neurobiology* 71, 201-220.
- Gallo, G. (2013). Mechanisms underlying the initiation and dynamics of neuronal filopodia: from neurite formation to synaptogenesis. *International review of cell and molecular biology* 301, 95-156.
- Ganguly, A., Tang, Y., Wang, L., Ladit, K., Loi, J., Dargent, B., Leterrier, C., and Roy, S. (2015). A dynamic formin-dependent deep F-actin network in axons. *The Journal of cell biology* 210, 401-417.
- Goldstein, A.Y., Wang, X., and Schwarz, T.L. (2008). Axonal transport and the delivery of pre-synaptic components. *Current opinion in neurobiology* 18, 495-503.
- Goley, E.D., and Welch, M.D. (2006). The ARP2/3 complex: an actin nucleator comes of age. *Nature reviews Molecular cell biology* 7, 713-726.
- Gross, S.P., Welte, M.A., Block, S.M., and Wieschaus, E.F. (2002). Coordination of opposite-polarity microtubule motors. *The Journal of cell biology* 156, 715-724.
- Guillaud, L., Setou, M., and Hirokawa, N. (2003). KIF17 dynamics and regulation of NR2B trafficking in hippocampal neurons. *The Journal of neuroscience : the official journal of the Society for Neuroscience* 23, 131-140.
- Gundelfinger, E.D., and Fejtova, A. (2012). Molecular organization and plasticity of the cytomatrix at the active zone. *Current opinion in neurobiology* 22, 423-430.
- Hall, D.H., and Hedgecock, E.M. (1991). Kinesin-related gene *unc-104* is required for axonal transport of synaptic vesicles in *C. elegans*. *Cell* 65, 837-847.
- Halpain, S. (2003). Actin in a supporting role. *Nature neuroscience* 6, 101-102.
- Hammarlund, M., Jorgensen, E.M., and Bastiani, M.J. (2007). Axons break in animals lacking beta-spectrin. *The Journal of cell biology* 176, 269-275.
- Hammond, J.W., Huang, C.F., Kaech, S., Jacobson, C., Banker, G., and Verhey, K.J. (2010). Posttranslational modifications of tubulin and the polarized transport of kinesin-1 in neurons. *Molecular biology of the cell* 21, 572-583.
- Hayashi-Takagi, A., Takaki, M., Graziane, N., Seshadri, S., Murdoch, H., Dunlop, A.J., Makino, Y., Seshadri, A.J., Ishizuka, K., Srivastava, D.P., et al. (2010). Disrupted-in-Schizophrenia 1 (DISC1) regulates spines of the glutamate synapse via Rac1. *Nature neuroscience* 13, 327-332.
- He, J., Zhou, R., Wu, Z., Carrasco, M.A., Kurshan, P.T., Farley, J.E., Simon, D.J., Wang, G., Han, B., Hao, J., et al. (2016). Prevalent presence of periodic actin-spectrin-based membrane skeleton in a broad range of neuronal cell types and animal species. *Proceedings of the National Academy of Sciences of the United States of America* 113, 6029-6034.
- Hering, H., and Sheng, M. (2003). Activity-dependent redistribution and essential role of cortactin in dendritic spine morphogenesis. *The Journal of neuroscience : the official journal of the Society for Neuroscience* 23, 11759-11769.
- Hetrick, B., Han, M.S., Helgeson, L.A., and Nolen, B.J. (2013). Small molecules CK-666 and CK-869 inhibit actin-related protein 2/3 complex by blocking an activating conformational change. *Chemistry & biology* 20, 701-712.
- Hirokawa, N., Niwa, S., and Tanaka, Y. (2010). Molecular motors in neurons: transport mechanisms and roles in brain function, development, and disease. *Neuron* 68, 610-638.
- Hirokawa, N., and Takemura, R. (2005). Molecular motors and mechanisms of directional transport in neurons. *Nature reviews Neuroscience* 6, 201-214.
- Hong, N.H., Qi, A., and Weaver, A.M. (2015). PI(3,5)P2 controls endosomal branched actin dynamics by regulating cortactin-actin interactions. *The Journal of cell biology* 210, 753-769.
- Honkura, N., Matsuzaki, M., Noguchi, J., Ellis-Davies, G.C., and Kasai, H. (2008). The subspine organization of actin fibers regulates the structure and plasticity of dendritic spines. *Neuron* 57, 719-729.
- Hotulainen, P., and Hoogenraad, C.C. (2010). Actin in dendritic spines: connecting dynamics to function. *The Journal of cell biology* 189, 619-629.
- Hu, X., Viesselmann, C., Nam, S., Merriam, E., and Dent, E.W. (2008). Activity-dependent dynamic microtubule invasion of dendritic spines. *The Journal of neuroscience : the official journal of the Society for Neuroscience* 28, 13094-13105.
- Huang, C.F., and Banker, G. (2012). The translocation selectivity of the kinesins that mediate neuronal organelle transport. *Traffic* 13, 549-564.
- Ikegami, K., and Setou, M. (2010). Unique post-

- translational modifications in specialized microtubule architecture. *Cell structure and function* 35, 15-22.
- Ivanov, A., Esclapez, M., Pellegrino, C., Shirao, T., and Ferhat, L. (2009). Drebrin A regulates dendritic spine plasticity and synaptic function in mature cultured hippocampal neurons. *Journal of cell science* 122, 524-534.
- Jacob, T.C., Moss, S.J., and Jurd, R. (2008). GABA(A) receptor trafficking and its role in the dynamic modulation of neuronal inhibition. *Nature reviews Neuroscience* 9, 331-343.
- Jaworski, J., Kapitein, L.C., Gouveia, S.M., Dortland, B.R., Wulf, P.S., Grigoriev, I., Camera, P., Spangler, S.A., Di Stefano, P., Demmers, J., et al. (2009). Dynamic microtubules regulate dendritic spine morphology and synaptic plasticity. *Neuron* 61, 85-100.
- Kamal, A., Stokin, G.B., Yang, Z., Xia, C.H., and Goldstein, L.S. (2000). Axonal transport of amyloid precursor protein is mediated by direct binding to the kinesin light chain subunit of kinesin-I. *Neuron* 28, 449-459.
- Kandel, E.R. (2001). The molecular biology of memory storage: a dialogue between genes and synapses. *Science* 294, 1030-1038.
- Kapitein, L.C., and Hoogenraad, C.C. (2011). Which way to go? Cytoskeletal organization and polarized transport in neurons. *Molecular and cellular neurosciences* 46, 9-20.
- Kapitein, L.C., Schlager, M.A., Kuijpers, M., Wulf, P.S., van Spronsen, M., MacKintosh, F.C., and Hoogenraad, C.C. (2010). Mixed microtubules steer dynein-driven cargo transport into dendrites. *Current biology : CB* 20, 290-299.
- Karcher, R.L., Deacon, S.W., and Gelfand, V.I. (2002). Motor-cargo interactions: the key to transport specificity. *Trends in cell biology* 12, 21-27.
- Kardon, J.R., and Vale, R.D. (2009). Regulators of the cytoplasmic dynein motor. *Nature reviews Molecular cell biology* 10, 854-865.
- Kessels, M.M., Schwintzer, L., Schlobinski, D., and Qualmann, B. (2011). Controlling actin cytoskeletal organization and dynamics during neuronal morphogenesis. *European journal of cell biology* 90, 926-933.
- Kevenaar, J.T., Bianchi, S., van Spronsen, M., Olieric, N., Lipka, J., Frias, C.P., Mikhaylova, M., Harterink, M., Keijzer, N., Wulf, P.S., et al. (2016). Kinesin-Binding Protein Controls Microtubule Dynamics and Cargo Trafficking by Regulating Kinesin Motor Activity. *Current biology : CB* 26, 849-861.
- Klemmer, P., Meredith, R.M., Holmgren, C.D., Klychnikov, O.I., Stahl-Zeng, J., Loos, M., van der Schors, R.C., Wortel, J., de Wit, H., Spijker, S., et al. (2011). Proteomics, ultrastructure, and physiology of hippocampal synapses in a fragile X syndrome mouse model reveal presynaptic phenotype. *The Journal of biological chemistry* 286, 25495-25504.
- Koch, N., Kobler, O., Thomas, U., Qualmann, B., and Kessels, M.M. (2014). Terminal axonal arborization and synaptic bouton formation critically rely on abp1 and the arp2/3 complex. *PloS one* 9, e97692.
- Kojima, N., Hanamura, K., Yamazaki, H., Ikeda, T., Itohara, S., and Shirao, T. (2010). Genetic disruption of the alternative splicing of drebrin gene impairs context-dependent fear learning in adulthood. *Neuroscience* 165, 138-150.
- Kollins, K.M., Bell, R.L., Butts, M., and Withers, G.S. (2009). Dendrites differ from axons in patterns of microtubule stability and polymerization during development. *Neural development* 4, 26.
- Kondo, M., Takei, Y., and Hirokawa, N. (2012). Motor protein KIF1A is essential for hippocampal synaptogenesis and learning enhancement in an enriched environment. *Neuron* 73, 743-757.
- Korobova, F., and Svitkina, T. (2010). Molecular architecture of synaptic actin cytoskeleton in hippocampal neurons reveals a mechanism of dendritic spine morphogenesis. *Molecular biology of the cell* 21, 165-176.
- Kreis, P., and Barnier, J.V. (2009). PAK signalling in neuronal physiology. *Cellular signalling* 21, 384-393.
- Kuijpers, M., and Hoogenraad, C.C. (2011). Centrosomes, microtubules and neuronal development. *Molecular and cellular neurosciences* 48, 349-358.
- Kuijpers, M., van de Willige, D., Freal, A., Chazeau, A., Franker, M.A., Hofenck, J., Rodrigues, R.J., Kapitein, L.C., Akhmanova, A., Jaarsma, D., et al. (2016). Dynein Regulator NDEL1 Controls Polarized Cargo Transport at the Axon Initial Segment. *Neuron* 89, 461-471.
- Lamprecht, R., and LeDoux, J. (2004). Structural plasticity and memory. *Nature reviews Neuroscience* 5, 45-54.
- Landis, D.M., and Reese, T.S. (1983). Cytoplasmic organization in cerebellar dendritic spines. *The Journal of cell biology* 97, 1169-1178.
- Leterrier, C., Potier, J., Caillol, G., Debarnot, C., Rueda Boroni, F., and Dargent, B. (2015). Nanoscale Architecture of the Axon Initial Segment Reveals

- an Organized and Robust Scaffold. *Cell reports* 13, 2781-2793.
- Letourneau, P.C. (2009). Actin in axons: stable scaffolds and dynamic filaments. Results and problems in cell differentiation 48, 65-90.
- Lipka, J., Kapitein, L.C., Jaworski, J., and Hoogenraad, C.C. (2016). Microtubule-binding protein doublecortin-like kinase 1 (DCLK1) guides kinesin-3-mediated cargo transport to dendrites. *The EMBO journal* 35, 302-318.
- Lo, K.Y., Kuzmin, A., Unger, S.M., Petersen, J.D., and Silverman, M.A. (2011). KIF1A is the primary anterograde motor protein required for the axonal transport of dense-core vesicles in cultured hippocampal neurons. *Neuroscience letters* 491, 168-173.
- Lowery, L.A., and Van Vactor, D. (2009). The trip of the tip: understanding the growth cone machinery. *Nature reviews Molecular cell biology* 10, 332-343.
- MacLean-Fletcher, S., and Pollard, T.D. (1980). Mechanism of action of cytochalasin B on actin. *Cell* 20, 329-341.
- Miller, K.E., DeProto, J., Kaufmann, N., Patel, B.N., Duckworth, A., and Van Vactor, D. (2005). Direct observation demonstrates that Liprin-alpha is required for trafficking of synaptic vesicles. *Current biology : CB* 15, 684-689.
- Mitchison, T., and Kirschner, M. (1984). Dynamic instability of microtubule growth. *Nature* 312, 237-242.
- Morrison, E.E., Wardleworth, B.N., Askham, J.M., Markham, A.F., and Meredith, D.M. (1998). EB1, a protein which interacts with the APC tumour suppressor, is associated with the microtubule cytoskeleton throughout the cell cycle. *Oncogene* 17, 3471-3477.
- Morton, A.M., Cunningham, A.L., and Diefenbach, R.J. (2010). Kinesin-1 plays a role in transport of SNAP-25 to the plasma membrane. *Biochemical and biophysical research communications* 391, 388-393.
- Muller, M.J., Klumpp, S., and Lipowsky, R. (2008). Tug-of-war as a cooperative mechanism for bidirectional cargo transport by molecular motors. *Proceedings of the National Academy of Sciences of the United States of America* 105, 4609-4614.
- Nelson, J.C., Stavoe, A.K., and Colon-Ramos, D.A. (2013). The actin cytoskeleton in presynaptic assembly. *Cell adhesion & migration* 7, 379-387.
- Niwa, S., Tanaka, Y., and Hirokawa, N. (2008). KIF1Bbeta- and KIF1A-mediated axonal transport of presynaptic regulator Rab3 occurs in a GTP-dependent manner through DENN/MADD. *Nature cell biology* 10, 1269-1279.
- Okada, Y., Yamazaki, H., Sekine-Aizawa, Y., and Hirokawa, N. (1995). The neuron-specific kinesin superfamily protein KIF1A is a unique monomeric motor for anterograde axonal transport of synaptic vesicle precursors. *Cell* 81, 769-780.
- Okamoto, K., Nagai, T., Miyawaki, A., and Hayashi, Y. (2004). Rapid and persistent modulation of actin dynamics regulates postsynaptic reorganization underlying bidirectional plasticity. *Nature neuroscience* 7, 1104-1112.
- Okamoto, K., Narayanan, R., Lee, S.H., Murata, K., and Hayashi, Y. (2007). The role of CaMKII as an F-actin-bundling protein crucial for maintenance of dendritic spine structure. *Proceedings of the National Academy of Sciences of the United States of America* 104, 6418-6423.
- Ozkan, E., Chia, P.H., Wang, R.R., Goriatcheva, N., Borek, D., Otwinowski, Z., Walz, T., Shen, K., and Garcia, K.C. (2014). Extracellular architecture of the SYG-1/SYG-2 adhesion complex instructs synaptogenesis. *Cell* 156, 482-494.
- Pacheco, A., and Gallo, G. (2016). Actin filament-microtubule interactions in axon initiation and branching. *Brain research bulletin* 126, 300-310.
- Patil, H., Cho, K.I., Lee, J., Yang, Y., Orry, A., and Ferreira, P.A. (2013). Kinesin-1 and mitochondrial motility control by discrimination of structurally equivalent but distinct subdomains in Ran-GTP-binding domains of Ran-binding protein 2. *Open biology* 3, 120183.
- Quinlan, E.M., and Halpain, S. (1996). Emergence of activity-dependent, bidirectional control of microtubule-associated protein MAP2 phosphorylation during postnatal development. *The Journal of neuroscience : the official journal of the Society for Neuroscience* 16, 7627-7637.
- Quinlan, M.E., Heuser, J.E., Kerkhoff, E., and Mullins, R.D. (2005). *Drosophila* Spire is an actin nucleation factor. *Nature* 433, 382-388.
- Racz, B., and Weinberg, R.J. (2008). Organization of the Arp2/3 complex in hippocampal spines. *The Journal of neuroscience : the official journal of the Society for Neuroscience* 28, 5654-5659.
- Ramachandran, B., and Frey, J.U. (2009). Interfering with the actin network and its effect on long-term potentiation and synaptic tagging in hippocampal CA1 neurons in slices *in vitro*. *The Journal of neuroscience : the official journal of the Society for Neuroscience* 29, 12167-12173.
- Rizvi, S.A., Neidt, E.M., Cui, J., Feiger, Z., Skau,

- C.T., Gardel, M.L., Kozmin, S.A., and Kovar, D.R. (2009). Identification and characterization of a small molecule inhibitor of formin-mediated actin assembly. *Chemistry & biology* 16, 1158-1168.
- Roy, S. (2016). Waves, rings, and trails: The scenic landscape of axonal actin. *The Journal of cell biology* 212, 131-134.
- Rust, M.B., and Maritzen, T. (2015). Relevance of presynaptic actin dynamics for synapse function and mouse behavior. *Experimental cell research* 335, 165-171.
- Sankaranarayanan, S., Atluri, P.P., and Ryan, T.A. (2003). Actin has a molecular scaffolding, not propulsive, role in presynaptic function. *Nature neuroscience* 6, 127-135.
- Schlager, M.A., and Hoogenraad, C.C. (2009). Basic mechanisms for recognition and transport of synaptic cargos. *Molecular brain* 2, 25.
- Schuh, M. (2011). An actin-dependent mechanism for long-range vesicle transport. *Nature cell biology* 13, 1431-1436.
- Setou, M., Nakagawa, T., Seog, D.H., and Hirokawa, N. (2000). Kinesin superfamily motor protein KIF17 and mLin-10 in NMDA receptor-containing vesicle transport. *Science* 288, 1796-1802.
- Setou, M., Seog, D.H., Tanaka, Y., Kanai, Y., Takei, Y., Kawagishi, M., and Hirokawa, N. (2002). Glutamate-receptor-interacting protein GRIP1 directly steers kinesin to dendrites. *Nature* 417, 83-87.
- Sheng, M., and Hoogenraad, C.C. (2007). The postsynaptic architecture of excitatory synapses: a more quantitative view. *Annual review of biochemistry* 76, 823-847.
- Shin, O.H., Rhee, J.S., Tang, J., Sugita, S., Rosenmund, C., and Sudhof, T.C. (2003). Sr2+ binding to the Ca2+ binding site of the synaptotagmin 1 C2B domain triggers fast exocytosis without stimulating SNARE interactions. *Neuron* 37, 99-108.
- Sidenstein, S.C., D'Este, E., Bohm, M.J., Danzl, J.G., Belov, V.N., and Hell, S.W. (2016). Multicolour Multilevel STED nanoscopy of Actin/Spectrin Organization at Synapses. *Scientific reports* 6, 26725.
- Song, A.H., Wang, D., Chen, G., Li, Y., Luo, J., Duan, S., and Poo, M.M. (2009). A selective filter for cytoplasmic transport at the axon initial segment. *Cell* 136, 1148-1160.
- Sousa, V.L., Bellani, S., Giannandrea, M., Yousuf, M., Valtorta, F., Meldolesi, J., and Chieregatti, E. (2009). α -synuclein and its A30P mutant affect actin cytoskeletal structure and dynamics. *Molecular biology of the cell* 20, 3725-3739.
- Spector, I., Shochet, N.R., Kashman, Y., and Groweiss, A. (1983). Latrunculin: novel marine toxins that disrupt microfilament organization in cultured cells. *Science* 219, 493-495.
- Spillane, M., Ketschek, A., Jones, S.L., Korobova, F., Marsick, B., Lanier, L., Svitkina, T., and Gallo, G. (2011). The actin nucleating Arp2/3 complex contributes to the formation of axonal filopodia and branches through the regulation of actin patch precursors to filopodia. *Developmental neurobiology* 71, 747-758.
- Star, E.N., Kwiatkowski, D.J., and Murthy, V.N. (2002). Rapid turnover of actin in dendritic spines and its regulation by activity. *Nature neuroscience* 5, 239-246.
- Su, Q., Cai, Q., Gerwin, C., Smith, C.L., and Sheng, Z.H. (2004). Syntabulin is a microtubule-associated protein implicated in syntaxin transport in neurons. *Nature cell biology* 6, 941-953.
- Sudhof, T.C. (2004). The synaptic vesicle cycle. *Annual review of neuroscience* 27, 509-547.
- Sudhof, T.C. (2012). The presynaptic active zone. *Neuron* 75, 11-25.
- Takano, T., Xu, C., Funahashi, Y., Namba, T., and Kaibuchi, K. (2015). Neuronal polarization. *Development* 142, 2088-2093.
- Tanaka, Y., Kanai, Y., Okada, Y., Nonaka, S., Takeda, S., Harada, A., and Hirokawa, N. (1998). Targeted disruption of mouse conventional kinesin heavy chain, kif5B, results in abnormal perinuclear clustering of mitochondria. *Cell* 93, 1147-1158.
- Terry-Lorenzo, R.T., Roadcap, D.W., Otsuka, T., Blanpied, T.A., Zamorano, P.L., Garner, C.C., Shenolikar, S., and Ehlers, M.D. (2005). Neurabin/protein phosphatase-1 complex regulates dendritic spine morphogenesis and maturation. *Molecular biology of the cell* 16, 2349-2362.
- Thirumurugan, K., Sakamoto, T., Hammer, J.A., 3rd, Sellers, J.R., and Knight, P.J. (2006). The cargo-binding domain regulates structure and activity of myosin 5. *Nature* 442, 212-215.
- Vale, R.D. (2003). The molecular motor toolbox for intracellular transport. *Cell* 112, 467-480.
- van Spronsen, M., Mikhaylova, M., Lipka, J., Schlager, M.A., van den Heuvel, D.J., Kuijpers, M., Wulf, P.S., Keijzer, N., Demmers, J., Kapitein, L.C., et al. (2013). TRAK/Milton motor-adaptor proteins steer mitochondrial trafficking to axons and dendrites. *Neuron* 77, 485-502.
- van Woerden, G.M., Hoebeek, F.E., Gao, Z., Nagaraja, R.Y., Hoogenraad, C.C., Kushner, S.A., Hansel,

- C., De Zeeuw, C.I., and Elgersma, Y. (2009). betaCaMKII controls the direction of plasticity at parallel fiber-Purkinje cell synapses. *Nature neuroscience* 12, 823-825.
- Verhey, K.J., and Hammond, J.W. (2009). Traffic control: regulation of kinesin motors. *Nature reviews Molecular cell biology* 10, 765-777.
- Wang, Z., Edwards, J.G., Riley, N., Provance, D.W., Jr., Karcher, R., Li, X.D., Davison, I.G., Ikebe, M., Mercer, J.A., Kauer, J.A., et al. (2008). Myosin Vb mobilizes recycling endosomes and AMPA receptors for postsynaptic plasticity. *Cell* 135, 535-548.
- Watanabe, K., Al-Bassam, S., Miyazaki, Y., Wandless, T.J., Webster, P., and Arnold, D.B. (2012). Networks of polarized actin filaments in the axon initial segment provide a mechanism for sorting axonal and dendritic proteins. *Cell reports* 2, 1546-1553.
- Welte, M.A. (2004). Bidirectional transport along microtubules. *Current biology : CB* 14, R525-537.
- Westermann, S., and Weber, K. (2003). Post-translational modifications regulate microtubule function. *Nature reviews Molecular cell biology* 4, 938-947.
- Witte, H., and Bradke, F. (2008). The role of the cytoskeleton during neuronal polarization. *Current opinion in neurobiology* 18, 479-487.
- Witte, H., Neukirchen, D., and Bradke, F. (2008). Microtubule stabilization specifies initial neuronal polarization. *The Journal of cell biology* 180, 619-632.
- Wolf, M., Zimmermann, A.M., Gorlich, A., Gurniak, C.B., Sassoe-Pognetto, M., Friauf, E., Witke, W., and Rust, M.B. (2015). ADF/Cofilin Controls Synaptic Actin Dynamics and Regulates Synaptic Vesicle Mobilization and Exocytosis. *Cereb Cortex* 25, 2863-2875.
- Wu, L.J., Ren, M., Wang, H., Kim, S.S., Cao, X., and Zhuo, M. (2008). Neurabin contributes to hippocampal long-term potentiation and contextual fear memory. *PloS one* 3, e1407.
- Xu, K., Zhong, G., and Zhuang, X. (2013). Actin, spectrin, and associated proteins form a periodic cytoskeletal structure in axons. *Science* 339, 452-456.

Positioning of AMPA receptor-containing endosomes regulates synapse architecture

Marta Esteves da Silva¹, Max Adrian¹, Philipp Schätzle¹, Joanna Lipka^{1,3}, Takuya Watanabe⁴, Sukhee Cho⁴, Kensuke Futai⁴, Corette J. Wierenga¹, Lukas C. Kapitein^{1,2} and Casper C. Hoogenraad^{1,2}

Cell Reports, November 2015, 13(5):933-943

¹Cell Biology, Faculty of Science, Utrecht University, Utrecht, The Netherlands.

²Department of Neuroscience, Erasmus Medical Center, Rotterdam, The Netherlands.

³International Institute of Molecular and Cell Biology, Warsaw, Poland. ⁴Department of Psychiatry, Brudnick Neuropsychiatric Research Institute, University of Massachusetts Medical School, Worcester MA, USA.

ABSTRACT

Lateral diffusion in the membrane and endosomal trafficking both contribute to the addition and removal of AMPA receptors (AMPARs) at postsynaptic sites. However the spatial coordination between these mechanisms has remained unclear, because little is known about the dynamics of AMPAR containing endosomes. In addition, how the positioning of AMPAR-containing endosomes affects synapse organization and functioning has never been directly explored. Here, we used live-cell imaging in hippocampal neuron cultures to show that intracellular AMPARs are transported in Rab11-positive recycling endosomes, which frequently enter dendritic spines and depend on the microtubule and actin cytoskeleton. By using chemically-induced dimerization systems to recruit kinesin (KIF1C) or myosin (MyosinV/VI) motors to Rab11-positive recycling endosomes, we control their trafficking and found that induced removal of recycling endosomes from spines decreases surface AMPAR expression and PSD-95 clusters at synapses. Our data suggest a mechanistic link between endosome positioning and the postsynaptic structure and composition.

INTRODUCTION

Most fast excitatory signaling in the brain is mediated by AMPA-type glutamate receptors and changes in the number of these receptors at synapses are thought to underlie information storage in the brain (Huganir and Nicoll, 2013). AMPA receptors (AMPA receptors) exchange between synaptic and extrasynaptic sites by lateral diffusion in the plasma membrane, whereas endosomal recycling and trafficking followed by exocytosis is believed to maintain a supply of extrasynaptic AMPARs on the membrane (Czondor *et al.*, 2012; Newpher and Ehlers, 2008). However, the spatial coordination between these two major AMPAR transport mechanisms has remained unclear, because, in contrast to lateral receptor diffusion, little is known about the dynamics of AMPAR containing endosomes.

Excitatory synapses are mostly located at small dendritic protrusions, called spines, which are often connected to dendritic shaft through a narrow membrane tube of 100 - 200 nm diameter, called the spine neck. This architecture is believed to biochemically isolate the spine from the rest of dendrite, because it slows down both cytoplasmic and membrane-based diffusion. Simulations suggested that secretion inside spines dramatically increases the fraction of receptors captured at synapses, compared to secretion near the base of the spine neck (Adrian *et al.*, 2014). In addition, endosomes are known to often function as signaling hub, and their precise position either inside or outside spines would also strongly affect signaling persistence, given the biochemical isolation of spines (Colgan and Yasuda, 2014). However, how the positioning of AMPAR-containing endosomes affects synapse architecture has never been directly explored.

Here we use high-resolution live-cell imaging to examine the intracellular dynamics of AMPAR-containing endosomes. We found that AMPARs move in highly dynamic Rab11 endosomes that frequently enter and exit dendritic spines. Whereas long-range transport is largely microtubule (MT)-based, spine entries mostly depend on actin-based myosin motors. By repositioning endosomes, we found that removal of recycling endosomes from dendritic spines decreased the level of AMPAR at the spine membrane, as well as PSD-95 clusters at synapses. Our data demonstrate that recycling endosome trafficking directly affects synaptic function and suggest a mechanistic link between endocytic recycling and the structure and composition of the synapse.

RESULTS

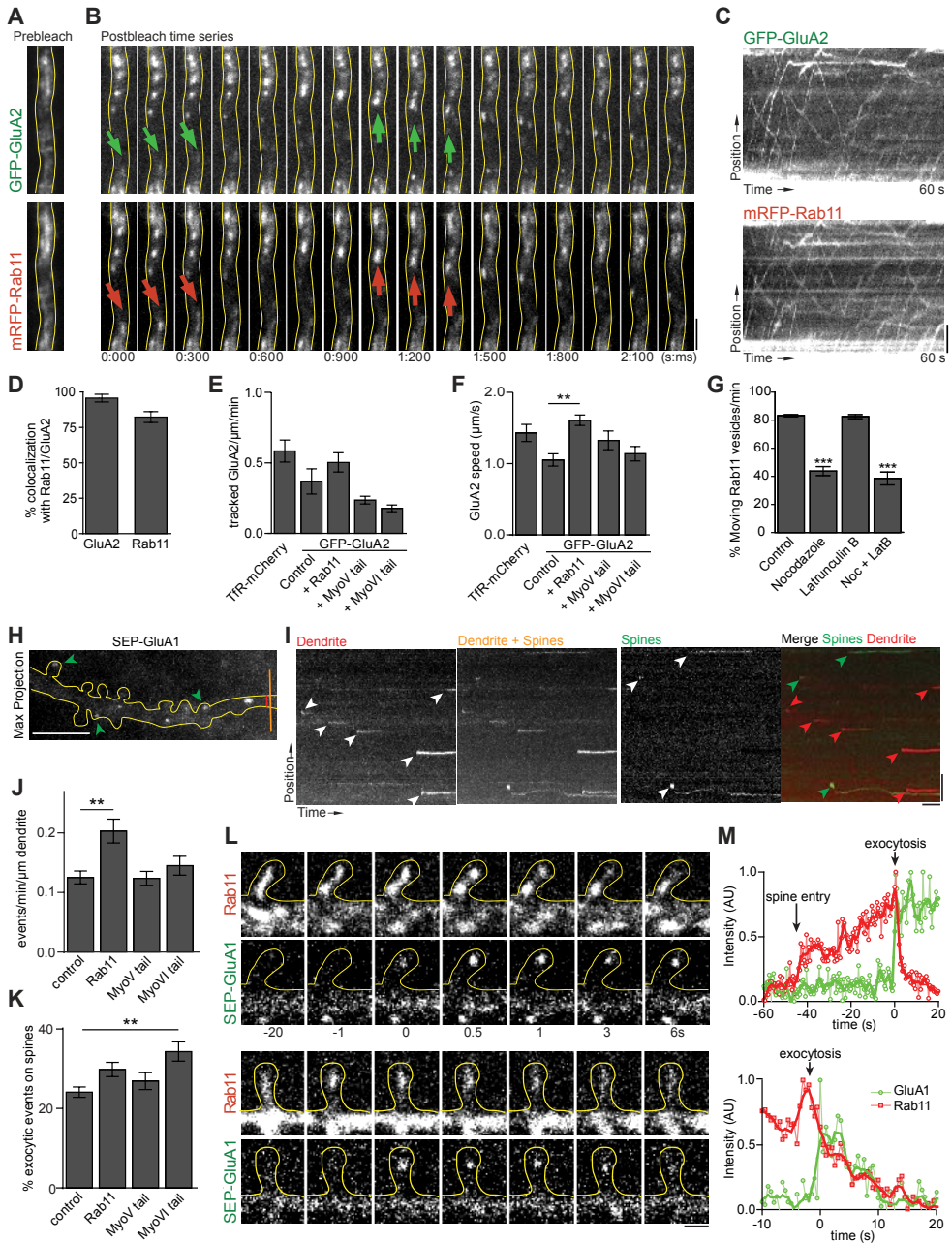
Intracellular AMPA receptors are transported in recycling endosomes

To directly probe AMPAR vesicle trafficking in hippocampal neurons, we co-express HA-GluA1 and GFP-GluA2 and precisely control the timing and level of GFP-GluA2 receptor expression using a doxycycline regulated gene expression system. The majority of the GluA2 receptors is localized to the plasma membrane or retained in the endoplasmic reticulum, which appear as diffusive signals throughout the dendrites (Fig.1A). To selectively visualize intracellular vesicular GFP-GluA2, most of the fluorescence from the dendritic part in the field

of view was bleached before image acquisition. Neurons expressing low levels of GFP-GluA2 revealed vesicle-like structures in the dendritic shaft and dendritic spines that were rapidly moving (Fig.1A,B). In the dendritic shaft, GFP-GluA2 motility was directed both away from and towards the cell body and reversals were also frequently observed (Fig.1C). Intracellular AMPARs most likely follow the endosomal transport routes (Brown *et al.*, 2007; Hoogenraad *et al.*, 2010; Park *et al.*, 2004; Park *et al.*, 2006; Wang *et al.*, 2008). To examine the identity of GFP-GluA2 containing vesicles, neurons were co-transfected with HA-GluA1 and GFP-GluA2 and stained for Rab11, a marker for recycling endosomes. Due to the high abundance of GluA1/2 in other cellular compartments only a minor fraction is colocalized with endogenous Rab11 in fixed neurons (Fig.S1A,B). Live-cell imaging in conditioned medium with constant osmolality, showed that ~80% of Rab11-positive recycling endosomes in the dendrites are motile (Fig.S2A-E). Live imaging directly after bleaching revealed that 96.0 ± 1.5 % of the motile GFP-GluA2 containing vesicles contained mRFP-Rab11, whereas 77.6 ± 1.2 % of all motile Rab11 positive vesicles also contained GluA2 (Fig.1D, Table S1). The average density of moving GFP-GluA2 vesicles per $\mu\text{m}/\text{min}$ was 0.37 ± 0.09 (Fig.1E) with a mean vesicle velocity of 1.05 ± 0.09 $\mu\text{m}/\text{s}$ in control conditions (Fig.1F). Co-expression of Rab11 increased the GluA2 vesicle speed to values similar to those for endosomal vesicles with Transferrin Receptor (TfR) (Fig.1F). Interestingly, highly dynamic clusters of GluA2 could be observed within the motile Rab11-positive recycling endosomes (Fig.S1C-I). These intra-endosomal subdomains may localize signal responses or concentrate components for further endosomal sorting. We next determined whether Rab11 vesicle trafficking in dendrites depends on the actin or MT cytoskeleton. While blocking F-actin assembly by latrunculin B (10 μM) treatments did not affect Rab11 vesicles dynamics along the dendrites, addition of low concentrations of nocodazole (300 nM) to inhibit MT dynamics decreased their motility to ~40% (Fig.1G and S2F-G). After nocodazole treatment, the majority of the Rab11-positive recycling endosomes accumulate in enlarged and immobile clusters in the dendritic shaft. Addition of nocodazole and latrunculin

► **Figure 1. Rab11-positive recycling endosomes transport GluA1/A2 in dendrites and spines**

A-B. Stills from a dual-color time-lapse recording of a rat hippocampal neuron expressing GluA1, GFP-GluA2 (top) and mRFP-Rab11 (bottom). **A.** Prebleach overview of GFP-GluA2 and mRFP-Rab11; **B.** post-bleach time series. Arrows mark motile vesicles positive for both GFP-GluA2 and mRFP-Rab11. **C.** Kymograph of the recording in B showing prevalent co-motility of GFP-GluA2 and mRFP-Rab11. **D.** Average colocalization between intracellular GFP-GluA2 and mRFP-Rab11 in dendrites. **E-F.** Quantification of the number of tracked vesicles/ $\mu\text{m}/\text{min}$ (**E**) and the vesicle speeds (**F**) of neurons expressing TfR-mCherry or GFP-GluA2 under indicated conditions. **G.** Quantification of the percentage of motile Rab11-positive recycling endosomes in 1 min timelapse acquisition under the indicated conditions. **H-I.** Quantification of SEP-GluA1 exocytic events in dendrites. **H.** Maximum projection of SEP-GluA1 signal of 500 frames recorded at 5 fps after bleaching the dendrite. **I.** Kymographs of dendrite shown in **H** with different widths to visualize exocytosis in the dendritic shaft and spines. Yellow and red bar show projection width of kymograph, green arrows show exocytic events in spines detected by the kymograph. Scale bars are 10s and 5 μm . **J-K.** Quantification of the number of exocytic events per dendrite (**J**) and the fraction of events in dendritic spines (**K**) under indicated conditions. **L.** Stills from two time-lapse recordings of neurons expressing tagRFP-Rab11 (top panels) and SEP-GluA1 (bottom panels). Time is indicated relative to exocytic event in SEP channel. Solid line indicates outline of a single dendritic spine. **M.** Quantification of fluorescence intensity of tagRFP-Rab11 (red) and



SEP-GluA1 (green) in dendritic spines shown in L. Dots indicate measurements connected with dim lines, thick lines are smoothed values over 4 adjacent values. Upper graph reveals prolonged retention of SEP-GluA1 fluorescence in the spine head, while lower graph shows rapid loss of SEP-GluA1 signal. Graphs represent mean \pm SEM. Statistical significance was determined by using Kruskal-Wallis test or one-way ANOVA and Dunnett's multiple comparison post hoc test, respectively; ** $p < 0.01$, *** $p < 0.001$. Scale bar is 5 μm (B,C,I). See also Figure S1, S2 and Table S1.

B to the neurons has a similar effect as nocodazole alone (Fig.1G and Fig.S2F-G). Consistently, expression of dominant-negative constructs to abrogate MyosinV or MyosinVI function did not affect the GFP-GluA2 vesicle speed (Fig.1F). These results suggest that intracellular AMPARs are transported in Rab11-positive recycling endosomes along dynamic MT tracks within the dendritic shaft.

Endosomal entry in spines correlates with an increase in surface AMPA receptors

SEP-labeled GluA subunits have been used to visualize postsynaptic exocytosis in dendrites and AMPAR dynamics on the plasma membrane. Here, we determine the correlation between recycling endosome dynamics and AMPAR exocytosis by simultaneously imaging tagRFP-Rab11 and SEP-GluA1. As reported previously (Petrini *et al.*, 2009), AMPARs undergo exocytosis not only in dendritic shafts but also in dendritic spines (Fig.1I). Under basal conditions, generally few exocytic events releasing GluA1 could be observed (0.13 ± 0.01 events/min/ μm dendrite) (Fig.1J), but the number of events in spines contributes to $24.1 \pm 1.3\%$ of the total amount of events recorded on dendrites (Fig.1K). Co-expression of Rab11 leads to a slight increase in the total number exocytic GluA1 events (Fig.1J). Some of the events in spines followed the entry of dynamic Rab11 vesicles and the appearance of SEP-GluA1 was accompanied by the disappearance of the Rab11 signal (Fig.1L,M, Video S1), suggesting a correlation between Rab11-positive recycling endosomes trafficking and AMPAR exocytosis in spines. Expression of dominant-negative constructs to abrogate MyosinV or MyosinVI function did not affect GluA1 exocytosis in dendrites (Fig.1J). However, inhibiting MyosinVI increased the number of exocytic events in spines (Fig.1K). After exocytosis the SEP-GluA1 fluorescence showed two distinct behaviors in individual spines; it either remained in the spine head for prolonged times in the order of tens of seconds (Fig.1L, top) or fade within few seconds (Fig.1L, bottom), most likely reflecting the differential GluA1 retention in spine heads (Petrini *et al.*, 2009). Consistently, these data suggest that recycling endosomes in spines contribute to an increase in surface AMPARs.

Recycling endosomes move along both actin and microtubules in dendritic spines

We frequently observed Rab11 vesicles containing GFP-GluA2 in dendritic spines (Fig.2A and Video S2). Under basal conditions, GFP-GluA2 positive Rab11 vesicles move in and out of spines (Fig.2B and Fig.S2A). The recycling endosomes that enter spines did not necessarily emerge from immobile storage sites near the spine base, but frequently moved from distant dendritic regions. Similarly, GluA1/2 positive endosomal vesicles that left the spines were often not retained near the base of spine, but quickly move away in the anterograde or retrograde direction within the adjacent dendrite. On average $22.6 \pm 2.3\%$ of all immobile Rab11 vesicles were at the base of spine (Fig.S2D). To determine the role of MT and actin dynamics on Rab11-positive recycling endosomes trafficking in dendritic spines, neurons were treated with low concentrations of nocodazole (300 nM) and/or latrunculin B (10 μM). In untreated live neurons at DIV14, $\sim 65\%$ of dendritic spines are targeted by Rab11-positive recycling endosomes, and

~80% of the endosomes in spines are dynamic (Fig.2G-I, Fig.S3A). Both nocodazole and/or latrunculin B treatments increased the number of targeted spines (Fig.2G) and decreased the endosome dynamics in spines (Fig.2H). The effect on recycling endosomal dynamics is mild in the case of nocodazole but much more severe with latrunculin B and the combination of both drugs (Fig.2G-I, Fig.S3A). Consistent with previous data (Correia *et al.*, 2008; Wagner *et al.*, 2011; Wang *et al.*, 2008), we found that MyosinV is involved in proper endosome trafficking in spines (Fig.S3B-E). The data also suggest that MyosinVI has a role in Rab11 vesicle transport in spines (Fig.S3D). Previous studies have shown that MyosinVI is enriched in the postsynaptic density and disruption of its function leads to synaptic loss (Nash *et al.*, 2010; Osterweil *et al.*, 2005).

Since recent work demonstrated that spines contain dynamic MTs (Gu *et al.*, 2008; Hu *et al.*, 2008; Jaworski *et al.*, 2009), we next investigated in more detail the role of MT on Rab11 vesicle dynamics in spines. To visualize MT dynamics in spines, we expressed mCherry-MT+TIP to specifically label growing MT plus-ends (Yau *et al.*, 2014). MT spine entry events were readily detected from comet displacements, whereas depolymerizing MTs (lacking a clear comet at the tip) could also be observed within spines (Fig.2C-F). Co-expression of mCherry-MT+TIP and GFP-Rab11 revealed that recycling endosomes move in and out of spines in both the presence and absence of MTs (Fig.2C-F). In untreated neurons, fast imaging of Rab11 vesicle dynamics within spines revealed that the mean entry speed is $0.66 \pm 0.024 \mu\text{m}/\text{sec}$, the mean exit speed is $0.55 \pm 0.04 \mu\text{m}/\text{sec}$ and the average dwell time of dynamic Rab11 vesicles is 24 seconds (Fig.2J-L). Treating neurons with low concentrations of nocodazole (300 nM) decreased both the average entry and exit speeds of endosomes in spines (Fig.2K-L). Interestingly, inhibiting microtubule dynamics resulted in a marked shift of the velocity distribution profiles toward lower speeds (Fig.2K-L), suggesting that the velocity of Rab11 vesicles in spines is higher with MTs, compared to spines without MTs. This is consistent with microtubule-based motility being generally faster than actin-based motility (Kapitein *et al.*, 2013). At one point, the endosomal spine entry precisely coincided with the entry of a MT, suggesting that here Rab11 trafficking was limited by the MT growth speed (Fig.2E-F, entry speeds $\sim 0.05 \mu\text{m}/\text{s}$). Although we cannot exclude that drug treatments have an indirect effect on the Rab11 vesicle dynamics in spines, it seems likely that recycling endosomes can exploit both dynamic actin and MT-based strategies to enter dendritic spines.

Controlled transport of Rab11 positive recycling endosomes in dendritic spines

Translocation of Rab11-positive recycling endosomes to spines has been shown to be important for spine growth (Hoogenraad *et al.*, 2010; Park *et al.*, 2006). To determine the role of recycling endosomes for overall spine morphology and postsynaptic organization, we co-transfected neurons with GFP to highlight neuronal morphology and a Rab11 dominant negative construct (Rab11-S25N) or Rab11a shRNA. While expression of wildtype GFP-Rab11 does not affect spine morphology, blocking or depleting Rab11 highly affected the morphology of spines, showing a marked decrease in the total number of protrusions and dendritic spines (Fig.3A).

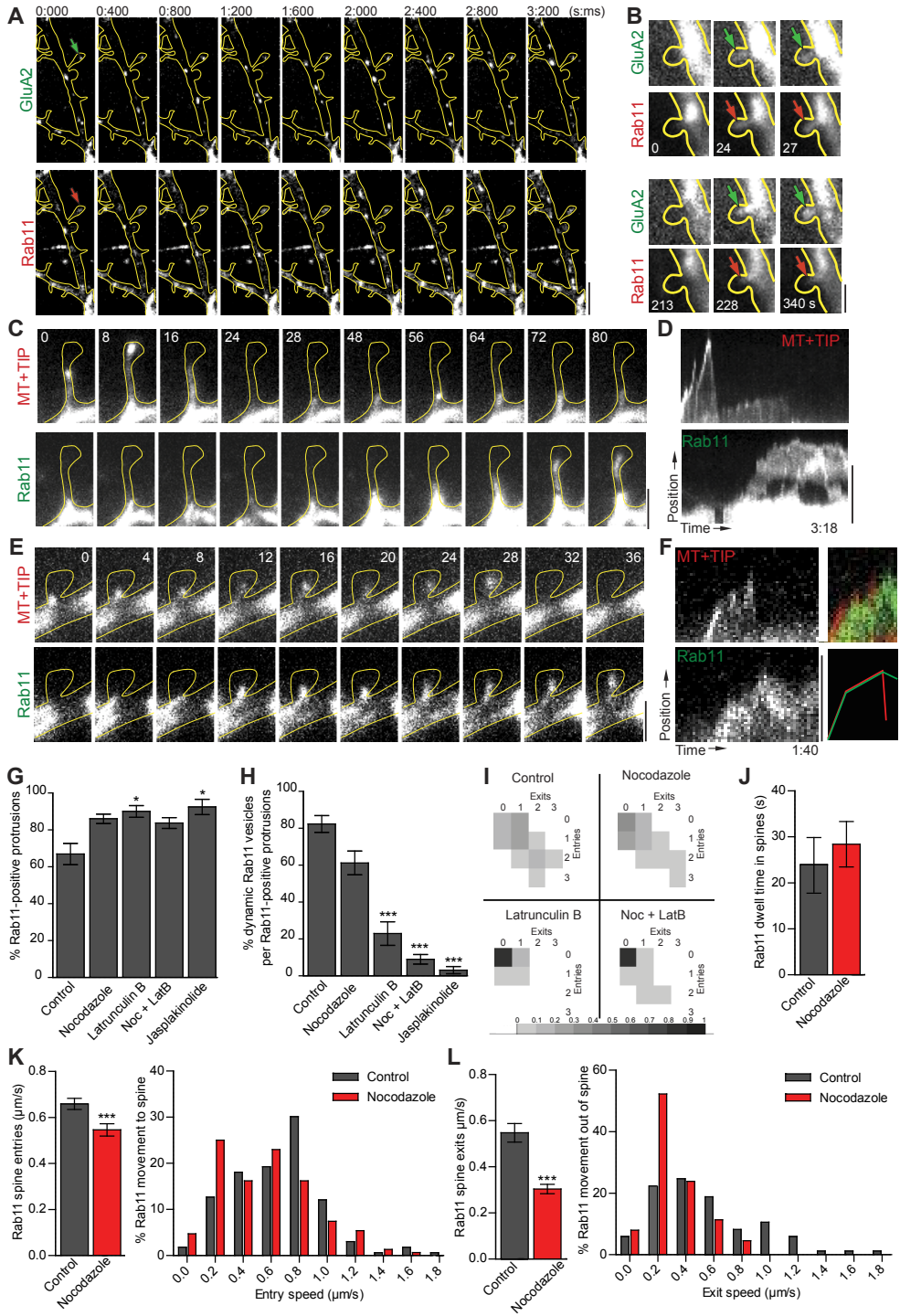
To determine if the morphological effect upon disruption of Rab11 correlates with changes in postsynaptic organization, alterations in the number and area of clusters of the postsynaptic marker Homer-1 were analyzed. The number of Homer-1 clusters in protrusions decreased in both Rab11 knockdown or dominant negative conditions (Fig.3B), without significantly affecting the area of the clusters (Fig.3C). Together, these data indicate that Rab11-positive recycling endosomes play an important role in dendritic spine morphology and postsynaptic organization.

To determine the short-term effects of Rab11-positive recycling endosomes trafficking on spine morphology and synaptic function, we developed an inducible trafficking assay to directly control endosomal transport in dendritic spines. In this assay, FRB-FKBP heterodimerization is used to induce the binding of kinesin motors, myosin motors or adaptors to Rab11 vesicles during live-cell recordings (Kapitein *et al.*, 2010). For these experiments, Rab11 vesicles were labeled by expressing FKBP-Rab11, a fusion construct of Rab11 with FKBP12, a domain that binds to an FRB domain in the presence of rapalog AP21967 (Fig.3D). FKBP-Rab11 targets specifically recycling endosomes (Fig.S1J). FRB is fused to truncated Kinesin-3 motor KIF1C, and MyosinVI motors, which contains the motor domain and coiled-coil dimerization region (KIF1C-FRB and MyosinVI-FRB). Alternatively, MyosinV was recruited through the MyosinV binding domain (MBD) of melanophilin (MBD-FRB). Inducing the FKBP-Rab11 interaction with various motor proteins did not affect SEP-TfR exocytosis (Fig.3D), indicating that attachment of FKBP-Rab11 to motors does not interfere with global recycling endosome function.

First we focused on KIF1C-induced Rab11 trafficking. Addition of rapalog to neurons co-expressing KIF1C-FRB and FKBP-GFP-Rab11 induced targeting of Rab11-positive recycling endosomes from the shaft into dendritic spines (Fig.S4A-C). Quantification in fixed neurons revealed a marked increase in the number of Rab11 targeted spines after 30 minutes of rapalog treatment (Fig.3E). Live-cell imaging of KIF1C-induced Rab11 vesicle dynamics within the spines showed no effect on the entry and exit speeds (Fig.S4D). Interestingly, we also found an

► **Figure 2. Recycling endosomes transport into dendritic spines depends on microtubule dynamics**

A-B. Stills from a dual-color time-lapse recording of a rat hippocampal neuron expressing GluA1, GFP-GluA2 (top) and mRFP-Rab11 (bottom). Arrows mark motile vesicles positive for both markers. **C-F.** Stills (**C,E**) and kymograph (**D,F**) from a dual-color time-lapse recording of a neuron expressing GFP-Rab11 (bottom) and mCherry-MT+TIP (top). (**F**) Overlay of green and red channels shows complete overlap. **G.** Quantification of the percentage of dendritic protrusions targeted by Rab11-positive recycling endosomes along 20 μm of dendrite during 5 minutes timelapse in the different conditions. **H.** Quantification of the percentage of dynamic Rab11-positive recycling endosomes, i.e. either one exit or one entry from a dendritic protrusion, per number of targeted protrusions, in the different conditions. **I.** Schematic heatmap showing the dynamic distribution of Rab11-positive recycling endosomes in dendritic spines during 5 minutes timelapse, under different conditions. **J.** Quantification of Rab11-vesicles dwell time in spines before and after nocodazole treatment. **K-L.** Quantification of Rab11-positive recycling endosomes entry (**K**) and exit (**L**) speeds in spines in control and nocodazole conditions. Graphs represent mean \pm SEM. Statistical significance was determined using Kruskal-Wallis test and Dunn's multiple comparison post hoc test, * $p < 0.05$, *** $p < 0.001$ (Fig.2G-H), and unpaired t-test with Mann Whitney correction, *** $p < 0.001$ (Fig.2J-L). Scale bar is 5 μm (A), 1 μm (B), 2 μm (C-F). See also Figure S3 and Table S1.



2

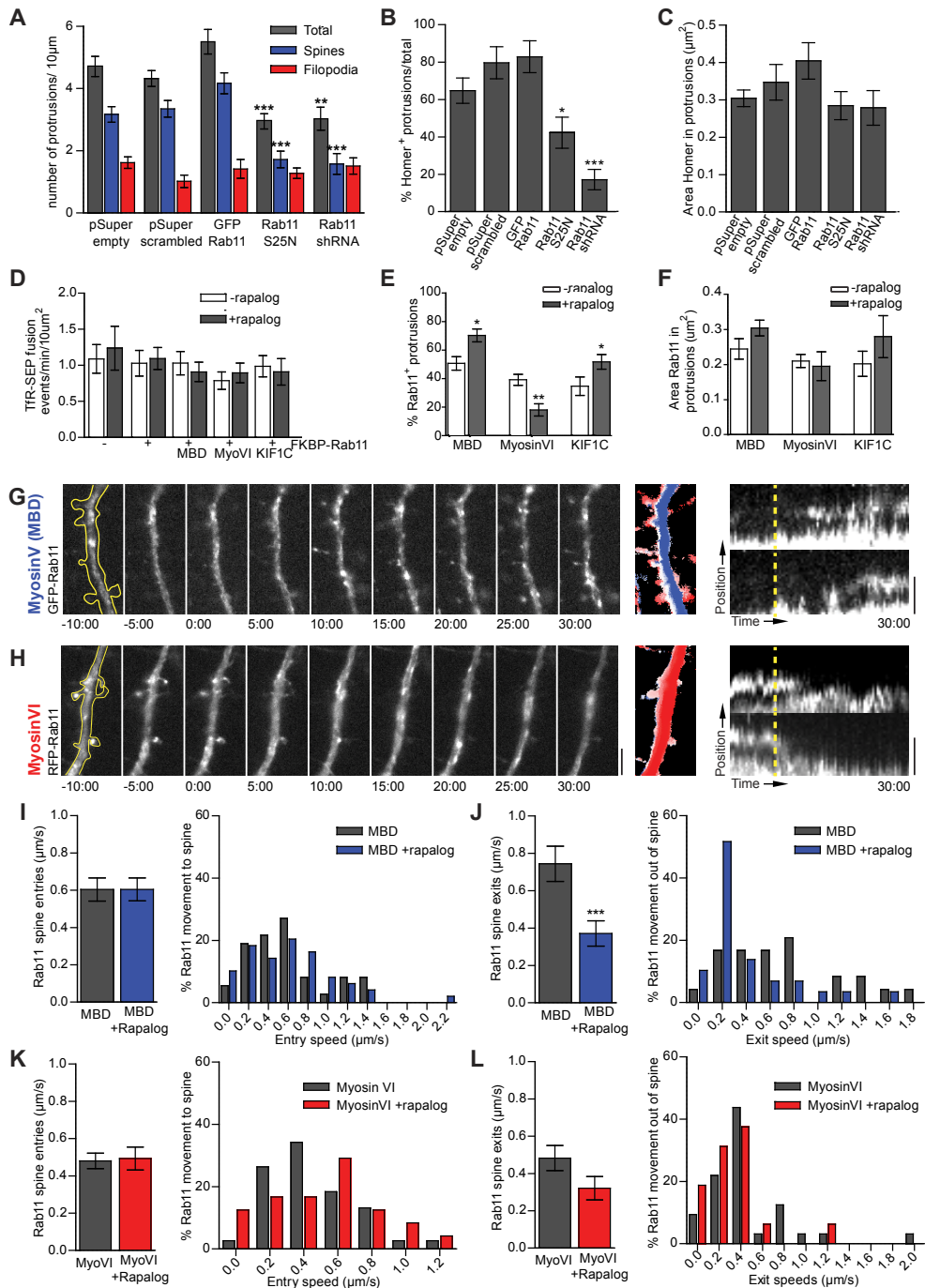


Figure 3. Time-dependent effect of recycling endosome removal from spines

A. Quantification of protrusions per 10 μm dendrite. Classification was based on head width/ length ratio (<0.5 =filopodia; >=0.5 = spine). **B-C.** Quantification of Homer-positive protrusions per 10 μm regions of dendrite (**B**)

and area of Homer clusters (C). **D.** Induced dimerization of Rab11-vesicles with different motors does not affect fusion of TfR to the surface of COS7 cells. **E-F.** Induced dimerization of MyosinV (MBD) and KIF1C to Rab11-positive recycling endosomes increases their number in dendritic protrusions, whereas coupling of MyosinV to Rab11-positive recycling endosomes removes them from spines. There is no significant effect in the area of Rab11 vesicles in protrusions upon dimerization. **G-H.** Left panels: Stills from time lapse recordings of Rab11-positive recycling endosomes during which rapalog was added at time 0:00 to recruit MyosinV through MBD (G) or MyosinVI (H). Scale bar is 5 μm . Middle panels: Overlay of sequential binarized frames, color coded for time from blue to white (-10:00 to 0:00) and white to red (0:00-30:00), first frames are on top. Right panels: corresponding kymographs along the length of spines, showing altered dynamics and localization of Rab11 vesicles upon addition of rapalog (marked with dotted lines). Time scale is min:sec. **I-L.** Quantification of Rab11-positive recycling endosomes entry (I,K) and exit (J,L) speeds in spines before and after induced recruitment of MBD (I,J) or MyosinVI (K,L). Graphs show mean \pm SEM. Statistical significance was determined using Kruskal-Wallis test and Dunn's multiple comparison post hoc test, * $p < 0.05$, *** $p < 0.001$ (A-C), unpaired t-test with Mann Whitney correction, * $p < 0.05$, ** $p < 0.01$, *** $p < 0.001$ (D-L). Scale bar is 2 μm (H). See also Figure S3 and Table S1.

increase of non-typical spine cargoes, such as peroxisomes (Kapitein *et al.*, 2010) into dendritic spines after KIF1C recruitment (Fig.S4I-K). In contrast, recruitment of non-processive mutant KIF1C-T306M (Fig.S4F-K) did not affect spine targeting. These results demonstrate that the recruitment of an active microtubule-based motor can result in spine entries.

We next focused on MyosinV- and VI-induced Rab11 trafficking. Addition of rapalog to neurons co-expressing MBD-FRB and FKBP-GFP-Rab11 induced a rapid burst of recycling endosomes from the shaft into many dendritic spines but are also able to move back out (Fig.3E-G; Video S3). Quantification showed that MyosinV-induced Rab11 trafficking does not increase the average entry speed (Fig.3I), but changes the number of targeted spines (Fig.3E,F). Interestingly, the mean exit speed is decreased by MBD recruitment, suggesting that MyosinV can oppose active spine exit events (Fig.3J). In contrast, addition of rapalog to neurons expressing MyosinVI-FRB caused Rab11-positive recycling endosomes to move away from the spines into the dendrites (Fig.3E,H; Video S4). Quantification showed that MyosinVI-induced Rab11 trafficking does not influence the average entry and exit speeds (Fig.3K-L). These data indicate that MyosinV- and MyosinVI-induced Rab11 trafficking primarily influence the number of targeted spines.

We next tested whether induced targeting or removal of recycling endosomes affects spine morphology. Under both conditions, we observed no differences in the total number of protrusions, spines or filopodia 30 minutes after rapalog addition (Fig.4A). Cumulative frequency plots revealed that also the width and length of spines on dendrites was not changed significantly (Fig.4B). We next determined whether these manipulations influence spine growth following chemical LTP (cLTP). Consistent with previous studies (Park *et al.*, 2004; Wang *et al.*, 2008), cLTP stimulation using glycine treatment increased spine size in control neurons (Fig.4C). In the rapalog experiments where MBD or MyosinVI is recruited to Rab11 vesicles, the increase in spine size after cLTP was still apparent (Fig.4C). These data suggest that under normal and cLTP conditions induced targeting or removal of recycling endosomes does not immediately affect the morphology of dendritic protrusions.

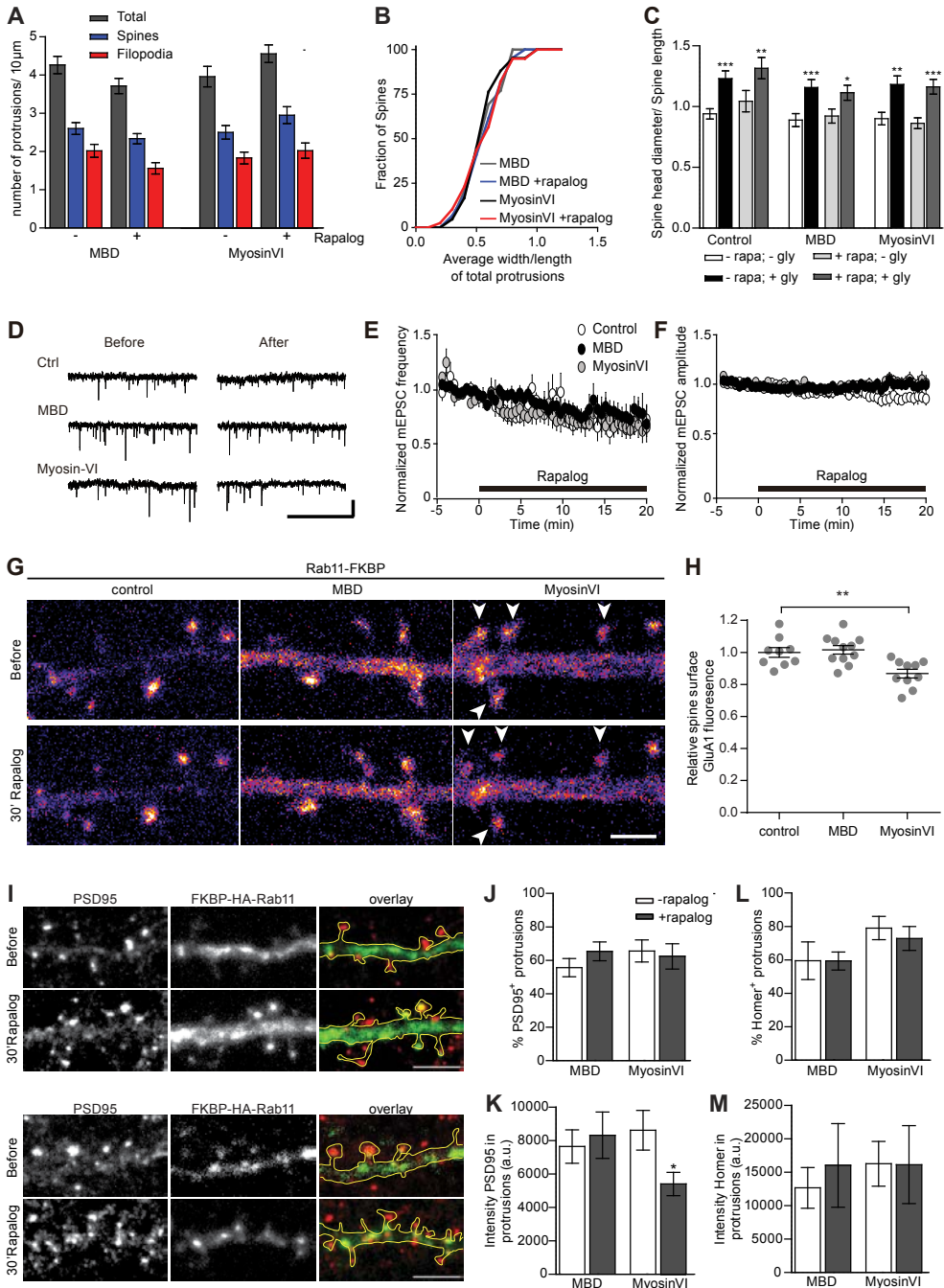


Figure 4. Removal of recycling endosomes decreases synaptic GluA1 levels and PSD-95 cluster size

A. Quantification of protrusions before and after induced dimerization of recycling endosomes to MyosinV(MBD)/VI motors. **B.** Cumulative frequency of average width/length of total protrusion before and after induced dimerization of Rab11 endosomes to MBD or MyosinVI. **C.** Rapallog (rapa)-induced recruitment of MBD or MyosinVI to recycling

endosomes following a glycine (gly)-based chemical LTP protocol. **D-F.** Sample traces of mEPSCs recorded before and 20 minutes after application of rapalog (scale bar: 20 pA/2 s). Summary graph of the averaged time course of frequency (**E**) and amplitude (**F**) of mEPSCs. Averaged mEPSP amplitudes and frequencies were measured every 30 sec, and the values were normalized to the values measured during the baseline period (-5 to 0 min). Rapalog (100 nM) was applied at 0 min. **G.** Typical examples of SEP-GluA1 levels in dendrites expressing Rab11-FKBP and mCherry (control), mRFP-MBD-FRB or MyosinVI-mRFP-FRB before and after 30 minutes of rapalog addition. Images are pseudocoloured for intensity (purple: low to yellow/white: high). **H.** Quantification of relative average SEP-GluA1 fluorescence intensity after 30 minutes rapalog treatment in dendritic spines of neurons expressing mCherry (control), mRFP-MBD-FRB or MyosinVI-mRFP-FRB. **I.** Immunostaining of dendritic protrusions with PSD-95 (red) before and after induced dimerization of Rab11 recycling endosomes (green) to MBD or MyosinVI. **J-K.** Quantification of number of PSD-95-positive protrusions (**J**) and PSD-95 intensity (**K**) per 10 μ m regions of dendrite before/after induced dimerization of Rab11 endosomes to MBD or MyosinVI. **L-M.** Quantification of number of Homer-positive protrusions (**L**) and Homer intensity (**M**) per 10 μ m dendritic region before/after induced dimerization of Rab11 to MBD or Myosin VI. Graphs show mean \pm SEM. Statistical significance was determined using an unpaired t-test with Mann Whitney correction, * $p < 0.05$, ** $p < 0.01$, *** $p < 0.001$ (C,J-M), one-way-ANOVA and Bonferroni's multiple comparison post hoc test, ** $p < 0.01$ (H). Scale bar is 2 μ m (G), 5 μ m (I). See also Table S1.

Removal of Rab11 from spines decreases surface GluA1 and PSD-95 clusters

Given that intracellular AMPARs are transported in recycling endosomes, we explored the functional effects on synapses of induced Rab11-positive recycling endosomes trafficking by measuring AMPAR-mediated miniature excitatory postsynaptic currents (mEPSCs). The influence of MyosinV-induced targeting and MyosinVI-induced removal of recycling endosomes was tested in DIV14-16 neurons transfected for 3 days. During the 20 minutes recordings after rapalog addition, we observed no changes in the frequency or amplitude of mEPSCs between all tested conditions (Fig.4D-F). We next analyzed surface AMPAR levels in individual spines of DIV20-22 neurons by measuring SEP-GluA1 intensity before and after rapalog treatment. MyosinVI-induced removal of Rab11-positive recycling endosomes from spines was associated with a marked decrease in SEP-GluA1 (Fig.4G-H). To determine if the short-term effects of altered Rab11-positive recycling endosomes trafficking affect the structural organization of the synapse, we visualized the postsynaptic marker PSD-95 and Homer-1 clusters (Fig.4I-M). There is a marked decrease in the intensity of PSD-95 clusters upon removal of recycling endosomes (Fig.4J-K), while no effect on Homer-1 was observed (Fig.4L-M). We conclude that removal of recycling endosomes from spines on the short-term decreases surface AMPARs and PSD-95 clusters without affecting spine morphology and overall PSD architecture.

DISCUSSION

Here we demonstrate that AMPARs are transported in Rab11-positive recycling endosomes along MT tracks within the dendritic shaft and use both the MT and actin cytoskeleton to enter dendritic spines. Inhibiting actin or microtubule dynamics both decrease endosome trafficking in spines. We also demonstrate that Rab11 can enter dendritic spines in a myosin (MyosinV) and kinesin (KIF1C) dependent manner. However, under basal conditions the frequency of MT-spine invasions is relatively low, making actin-based transport a more generic way of driving cargo trafficking in spines. By using chemically induced dimerization to recruit

2

MyosinV motors to Rab11-positive cargoes, we are able to control the position and trafficking of Rab11-positive recycling endosomes in spines. We demonstrate that targeting Rab11-positive recycling endosomes to spines does not significantly affect surface AMPAR levels, indicating that the supply of Rab11-positive recycling endosomes to spines is not the rate-limiting step in determining surface levels of AMPARs. On the other hand, we found that removal of Rab11-positive recycling endosomes from spines by MyosinVI was associated with a marked decrease in surface AMPAR levels and PSD-95 cluster size. We believe that this phenotype is the result of removal of the endosome from spines, however we cannot exclude that reduced AMPAR levels is an effect of globally disrupting endosome trafficking throughout the neuron. We envision two scenarios for this effect that are not mutually exclusive. First, Rab11-positive recycling endosomes could directly control the surface expression of AMPARs by reducing the AMPAR reserve pool and decreasing endocytic recycling within spines. Second, it is possible that Rab11-positive recycling endosomes controls synaptic AMPAR levels by directly or indirectly maintaining PSD-95 levels at synapses. This model fits with current observations that AMPAR density depends on structural alterations within the postsynaptic density (Bosch *et al.*, 2014; Meyer *et al.*, 2014). Our results also showed that induced addition and removal of Rab11 recycling endosomes from spines for short time periods does not have an impact on spine growth following chemical LTP stimulation. This is an interesting finding because it shows that local translocation of Rab11 vesicles for a short time interval (~30 minutes rapalog treatment), is not sufficient to cause the plasticity changes that were previously observed after longer-term blockage of endosomal recycling (Park *et al.*, 2004; Wang *et al.*, 2008). Future work will be needed to resolve the precise chronology of the various trafficking events during LTP and to determine which specific organelles and spine substructures are remodel over different time periods. Based on the involvement of endosomes in mediating signal transduction responses in other systems (Miaczynska *et al.*, 2004), our findings imply that the specific positioning of recycling endosomes is an important factor in controlling different aspect of synapse architecture.

AUTHORS CONTRIBUTIONS

M.E.d.S., M.A., P.S., J.L. and L.C.K. performed experiments. M.E.d.S., M.A. and L.C.K. analysed the data. T.W., S.C. and K.F. performed the electrophysiology experiments and analyzed the data. M.E.d.S., L.C.K. and C.C.H. designed the research and wrote the paper. C.J.W., L.C.K. and C.C.H. supervised the project.

ACKNOWLEDGEMENTS

We are grateful to Dr. Terunaga Nakagawa for pTRE-GFP-GluA1-FLAG, Dr. Daniel Choquet for SEP-GluA1, Dr. Folma Buss for Myosin VI tail construct. This work was supported by the Erasmus Medical Center (EMC fellowship, LCK), the Netherlands Organization for Scientific Research (NWO-ALW-VENI, LCK; NWO-ALW-VICI, CCH), the Netherlands Organization for Health Research and Development (ZonMW-TOP, CCH; ZonMW-VIDI,

CW), and EMBO Young Investigators Program (YIP, CCH). This work is part of the research programme of the Foundation for Fundamental Research on Matter (FOM), which is part of NWO. MEdS is supported by Fundação para a Ciência e Tecnologia (FCT-Portugal). PS is supported by the Swiss National Science Foundation (SNSF). JL is supported by International PhD Project Programme of Foundation for Polish Science (studies of nucleic acids and proteins-from basic to applied research) cofinanced by the European Union-Regional Development Fund and cosupervised by prof. Jacek Jaworski. KF was supported by the Whitehall Foundation (2012-08-44) and Japan Foundation for Pediatric Research (JFPR).

EXPERIMENTAL METHODS

Expression constructs

Fluorescently or HA-tagged MyosinVI(1-1041)-FRB, MBD(147-240)-FRB and PEX-FKBP heterodimerisation constructs have been described (Kapitein *et al.*, 2010). All other constructs were created using PCR based strategies. Fluorescently or HA-tagged FKBP-Rab11, KIF1C(1-496)-FRB, KIF1C(1-496)-T306M-FRB (rigor mutant) were generated in GW1 and/or p β actin expression vectors. For details see supplemental experimental methods.

Hippocampal neuron cultures, transfections and electrophysiology

Primary hippocampal cultures were prepared from embryonic day 18 (E18) rat brains (Jaworski *et al.*, 2009). For electrophysiology experiments, hippocampal primary cultures were prepared from postnatal 1-3 days old C57BL6 mice of either sex as described previously (Hooogenraad *et al.*, 2010). For details see supplemental experimental methods.

Live cell imaging microscopy

Live cell imaging was performed using two-color Total Internal Reflection Fluorescence (TIRF) or laser confocal spinning disk microscopy. All imaging was performed in full conditioned Neurobasal medium at 37°C and 5% CO₂ unless otherwise indicated. For details see supplemental experimental methods.

Live cell imaging of Rab11 and GFP-GluA2 dynamics

To probe intracellular AMPA receptor vesicle transport in neurons, we coexpressed pTRE-GFP-GluA2 with HA-GluA1 and precisely control the timing and level of GluA2 expression using a doxycycline (DOX) regulated gene expression system. To image Rab11-positive recycling endosomes dynamics in dendritic spines, time-lapses of 5 minutes were acquired, with 5 seconds interval between acquisitions. For details see supplemental experimental methods.

Live cell imaging and analysis of Rab11 and SEP-GluA1 dynamics

To visualize exocytic events of Rab11-positive recycling endosomes containing AMPA receptors, we performed simultaneous dual-color imaging of tagRFP-Rab11 and SEP-GluA1 at 2 frames per second for up to 3 minutes. Events showing sudden local increase of SEP fluorescence were manually counted in ImageJ and classified as spine or dendritic events. To quantify membrane bound amount of GluA1 in rapalog experiments, background-subtracted maximum projections of SEP-GluA1 fluorescence intensity before and after 30 min of rapalog treatment in -15 randomly selected spines per imaged dendrite was measured in ImageJ and expressed as a ratio. These ratios were then averaged per dendrite. For details see supplemental experimental methods.

Statistical Methods

Unless otherwise noted, the graphs represent mean \pm SEM. Statistical significance was determined using the Kruskal-Wallis test or one-way ANOVA and Dunn's multiple comparison post hoc test, Wilcoxon test for paired data, an unpaired t-test with Mann-Whitney correction. * $p < 0.05$, ** $p < 0.01$, *** $p < 0.001$. The statistical test(s) used

for each experiments is indicated in each figure legend. The exact value of n (number of neurons analyzed) and N (number of independent experiments) and the mean \pm SEM for each graph presented in the paper is summarized in Supplementary Table S1.

REFERENCES

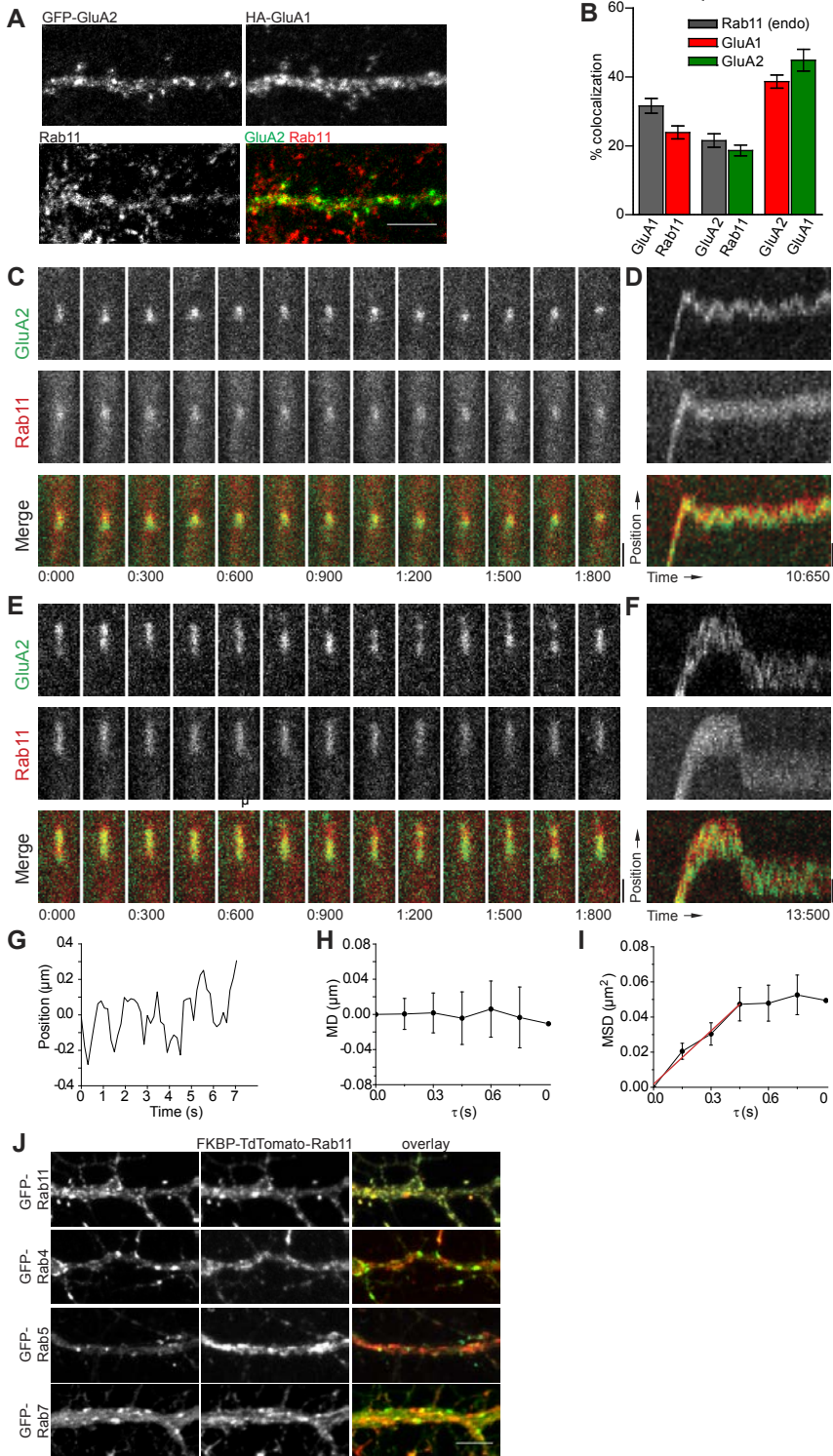
- Adrian, M., Kusters, R., Wierenga, C.J., Storm, C., Hoogenraad, C.C., and Kapitein, L.C. (2014). Barriers in the brain: resolving dendritic spine morphology and compartmentalization. *Frontiers in neuroanatomy* 8, 142.
- Bosch, M., Castro, J., Saneyoshi, T., Matsuno, H., Sur, M., and Hayashi, Y. (2014). Structural and Molecular Remodeling of Dendritic Spine Substructures during Long-Term Potentiation. *Neuron* 82, 444-459.
- Brown, T.C., Correia, S.S., Petrok, C.N., and Esteban, J.A. (2007). Functional compartmentalization of endosomal trafficking for the synaptic delivery of AMPA receptors during long-term potentiation. *The Journal of neuroscience : the official journal of the Society for Neuroscience* 27, 13311-13315.
- Colgan, L.A., and Yasuda, R. (2014). Plasticity of dendritic spines: subcompartmentalization of signaling. *Annual review of physiology* 76, 365-385.
- Correia, S.S., Bassani, S., Brown, T.C., Lise, M.F., Backos, D.S., El-Husseini, A., Passafaro, M., and Esteban, J.A. (2008). Motor protein-dependent transport of AMPA receptors into spines during long-term potentiation. *Nature neuroscience* 11, 457-466.
- Czondor, K., Mondin, M., Garcia, M., Heine, M., Frischknecht, R., Choquet, D., Sibarita, J.B., and Thoumine, O.R. (2012). Unified quantitative model of AMPA receptor trafficking at synapses. *Proceedings of the National Academy of Sciences of the United States of America* 109, 3522-3527.
- Gu, J., Firestein, B.L., and Zheng, J.Q. (2008). Microtubules in dendritic spine development. *The Journal of neuroscience : the official journal of the Society for Neuroscience* 28, 12120-12124.
- Hoogenraad, C.C., Popa, I., Futai, K., Martinez-Sanchez, E., Wulf, P.S., van Vlijmen, T., Dortland, B.R., Oorschot, V., Govers, R., Monti, M., et al. (2010). Neuron specific Rab4 effector GRASP-1 coordinates membrane specialization and maturation of recycling endosomes. *PLoS biology* 8, e1000283.
- Hu, X., Viesselmann, C., Nam, S., Merriam, E., and Dent, E.W. (2008). Activity-dependent dynamic microtubule invasion of dendritic spines. *The Journal of neuroscience : the official journal of the Society for Neuroscience* 28, 13094-13105.
- Huganir, R.L., and Nicoll, R.A. (2013). AMPARs and synaptic plasticity: the last 25 years. *Neuron* 80, 704-717.
- Jaworski, J., Kapitein, L.C., Gouveia, S.M., Dortland, B.R., Wulf, P.S., Grigoriev, I., Camera, P., Spangler, S.A., Di Stefano, P., Demmers, J., et al. (2009). Dynamic microtubules regulate dendritic spine morphology and synaptic plasticity. *Neuron* 61, 85-100.
- Kapitein, L.C., Schlager, M.A., van der Zwan, W.A., Wulf, P.S., Keijzer, N., and Hoogenraad, C.C. (2010). Probing intracellular motor protein activity using an inducible cargo trafficking assay. *Biophysical journal* 99, 2143-2152.
- Kapitein, L.C., van Bergeijk, P., Lipka, J., Keijzer, N., Wulf, P.S., Katrukha, E.A., Akhmanova, A., and Hoogenraad, C.C. (2013). Myosin-V opposes microtubule-based cargo transport and drives directional motility on cortical actin. *Curr Biol* 23, 828-834.
- Meyer, D., Bonhoeffer, T., and Scheuss, V. (2014). Balance and stability of synaptic structures during synaptic plasticity. *Neuron* 82, 430-443.
- Miaczynska, M., Pelkmans, L., and Zerial, M. (2004). Not just a sink: endosomes in control of signal transduction. *Curr Opin Cell Biol* 16, 400-406.
- Nash, J.E., Appleby, V.J., Correa, S.A., Wu, H., Fitzjohn, S.M., Garner, C.C., Collingridge, G.L., and Molnar, E. (2010). Disruption of the interaction between myosin VI and SAP97 is associated with a reduction in the number of AMPARs at hippocampal synapses. *Journal of neurochemistry* 112, 677-690.
- Newpher, T.M., and Ehlers, M.D. (2008). Glutamate receptor dynamics in dendritic microdomains. *Neuron* 58, 472-497.
- Osterweil, E., Wells, D.G., and Mooseker, M.S. (2005). A role for myosin VI in postsynaptic structure and glutamate receptor endocytosis. *The Journal of cell biology* 168, 329-338.
- Park, M., Penick, E.C., Edwards, J.G., Kauer, J.A., and Ehlers, M.D. (2004). Recycling endosomes supply AMPA receptors for LTP. *Science* 305, 1972-1975.

- Park, M., Salgado, J.M., Ostroff, L., Helton, T.D., Robinson, C.G., Harris, K.M., and Ehlers, M.D. (2006). Plasticity-induced growth of dendritic spines by exocytic trafficking from recycling endosomes. *Neuron* 52, 817-830.
- Petrini, E.M., Lu, J., Cognet, L., Lounis, B., Ehlers, M.D., and Choquet, D. (2009). Endocytic trafficking and recycling maintain a pool of mobile surface AMPA receptors required for synaptic potentiation. *Neuron* 63, 92-105.
- Wagner, W., Brenowitz, S.D., and Hammer, J.A., 3rd (2011). Myosin-Va transports the endoplasmic reticulum into the dendritic spines of Purkinje neurons. *Nature cell biology* 13, 40-48.
- Wang, Z., Edwards, J.G., Riley, N., Provance, D.W., Jr., Karcher, R., Li, X.D., Davison, I.G., Ikebe, M., Mercer, J.A., Kauer, J.A., et al. (2008). Myosin Vb mobilizes recycling endosomes and AMPA receptors for postsynaptic plasticity. *Cell* 135, 535-548.
- Yau, K.W., van Beuningen, S.F., Cunha-Ferreira, I., Cloin, B.M., van Battum, E.Y., Will, L., Schatzle, P., Tas, R.P., van Krugten, J., Katrukha, E.A., et al. (2014). Microtubule Minus-End Binding Protein CAMSAP2 Controls Axon Specification and Dendrite Development. *Neuron* 82, 1058-1073.

SUPPLEMENTARY FIGURES

► **Figure S1. related to Figure 1. AMPA-receptors undergo confined diffusion inside Rab11-positive recycling endosomes**

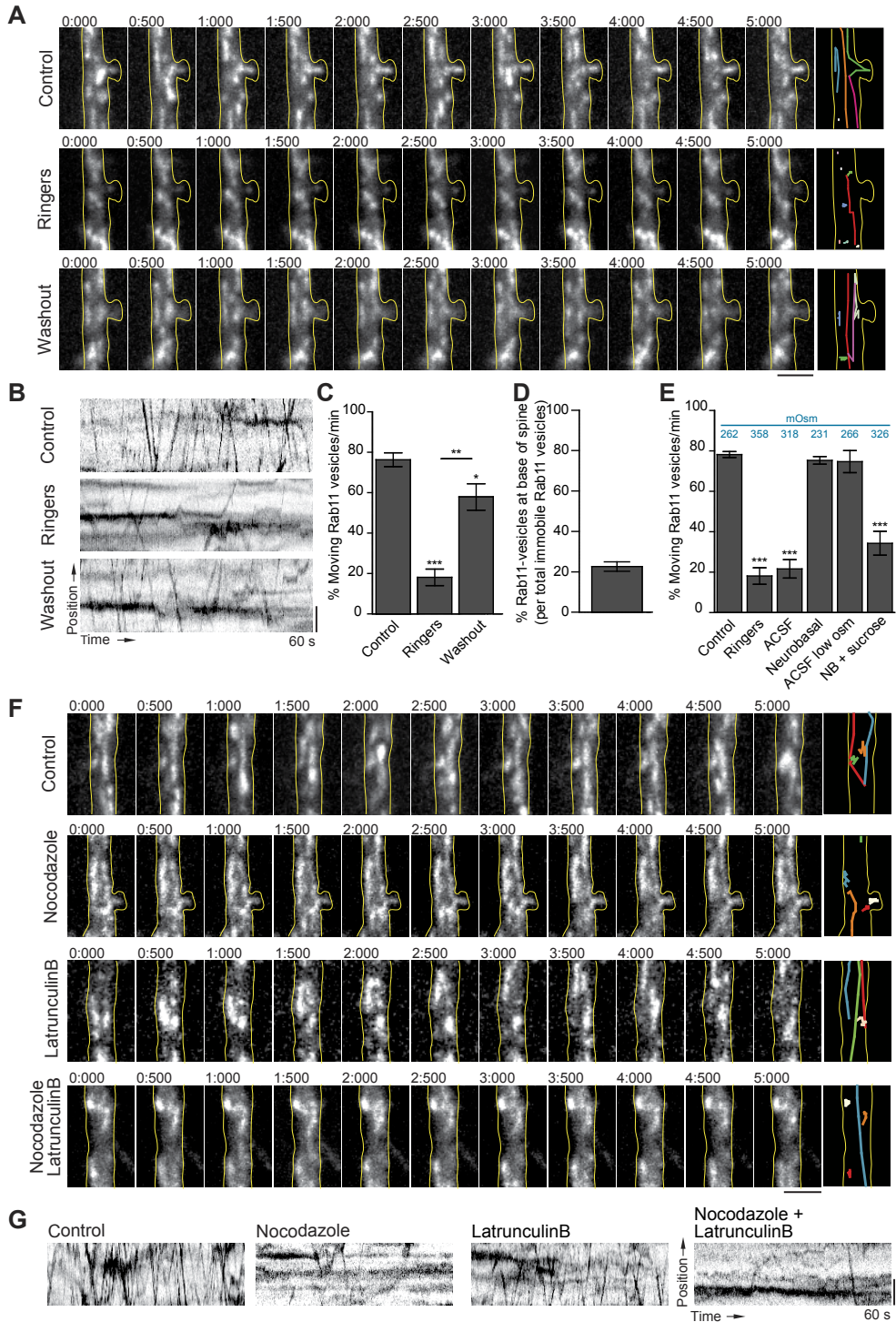
A. Immunostaining of endogenous Rab11 with coexpressed GluA1 and GluA2 shows partial colocalization. Scale bar is 5 μm . Zoomed area: scale bar is 2 μm . **B.** Quantification of colocalization between coexpressed GluA1, GluA2 and intracellular Rab11 (n=11; N=2). **C-E.** Stills from a dual-color time-lapse recording of a rat hippocampal neuron expressing GluA1, GFP-GluA2 (top) and mRFP-Rab11 (bottom). Time is indicated as seconds:milliseconds. Scale bar is 1 μm . **D-F.** Kymographs of the recording shown in **C** and **E**, respectively, showing motility of single (**D**) or multiple (**F**) GFP-GluA2 clusters inside the Rab11-positive recycling endosome. Scale bar is 1 μm . **G.** Example trajectory of a GFP-GluA2 cluster during a nonmotile episode of the Rab11-positive recycling endosome. **H.** Average mean displacement of 7 GFP-GluA2 clusters for different time intervals τ during nonmotile episodes of Rab11-positive recycling endosomes, revealing that clusters undergo no net displacements when the endosomes are immobile. **I.** Average mean squared displacement for different time intervals τ for 7 clusters during nonmotile endosome episodes, revealing that the clusters undergo confined diffusion limited by the endosome boundaries, with an initial diffusion constant of 0.05 $\mu\text{m}^2/\text{s}$. **J.** Dendritic colocalization of FKBP-tdTomato-Rab11 with other Rab11 construct and other overexpressed endosomal markers. There is a high degree of colocalization between the two Rab11 constructs, and only minor colocalization with the other endosomal markers. Scale bar is 5 μm .



2

► **Figure S2. related to Figure 1. Microtubule-targeting drug affect endosome motility in the dendritic shaft**

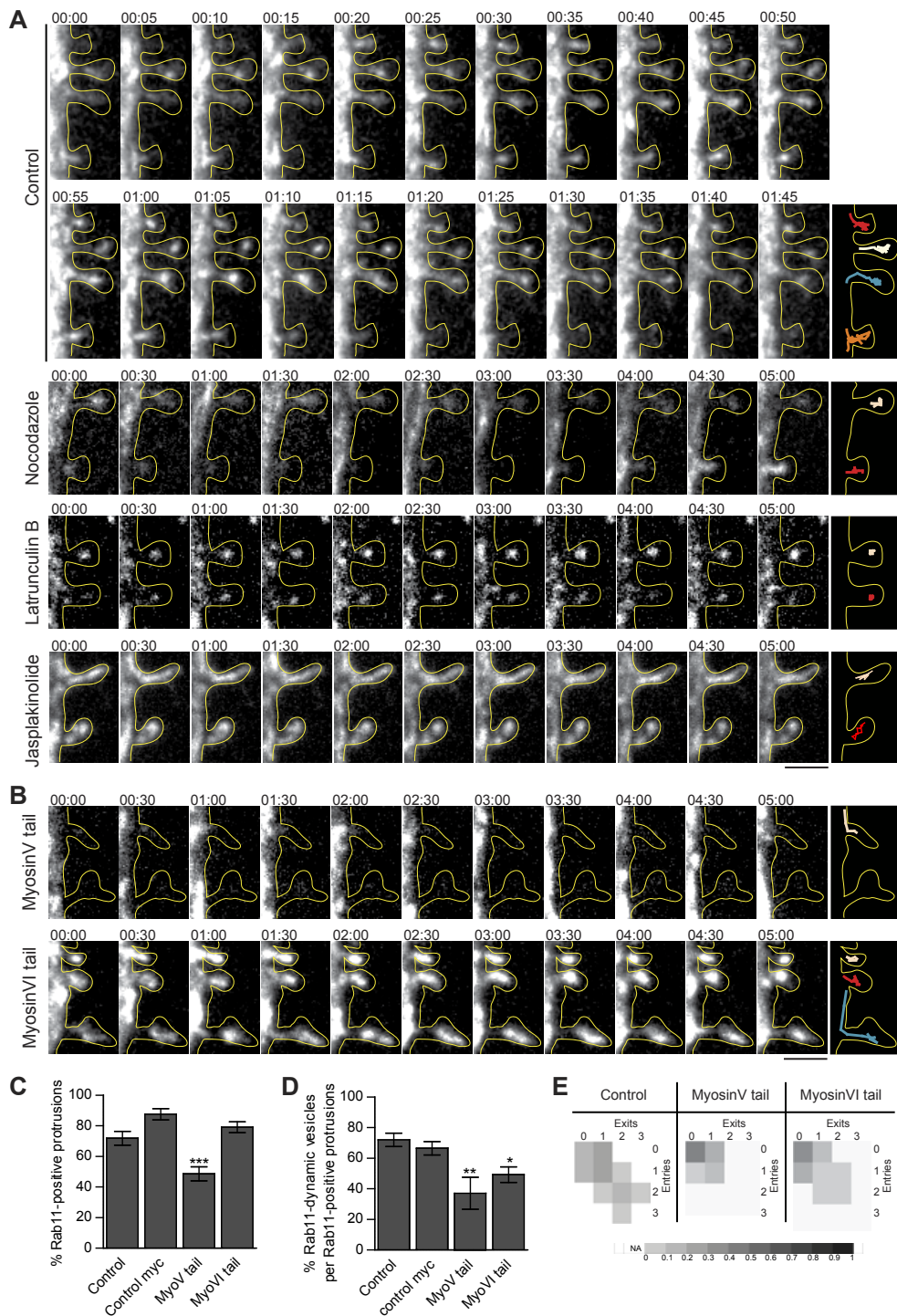
A. Stills from a 60 seconds time-lapse recording of rat hippocampal neurons at DIV14-17 expressing GFP-Rab11, when imaged in different solutions. Vesicle manual tracking shows motile and non-motile Rab11-positive recycling endosomes. Time is indicated as seconds:milliseconds. All cells were first imaged in conditioned medium (CM) which was replaced by Ringers buffer for 5 minutes and then washed out with CM for 15-20 minutes. Rab11-positive recycling endosomes are mobile in CM, but quickly become immobile in Ringers buffer. Motility is partially recovered after washout. Scale bar is 2 μm . **B.** Kymographs of the recordings in **A**, showing the motility of the recycling endosomes in the described conditions. Scale bar is 2 μm . **C.** Quantification of the percentage of motile Rab11-positive recycling endosomes in 1min timelapse acquisition under the indicated conditions (n=6, N=2). Replacing the CM before imaging with Ringer's or artificial cerebrospinal fluid (ACSF) solutions markedly reduced Rab11 vesicles motility in the dendrites, which was due to the difference in osmolarity of these solutions compared to CM. By returning the neurons to CM and washing out the Ringer's solution, most of the Rab11 vesicles motility is recovered. **D.** Quantification of the fraction of immobile Rab11-vesicles at the base of the spine (n=17, N=2). **E.** Quantification of the percentage of motile Rab11- positive vesicles in 1min timelapse acquisition under the indicated conditions (Control: n=10; Ringers: n=6; ACSF: n=6; Neurobasal: n=6; ACSF low osm: n=4; NB + Sucrose: n=4; N=2). Osmolality of each solution is indicated in blue. **F.** Stills from a 60 seconds time-lapse recording of rat hippocampal neurons expressing GFP-Rab11. Manual vesicle tracking shows motile and non-motile Rab11-positive recycling endosomes. Time is indicated as seconds:milliseconds. Neurons were imaged either in control conditions or after 3 minutes in 300nM nocodazole, 10 μM latrunculin B or a combination of both. Scale bar is 2 μm . **G.** Kymographs of the recordings in **F**, showing the motility of the vesicles in the different conditions. Scale bar is 2 μm . Graphs represent mean \pm SEM. Statistical significance was determined by using the Wilcoxon test for paired data, *p<0.05, **p<0.01, ***p<0.001 (C), Kruskal-Wallis test and Dunn's multiple comparison post hoc test, ***p<0.001 (E).



2

► **Figure S3. related to Figure 2. Blockade of MyosinV and MyosinVI differentially affects recycling endosome entry in spines**

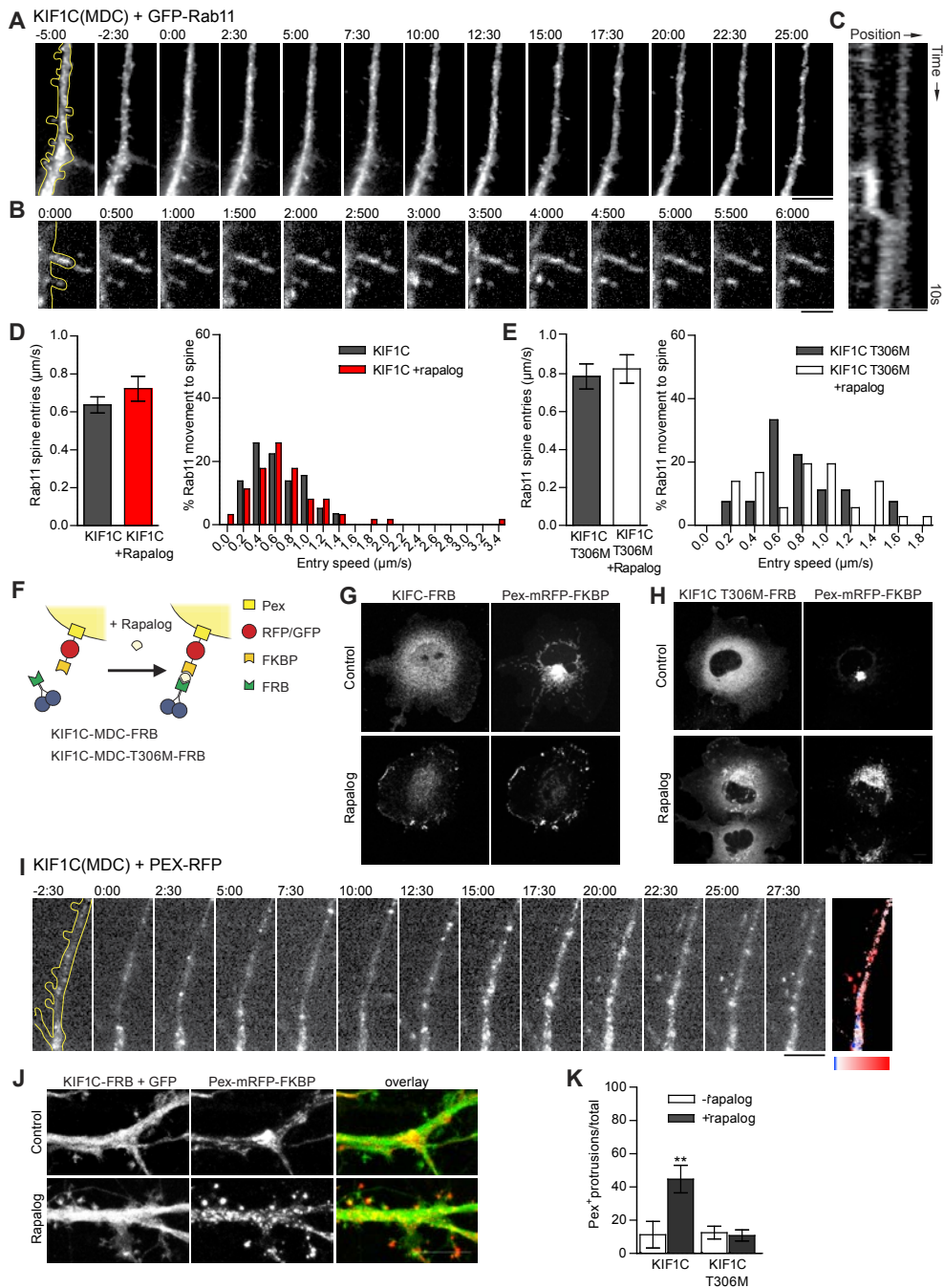
A. Stills from a 5 minutes time-lapse recording of rat hippocampal neurons expressing GFP-Rab11. Vesicle manual tracking shows motile and non-motile Rab11-positive recycling endosomes. Time is indicated as minutes:seconds. Neurons were imaged either in control conditions or after 5 minutes in 300nM nocodazole, 10 μ M latrunculin B or a combination of both, and 10 μ M jasplakinolide. Scale bar is 2 μ m. **B.** Stills from a 5 minutes time-lapse recording of rat hippocampal neurons expressing GFP-Rab11 and myc-MyosinV tail or myc-MyosinVI tail. Vesicle manual tracking shows motile and non-motile Rab11 endosomes. Time is indicated as minutes:seconds. Scale bar is 2 μ m. **C.** Rab11-positive recycling endosomes are less targeted to dendritic protrusion when MyosinV function is blocked but not MyosinVI. **D.** Rab11-positive recycling endosomes dynamics is affected when either MyosinV or MyosinVI function is inhibited (control: n=16; control myc: n=20; MyosinV tail: n=12; MyosinVI tail: n=21, N=2). **E.** Schematic heatmap showing the dynamic distribution of Rab11-positive recycling endosomes. Inhibition of MyosinV tail affects mostly entries in protrusions, whereas inhibition of MyosinVI tail halts Rab11 vesicles exits from protrusions. Graphs represent mean \pm SEM. Statistical significance was determined using Kruskal-Wallis test and Dunn's multiple comparison post hoc test, * p<0.05.



2

► **Figure S4. related to Figure 3. Chemically-induced recruitment of KIF1C to recycling endosomes promotes their targeting to dendritic spines**

A. Stills from a 45 minute time lapse recording. Dimerization of KIF1C to Rab11 endosomes increases their number along the dendritic shaft. Scale bar is 10 μm . **B.** Occasionally, induced dimerization also promotes the entry of new Rab11 endosomes in dendritic spines. Scale bar is 2 μm . **C.** Kymograph of the timelapse depicted in B, showing the translocation of the endosome to the dendritic spines. Scale bar is 1 μm . **D.** Quantification of Rab11-vesicles entry speeds in spines before and after induced recruitment of KIF1C. n=9; N=3. **E.** Quantification of Rab11-vesicles entry speeds in spines before and after induced recruitment of KIF1C T306M. n=9; N=3. **F.** Schematic diagram of the inducible recruitment of KIF1 motors to peroxisomes using rapalog-induced heterodimerization of FRB and FKBP. KIF1 motors are coupled to FRB. **G-H.** Recruitment of peroxisomes to KIF1 motors in COS7, shown translocation to the periphery of the cells upon dimerization with KIF1C (**G**) but not the mutant KIF1C T306M (**H**). Scale bar is 10 μm . **I.** Dimerization of KIF1C to peroxisomes causes their translocation from the dendritic shaft to spines. Scale bar is 10 μm . **J.** Representative fixed neuron showing recruitment of peroxisomes to spines upon KIF1C recruitment. Scale bar is 10 μm . **K.** Quantification of translocation of peroxisomes to spines upon recruitment to KIF1. Recruitment of KIF1C causes a significant increase in the number of peroxisomes in spines, but the mutant KIF1C T306M. (KIF1C: n=9; KIF1C T306M: n=12; N=2). Graphs show mean \pm SEM. Statistical significance was determined using an unpaired t-test with Mann Whitney correction, ** $p < 0.01$ (D-E,K).



SUPPLEMENTARY TABLE

► **Table S1. Overview of all data analyzed and quantified in this study**



Figure	Condition	n	N	Mean ± SEM
Fig.1D	GluA2	90 (Rab11 endosomes)	5 (neurons)	96.0 ± 1.5 %
	Rab11	79 (GluA2 clusters)	5 (neurons)	77.6 ± 1.2 %
Fig.1E-F	TIR-mCherry	6 (dendrites)	3	0.59 ± 0.08 GluA2/μm ² /min; 1.43 ± 0.12 μm/s
	GFP-GluA2 + Control	14 (dendrites)	3	0.37 ± 0.09 GluA2/μm ² /min; 1.05 ± 0.09 μm/s
	GFP-GluA2 + Rab11	30 (dendrites)	3	0.50 ± 0.07 GluA2/μm ² /min; 1.61 ± 0.07 μm/s
	GFP-GluA2 + MyoV tail	12 (dendrites)	3	0.24 ± 0.03 GluA2/μm ² /min; 1.33 ± 0.14 μm/s
	GFP-GluA2 + MyoVI tail	8 (dendrites)	3	0.18 ± 0.02 GluA2/μm ² /min; 1.14 ± 0.10 μm/s
Fig.1G	Control	30	6	83.2 ± 0.76 %
	Nocodazole	12	2	43.8 ± 3.21 %
	Latrunculin	11	2	82.56 ± 1.49 %
	Noc + LatB	8	2	38.53 ± 4.58 %
Fig.1J-K	Control	23 (dendrites)	3	0.13 ± 0.01 events/min/μm; 24.1 ± 1.3 %
	Rab11	24 (dendrites)	3	0.20 ± 0.02 events/min/μm; 29.8 ± 1.8 %
	MyoV tail	25 (dendrites)	3	0.13 ± 0.01 events/min/μm; 26.9 ± 2.1 %
	MyoVI tail	23 (dendrites)	3	0.14 ± 0.02 events/min/μm; 34.3 ± 2.4 %
Fig.2G-H	Control	23	4	66.9 ± 5.7 %; 82.2 ± 4.6 %
	Nocodazole	24	4	83.6 ± 2.3 %; 59.2 ± 5.4 %
	Latrunculin	18	3	90.0 ± 3.2 %; 22.8 ± 6.4 %
	Noc + LatB	17	2	83.7 ± 2.9 %; 8.9 ± 2.6 %
	Jasplakinolide	10	2	92.4 ± 4.2 %; 3.0 ± 1.9 %
Fig.2J-L	Control	16	2	23.9 ± 5.9 s; 0.66 ± 0.024 μm/s; 0.55 ± 0.04 μm/s
	Nocodazole	11	2	28.4 ± 4.9 s; 0.55 ± 0.03 μm/s; 0.30 ± 0.02 μm/s
Fig.3A-C	pSuper empty	29	3	4.70 ± 0.32; 3.17 ± 0.25; 1.61 ± 0.18
	pSuper scrambled	12	3	4.32 ± 0.26; 3.35 ± 0.27; 1.02 ± 0.20
	GFP-Rab11	12	3	5.50 ± 0.39; 4.17 ± 0.34; 1.41 ± 0.30
	Rab11 S25N	32	3	2.94 ± 0.24; 1.72 ± 0.26; 1.28 ± 0.17
	Rab11 shRNA	18	3	3.03 ± 0.37; 1.58 ± 0.33; 1.50 ± 0.26
Fig.3B-C	pSuper empty	19	3	64.8 ± 6.8 %; 0.30 ± 0.02 μm ²
	pSuper scrambled	12	3	79.7 ± 8.6 %; 0.35 ± 0.05 μm ²
	GFP-Rab11	12	3	82.9 ± 8.6 %; 0.40 ± 0.05 μm ²
	Rab11 S25N	19;15	3	42.28 ± 8.3 %; 0.28 ± 0.04 μm ²
	Rab11 shRNA	12;6	3	17.13 ± 5.4 %; 0.28 ± 0.05 μm ²
Fig.3D	Control	20 (COS7 cells)	2	1.085 ± 0.20; 1.23 ± 0.30 fusion/min/10μm ²
	FKBP-Rab11	16 (COS7 cells)	2	1.02 ± 0.18; 1.09 ± 0.15 fusion/min/10μm ²
	FKBP-Rab11 + MBD-FRB	16 (COS7 cells)	2	1.026 ± 0.16; 0.90 ± 0.13 fusion/min/10μm ²
	FKBP-Rab11 + MyoVI-FRB	15 (COS7 cells)	2	0.78 ± 0.12; 0.89 ± 0.14 fusion/min/10μm ²
	FKBP-Rab11 + Kif1C-FRB	16 (COS7 cells)	2	0.98 ± 0.15; 0.91 ± 0.18 fusion/min/10μm ²
Fig.3E	MBD	20	2	49.8 ± 4.7 %; 0.29 ± 0.04 μm ²
	MBD + rapalog	28	2	69.1 ± 4.4 %; 0.37 ± 0.03 μm ²
	MyosinVI	21	2	38.4 ± 3.8 %; 0.26 ± 0.02 μm ²
	MyosinVI + rapalog	15	2	17.5 ± 4.3 %; 0.24 ± 0.05 μm ²
	Kif1C	10	2	33.9 ± 6.4 %; 0.25 ± 0.04 μm ²
	Kif1C + rapalog	10	2	50.8 ± 5.1 %; 0.34 ± 0.07 μm ²
Fig.3I-J	MBD	8	3	0.60 ± 0.06 μm/s; 0.74 ± 0.09 μm/s
	MBD + rapalog	8	3	0.60 ± 0.06 μm/s; 0.37 ± 0.7 μm/s
Fig.3K-L	MyosinVI	8	3	0.50 ± 0.04 μm/s; 0.50 ± 0.07 μm/s
	MyosinVI + rapalog	8	3	0.49 ± 0.06 μm/s; 0.32 ± 0.06 μm/s
Fig.4A-B	MBD	38	2	4.26 ± 0.23; 2.60 ± 0.15; 2.02 ± 0.17
	MBD + rapalog	44	2	3.71 ± 0.20; 2.33 ± 0.13; 1.56 ± 0.15
	MyosinVI	44	2	3.96 ± 0.27; 2.50 ± 0.18; 1.83 ± 0.15
	MyosinVI + rapalog	38	2	4.56 ± 0.23; 2.95 ± 0.22; 2.02 ± 0.20
Fig.4C	Control	16; 14; 14; 16	2	0.94 ± 0.04; 1.23 ± 0.06; 1.045 ± 0.09; 1.316 ± 0.09
	MBD	14; 13; 13; 13	2	0.89 ± 0.05; 1.16 ± 0.07; 0.92 ± 0.06; 1.11 ± 0.06
	MyosinVI	15; 13; 15; 16	2	0.90 ± 0.05; 1.18 ± 0.07; 0.86 ± 0.04; 1.16 ± 0.06
Fig.4D-E-F	Control	10	2	
	MBD	8	2	
Fig.4H	MyosinVI	7	2	
	Control	9	3	1.00 ± 0.03
	MBD	11	3	1.01 ± 0.03
Fig.4J-K	MyosinVI	10	3	0.87 ± 0.03
	MBD	16	2	55.6 ± 5.4 %; 7639 ± 1001 a.u.
	MBD + rapalog	20	2	65.3 ± 5.6 %; 8317 ± 1389 a.u.
	MyosinVI	18	2	65.6 ± 6.6 %; 8613 ± 1183 a.u.
Fig.4L-M	MyosinVI + rapalog	15	2	62.4 ± 7.6 %; 5403 ± 697 a.u.
	MBD	8	2	59.5 ± 11.3 %; 12661 ± 3042 a.u.
	MBD + rapalog	8	2	59.3 ± 5.4 %; 16016 ± 6240 a.u.
	MyosinVI	8	2	79.0 ± 7.0 %; 16264 ± 3342 a.u.
	MyosinVI + rapalog	8	2	72.8 ± 7.2 %; 16131 ± 5839 a.u.

n = neurons analysed (except when mentioned otherwise)

N = number of independent experiments (except when mentioned otherwise)

SUPPLEMENTARY VIDEOS

Supplementary Video S1

This video corresponds to Fig.1L. Exocytosis of SEP-tagged GluA1 from a tagRFPt-labelled Rab11-positive recycling endosome in a dendritic spine. White line indicates spine outline. Total time: 80 seconds. Acquisition was performed at 1 second per frame. 20x sped up. (AVI, 1.5MB).

Supplementary Video S2

This video corresponds to Fig.2A. GFP-tagged AMPA receptor subunit GluA2 is transported in mRFP- tagged Rab11-positive recycling endosomes. Total time: 60 seconds. Acquisition was performed at 200 milliseconds per frame. 20x sped up. (AVI, 10.5MB).

Supplementary Video S3

This video corresponds to Fig.3G. MBD recruitment to GFP-tagged Rab11-positive recycling endosomes upon rapalog application causes relocation of recycling endosomes from dendritic shafts to spines. Total time: 40 minutes. Acquisition was performed at 30 seconds per frame. 20x sped up. (AVI, 0.5 MB).

Supplementary Video S4

This video corresponds to Fig.3H. MyosinVI recruitment to GFP-tagged Rab11-positive recycling endosomes upon rapalog application causes translocation of recycling endosomes from spines to the dendritic shafts. Total time: 40 minutes. Acquisition was performed at 30 seconds per frame. 20x sped up. (AVI, 0.4 MB).

Videos available online

<http://dx.doi.org/10.1016/j.celrep.2015.09.062>



MATERIAL AND METHODS

Ethics Statement

All animal experiments were performed in compliance with the guidelines for the welfare of experimental animals issued by the Government of The Netherlands. All animal experiments were approved by the Animal Ethical Review Committee (DEC) of the Erasmus Medical Center and Utrecht University and the Institutional Animal Care and Use Committee (IACUC) at University of Massachusetts Medical School.

Expression constructs

The following mammalian expression plasmids have been described previously: pGW1-mRFP, pGW1-GFP, p β actin-HA- β -Galactosidase (Jaworski *et al.*, 2009), pSuper vector (Brummelkamp *et al.*, 2002), SEP-GluA1 (Petrini *et al.*, 2009), HA-GluA1 and HA-GluA2 (Hoogenraad *et al.*, 2005), pTRE-GFP-GluA1, pTRE-GFP-GluA2-FLAG and pTet-on-Ad (Shanks *et al.*, 2010), mCherry-MT+TIP (Yau *et al.*, 2014), mRFP-Rab11a, GFP-Rab11a, HA-Rab11a, GFP-Rab11-S25N (Hoogenraad *et al.*, 2010), mRFP-Rab6 (Schlager *et al.*, 2010), rat Rab11a shRNA (Bravo-Cordero *et al.*, 2007), MyosinVa and MyosinVb tails (Nedvetsky *et al.*, 2007), MyosinVI tail (Buss *et al.*, 2001), MyosinVI-(aa1-1041)-FRB, GFP-, mRFP- and HA-MBD-(aa147-240)-FRB, Pex-mRFP-FKBP (Kapitein *et al.*, 2010b), TFR-SEP (Park *et al.* 2004), MARCKS-eGFP (Schatzle *et al.*, 2011). All other constructs were created using PCR based strategies. KIF1C-(aa1-496)-HA-FRB, KIF1C(aa1-496)-T306M-GFP-FRB (rigor mutant, adapted from

a KIF1A mutation (Lee *et al.*, 2003)), and FKBP-TdTomato-Rab11 were generated in pβactin expression vector. TagRFP-Rab11a, FKBP-GFP-Rab11a and FKBP-HA-Rab11a fusions were generated in GW1 expression vectors. The dominant-negative MyosinVa (aa1242-1830) and MyosinVb (aa1233-1848) constructs (MyoV-tail) and MyosinVI construct (aa846-1277, MyoVI-tail) were cloned into GW1 expression vectors.

Hippocampal neuron cultures, transfections and drug treatments

Primary hippocampal cultures were prepared from embryonic day 18 (E18) rat brains (Goslin and Banker, 1989; Kapitein *et al.*, 2010a). Cells were plated on coverslips coated with poly-L-lysine (30 µg/ml) and laminin (2 µg/ml) at a density of 100,000/well. Hippocampal cultures were grown in Neurobasal medium (NB) supplemented with B27, 0.5 mM glutamine, 12.5 µM glutamate and penicillin/streptomycin. Hippocampal neurons at 14-21DIV were transfected using Lipofectamine 2000 (Invitrogen). Briefly, DNA (3.6 µg /well) was mixed with 3 µl Lipofectamine 2000 in 200 µl NB, incubated for 30 minutes and then added to the neurons in NB with 0.5mM glutamine at 37°C in 5% CO₂ for 45 min to 1 hour. Next, neurons were washed with NB and transferred in the original medium at 37°C in 5% CO₂ for 2-4 days. To induce expression of GFP-GluA2 + HA-GluA1 in hippocampal neurons, doxycycline (Sigma) was added to a final concentration of 1µg/ml 24-30 hours prior to microscopy. 300 nM nocodazole, 10 µM latrunculin B (Sigma) or 10 µM jasplakinolide (Tocris) were added to neuron cultures and imaged after 1 min and up to 1hr after addition. Rapalog (AP21967) was dissolved to 0.1 mM in ethanol. 5 minutes prior to imaging, 0.2 ml of culture medium with rapalog (400 nM) was added to establish a final rapalog concentration of 100 nM.

The cLTP protocol was used combined with rapalog treatment transfected neurons were either left untreated (- rapalog) or treated with 100nM rapalog (+ rapalog) for 15 minutes at 37°C in 5% CO₂. After that, neurons were washed with warm extracellular solution (ECS) of the following composition (mM): NaCl, 120; CaCl₂, 1.3; MgCl₂, 2; KCl, 3.0; HEPES, 10; glucose, 10; Bicuculline, 0.02 (pH 7.4 and osmolarity between 240 and 250mOsmol). Neurons were either left untreated (- rapalog; - glycine) or treated with 200µM glycine (- rapalog; + glycine) or 100nM rapalog (+ rapalog; - glycine) or 200µM glycine plus 100nM rapalog (+ rapalog; + glycine; all conditions in ECS). After 20 minutes at 37°C in 5% CO₂, neurons were fixed for 10 min with 4% paraformaldehyde (PFA)/4% sucrose in PBS at room temperature.

Immunohistochemistry and dendritic spine analysis

For immunohistochemistry, neurons were fixed for 10 min with 4% paraformaldehyde (PFA)/4% sucrose in PBS at room temperature. In rapalog experiments, neurons were fixed after 30 minutes of 100nM rapalog treatment. After fixation cells were washed 3 times for 5 minutes in PBS at room temperature and incubated with the primary-antibody mix in GDB buffer (0.2% BSA, 0.8M NaCl, 0.5% Triton X-100, 30mM phosphate buffer, pH 7.4) overnight at 4°C. Next the neurons were washed 3 times for 5 minutes in PBS at room temperature and incubated with the secondary-antibody mix in GDB buffer for at most 1 hour at room temperature. Neurons were then washed 3 times for 5 min in PBS at room temperature and subsequently mounted on slides in Vectashield mounting medium (Vector Laboratories). Confocal images were acquired using LSM700 (Zeiss) with a 63x/1.40 Oil DIC objective and additional 1.3 zoom using 488nm, 555nm and 633 nm laser lines. A total thickness of 5 µm was scanned for each position and maximum intensity projections were generated for analysis. Imaging settings were kept the same when pictures were compared for fluorescence intensity. The following primary and secondary antibodies were used in this study: mouse anti-PSD-95 antibody (Neuromab, catalog number 75-028), rabbit anti-Homer1 antibody (Synaptic Systems, catalog number 160 002), and rabbit anti Rab11 antibody (Invitrogen, catalog number 71-5300) and Alexa 488-, Alexa 568- and Alexa 633- conjugated secondary antibodies (Invitrogen). Morphology of dendritic protrusions was measured manually in ImageJ, by tracing the width of heads and the length of the protrusion along 10 µm dendritic regions. Protrusions were classified as spines or filopodia according to head width to length ratio (filopodia corresponds to protrusions with ratio below 0.5 and spines have ratio equal to or bigger than 0.5). On the same selected regions, the number and size of PSD-95 and Homer1 clusters were measured manually. The colocalization of overexpressed GluA subunits and endogenous Rab11 was performed using ComDet ImageJ plugin version 0.3.4 (<https://github.com/ekatruxha/ComDet>).

Live cell imaging microscopy

All imaging was performed in full conditioned medium at 37°C and 5% CO₂ unless otherwise indicated. Most live cell imaging was performed using two-color Total Internal Reflection Fluorescence (TIRF) or laser confocal

spinning disk microscopy. For TIRF microscopy, a Nikon Eclipse TE2000E (Nikon) with a CFI Apo TIRF 100x 1.49 N.A. oil objective (Nikon) was used, as described previously (Jaworski *et al.*, 2009; Kapitein *et al.*, 2010a). Briefly, simultaneous dual-color TIRFM was achieved using a DualView (DV2, Photometrics) with beam splitter (Chroma, 565DCXR) and additional emitter (Chroma, ET525/25) in the GFP light path, generating two images on the same chip of a sensitive EMCCD camera (QuantEM or Evolve, both Photometrics). An additional 2.5x magnification lens (Nikon, VM Lens C-2.5x) was employed to compensate the larger pixel size and prevent undersampling of the point-spread function. To visualize intracellular vesicular GFP-GluA2, most of the fluorescence from the dendritic part in the field of view was bleached before image acquisition using the FRAP scanning head 3 FRAP L5 D-CURIE (Curie Institute) in combination with both the 488 nm and 561 nm laser line. Kymographs were created in Metamorph (Universal Imaging) or ImageJ. Experiments in which Rab11 was redistributed using rapalog were performed on the same setup, but using a 40x 1.4 N.A. oil objective, a mercury lamp for excitation and a Coolsnap camera for detection (Photometrics) (Kapitein *et al.*, 2013).

For spinning disk microscopy, a Nikon Eclipse-Ti (Nikon) microscope with CFI Apo TIRF 100x, 1.49 NA, Plan Apo VC 100x N.A. 1.40 or Plan Apo 60x N.A. 1.30 oil objectives (Nikon) was used. The microscope is equipped with a motorized stage (ASI; MS-2000), a Perfect Focus System (Nikon), an incubation chamber (Tokai Hit; INUBG2E-ZILCS) and uses MetaMorph 7.7.6 software (Molecular Devices) to control the camera and all motorized parts. Confocal excitation and detection is achieved using 100 mW Cobolt Calypso 491nm and 100mW Cobolt Jive 561nm lasers and a Yokogawa spinning disk confocal scanning unit (CSU-X1-A1; Yokogawa) equipped with a triple-band dichroic mirror (z405/488/568trans-pc; Chroma) and a filter wheel (CSU-X1-FW-06P-01; Yokogawa) containing GFP (ET-GFP (49002)), mCherry (ET-mCherry (49008)) and mCherry/GFP (ET-mCherry/GFP (59022)) emission filters (all Chroma). Confocal images were acquired with a Evolve 512 EMCCD camera (Photometrics) at a final magnification of 66 nm/pixel, including the additional 2.0x magnification introduced by an additional lens mounted between scanning unit and camera (Edmund Optics). Simultaneous dual-color imaging was performed using a DualView beam splitter (DV2, Roper).

Live cell imaging and analysis of GFP-GluA2 and Rab11 dynamics

To probe intracellular AMPA receptor vesicle transport in neurons, we precisely control the timing and level of receptor expression using a doxycycline (DOX) regulated gene expression system. pTRE-GFP-GluA2 expression was silenced by binding of the reverse tetracycline-controlled transcriptional activator (pTet-on-Ad) in the absence of doxycycline (DOX) to the cultures (Shanks *et al.*, 2010). To facilitate the formation of heterotetrameric complexes we coexpressed pTRE-GFP-GluA2 with HA-GluA1. After incubation with DOX for 25-30 hours, high-resolution total-internal reflection (TIRF) microscopy was performed. In GFP-GluA2 expressing neurons there is a major contribution from surface receptors, which appear as diffusive signals on the plasma membrane. However, we visualized the intracellular pool of GluA2 receptors directly after bleaching a large dendritic area by fast image acquisition over relatively short time intervals. During this imaging period, ~95% of the GFP-GluA2 signal is observed in fast moving Rab11-positive vesicles, suggesting that these GluA2 receptors are located inside the cell rather than on its cell membrane. After ~100 seconds, we observe recovery of fluorescence by a diffusive distribution throughout the bleached area, most likely due to the lateral diffusion of GFP-GluA2 receptors at the plasma membrane. As a result of the increase in the diffusive fluorescent signal it is challenging to detect and follow intracellular GluA2 receptor trafficking for longer time periods after bleaching. Thus our approach is limited to pools of GFP-GluA2 receptor that are mobile and move quickly into the bleached area. Cui-Wang and colleagues (Cui-Wang *et al.*, 2012) showed that the internal diffusion of ER retained GluA2 receptors is around the same time scale as that of mobile receptors at the plasma membrane, suggesting that GluA2 receptor diffusion at the ER could also contribute to the increase in overall fluorescent signal in the dendrites. The ER retained GluA2 receptors are also bleached in our experiments and we probably do not detect the slow release of receptors from ER exit sites due to the increase in diffusive fluorescent signal throughout the bleached area (from both the plasma membrane and ER pools).

To visualize Rab11-positive recycling endosomes transport in cultured hippocampal neurons, we performed imaging of GFP-Rab11 in dendritic shafts for 1 minute at an acquisition rate of 4 frames per second. To image Rab11-positive recycling endosomes dynamics in dendritic spines, time-lapses of 5 minutes were acquired, with 5 seconds interval between acquisition and a z-stack stream at every timepoint, to guarantee the entire dendritic complexity is imaged. mRFP was also imaged to assess neuronal morphology. To quantify speeds of Rab11-positive recycling endosomes entry or exits in spines, 5 minutes stream acquisition was performed, at an acquisition rate of 5 frames per

second. To visualize the distribution of spine entry and exit speeds, data was plotted in cumulative frequency plots with bins of 0.2 μm (the first bin in each plot is only 0.1 μm). In rapalog experiments, 3 minutes of stream acquisition was performed, at an acquisition rate of 5 frames per second. The same neurons were imaged before and after rapalog from 0 to 10 minutes (3 neurons per coverslip). All imaging experiments are performed in conditioned Neurobasal medium. Other solutions used to test different imaging conditions, include Ringers solution (10 mM HEPES, 155 mM NaCl, 1-2 mM CaCl_2 , 1 mM MgCl_2 , 2 mM NaH_2PO_4 , 10 mM glucose, pH 7.2), and Artificial CerebroSpinal Fluid (ACSF, 126 mM NaCl, 3 mM KCl, 2.5 mM CaCl_2 , 1.3 mM MgCl_2 , 1.25 mM NaH_2PO_4 , 26 mM NaHCO_3 , 20 mM glucose). The osmolality was measured using a semi-micro osmometer K-7400 (Knauer). To quantify Rab11-positive recycling endosomes movements along the dendritic shafts, kymographs of 5 μm dendritic fractions were made in ImageJ and manually counted. Rab11-positive recycling endosomes dynamic entries or exits from dendritic spines were also manually counted, along 20 μm of dendrite. Manual tracking of the timelapse videos was obtained by tracking individual clustered vesicle displacements on each frame.

Live cell imaging and analysis of Rab11 and SEP-GluA1 dynamics

To visualize exocytic events of Rab11-positive recycling endosomes containing AMPA receptors, we performed simultaneous dual-color imaging of tagRFP-Rab11 and SEP-GluA1 at 2 frames per second for up to 3 minutes. Events showing sudden local increase of SEP fluorescence were manually counted in ImageJ and classified as spine or dendritic events. To quantify membrane bound amount of GluA1 in rapalog experiments, background-subtracted maximum projections of SEP-GluA1 fluorescence intensity before and after 30min of rapalog treatment in -15 randomly selected spines per imaged dendrite was measured in ImageJ and expressed as a ratio. These ratios were then averaged per dendrite. Representative examples of these spines are shown in ImageJ's "Fire" LUT. Only cells in which the SEP signal was sensitive to an acid wash at pH 6.0 were analyzed in these experiments.

Electrophysiology

Hippocampal primary cultures were prepared from postnatal 1-3 days old C57BL6 mice of either sex as described previously (Futai *et al.*, 2013). Neurons were transfected at days 11-13 *in vitro* (DIV) using Lipofectamine 2000 (Invitrogen), and were assayed 3 days after transfection. Expression vectors for FKBP-HA-Rab11 and HA-MBD-FRB or MyoVI-MD-GFP-FRB were transfected together with pCAG-EGFP at a ratio of 1:1:0.5 by weight. The extracellular solution was (in mM): 119 NaCl, 2.5 KCl, 4 CaCl_2 , 4 MgCl_2 , 26 NaHCO_3 , 1 NaH_2PO_4 and 11 glucose, gassed with 5% CO_2 /95% O_2 , pH 7.4. Whole-cell voltage clamp recordings were made from gene transfected hippocampal pyramidal neurons (visualized by co-transfecting GFP). The patch recording pipettes (2-4 M Ω) were filled with internal solution containing (in mM): 115 cesium methanesulfonate, 20 CsCl, 10 HEPES, 2.5 MgCl_2 , 4 adenosine triphosphate disodium salt, 0.4 guanosine triphosphate trisodium salt, 10 sodium phosphocreatine, and 0.6 EGTA, at pH 7.25 with CsOH. To measure AMPA receptor-mediated miniature EPSC, picrotoxin (0.1 mM, Sigma) and tetrodotoxin (0.001 mM, Ascent Scientific) was added to ACSF and neurons were voltage clamped at $V_{\text{hold}} = -70$ mV. Events smaller than 5 pA were excluded from the analysis. Experiments and analysis were done blind to the DNA constructs used.

COS7 cell culture, transfection and imaging

COS7 cells were cultured in Dulbecco's modified Eagle's medium/Ham's F10 medium (50/50%) containing 10% fetal calf serum and 1% penicillin/streptomycin, and 2 days before transfection the cells were plated on 24 mm diameter coverslips. Cells were transfected with Eugene6 transfection reagent (Roche) according to the manufacturer's protocol and grown for 24 hours prior to imaging or fixation. 1 minute of stream acquisition was performed, at an acquisition rate of 4 frames per second. On rapalog experiments, cells were imaged after 1 to 30 minutes of 100nM rapalog.

SUPPLEMENTARY REFERENCES

Bravo-Cordero, J.J., Marrero-Diaz, R., Megias, D., Genis, L., Garcia-Grande, A., Garcia, M.A., Arroyo, A.G., and Montoya, M.C. (2007). MT1-MMP proinvasive activity is regulated by a novel

Rab8-dependent exocytic pathway. The EMBO journal 26, 1499-1510.
Brummelkamp, T.R., Bernards, R., and Agami, R. (2002). A system for stable expression of short

- interfering RNAs in mammalian cells. *Science* 296, 550-553.
- Buss, F., Arden, S.D., Lindsay, M., Luzio, J.P., and Kendrick-Jones, J. (2001). Myosin VI isoform localized to clathrin-coated vesicles with a role in clathrin-mediated endocytosis. *The EMBO journal* 20, 3676-3684.
- Cui-Wang, T., Hanus, C., Cui, T., Helton, T., Bourne, J., Watson, D., Harris, K.M., and Ehlers, M.D. (2012). Local zones of endoplasmic reticulum complexity confine cargo in neuronal dendrites. *Cell* 148, 309-321.
- Futai, K., Doty, C.D., Baek, B., Ryu, J., and Sheng, M. (2013). Specific trans-synaptic interaction with inhibitory interneuronal neuroligin underlies differential ability of neuroligins to induce functional inhibitory synapses. *The Journal of neuroscience : the official journal of the Society for Neuroscience* 33, 3612-3623.
- Goslin, K., and Banker, G. (1989). Experimental observations on the development of polarity by hippocampal neurons in culture. *J Cell Biol* 108, 1507-1516.
- Hoogenraad, C.C., Milstein, A.D., Ethell, I.M., Henkemeyer, M., and Sheng, M. (2005). GRIP1 controls dendrite morphogenesis by regulating EphB receptor trafficking. *Nature neuroscience* 8, 906-915.
- Hoogenraad, C.C., Popa, I., Futai, K., Martinez-Sanchez, E., Wulf, P.S., van Vlijmen, T., Dortland, B.R., Oorschot, V., Govers, R., Monti, M., et al. (2010). Neuron specific Rab4 effector GRASP-1 coordinates membrane specialization and maturation of recycling endosomes. *PLoS biology* 8, e1000283.
- Jaworski, J., Kapitein, L.C., Gouveia, S.M., Dortland, B.R., Wulf, P.S., Grigoriev, I., Camera, P., Spangler, S.A., Di Stefano, P., Demmers, J., et al. (2009). Dynamic microtubules regulate dendritic spine morphology and synaptic plasticity. *Neuron* 61, 85-100.
- Kapitein, L.C., Schlager, M.A., Kuijpers, M., Wulf, P.S., van Spronsen, M., MacKintosh, F.C., and Hoogenraad, C.C. (2010a). Mixed microtubules steer dynein-driven cargo transport into dendrites. *Curr Biol* 20, 290-299.
- Kapitein, L.C., Schlager, M.A., van der Zwan, W.A., Wulf, P.S., Keijzer, N., and Hoogenraad, C.C. (2010b). Probing intracellular motor protein activity using an inducible cargo trafficking assay. *Biophysical journal* 99, 2143-2152.
- Kapitein, L.C., van Bergeijk, P., Lipka, J., Keijzer, N., Wulf, P.S., Katrukha, E.A., Akhmanova, A., and Hoogenraad, C.C. (2013). Myosin-V opposes microtubule-based cargo transport and drives directional motility on cortical actin. *Curr Biol* 23, 828-834.
- Lee, J.R., Shin, H., Ko, J., Choi, J., Lee, H., and Kim, E. (2003). Characterization of the movement of the kinesin motor KIF1A in living cultured neurons. *The Journal of biological chemistry* 278, 2624-2629.
- Nedvetsky, P.I., Stefan, E., Frische, S., Santamaria, K., Wiesner, B., Valenti, G., Hammer, J.A., 3rd, Nielsen, S., Goldenring, J.R., Rosenthal, W., et al. (2007). A Role of myosin Vb and Rab11-FIP2 in the aquaporin-2 shuttle. *Traffic* 8, 110-123.
- Petrini, E.M., Lu, J., Cognet, L., Lounis, B., Ehlers, M.D., and Choquet, D. (2009). Endocytic trafficking and recycling maintain a pool of mobile surface AMPA receptors required for synaptic potentiation. *Neuron* 63, 92-105.
- Schatzle, P., Ster, J., Verbich, D., McKinney, R.A., Gerber, U., Sonderegger, P., and Mateos, J.M. (2011). Rapid and reversible formation of spine head filopodia in response to muscarinic receptor activation in CA1 pyramidal cells. *The Journal of physiology* 589, 4353-4364.
- Schlager, M.A., Kapitein, L.C., Grigoriev, I., Burzynski, G.M., Wulf, P.S., Keijzer, N., de Graaff, E., Fukuda, M., Shepherd, I.T., Akhmanova, A., et al. (2010). Pericentrosomal targeting of Rab6 secretory vesicles by Bicaudal-D-related protein 1 (BICDR-1) regulates neuritogenesis. *EMBO J* 29, 1637-1651.
- Shanks, N.F., Maruo, T., Farina, A.N., Ellisman, M.H., and Nakagawa, T. (2010). Contribution of the global subunit structure and stargazin on the maturation of AMPA receptors. *The Journal of neuroscience : the official journal of the Society for Neuroscience* 30, 2728-2740.
- Yau, K.W., van Beuningen, S.F., Cunha-Ferreira, I., Cloin, B.M., van Battum, E.Y., Will, L., Schatzle, P., Tas, R.P., van Krugten, J., Katrukha, E.A., et al. (2014). Microtubule Minus-End Binding Protein CAMSAP2 Controls Axon Specification and Dendrite Development. *Neuron* 82, 1058-1073.

Activity-dependent actin remodeling at the base of dendritic spines promotes microtubule entry

Philipp Schätzle, **Marta Esteves da Silva**, Roderick Tas, Eugene A. Katrukha, Hai Yin Hu, Corette J. Wierenga, Lukas C. Kapitein and Casper C. Hoogenraad

Cell Biology, Faculty of Science, Utrecht University, Utrecht, The Netherlands.

ABSTRACT

Microtubules are dynamic polymers that grow from their plus ends along the length of the axon and dendrites. Occasionally, microtubules can polymerize from the shaft directly into dendritic spines. Microtubules seem to specifically target dendritic spines that are undergoing activity-dependent changes, but the mechanism by which microtubules enter spines has remained poorly understood. Using live-cell imaging, high-resolution microscopy and local glutamate uncaging, we show that local actin remodeling at the base of a spine promotes local microtubule spine targeting. Microtubule spine entry is triggered by activation of NMDA receptors and calcium influx, and can be regulated by dynamic actin remodeling. Activity-dependent translocation of the actin remodeling protein cortactin out of the spine correlates with increased microtubule targeting at the single spine level. Our data shows that the structural changes in the actin cytoskeleton at the base of the spine are directly involved in microtubule entry, and emphasize the importance of actin-microtubule crosstalk in orchestrating synapse function and plasticity.

3

INTRODUCTION

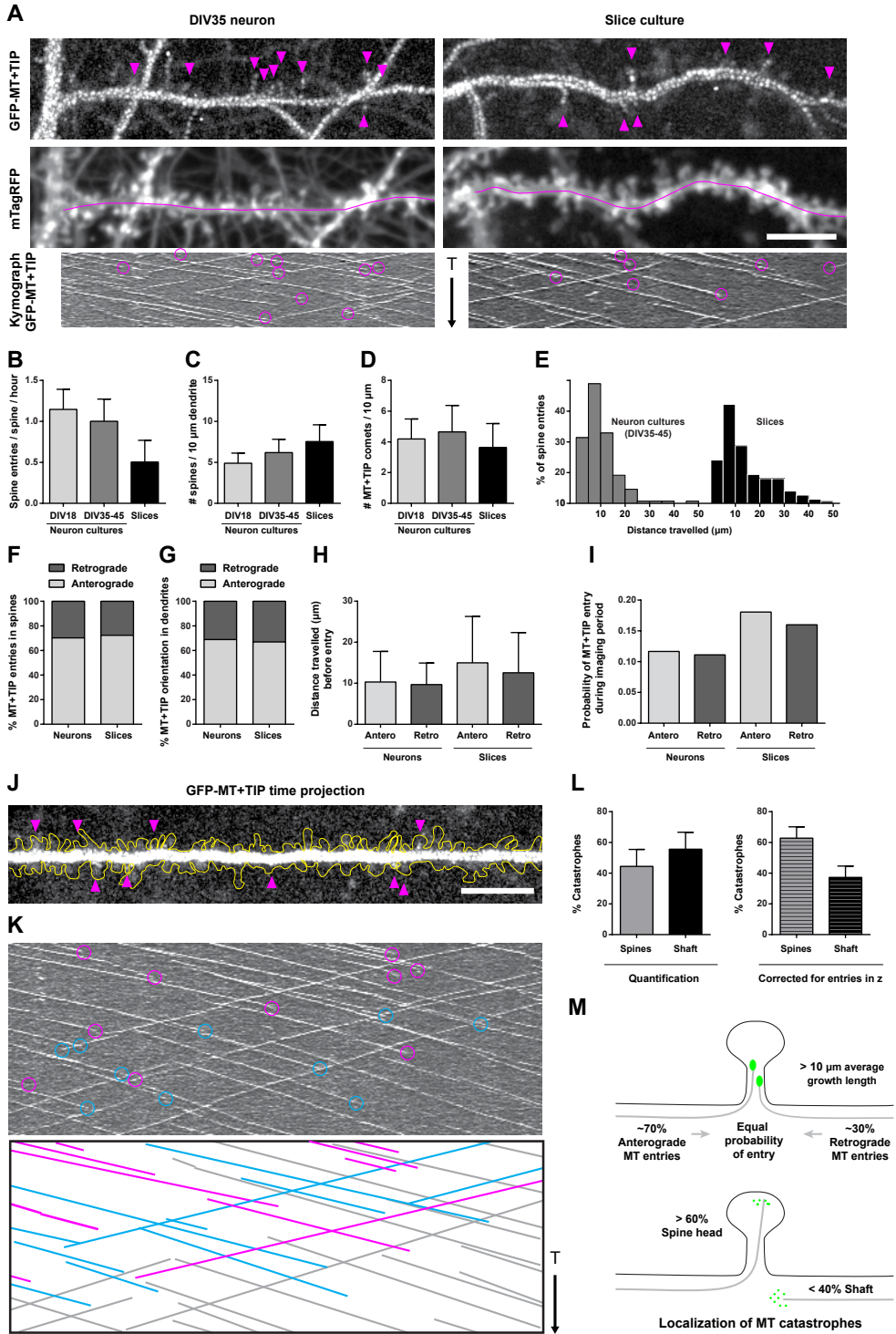
Microtubules are regarded as critical structures for stable neuronal morphology because they serve as tracks for long-distance transport, provide dynamic and mechanical functions, and control local signaling events (Kapitein and Hoogenraad, 2015). In dendrites, microtubules polymerize from their plus ends along the length of the dendrite in both anterograde and retrograde directions (Stepanova *et al.*, 2003). Equal numbers of opposing microtubule orientations throughout the dendritic processes have been reported *in vitro* and *in vivo* (Yau *et al.*, 2016). Occasionally, microtubules can polymerize from the dendritic shaft directly into dendritic spines (Hu *et al.*, 2008; Jaworski *et al.*, 2009). Even though microtubules enter spines spontaneously, subsequent studies have shown that these microtubule invasions of spines are regulated by synaptic activity. Recent work has shown that microtubule invasion frequency increases after induction of chemical long-term potentiation (cLTP) (Merriam *et al.*, 2011). In contrast, applying a paradigm that induces chemical long-term depression (cLTD) results in a loss of microtubule dynamics in dendritic spines (Kapitein *et al.*, 2011). However, the mechanistic link between neuronal activity and microtubule entry into spines remains largely unclear.

Dynamic microtubule entry in dendritic spines has been thought to contribute to processes related to synaptic maintenance and plasticity. For instance, recent data showed that microtubules entering dendritic spines provide a direct route for microtubule-based motor-driven transport of selective synaptic cargo into spines (Esteves da Silva *et al.*, 2015). Under basal conditions, the frequency of microtubule-spine invasions is relatively low, making actin-based transport a more generic way of driving cargo trafficking in spines. For example, it has been shown that endoplasmic reticulum and recycling endosomes use myosin V motors to enter spines (Correia *et al.*, 2008; Wagner *et al.*, 2011; Wang *et al.*, 2008). However, kinesin-3 family proteins (KIF1A and KIF1C) can act as microtubule-based motors that transport cargo along newly polymerized microtubules directly into spines (Esteves da Silva *et al.*, 2015; McVicker *et al.*, 2016). The mechanism by which microtubules enter dendritic spines has remained poorly understood. Therefore, in this study we investigate which processes regulate microtubule entry into spines.

RESULTS

Microtubules enter dendritic spines in cultured neurons and organotypic slices

The invasion of dendritic spines by dynamic microtubules was recently shown in developing neuron culture systems (Hu *et al.*, 2011; Hu *et al.*, 2008; Jaworski *et al.*, 2009; Merriam *et al.*, 2011). Using a lentivirus-based inducible expression system we demonstrate microtubule entry in spines in very mature dissociated neuron cultures and in dentate gyrus granule cells of organotypic hippocampal slice cultures (Fig.1A). We observed frequent microtubule invasions in spines in both culture types and at different stages of maturation indicating that this phenomenon is not limited to a transient phase during development (Fig.1B). The average



3

◀ Figure 1. Microtubules invade spines in mature cultured neuron and organotypic slice

A. Dendrites from lentiviral-transduced dissociated neurons and slice cultures expressing a marker for dynamic microtubules (MT+TIP, top) and cellular morphology (mTagRFP, middle). Top panel shows maximum projections of average-subtracted time-lapse recordings of MT+TIP comets (6 min). Arrowheads highlight examples of microtubules entering spines. Middle panel shows average projections of the full time-lapse and the line displays the dendritic sections used for kymographs. Bottom panels show kymographs of the MT+TIP comets from the top panels. Magenta circles indicate microtubules invading spines. **B.** Quantification of spine entry frequency in cultured neurons and slice cultures. Cultured neurons DIV18: $n = 10$, DIV35-45: $n = 25$, slices: $n = 37$ analyzed neurons. **C.** Quantification of spine number per 10 μm dendrite ($n =$ identical to **B**). **D.** Density of MT+TIP comets per 10 μm dendrite. **E.** Histogram of distance travelled by MT+TIP comets entering a spine in neuron (left graph) and slice cultures (right graph). Bin size = 5 μm , neurons: $n = 131$ comets, slices: $n = 149$ comets. **F.** Orientation of microtubules invading spines ($n =$ identical to **E**). **G.** Distribution of anterograde and retrograde oriented MT+TIP comets in neurons and slice cultures. DIV35-45: $n = 1140$ comets, slices: $n = 859$ comets. **H.** Average distance MT+TIP comets travelled before entering a spine. **I.** Probability of MT+TIP comets entering a spine relative to its orientation (pooled data). **D-I.** Make use of the same dataset. Cultured neurons DIV18: $n = 14$ dendrites from 2 preparations, DIV35-45: $n = 25$ dendrites from 2 preparations, slices: $n = 21$ dendrites from 6 preparations. **J.** Maximum intensity projection of MT+TIP comets time-lapse recording in slices. The spine outline was generated from mTagRFP signal. Arrowheads indicate microtubule entries in spines. **K.** Kymograph of the MT+TIP comets shown in **J**. Microtubule catastrophes within spines are highlighted by magenta circles, catastrophes without detectable spine entries (shaft) by cyan circles. Bottom graph shows a drawing of the kymograph using the same color code. Gray lines represent microtubule traces without observable catastrophes. Scale and time lapse length is identical to **J**. **L.** Localization of microtubule catastrophes in dendrites of slice cultures. Right graph is corrected for false positive shaft catastrophes resulting from limited z -resolution. $n = 203$ comets of 12 dendrites from 10 slices of 4 preparations. **M.** Summary of findings: Spine targeting is not selective for microtubule polarity but the higher number of anterograde growing microtubules results in a more frequent targeting of this orientation. Spines represent preferred localizations for microtubule growth termination. Scale bars, 10 μm . Vertical arrow, 4 min. Bars diagrams show mean + SD.

spine entry frequency in slices was about half of the value observed for cultured neurons (Fig.1B), which could be partially explained by a higher spine density compared to the number of dynamic microtubules in granule cells (Fig.1C,D). We found that microtubules travelled remarkable distances before entering a spine (Fig.1E). This was even more pronounced in slice cultures, where 25% of all spine entries were preceded by distances between 20-50 microns. Furthermore, a considerable number of comet traces crossed the acquisition borders in time and/or space, which means that the actual length of many comets was actually underestimated. This observation is in conflict with a recent publication where it is reported that microtubules travel short distances before spine invasions (Merriam *et al.*, 2013). In our opinion, this discrepancy is the result of limitations in z -resolution of TIRF microscopy used in the aforementioned study. The bidirectional polarity of growing microtubules in dendrites (Yau *et al.*, 2016) could entail that one orientation is favored for spine entries. However, the polarity of microtubules entering spines (Fig.1F) was identical to the orientation of the total dynamic microtubule population (Fig.1G). Consistently, microtubules of opposed polarity did not show differences for the covered distances before spine entries (Fig.1H) and spine entry probabilities (Fig.1I). This data demonstrate that the polarity of microtubules is not a determinant factor for the targeting of dendritic spines.

The majority of microtubule catastrophes in dendrites occur at spines

The growth and shrinkage of microtubules is controlled by a variety of regulatory proteins that interact with the plus-tip or the microtubule lattice (Akhmanova and Steinmetz, 2008). In slice cultures the majority of microtubule catastrophes were not followed by an observable microtubule rescue event (see for instance the kymograph in Fig.1K). As spine entries always result in a microtubule catastrophe, we wondered to which extent this scenario accounts for the termination of microtubule growth in the dendrite. Based on kymographs, we identified microtubule catastrophes in slices and analyzed if these occur within the dendrite or in spines (Fig.1J,K). Surprisingly, more than 40% of the microtubule catastrophes could directly be associated with entries in spines (magenta circles in Fig.1K). However, this number reflects only spine entries identified in x,y dimensions because the axial resolution of the microscope is two times less than the lateral resolution, thus hindering the identification of entries in spines in the z-axis. To correct for this limitation, we applied a z-correction factor by assuming that spine entries cannot be resolved if the spine is more than ± 60 degrees out of the imaging plane. This correction increased the proportion of catastrophes occurring in spines to more than 60% (Fig.1L), suggesting that spine entries may represent the default pathway of terminating the growth of dynamic microtubules in mature neurons.

Increasing dendritic calcium levels increase microtubule entries in spines

Previous studies in dissociated neurons suggest a regulatory effect of synaptic activation on spine invasions by microtubules (Kapitein *et al.*, 2011; Merriam *et al.*, 2011; Merriam *et al.*, 2013). To verify this in slices, we applied pharmacological treatments that modulate the pattern of synaptic activation in hippocampal slice cultures and analyzed microtubule dynamics in spines. While decreasing (TTX) or increasing (PTX) network activity did not affect spine entry frequencies in slices, we observed a small but significant decrease using low concentrations of DHPG, known to induce chemical LTD in slices (Fig.2A). The most striking effect was found after application of the muscarinic agonist methacholine (MCh). Cholinergic stimulation has been used by several groups to induce LTP in hippocampal slice cultures and acute slices (De Roo *et al.*, 2008; Fernandez de Sevilla *et al.*, 2008). Following methacholine stimulation we observed a doubling of spine entry events compared to control conditions (Fig.2A-C and Supplementary Video S1). Interestingly, TTX-induced blocking of action potentials did not abolish the potentiating effect of methacholine, indicating that the G protein-coupled release of calcium from IP₃-sensitive stores is sufficient to increase microtubule invasions in spines (Fig.2A,C). Our data is in agreement with a recent study demonstrating an increase of microtubule invasions in spines of dissociated cultures after stimulation with a glycine-based chemical LTP protocol (Merriam *et al.*, 2013). To confirm the role of dendritic calcium levels in this process, we applied brief local puff applications of NMDA on TTX-silenced neuron cultures (Fig.2D). Quantifications of spine entry frequencies before and after application revealed a significant increase following NMDA-induced increase in calcium levels (Fig.2E). Together, these experiments demonstrate that intracellular calcium transients are involved in

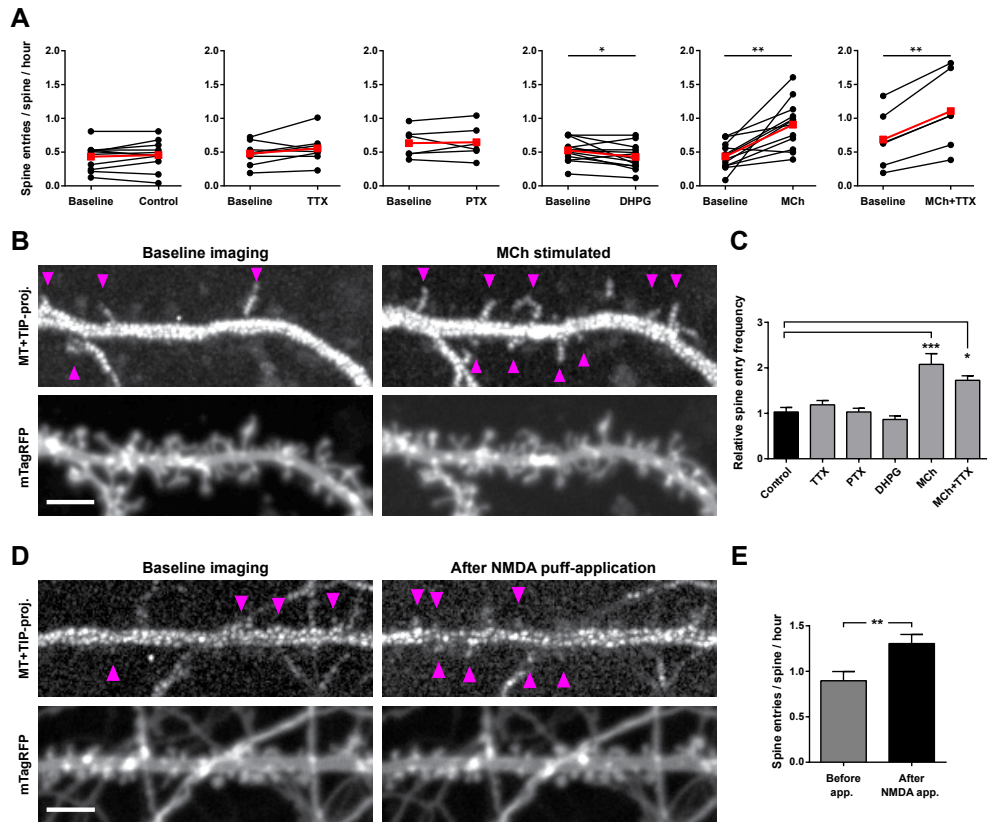


Figure 2. Specific synaptic activation modulates microtubule invasions in spines

A. Synaptic activation in slice cultures was altered by indicated pharmacological treatments. Cultures were transduced with lentivirus expressing GFP-tagged MT+TIP marker and mTagRFP. Red points represent the mean values of the dataset. * $p < 0.05$, ** $p < 0.01$, paired t-test; control: $n = 11$, TTX: $n = 8$, PTX: $n = 6$, DHPG: $n = 13$, methacholine (MCh): $n = 12$, MCh+TTX: $n = 6$ dendrites. **B.** Example of MCh-stimulated dendrite showing projections of MT+TIP comets (upper panel) and dendrite morphology (lower panel), before and after stimulation. Arrowheads indicate examples of MT+TIP entries in spines. See also Supplementary Video S1. **C.** Relative change of spine entry frequency (stimulation/baseline) for each treatment in **A**. * $p < 0.05$, *** $p < 0.0001$, one-way ANOVA with posthoc Dunnett's test. **D.** Neuron culture infected with virus expressing MT+TIP marker and mTagRFP. Dendrite recorded 4 min before and after local puff-application of NMDA. Panels are arranged as in **B**. **E.** Quantification of spine entry frequency before and after local NMDA application. ** $p < 0.01$, paired t-test; $n = 12$ dendrites. Scale bars, 5 μm . Bars diagrams show mean + SEM.

the regulation of spine targeting by microtubules.

Regulation of spine targeting on the level of single synapses

To our knowledge, all previous experiments addressing the effects of synaptic activity on microtubule dynamics in spines were performed using global stimulation protocols. The above described local NMDA applications were our first attempts to target individual synapses.

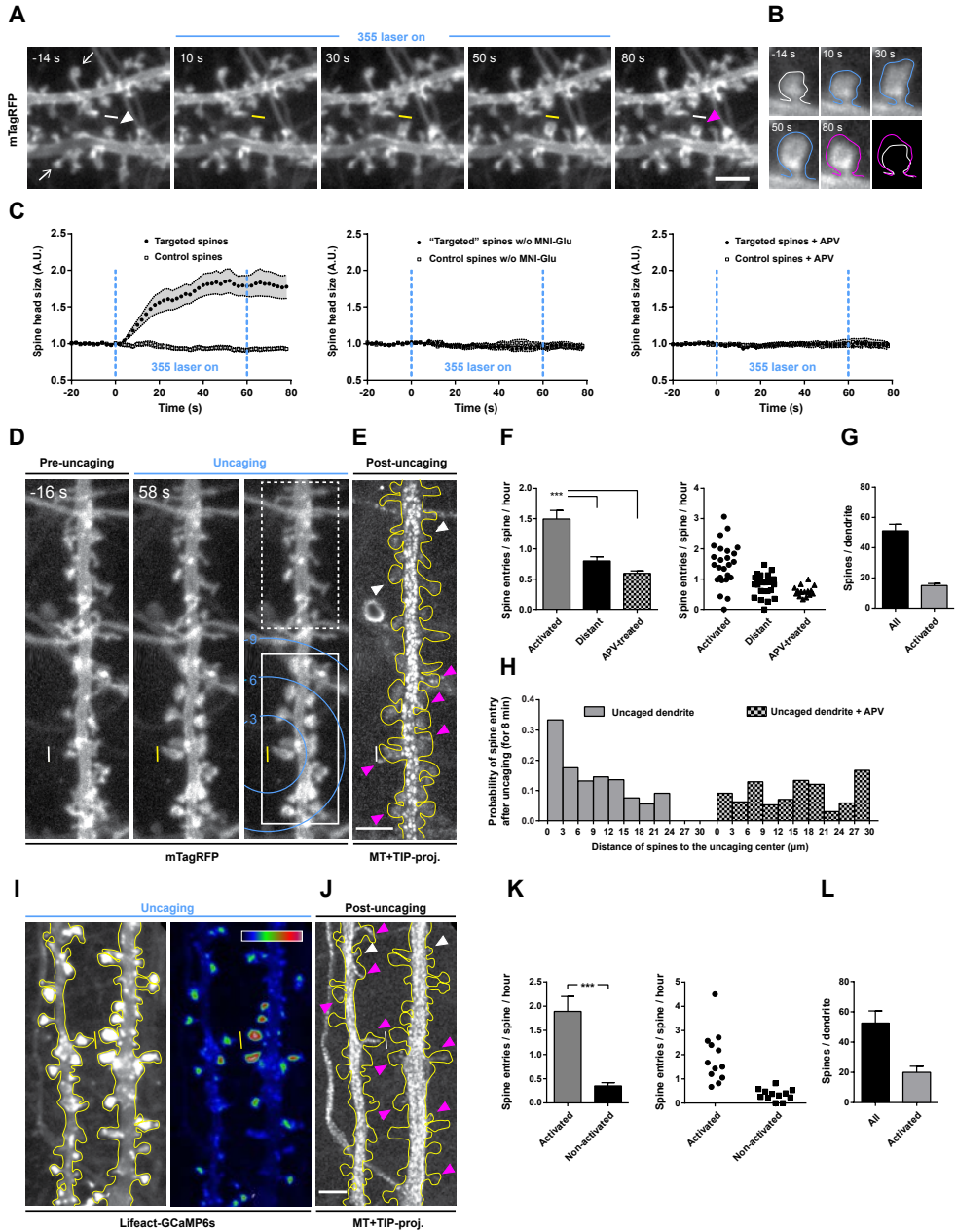


Figure 3. NMDA receptor activation triggers microtubule entry in spines

A. Still frames of a dissociated neuron expressing mTagRFP. The first and last images represent time points before and after single-photon glutamate uncaging. Uncaging intervals were 0.5 Hz starting from 0 s for 1 min. The white/yellow line marks the uncaging spot; arrowhead indicates a targeted spine and the arrows point to examples of spines that do not respond by size changes. **B.** The targeted spine in **A** at higher magnification. Spine outline was traced and the last image shows an overlay of the before and after uncaging situation. **C.** Quantification of the change in

spine head size in response to the uncaging stimulus over time. Targeted spines lay in close proximity to the uncaging spot, while control spines were chosen with a maximum possible distance to this position. Left graph shows the results of the standard uncaging protocol (targeted: $n = 21$, control: $n = 26$ spines). Middle graph represents a control condition in which the light pulse is applied in the absence of caged glutamate (targeted: $n = 9$, control: $n = 9$ spines) and right graph shows the uncaging experiment in the presence of the NMDA-receptor blocker APV (targeted: $n = 10$, control: $n = 11$ spines). Error bars indicates SEM **D**. Dendrite morphology before (left) and during glutamate uncaging (middle). Based on the morphological response to the stimulation, spines were classified as “activated” (white box) and “non-activated” (dashed box). White/yellow line marks the uncaging spot and the circles indicate the distance to the center of the uncaging region. See also Supplementary Video S2. **E**. Maximum projection of the MT+TIP comets time-lapse recorded after the uncaging session. Magenta arrowheads show MT+TIP spine entries in activated spines, white arrowheads in a non-activated spine. See also Supplementary Video S3. **F**. Quantification of spine entries following glutamate uncaging. Entry frequencies for activated and non-activated spines are shown separately, while this separation was not made for APV experiments. Right graph shows the individual experiments, where each point represents the mean spine entry frequency of an uncaged dendrite. $***p < 0.0001$, one-way ANOVA with posthoc Tukey’s test; uncaged: $n = 25$, APV silenced: $n = 17$ dendrites. **G**. Average spine numbers of the analyzed experiments and the fraction considered activated. **H**. Histogram showing the probability of spine entries in relation to the localization of spines to the uncaging region. Microtubule dynamics were recorded for 8 min after uncaging. Invaded and non-invaded spines were quantified together with their distance to the uncaging region. Data is presented in bins of 3 μm intervals for uncaged control and APV treated dendrites (uncaged: $n = 20$, APV: $n = 17$ dendrites). **I**. Maximum projection of a Lifeact-GCaMP6s time-lapse acquired during uncaging of glutamate. The levels are strongly enhanced to identify all spines on the dendrite (left). The color coded sum projection allows the identification of activated spines (right). Yellow line marks the uncaging region, insert in top right corner shows lookup table for the color code. See also Supplementary Video S4. **J**. Projection of MT+TIP comets time-lapse recorded after the uncaging session. Microtubule entries in activated spines are highlighted with magenta arrowheads, entries in non-activated spines with white arrowheads. See also Supplementary Video S5. **K**. Quantification of spine entry frequency following glutamate uncaging. Activated and non-activated spines are identified on their GCaMP6s signal. $***p < 0.0001$, Mann Whitney test; $n = 12$ dendrites. The scatter blot on the right shows the results of the individual experiments. **L**. Average spine numbers of the analyzed experiments and the fraction considered activated. Scale bars, 3 μm . Bars diagrams show mean + SEM.

However, recordings of calcium dynamics showed that the majority of synapses within the field of view became activated and their stimulation evoked calcium waves extending throughout the dendrite (data not shown). To activate only a small population of synapses along a dendrite, we performed local glutamate uncaging on cultured neurons. Two-photon uncaging in slice cultures is associated with an NMDA-receptor-dependent increase in spine size (Matsuzaki *et al.*, 2004; Ross, 2012). We used spine growth as read-out of successful single-photon glutamate uncaging in our neuronal cultures. Spines close to the uncaging region showed an almost 2-fold increase in size while distant control spines were unchanged (Fig.3A-D). Additional control experiments demonstrated that the spine size changes were not a direct result of the 355 nm laser excitation but dependent on the activation of NMDA receptors (Fig.3C). Next, we combined the uncaging protocol with subsequent recording of microtubule dynamics (Fig.3E and Supplementary Video S2,S3). Quantifications of microtubule invasions showed that the population of activated spines was almost two times more often invaded than distant spines (Fig.3F). Uncaging in the presence of APV resulted in an unchanged invasion frequency in activated and distant spines. As an alternative quantification, we determined the spine entry frequency relative to the distance to the uncaging center, which confirmed that spines in close

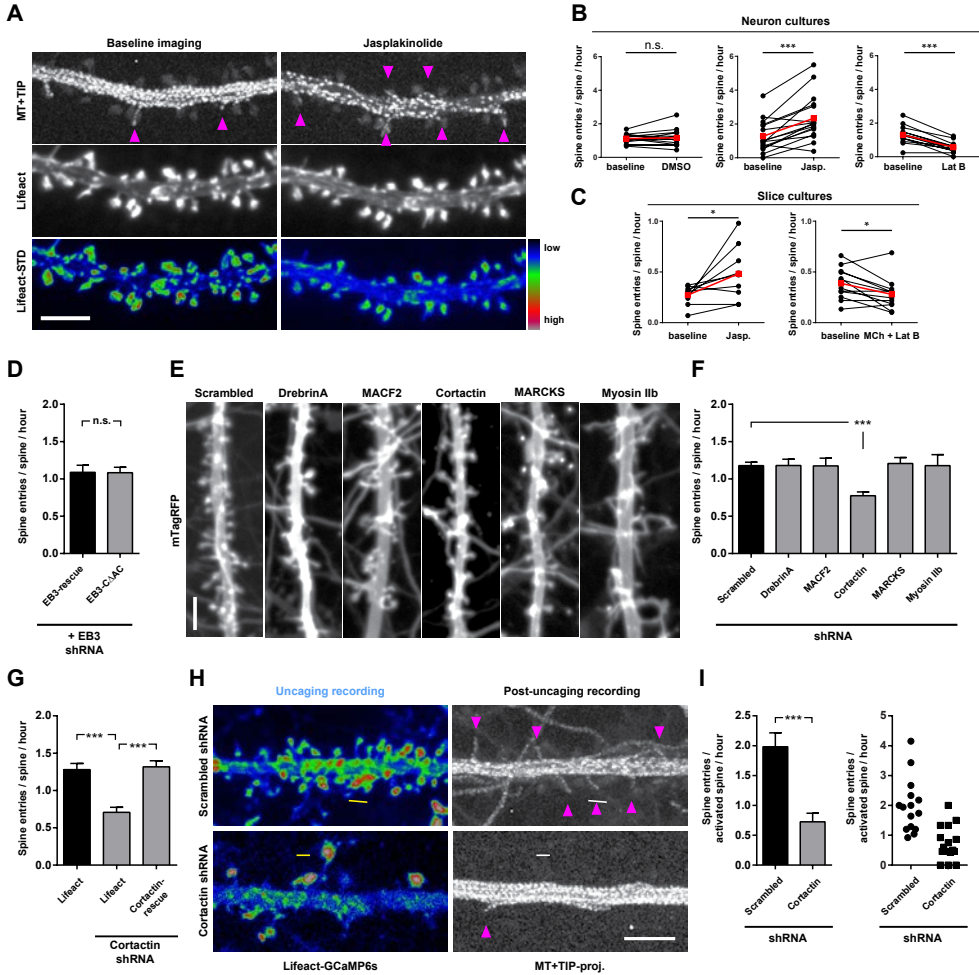


Figure 4. Actin is important for mediating microtubule entries in spines

A. Dendrite of a dissociated neuron before and after treatment with jasplakinolide. Neurons were infected with virus co-expressing MT+TIP marker and Lifeact. Top panel shows the projection of the MT+TIP comets, middle panel is a still frame of the Lifeact signal and bottom panel is a projection of the standard deviation of the complete Lifeact time-lapse recording. Note that following jasplakinolide treatment there is a reduction in the number of MT+TIP comets and spine head dynamics but no increase in spine size. **B.** Effects on spine entry frequency in neuron cultures treated with DMSO (left) or actin targeting drugs jasplakinolide (middle) and Latrunculin B (right). ***p < 0.001, n.s. = not significant, paired t-test; Jasp.: n = 16, Lat B: n = 14 dendrites. **C.** Slice culture experiments with either Jasp. (left) or a combination of MCh and Lat B (right). *p < 0.05, paired t-test; Jasp.: n = 9, MCh+Lat B: n = 12 dendrites. **D.** Neuron cultures coinfecting with EB3 shRNA virus and either the full-length GFP-EB3-rescue or GFP-EB3-CΔAC virus. Not significant, unpaired t-test; EB3-rescue: n = 21, EB3-CΔAC: n = 22 dendrites. **E.** Representative examples of dendritic morphology after lentivirus-mediated depletion of indicated target proteins in cultured neurons. Neurons were coinfecting with virus expressing indicated shRNAs and virus expressing mTagRFP and the MT+TIP marker. **F.** Quantification of microtubule invasion frequencies in knockdown conditions. ***p < 0.001, one-way ANOVA with posthoc Dunnett's test; scrambled: n = 45, DrebrinA: n = 21, MACF2: n = 7, Cortactin: n = 20, MARCKS: n = 15, Myosin IIb: n = 17 dendrites. **G.** Quantification of MT+TIP spine entries in baseline, cortactin-knockdown or

cortactin-rescue conditions. Neurons were depleted for endogenous cortactin with lentivirus and spines identified based on the Lifeact or the shRNA-resistant cortactin signals. *** $p < 0.0001$, one-way ANOVA with posthoc Tukey's test; Lifeact: $n = 17$, Lifeact+shRNA: $n = 13$, cortactin-rescue+shRNA: $n = 14$ dendrites. **H.** Glutamate uncaging experiment in control (upper) and cortactin-knockdown (lower) neuron cultures. Neuron cultures were coinfecting with the cortactin-shRNA virus and virus expressing the MT+TIP marker and Lifeact-GCaMP6s. Left panel shows a sum projection of the Lifeact-GCaMP6s signal recorded during the glutamate uncaging protocol (yellow/white line marks uncaging region). The majority of spines within the field of view were activated because of a slightly stronger uncaging stimulation as in previous experiments (same color coding as in **A**). Right panel shows a projection of MT+TIP comets acquired after the uncaging session. Magenta arrowheads indicate microtubule entries in spines. **I.** Spine entry frequency after uncaging of glutamate for control and cortactin knockdown neurons. *** $p < 0.0001$, unpaired t-test; scrambled: $n = 15$, Cortactin: $n = 16$ dendrites. Right graph depicts the single experiments, where each data point represents the mean spine entry frequency for an individual dendrite. Scale bars, 5 μm . Bars diagrams show mean + SEM.

proximity to the uncaging region were more frequently targeted than more distant spines (Fig.3H). This effect could not be observed in the presence of APV. Although these uncaging experiments strongly suggest that local activation induces local targeting, our approach could not indisputably resolve the activation state of individual spines. To overcome this we combined the uncaging experiments with a read-out of the NMDA-evoked calcium transients. A fusion construct of Lifeact and GCaMP6s resulted in a highly specific indicator for calcium signals in spines. The combined recording of calcium signals and microtubule dynamics (Fig 3I,J and Supplementary Video S4,S5), showed a strong correlation between activated spines and microtubule targeting events in the uncaging experiments (Fig 3K). Additionally, the calcium imaging confirmed that the applied stimulation protocol did not induce global calcium events. In summary, the activation of small number of dendritic spines using glutamate uncaging yielded direct evidence for a coupling between synaptic activation and increased probability of targeting by dynamic microtubules on the level of single spines.

Microtubule targeting in spines depends on actin remodeling

The actin cytoskeleton in spines is a major downstream target of activity-induced plastic changes at synapses (Hotulainen and Hoogenraad, 2010). To determine whether actin plays a role in microtubule entries in spines, we pharmacologically interfered with actin dynamics. We monitored spine size and actin in neuron cultures expressing the actin marker Lifeact in control conditions and after incubation with the actin stabilizing drug jasplakinolide. The treatment did not increase spine size but reduced actin-based motility of the spine heads (Fischer *et al.*, 1998) (Fig.4A). Interestingly, microtubule entries in spines were strongly increased by jasplakinolide, while the total number of comets was reduced (Fig.4A,B). In contrast, disruption of actin structures with latrunculin B induced a significant decrease of spine entry frequency in dissociated neurons (Fig.4B). We found similar results in slice cultures, in which jasplakinolide also increased spine entry frequency (Fig.4C). Remarkably, the methacholine-induced potentiating effect on spine entry frequency in slices (Fig.2A) was completely abolished in the presence of latrunculin B (Fig.4C). These data demonstrate a clear involvement of actin in the microtubule invasion of spines.

The localization of endoplasmic reticulum (ER) in spines is another actin-dependent process (Wagner *et al.*, 2011) that is further affected by synaptic activity (Holbro *et al.*, 2009), reminiscent of our microtubule spine invasions. As microtubule plus-tips can interact with the ER (Grigoriev *et al.*, 2008) we wondered if growing microtubules were guided into spines by following previously established ER-structures. To address this possibility, we overexpressed a dominant negative MyosinVa construct in neuron cultures to disrupt spine targeting of ER. Although we noticed a more than 5 times reduction of ER positive spines in these experiments, there was no effect on the microtubule spine entry frequency (Supplementary Fig.S1), indicating that microtubule invasions occur independent of ER in spines.

End-binding proteins (EBs) recognize growing microtubule plus-tips and interact via their acidic C-terminal tail region with a multitude of proteins (Akhmanova and Steinmetz, 2008). Protein interactions between EBs and an actin associated protein could well explain the observed pattern of microtubule targeting in spines. We therefore tested if specifically disrupting these EB3-interactions would interfere with microtubule spine invasions. However, we observed full rescue of spine targeting after knockdown of EB3 and coexpression of full-length EB3-rescue as well as EB3-C Δ AC (Fig.4D), suggesting that microtubule-actin interlinking proteins are not required in this process. Control experiments with coexpression of EB3 shRNA and the MT+TIP marker did not allow recording of microtubule comets, indicating strong depletion of endogenous EB3 (data not shown).

Next, we investigated if the knockdown of actin interacting/regulating proteins affects the targeting of spines by microtubules. Cortactin, MARCKS and MyosinIIb represent important regulators of actin dynamics in spines (Calabrese and Halpain, 2005; Hering and Sheng, 2003; Rex *et al.*, 2010), while DrebrinA and MACF2 have the additional ability to interact with growing microtubule plus-ends (Geraldo *et al.*, 2008; Leung *et al.*, 1999). Lentiviral induced RNAi of the actin-interacting candidate proteins differently affected spine morphology and density (Fig.4E and Supplementary Fig.S2). Interestingly, only the knockdown of cortactin resulted in a significant effect on microtubule spine entry frequency in the neuron cultures (Fig.4F). To exclude potential off target-effects of the used cortactin-shRNA, we performed rescue experiments using a knockdown-resistant version of cortactin, which resulted in a comparable spine entry frequency as in control conditions (Fig.4G). The involvement of the actin regulator cortactin suggests that the actin cytoskeleton per se may facilitate microtubule spine targeting and that actin-microtubule interactions may be less important. An activity-dependent redistribution of cortactin (Hering and Sheng, 2003; Iki *et al.*, 2005; Seese *et al.*, 2012) may be linked to a role for cortactin in activity-dependent targeting of microtubules to spines. Using glutamate uncaging in combination with knockdown, we found a significant reduction of microtubule spine targeting confirming the importance of cortactin in promoting actin dynamics that facilitate spine entries (Fig.4H,J).

Actin remodelling at the base of the spine

Actin dynamics have been extensively studied in the spine head but relatively little data exists

about actin remodelling at the base of the spine. Electron microscopy has demonstrated a branched actin network at the base of the spine, which often overlapped with microtubules at the intersection between the spine neck and dendritic shaft (Korobova and Svitkina, 2010). We reasoned that the base of the spine is an important area for guiding microtubule entry into spines and we analyzed actin dynamics at single spine level in greater detail. Glutamate uncaging-induced stimulation of spines in control neurons markedly increased actin fluorescence intensities (Lifect) in spine heads and at the spine base (Fig.5A). Interestingly, the knockdown of cortactin significantly blocked the actin increase at the spine head and spine base in response to stimulation (Fig.5A-C, Supplementary Fig.S3, Video S6). These data suggest that the reduction of microtubule entries in spines observed after knockdown of cortactin (Fig.4E,F) may result from the disturbed actin dynamics at the spine base. To test if microtubule entries in spines correlate with actin dynamics at the base of the spine, we recorded actin dynamics in neuron cultures under baseline conditions. We frequently observed increased actin dynamics at the base of spines that were invaded by microtubules in the analyzed time-lapses (Fig.5D,E). Analysis of the signal intensities for actin and dynamic microtubules confirmed these observations (Fig.5G). Quantification of the live-imaging data demonstrated that 76% of the invaded spines exhibit increased actin dynamics at the spine base (Fig.5H). Together, our results suggest a model in which synaptic activation induces actin dynamics at the spine base that promotes microtubule invasion in spines (Fig.5I).

Consistent with the live-imaging data, dSTORM imaging of Lifect-myc labelled expressing neuron cultures revealed actin structures at the base of some spines (Fig.6A). Intriguingly, long actin filaments at the spine base were observed extending throughout the dendritic shaft. Similar actin structures were also seen in non-transduced neurons by applying purified Lifect-GFP-post fixation for single molecule detection (Kiuchi *et al.*, 2015) (Fig.6B). Based on these observations it is tempting to speculate that microtubules may be directed into spines by cooperative interaction between dendritic and spinal actin structures. Together, our results suggest that increasing dynamics and remodelling of a specialized actin organization at the base of the spine is correlated with microtubule entries.

DISCUSSION

Here we have identified a mechanism by which synaptic activity locally regulates microtubule entry into spines. We found that microtubule-spine entry is regulated by NMDA receptor activation and calcium influx and that actin remodeling is directly involved in microtubule entry. Our data demonstrate that structural changes in the actin cytoskeleton at the base of the spine are directly involved in microtubule entry.

Microtubule spine entry is triggered by activation of NMDA receptor and calcium influx

We used a lentivirus-based inducible expression system of fluorescently labeled microtubule plus-ends combined with fast live cell imaging to examine microtubule entry in dendritic spines in mature neurons in dissociated cultures and in organotypic hippocampal slices. Our

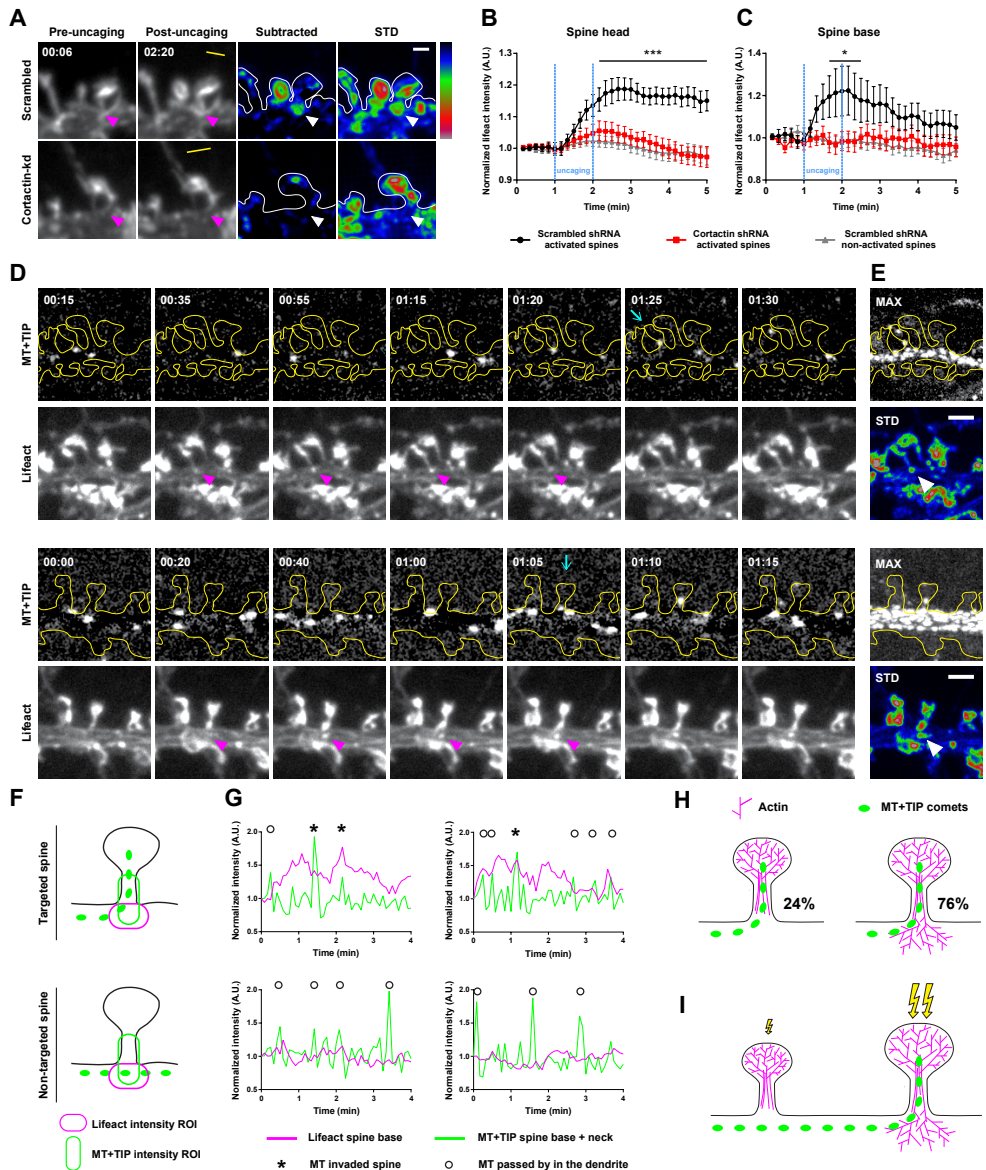


Figure 5. Actin dynamics at the spine base

A. Glutamate uncaging in neuron cultures expressing virus delivered Lifact and either scrambled or cortactin shRNAs. First two columns show still frames before and after uncaging and the yellow line indicates uncaging region. Next, subtraction of the pre- from the post-uncaging Lifact signals to visualize the increases in fluorescence intensity. Right column is a projection of the Lifact signal SD over the full 5 min recording to visualize hot spots of actin dynamics. Arrowheads point on the same position at the base of the spine. Scale bar, 1 μ m. Full length recordings of these and additional examples are shown in Supplementary Video S6. **B.** Quantification of Lifact average intensities at the spine head in response to glutamate uncaging. Relative signals for activated spines in control or cortactin knockdown conditions and non-activated spines in control conditions are plotted over time. Data points represent means \pm SEM.; *** $p < 0.001$, two-way ANOVA with posthoc Bonferroni test; scrambled activated: $n = 20$

spines, cortactin activated: $n = 19$ spines, scrambled non-activated: $n = 22$ spines. Spines from each condition were imaged from ≥ 15 dendrites of two independent cultures. **C.** Same dataset representation as in **B** showing quantified intensities for the corresponding spine bases. $*p < 0.05$, two-way ANOVA with posthoc Bonferroni test **D.** Still frames of two example neurons expressing MT+TIP and Lifeact. The moment of spine entries are indicated by a cyan arrow in the upper rows. Arrowheads indicate actin dynamics at the spine base. Note that time intervals change within the panel as indicated. Full time-lapse recordings of both examples can be found in Supplementary Video S7. **E.** Maximum projection of the MT+TIP channel (upper) and a projection of the SD of the Lifeact signal to highlight actin dynamics (bottom). Scale bar, $2 \mu\text{m}$. **F.** Schematic representation of the regions of interest (ROIs) used in the quantification of actin and MT+TIP comets signals (left). **G.** Measurements of actin and MT+TIP signals of two targeted (examples from **D**) and two non-targeted spines. Curves represent the mean signal intensities measured in the ROIs at the spine base or spine base and neck. Asterisks indicate microtubules entering spines, while circles depict comets that passed by in the shaft. **H.** Schematic diagram of the quantification of microtubule entries in correlation with actin dynamics at the spine base. Correlation was considered positive when increased actin dynamics coincide in a window of 1 min before the microtubule enters the spine. Spines: $n = 42$ of 21 dendrites from two preparations. **I.** Summary of findings: Synaptic activation induces actin reorganization at the spine base, which increases the chance for a nearby microtubule to enter the activated spine.

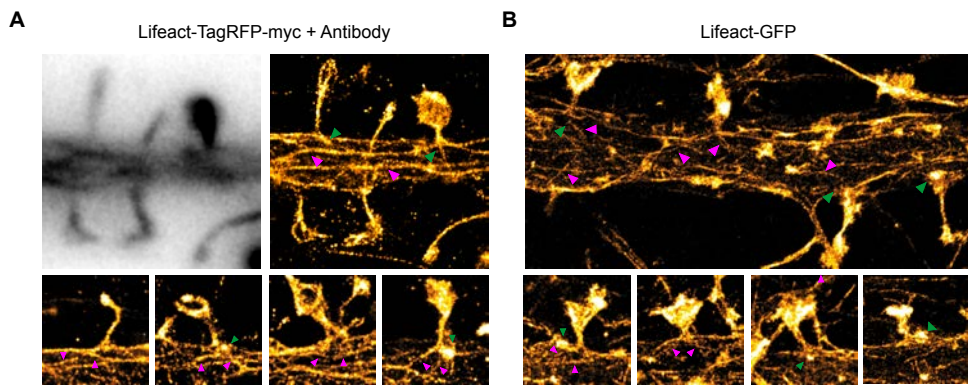


Figure 6. Super-resolution imaging of actin in dendrites

A. Lentivirus infected neurons expressing Lifact-TagRFP-Myc were fixed and stained against the with Myc-tag with a primary and a secondary Alexa647 antibody. Top panel shows a diffraction limited and a dSTORM reconstruction of the dendritic shaft and spines. Bottom panels shows more examples of actin structures individual spines. Green arrowheads point on examples of actin structures at the spine base; Magenta arrowheads indicate actin cables. **B.** Untreated neuron cultures were fixed and imaged through transient binding of purified Lifact-GFP. Regions of interest were identified through sparse labelling with Phalloidin 568. Top panel shows a dSTORM reconstruction of the dendritic shaft and spines. Bottom panels shows more examples of actin structures individual spines. Green arrowheads point on examples of actin structures at the spine base; Magenta arrowheads indicate actin cables. Scale bar: $1 \mu\text{m}$.

findings demonstrate that microtubule entry in spines is not a transient event during neuronal development, but that it is very common and even the default pathway for terminating dendritic microtubule growth in mature neurons. We found that more than 40% of the microtubule catastrophes is directly associated with entries in spines. Anterograde or retrograde growing microtubules did not show differences in spine entry probabilities, indicating that the polarity of microtubules in dendrites is not a determinant factor for the targeting of dendritic spines.

Previous studies in dissociated neurons suggested a regulatory effect of synaptic activity on microtubule spine entry (Kapitein *et al.*, 2011; Merriam *et al.*, 2011; Merriam *et al.*, 2013). To investigate whether synaptic activity correlates with microtubule spine entry at the level of individual spines, we applied pharmacological treatments that modulate the pattern of synaptic activation in hippocampal slice cultures and analyzed microtubule dynamics in spines. We found that microtubule spine entry frequency was strongly increased following a cLTP protocol which ultimately increases intracellular calcium levels. In addition, using glutamate uncaging in neuron cultures we showed direct evidence for a coupling between NMDAR-dependent synaptic activation and increased microtubule targeting on the level of single spines. Together, these data indicate that dynamic microtubules preferentially target dendritic spines that have recently experienced NMDAR-mediated calcium influx.

Local actin remodeling links synaptic activity and microtubule spine entry

Calcium influx through NMDA receptors has been shown to alter the actin dynamics within dendritic spines (Hotulainen and Hoogenraad, 2010). Previous findings suggested that the microtubule plus-end binding protein EB3 is involved in dendritic spine entries through the interaction of microtubule actin-associated protein Drebrin (Merriam *et al.*, 2013). These conclusions are largely based on Drebrin overexpression experiments, where increased levels of Drebrin increase microtubule invasion frequency and the number of spines invaded by microtubules (Merriam *et al.*, 2013). EB proteins interact via their acidic C-terminal tail region with SxIP motif containing proteins (Akhmanova and Hoogenraad, 2015). Our data indicate that knockdown of EB3 can be rescued by an EB3 construct lacking the C-terminal SxIP binding site. These results suggest that SxIP-mediated interactions between microtubule plus-ends and components of the actin cytoskeleton are not required for microtubule spine targeting. Super resolution microscopy imaging revealed that actin filaments at the spine base extend throughout the dendritic shaft. Consistent with microtubule-actin cooperation in various other cellular processes (Rodriguez *et al.*, 2003), it is possible that the actin filaments directly guide the entry of microtubules in dendritic spines. Therefore, we propose a model in which structural changes in the actin cytoskeleton at the base of the spine are involved with microtubule entry through steric interactions, rather than specific protein-protein interactions. In this way, activity-dependent remodeling of the actin cytoskeleton at the base of the spine may allow for regulated microtubule targeting. An increase in actin dynamics at the spine base has also been observed using glutamate uncaging combined with actin photoactivation (Honkura *et al.*, 2008). In approximately half of the stimulated spines, an outflow of actin and release of actin filaments from the spine head into the dendritic shaft have been observed (Honkura *et al.*, 2008). This is consistent with the data that the activity-dependent redistribution of cortactin (Hering and Sheng, 2003; Iki *et al.*, 2005; Seese *et al.*, 2012) may be involved in local actin remodelling and facilitating microtubule spine entries. Together our data show that dynamic microtubules preferentially target spines that are undergoing actin reorganization in an activity-regulated manner.

ACKNOWLEDGMENTS

P.S. was supported by postdoctoral fellowships from the Marie-Curie Program (grant 326425) and the Swiss National Science Foundation (PBZHP3_147307). M.E.d.S. is supported by Fundação para a Ciência e Tecnologia (FCT, Portugal; grant SFRH/BD/68642/2010). This work was further supported by the Netherlands Organization for Scientific Research (NWO-ALW-VICI, CCH; NWO ZonMW-VIDI, CJW and HYH), the Netherlands Organization for Health Research and Development (ZonMW-TOP, CCH), the European Research Council (ERC) (ERC-consolidator, CCH).

AUTHOR CONTRIBUTIONS

P.S. designed and performed the live cell imaging experiments and analyzed the data; M.E.d.S. performed lentiviral transduction of neuronal cultures and live cell imaging experiments; R.T prepped purified Lifeact-GFP and performed super resolution of actin structures in the dendrites; H.Y.H. assisted with the uncaging experiments. C.J.W. provided critical input for experimental design and data analysis. C.C.H. supervised the project and coordinated the study; P.S. and C.C.H wrote the manuscript with comments by all other authors.

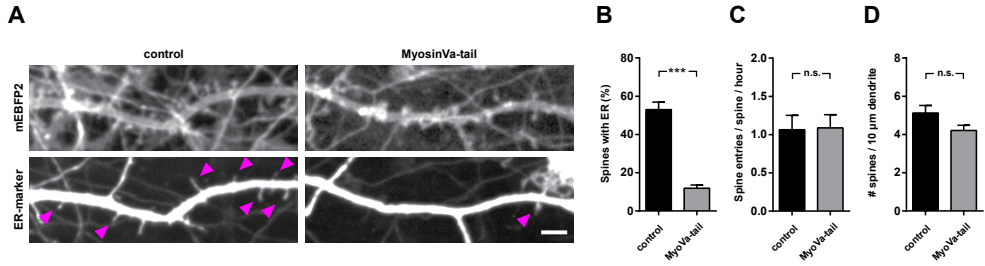
REFERENCES

- Akhmanova, A., and Hoogenraad, C.C. (2015). Microtubule minus-end-targeting proteins. *Current biology* : CB 25, R162-171.
- Akhmanova, A., and Steinmetz, M.O. (2008). Tracking the ends: a dynamic protein network controls the fate of microtubule tips. *Nature reviews Molecular cell biology* 9, 309-322.
- Calabrese, B., and Halpain, S. (2005). Essential role for the PKC target MARCKS in maintaining dendritic spine morphology. *Neuron* 48, 77-90.
- Correia, S.S., Bassani, S., Brown, T.C., Lise, M.F., Backos, D.S., El-Husseini, A., Passafaro, M., and Esteban, J.A. (2008). Motor protein-dependent transport of AMPA receptors into spines during long-term potentiation. *Nature neuroscience* 11, 457-466.
- De Roo, M., Klauser, P., and Muller, D. (2008). LTP promotes a selective long-term stabilization and clustering of dendritic spines. *PLoS biology* 6, e219.
- Esteves da Silva, M., Adrian, M., Schatzle, P., Lipka, J., Watanabe, T., Cho, S., Futai, K., Wierenga, C.J., Kapitein, L.C., and Hoogenraad, C.C. (2015). Positioning of AMPA Receptor-Containing Endosomes Regulates Synapse Architecture. *Cell reports* 13, 933-943.
- Fernandez de Sevilla, D., Nunez, A., Borde, M., Malinow, R., and Buno, W. (2008). Cholinergic-mediated IP₃-receptor activation induces long-lasting synaptic enhancement in CA1 pyramidal neurons. *The Journal of neuroscience : the official journal of the Society for Neuroscience* 28, 1469-1478.
- Fischer, M., Kaeck, S., Knutti, D., and Matus, A. (1998). Rapid actin-based plasticity in dendritic spines. *Neuron* 20, 847-854.
- Geraldo, S., Khanzada, U.K., Parsons, M., Chilton, J.K., and Gordon-Weeks, P.R. (2008). Targeting of the F-actin-binding protein drebrin by the microtubule plus-tip protein EB3 is required for neuritogenesis. *Nature cell biology* 10, 1181-1189.
- Grigoriev, I., Gouveia, S.M., van der Vaart, B., Demmers, J., Smyth, J.T., Honnappa, S., Splinter, D., Steinmetz, M.O., Putney, J.W., Jr., Hoogenraad, C.C., et al. (2008). STIM1 is a MT-plus-end-tracking protein involved in remodeling of the ER. *Current biology* : CB 18, 177-182.
- Hering, H., and Sheng, M. (2003). Activity-dependent redistribution and essential role of cortactin in dendritic spine morphogenesis. *J Neurosci* 23, 11759-11769.
- Holbro, N., Grunditz, A., and Oertner, T.G. (2009). Differential distribution of endoplasmic reticulum controls metabotropic signaling and plasticity at hippocampal synapses. *Proceedings of the National*

- Academy of Sciences of the United States of America 106, 15055-15060.
- Honkura, N., Matsuzaki, M., Noguchi, J., Ellis-Davies, G.C., and Kasai, H. (2008). The subspine organization of actin fibers regulates the structure and plasticity of dendritic spines. *Neuron* 57, 719-729.
- Hotulainen, P., and Hoogenraad, C.C. (2010). Actin in dendritic spines: connecting dynamics to function. *The Journal of cell biology* 189, 619-629.
- Hu, X., Ballo, L., Pietila, L., Viesselmann, C., Ballweg, J., Lombard, D., Stevenson, M., Merriam, E., and Dent, E.W. (2011). BDNF-induced increase of PSD-95 in dendritic spines requires dynamic microtubule invasions. *The Journal of neuroscience : the official journal of the Society for Neuroscience* 31, 15597-15603.
- Hu, X., Viesselmann, C., Nam, S., Merriam, E., and Dent, E.W. (2008). Activity-dependent dynamic microtubule invasion of dendritic spines. *The Journal of neuroscience : the official journal of the Society for Neuroscience* 28, 13094-13105.
- Iki, J., Inoue, A., Bito, H., and Okabe, S. (2005). Bi-directional regulation of postsynaptic cortactin distribution by BDNF and NMDA receptor activity. *The European journal of neuroscience* 22, 2985-2994.
- Jaworski, J., Kapitein, L.C., Gouveia, S.M., Dortland, B.R., Wulf, P.S., Grigoriev, I., Camera, P., Spangler, S.A., Di Stefano, P., Demmers, J., et al. (2009). Dynamic microtubules regulate dendritic spine morphology and synaptic plasticity. *Neuron* 61, 85-100.
- Kapitein, L.C., and Hoogenraad, C.C. (2015). Building the Neuronal Microtubule Cytoskeleton. *Neuron* 87, 492-506.
- Kapitein, L.C., Yau, K.W., Gouveia, S.M., van der Zwan, W.A., Wulf, P.S., Keijzer, N., Demmers, J., Jaworski, J., Akhmanova, A., and Hoogenraad, C.C. (2011). NMDA receptor activation suppresses microtubule growth and spine entry. *The Journal of neuroscience : the official journal of the Society for Neuroscience* 31, 8194-8209.
- Kiuchi, T., Higuchi, M., Takamura, A., Maruoka, M., and Watanabe, N. (2015). Multitarget super-resolution microscopy with high-density labeling by exchangeable probes. *Nature methods* 12, 743-746.
- Komarova, Y., Lansbergen, G., Galjart, N., Grosveld, F., Borisy, G.G., and Akhmanova, A. (2005). EB1 and EB3 control CLIP dissociation from the ends of growing microtubules. *Molecular biology of the cell* 16, 5334-5345.
- Korobova, F., and Svitkina, T. (2010). Molecular architecture of synaptic actin cytoskeleton in hippocampal neurons reveals a mechanism of dendritic spine morphogenesis. *Molecular biology of the cell* 21, 165-176.
- Leung, C.L., Sun, D., Zheng, M., Knowles, D.R., and Liem, R.K. (1999). Microtubule actin cross-linking factor (MACF): a hybrid of dystonin and dystrophin that can interact with the actin and microtubule cytoskeletons. *The Journal of cell biology* 147, 1275-1286.
- MacGillavry, H.D., Kerr, J.M., Kassner, J., Frost, N.A., and Blanpied, T.A. (2016). Shank-cortactin interactions control actin dynamics to maintain flexibility of neuronal spines and synapses. *The European journal of neuroscience* 43, 179-193.
- Matsuzaki, M., Honkura, N., Ellis-Davies, G.C., and Kasai, H. (2004). Structural basis of long-term potentiation in single dendritic spines. *Nature* 429, 761-766.
- McVicker, D.P., Awe, A.M., Richters, K.E., Wilson, R.L., Cowdrey, D.A., Hu, X., Chapman, E.R., and Dent, E.W. (2016). Transport of a kinesin-cargo pair along microtubules into dendritic spines undergoing synaptic plasticity. *Nature communications* 7, 12741.
- Merriam, E.B., Lombard, D.C., Viesselmann, C., Ballweg, J., Stevenson, M., Pietila, L., Hu, X., and Dent, E.W. (2011). Dynamic microtubules promote synaptic NMDA receptor-dependent spine enlargement. *PloS one* 6, e27688.
- Merriam, E.B., Millette, M., Lombard, D.C., Saengsawang, W., Fothergill, T., Hu, X., Ferhat, L., and Dent, E.W. (2013). Synaptic regulation of microtubule dynamics in dendritic spines by calcium, F-actin, and drebrin. *The Journal of neuroscience : the official journal of the Society for Neuroscience* 33, 16471-16482.
- Mikhaylova, M., Cloin, B.M., Finan, K., van den Berg, R., Teeuw, J., Kijanka, M.M., Sokolowski, M., Katrukha, E.A., Maidorn, M., Opazo, F., et al. (2015). Resolving bundled microtubules using anti-tubulin nanobodies. *Nature communications* 6, 7933.
- Rex, C.S., Gavin, C.F., Rubio, M.D., Kramar, E.A., Chen, L.Y., Jia, Y., Hugarir, R.L., Muzyczka, N., Gall, C.M., Miller, C.A., et al. (2010). Myosin IIb regulates actin dynamics during synaptic plasticity and memory formation. *Neuron* 67, 603-617.
- Riedl, J., Crevenna, A.H., Kessenbrock, K., Yu, J.H., Neukirchen, D., Bista, M., Bradke, F., Jenne, D., Holak, T.A., Werb, Z., et al. (2008). Lifeact: a

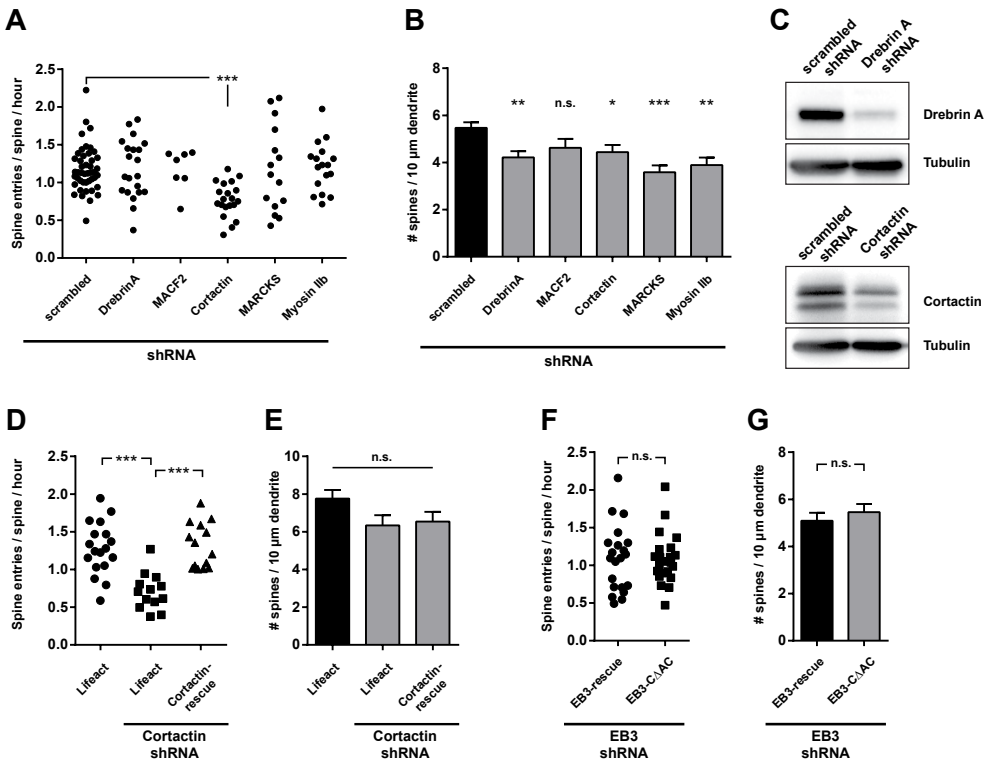
- versatile marker to visualize F-actin. *Nat Methods* 5, 605-607.
- Rodriguez, O.C., Schaefer, A.W., Mandato, C.A., Forscher, P., Bement, W.M., and Waterman-Storer, C.M. (2003). Conserved microtubule-actin interactions in cell movement and morphogenesis. *Nature cell biology* 5, 599-609.
- Ross, W.N. (2012). Understanding calcium waves and sparks in central neurons. *Nature reviews Neuroscience* 13, 157-168.
- Schatzle, P., Kapitein, L.C., and Hoogenraad, C.C. (2016). Live imaging of microtubule dynamics in organotypic hippocampal slice cultures. *Methods in cell biology* 131, 107-126.
- Seese, R.R., Babayan, A.H., Katz, A.M., Cox, C.D., Lauterborn, J.C., Lynch, G., and Gall, C.M. (2012). LTP induction translocates cortactin at distant synapses in wild-type but not Fmr1 knock-out mice. *The Journal of neuroscience : the official journal of the Society for Neuroscience* 32, 7403-7413.
- Stepanova, T., Slemmer, J., Hoogenraad, C.C., Lansbergen, G., Dortland, B., De Zeeuw, C.I., Grosveld, F., van Cappellen, G., Akhmanova, A., and Galjart, N. (2003). Visualization of microtubule growth in cultured neurons via the use of EB3-GFP (end-binding protein 3-green fluorescent protein). *The Journal of neuroscience : the official journal of the Society for Neuroscience* 23, 2655-2664.
- Szymczak-Workman, A.L., Vignali, K.M., and Vignali, D.A. (2012). Design and construction of 2A peptide-linked multicistronic vectors. *Cold Spring Harb Protoc* 2012, 199-204.
- van Beuningen, S.F., Will, L., Harterink, M., Chazneau, A., van Battum, E.Y., Frias, C.P., Franker, M.A., Katrukha, E.A., Stucchi, R., Vocking, K., et al. (2015). TRIM46 Controls Neuronal Polarity and Axon Specification by Driving the Formation of Parallel Microtubule Arrays. *Neuron* 88, 1208-1226.
- Wagner, W., Brenowitz, S.D., and Hammer, J.A., 3rd (2011). Myosin-Va transports the endoplasmic reticulum into the dendritic spines of Purkinje neurons. *Nature cell biology* 13, 40-48.
- Wang, Z., Edwards, J.G., Riley, N., Provance, D.W., Jr., Karcher, R., Li, X.D., Davison, I.G., Ikebe, M., Mercer, J.A., Kauer, J.A., et al. (2008). Myosin Vb mobilizes recycling endosomes and AMPA receptors for postsynaptic plasticity. *Cell* 135, 535-548.
- Yau, K.W., Schatzle, P., Tortosa, E., Pages, S., Holtmaat, A., Kapitein, L.C., and Hoogenraad, C.C. (2016). Dendrites *In Vitro* and *In Vivo* Contain Microtubules of Opposite Polarity and Axon Formation Correlates with Uniform Plus-End-Out Microtubule Orientation. *The Journal of neuroscience : the official journal of the Society for Neuroscience* 36, 1071-1085.
- Yau, K.W., van Beuningen, S.F., Cunha-Ferreira, I., Cloin, B.M., van Battum, E.Y., Will, L., Schatzle, P., Tas, R.P., van Krugten, J., Katrukha, E.A., et al. (2014). Microtubule minus-end binding protein CAMSAP2 controls axon specification and dendrite development. *Neuron* 82, 1058-1073.

SUPPLEMENTARY FIGURES



Supplementary Figure S1. ER structures do not guide microtubules into spines

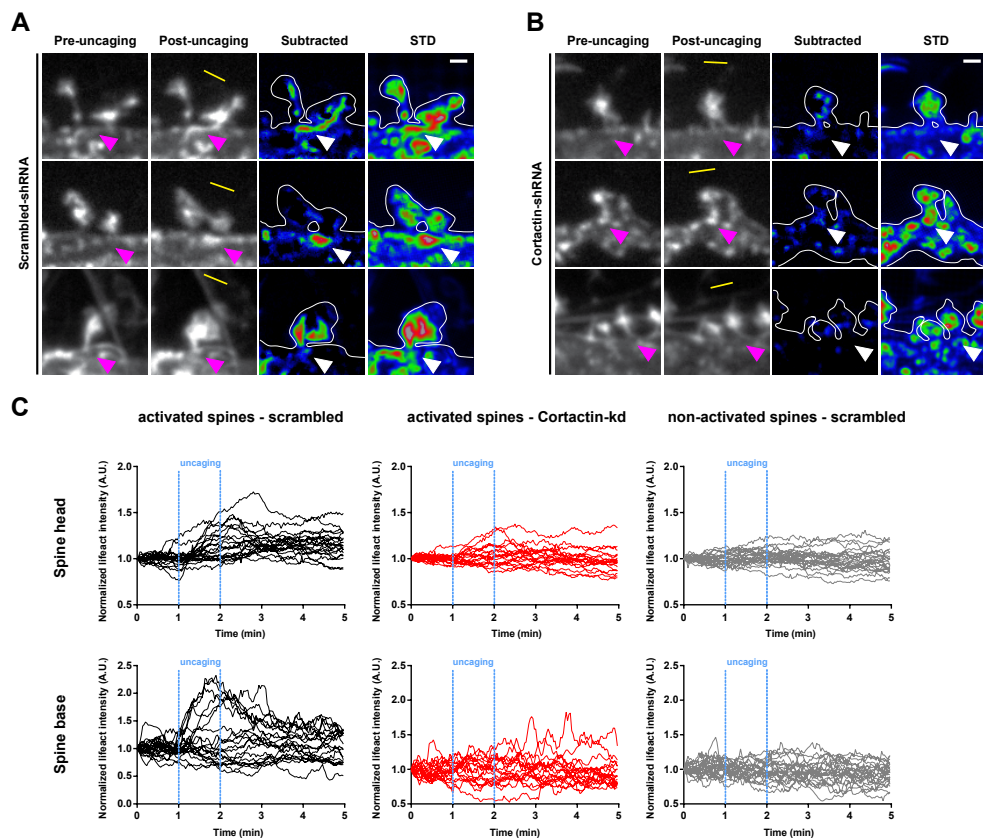
A. Neuron cultures were double infected with virus expressing a marker of ER and MT+TIP, as well as mEBFP2 (control) or mEBFP2 and MyosinVa-tail (dominant negative construct). **B.** Quantification of ER positive spines for both conditions. **C.** Spine entry frequencies were quantified based on MT+TIP signals. **D.** Spine density quantification. *** $p < 0.0001$ all others not significant, unpaired t-test; control: $n = 12$, MyosinVa-tail: $n = 15$ dendrites. Scale bars, 5 μ m. Bars diagrams show mean + SEM.



Supplementary Figure S2. Knockdown of microtubule-actin interactors

A. Spine entry frequencies after depletion of candidate proteins potentially mediating microtubule invasions in spines. Each data point shows the spine entries for an individual recorded dendrite. Average values for each condition are identical to the bar diagram shown in Fig.4E. **B.** Effects of the depletion of actin interactors on spine density.

* $p < 0.05$, ** $p < 0.01$, *** $p < 0.001$, n.s. = not significant, one-way ANOVA with posthoc Dunnett's test. **C.** Efficiency of lentivirus induced shRNA knockdown for DrebrinA (upper) and cortactin (lower) by Western Blot. The reduction of signal intensities compared to controls and normalized to the Tubulin signals were as follows: DrebrinA: = 15% and cortactin: = 47% remaining signal after 8 days. **D.** Individual experiments for the cortactin-rescue experiments from Fig.4F. **E.** Quantification of spine density in control, knockdown and cortactin-rescue conditions (8 days of knockdown). While the expression of cortactin-rescue restores microtubule entries in spines it does not recover the loss in spine numbers. One-way ANOVA. **F.** Individual experiments for the EB3-rescue experiments from Fig.4G. **G.** Spine density does not vary between the used EB3-rescue constructs. Unpaired t-test. Bars diagrams show mean + SEM.



Supplementary Figure S3. Knockdown of microtubule-actin interactors

A,B. Additional examples of glutamate uncaging-induced actin dynamics in spines for control (**A**) and cortactin knockdown (**B**). The first two columns show still frames before and after uncaging. Next, subtraction of the pre- from the post-uncaging Lifect signals to visualize the increases in fluorescence intensity. Right column is a projection of the Lifect signal SD over the full 5 min recording to visualize hot spots of actin dynamics. Arrowheads point on the same position at the base of a spine. Scale bar, 1 μ m. Full length videos of these and the example in Fig.5A are shown in Supplementary Video S6. **C.** Single traces of mean intensities in spine heads (upper panel) and base (lower panel) for all quantified spines. Scrambled activated: n = 20 spines, cortactin activated: n = 19 spines, scrambled non-activated: n = 22 spines.

SUPPLEMENTARY VIDEOS

Supplementary Video S1. MCh stimulation in slice cultures (refers to Fig.2B)

Time-lapse recording of MT+TIP marker and mTagRFP in a hippocampal organotypic slice culture. The granule cell was infected with lentivirus and the same neuron is shown before and after stimulation with methacholine. MT+TIP comets were imaged with 5 sec intervals (middle), while mTagRFP was recorded only for every 5th frame (right). The left side shows a maximum projection of the MT+TIP recording to better localize spine entries. Dashed box marks the dendritic region shown in Fig.2B. Time runs as indicated with 20 fps. Spine entry frequency strongly increased after stimulation with methacholine.

Supplementary Video S2. Local spine stimulation with glutamate uncaging (refers to Fig.3D)

Example dendrite of a dissociated neuron expressing mTagRFP during photoactivation. The uncaging laser was targeted to the white line and is active with appearance of the asterisk. Spines in close proximity to the uncaging region respond with morphological changes, while more distant spines are not affected. Time-lapse was recorded at 2 s intervals and is identical to the example shown in Fig.3D.

Supplementary Video S3. Activated spines are more frequently targeted by microtubules (refers to Fig.3D)

Same dendrite as in Video 2 recorded for MT+TIP and mTagRFP. Images were taken at 5 s intervals and time-lapse started directly after the uncaging session. Arrowhead highlights spines targeted by dynamic microtubules.

Supplementary Video S4. Glutamate uncaging combined with calcium imaging (refers to Fig.3I)

Two dendrites from the same dissociated neuron expressing Lifeact-GCaMP6s. Uncaging starts at the white line with appearance of the asterisk. The left side represents the sum projection of the recorded GCaMP6s signals shown in Fig 3I.

Supplementary Video S5. Spines with elevated calcium are preferentially targeted by microtubules (refers to Fig.3I)

Same dendrite as in Video 4 imaged for MT+TIP right after the photostimulation was finished. Comet signals were improved using a running average subtraction and low-pass filtering. Dendritic outline was drawn based on a maximum projection of the calcium signals during uncaging. Spines receiving microtubule entries and being classified as activated were labeled with magenta arrowheads, while white arrowheads indicate non-activated spines.

Supplementary Video S6. Actin dynamics induced by synaptic activation (refers to Fig.5A)

Individual spines expressing Lifeact-TagRFP were recorded during uncaging of glutamate in neuron cultures co-expressing scrambled shRNA (upper panel) or cortactin shRNA (lower panel). First spines on the left side represent the examples shown in Fig.5A. The appearance of asterisks indicate the time of uncaging and white lines mark the regions of photoactivation. Spines were imaged with 2 s intervals in the presence of TTX. The transient increase of actin dynamics in spine head and base is considerably reduced in cortactin knockdown conditions.

Supplementary Video S7. Actin dynamics induced by synaptic activation (refers to Fig.5D)

Full time sequences of the MT+TIP and Lifeact imaging shown in Fig.5D. The orange asterisks in the Lifeact channel appear 1 min before a microtubule comet enters the spine and turn red during the invasion period. Images were acquired at 5 s intervals in sequential mode. Increased actin dynamics at the base of the spines precede the invasion of microtubules in spines.

EXPERIMENTAL METHODS

Animals

All experiments with animals were performed in compliance with the guidelines for the welfare of experimental animals issued by the Government of The Netherlands, and were approved by the Animal Ethical Review Committee (DEC) of the Utrecht University.

DNA plasmids and lentivirus

Fluorescently tagged constructs. Membrane-targeted TagRFP-T (mTagRFP, generated from N-terminal first 41 amino acids of MARCKS) and the microtubule plus-tip marker (MT+TIP) GFP-MACF18 have been described previously (Schatzle *et al.*, 2016). Tomato-MACF18 is identical to GFP-MACF18 except for the replacement of GFP by tandem dimer Tomato. Lifeact-TagRFP-Myc was PCR generated by cloning the 17 amino acid (aa) Lifeact sequence (Riedl *et al.*, 2008) linked by a 7 aa linker (GDPPVAT) to the N-terminus of TagRFP-T (Evrogen). The TagRFP-T stop codon was replaced by a 4 aa linker (SSGS) followed by the 10 aa Myc sequence. Lifeact-GCaMP6s was based on the pGP-CMV-GCaMP6s (addgene #40753) vector. The start codon within this construct was replaced by the Lifeact sequence by a PCR based strategy. The TagRFP-ER construct is composed of the 17 amino acid rat calreticulin signal sequence fused to the N-term of TagRFP-T and a C-terminally located ER retention signal (KDEL). GFP-EB3-ΔAc and GFP-EB3-rescue constructs are identical to our previous publication (Jaworski *et al.*, 2009). Membrane-targeted EBFP2-HA was generated with a cryptic splice site corrected version of EBFP2 containing a C-terminal HA-tag. Cortactin-dsRed (MacGillavry *et al.*, 2016) was made shRNA resistant by introducing silent mutations in the target sequence using a PCR based strategy (GCATTGCTCTCAGGTGGAT).

Bicistronic expression constructs were generated based on the attenuated IRES site, derived from pIRES (Clontech). This design allows high expression of the coding sequence upstream of the IRES site and relative low expression of the inserted downstream construct. The following plasmids were generated by conventional cloning strategies: mTagRFP_IRES_GFP-MACF18, mTagRFP_IRES_GFP-EB3-rescue, mTagRFP_IRES_GFP-EB3-ΔAc, Lifeact-TagRFP-Myc_IRES_GFP-MACF18, Lifeact-GCaMP6s_IRES_Tomato-MACF18, TagRFP-ER_IRES_GFP-MACF18, Cortactin-dsRed_IRES_GFP-MACF18. Equal expression of two constructs was achieved in the mEBFP2-HA_P2A_Myc-MyoVa-tail construct by using the 2A sequence of the porcine teschovirus-1 (Szymczak-Workman *et al.*, 2012).

Lentiviral transfer vectors are based on the pSIN-TRE-MCS-Synapsin-rTA2 plasmid (Schatzle *et al.*, 2016). The bicistronic expression cassettes described above were subcloned in the multiple cloning site resulting in a TET-On inducible expression of the target proteins. Sequence information of all constructs can be provided on request.

RNAi-induced knockdown of target genes by lentivirus was based on a modified pLVTHM (addgene #12247) vector. The original EF-1α promoter and GFP sequences were replaced by a central polypurine tract/central termination sequence (cPPT/CTS), followed by a short 0.5kb Synapsin promoter and mEBFP2-HA. Individual shRNA sequences were subcloned from the original pSuper vectors via BamHI and ClaI sites. Following shRNA target sequences were used: scrambled GGTTTATATCGCGTTATT, Cortactin GCACTGCTCACAAGTGGAC (Hering and Sheng, 2003), DrebrinA GAGAACCAGAAAGTGATGTAC (Geraldo *et al.*, 2008), EB3 ACTATGATGGAAGGATTAC (Komarova *et al.*, 2005), MACF2 GCCGTGGTCAGAGTTGCTGAT, MARCKS CTGTACCAGTCAGTAATTA (Calabrese and Halpain, 2005), Myosin IIb GATCAAAGTTGGCCGAGAT (Rex *et al.*, 2010).

Lentiviral particles were generated by transfecting the transfer plasmid together with the packaging plasmids p.MDG2 (addgene #12259) and psPAX (addgene #12260) in HEK293T cells. Detailed information about the lentivirus production has been described elsewhere (Schatzle *et al.*, 2016).

Cell/tissue cultures and viral transduction

Neuron cultures. High density hippocampal cultures on coverslips were prepared as described elsewhere (Yau *et al.*, 2016). Experiments were performed with mature neuron cultures ranging from DIV 25-45, except for the analysis of spine entry frequencies in DIV18 neurons. Cultures were fed weekly by replacing 1/3 of the medium with fresh neuron culture medium (Neurobasal medium supplemented with 2% B27, 0.5 mM glutamine, and 1% penicillin/streptomycin (all from Gibco)). Lentiviral infections were carried out 8-14 days before experiments and protein expression was induced 2-4 days prior imaging. All infections with shRNA containing virus were carried out 8-9 days before experiments. Dendrites in knockdown experiments were routinely checked for clear mEBFP2 signals, confirming the infection with shRNA virus, before starting the actual experiments.

Organotypic slice cultures. Hippocampal interface slice cultures were generated from P5-6 mice pups and infected with lentivirus within 2 hours after plating. Detailed information about slice preparation and viral transduction has been published recently (Schatzle *et al.*, 2016). Experiments were made with slices kept for 2-4 weeks in culture.

Pharmacological treatments

Neurons. 1st imaging session was performed in the original neuron culture medium. For the 2nd recording session Jasplakinolide (10 μM) or Latrunculin B (1 μM) were diluted in 100 μl culture medium, transferred into the recording chamber and incubated for 30 min before starting of the recording.

Slices. 1st imaging session in ACSF (126 mM NaCl, 3 mM KCl, 2.5 mM CaCl_2 , 1.3 mM MgCl_2 , 1.25 mM Na_2HPO_4 , 26 mM NaHCO_3 , 20 mM glucose, and 1 mM Trolox (Sigma, 238813)). All drugs were diluted in ACSF and applied using following protocols: Control application: 0.1% DMSO incubated for 30min before the start of the 2nd recording session; TTX: 1 μM tetrodotoxin incubated for 30 min before the start of the 2nd recording; PTX: 100 μM picrotoxin incubated for 30 min before the start of the 2nd recording; DHPG: 50 μM dihydroxyphenylglycine incubated for 5 min + 5 min washout before the start of the 2nd recording; MCh: 25 μM methacholine incubated for 15 min + 15 min washout before the start of the 2nd recording; MCh + TTX: 10 min preincubation of 1 μM TTX + 25 μM MCh & 1 μM TTX incubated for 15 min + 15 min washout before the start of the 2nd recording; MCh + LatB: 15 min preincubation of 10 μM latrunculin B + 25 μM MCh & 10 μM LatB incubated for 15 min + washout in the presence of LatB + 15 min incubation in ACSF before the start of the 2nd recording; Jasp: 10 μM jasplakinolide incubated for 20 min before the start of the 2nd recording. Drugs were purchased from Abcam (TTX), Bio-Connect (Latrunculin B), Sigma (Methacholine, NMDA), Tocris (APV, jasplakinolide, MNI-Glutamate, Picrotoxin).

Live-cell imaging

Spinning-disk confocal microscopy was performed on an inverted Nikon Eclipse Ti with a Perfect Focus System. Glutamate uncaging experiments were imaged with a S Fluor 100 \times , 0.5–1.3 NA oil, all other neuron cultures with Plan Fluor 40 \times , 1.3 NA oil-immersion objective; slice cultures with a CFI Apo Lambda S LWD 40 \times , 1.15 NA water-immersion objective (all Nikon). The Yokogawa spinning disk confocal scanning unit (CSU-X1-A1NeE) is equipped with a triple-band dichroic mirror (z405/488/568trans-pc; Chroma) and a filter wheel (CSU-X1-FW-06P-01; Yokogawa) containing ET-BFP2 (49021), ET-GFP (49002), ET-mCherry (49008) emission filters from Chroma. Excitation is based on Vortran Stradus 405 nm (100 mW), Cobolt Calypso 491 nm (100 mW) and Cobolt Jive 561 nm (100 mW) lasers, photoactivation on a Teem Photonics 355 nm Q-switched pulsed laser. The UV laser light is controlled by the Ilas-2 system (Roper Scientific, France) and is tunable in intensity via an AOTF filter. Images were acquired in sequential mode with a Photometrics Evolve 512 EMCCD camera equipped with an additional 2.0 \times lens (Edmund Optics) resulting in a final resolution of 66nm/pixel. Neuron and slice cultures were imaged in a Ludin chamber (LIS, Switzerland), positioned in a Tokai Hit Stage Top Incubator (INUBG2E-ZILCS), which is mounted on a ASI motorized stage MS-2000-XYZ enabling multi-position imaging. The camera, lasers and all motorized parts are controlled by MetaMorph software.

Imaging of microtubule entries in spines and actin dynamics. Neuron cultures were imaged in full conditioned medium at 37°C and 5% CO_2 with 5 sec intervals and z-stacks of 0.7 μm step sizes (4–7 depending on the z orientation of the dendrite). Slices were recorded with the same settings except for a continuous perfusion with ACSF (oxygenated with 95% O_2 , 5% CO_2).

Local NMDA application. Dissociated neurons were silenced with 1 μM TTX for 14–18 hours prior recording. MT+TIP comets were recorded for 4 min at 5 sec intervals and mTagRFP only every 5th frame in the original culture medium. Puff-applications of 10 mM NMDA through a patch pipette were applied for 2 \times 50 ms (with a 10 sec break) using a picrospritzer. The second imaging session was started 1 min after the second application with the same settings as in the first recording.

Glutamate uncaging. Neurons were imaged at 2 sec intervals with 4 \times 0.8 μm z-stacks in modified Tyrod's buffer + 1 μM TTX (119 mM NaCl, 5 mM KCl, 2 mM CaCl_2 , 10 mM HEPES and 10 mM glucose; pH 7.25 and osmolarity adjusted with glucose to 0.265 mOsm). MNI-glutamate (0.5 mM) was added in 100 μl buffer to the darkened recording chamber on the microscope stage. Uncaging regions were defined as lines with about 2 μm in length and a distance of 1–1.5 μm to the spine head. The uncaging pulse lasted for 3–4 ms and preceded the actual recording. Several time points were recorded before and after the uncaging session (0.5 Hz for 1 min) to compare results. The laser power was adjusted to activate around 30% of the imaged spines, except for the uncaging experiments in combination with cortactin knockdown (Fig.4H,I), where a slightly stronger activation stimulus was used. Note that results recorded from different dendrites on the same coverslip sometimes varied in their response to the uncaging stimulus, which probably represent artefacts of the single-photon uncaging as for instance light scattering by dense structures in the neuron cultures. Unusual recordings were excluded from the quantification. The intensity of the

uncaging laser is sufficient to bleach mTagRFP signals within a few frames if the uncaging region is directly targeted on the spine head (not shown). Because we never observe bleaching in our uncaging experiments we conclude together with our control experiments in Fig.3C that the observed morphological changes of spines were not an artifact of light stress. The dependence on NMDA receptor activation was tested by uncaging glutamate in the presence of 150 μ M DL-2-amino-5-phosphopentanoic acid (APV).

Lifeact-GFP cloning and purification

The full Codon optimized Lifeact fragment was inserted through PCR into a pET28a vector containing an EcoRI/XhoI flanked GFP sequence. The full vector was amplified with the lifeAct fragment and the template was digested with DPN1. The resulting construct was transformed in *E.coli* BL21DE3 and sequenced.

LifeAct-GFP-6xHis was purified using standard His-tag purification methods. Bacteria were induced at OD 0.6 for overnight expression at 20 °C. After pelleting the cells were lysed through sonication in the presence of lysozyme and a protease inhibitor cocktail (Roche). The soluble fraction was filtered and bound to a His-Trap HP 1 ml column (GE healthcare). Elution was performed on an AKTExpress (GE healthcare). After buffer exchange to PBS the pure protein sample was frozen in 10% glycerol.

Super resolution imaging

For super resolution imaging of lentivirus infected neurons expressing Lifeact-TagRFP-Myc, Div18+ neurons were fixed with 4% PFA. After fixation cells were washed and permeabilized with 0.25% triton-X in PBS. After 3 washes the samples were blocked (2% BSA/ 0.2% Gelatin/ 10mM Glycin, 50mM NH₄Cl, pH 7.4) for 1 hour at room temperature. Cells were incubated overnight at 4°C with a combination of two mouse anti-myc primary antibodies (Santa Cruz; 9E10 and Oncogene; AB-1 both diluted 1:400). After three more washes in PBS the cells were incubated with secondary anti-mouse Alexa647 for 1 hour at room temperature and washed 3 more times. Super resolution imaging was then performed in on the setup in buffer optimal for Alexa 647 as described before (van Beuningen *et al.*, 2015; Yau *et al.*, 2014).

To perform super resolution of actin by transient binding of diffusing Lifeact-GFP, cells were first extracted in 0.25% Triton-x in CB (10 mM MES, 150 mM NaCl, 5mM MgCl₂, 5mM EGTA, 5mM Glucose, pH6.1) for 1 minute at 37 °C. Cells were fixed in 4% PFA + 0.25% Triton-x in CB at 37 °C, washed 3 times and blocked in 3% BSA for 30 minutes. To visualize regions for imaging cells were mildly stained with Phalloidin 568 (Life Technologies, 1/1000). After 3 thorough washes in PBS cells were mounted in PBS supplemented with low concentrations of LifeAct-GFP so that transient single molecule binding could be observed with 150 ms exposure time. Images were reconstructed using DoM Utrecht (Detection of Molecules, https://github.com/ekatruxha/DoM_Utrecht) (Mikhaylova *et al.*, 2015).

Image processing and quantifications

The four dimensional time-lapse data was reduced in complexity by generating average z-stack projections before additional image processing and quantifications were performed in FIJI. Time-lapse recordings were corrected for x-y drifts using the MultiStackReg plugin whenever required. Curved dendrites in Fig.1J, Fig.3D.E and Supplementary videos S2,S3 were straightened because of space limitations or for better illustration using the “Straighten” plugin.

Quantification of spine entries. Time-lapse recordings of MT+TIP comets were processed with a moving average subtraction and additional low pass filtering to amplify comet signals (Schatzle *et al.*, 2016). Spine entries were manually identified based on maximum intensity projections of the processed data and visually confirmed in the movies. Spine entry frequency is presented as “Spine entries / spine / hour” in order to compensate for variations in recording time and spine density between dendrites. Multiple targeting of the same spine within short time intervals is often caused by alternating catastrophe and rescue events of the same microtubule. Because we rather focused on the microtubule targeting mechanism than on the functional consequences for the spines, we counted multiple spine targeting as a single event if the imaging data did not clearly indicate independent microtubules as the source of multiple invasions.

Quantification of MT+TIP comet properties. Kymographs were generated from average subtracted and low pass filtered MT+TIP recordings using the FIJI “KymoResliceWide” plugin. The “Cell Counter” plugin was used to label the start and end points of individual microtubule traces. All coordinates were exported to Matlab and used to calculate microtubule density, orientation and length. It is important to state that a substantial proportion of microtubule traces crossed the observation limits in space or time. Therefore, our analysis underestimates the

actual length of some of the microtubule traces before entering a spine, which should be kept in mind for a correct interpretation of the results presented in Fig.1E,F.

Correlation analysis of spine entries and catastrophes. Time-lapse recordings were processed as in the previous section with the exception that curved dendrites were additionally straightened using the corresponding function in FIJI. All endings of microtubule traces in the kymograph were visually verified in the videos for coincidental spine entries.

Spine size changes following glutamate uncaging. Recordings of mTagRFP were bleach corrected (exponential fit method) and thresholded (percentile method). ROIs were defined around the heads of activated and distant non-activated spines. Areas corresponding to the spine head sizes were quantified over time using the “Analyze Particles” function. Data was normalized to the average spine size of the first 10 time points representing baseline conditions.

Quantification of actin signals at the spine head and base. Mean intensities of the Lifeact signals over time were quantified in manually defined regions of interest (ROI) at the spine base and head. Resulting mean intensities were adjusted for bleaching based on the mean Lifeact signals of the full image over time and then normalized to the first time point in the time-lapse. The graph in Fig.5B,C presents averaged signals from 10s intervals (5 time points) for a better visual arrangement, while Supplementary Fig.S3 shows the raw data of all quantified ROIs.

Quantification of actin and MT+TIP signals at the spine baselneck. ROIs covering the spine base (Lifeact) or spine base and neck (MT+TIP) of the same spine were defined and mean intensities quantified. The same method for bleach correction and normalization was used for both channels as described in the previous section. Peaks in the MT+TIP intensities were rechecked in the time-lapse recordings whether they represent spine entries or passing microtubule comets.

3

Three-step model for polarized sorting of KIF17 into dendrites

Mariella A. Franker*, **Marta Esteves da Silva***, Roderick P. Tas*, Elena Tortosa, Yujie Cao, Cátia P. Frias, Anne F. J. Janssen, Phebe S. Wulf, Lukas C. Kapitein and Casper C. Hoogenraad

Current Biology, July 2016, 26(13):1705-1712

Cell Biology, Faculty of Science, Utrecht University, Utrecht, The Netherlands.

*These authors contributed equally to this work.

ABSTRACT

Kinesin and dynein motors drive bidirectional cargo transport along microtubules and have a critical role in polarized cargo trafficking in neurons (Kapitein and Hoogenraad, 2011; Rolls, 2011). The kinesin-2 family protein KIF17 is a dendrite-specific motor protein and has been shown to interact with several dendritic cargoes (Chu *et al.*, 2006; Guillaud *et al.*, 2003; Irla *et al.*, 2007; Kayadjanian *et al.*, 2007; Setou *et al.*, 2000). However, the mechanism underlying the dendritic targeting of KIF17 remains poorly understood (Huang and Banker, 2012; Kapitein *et al.*, 2010a; Nakata and Hirokawa, 2003; Song *et al.*, 2009). Using live cell imaging combined with inducible trafficking assays to directly probe KIF17 motor activity in living neurons, we found that the polarized sorting of KIF17 to dendrites is regulated in multiple steps. First, cargo binding of KIF17 relieves autoinhibition and initiates microtubule-based cargo transport. Second, KIF17 does not autonomously target dendrites, but enters the axon where the actin cytoskeleton at the axon initial segment (AIS) prevents KIF17 vesicles from moving further into the axon. Third, dynein-based motor activity is able to redirect KIF17 coupled cargoes into dendrites. We propose a three-step model for polarized targeting of KIF17, in which the collective function of multiple motor teams is required for proper dendritic sorting.

RESULTS AND DISCUSSION

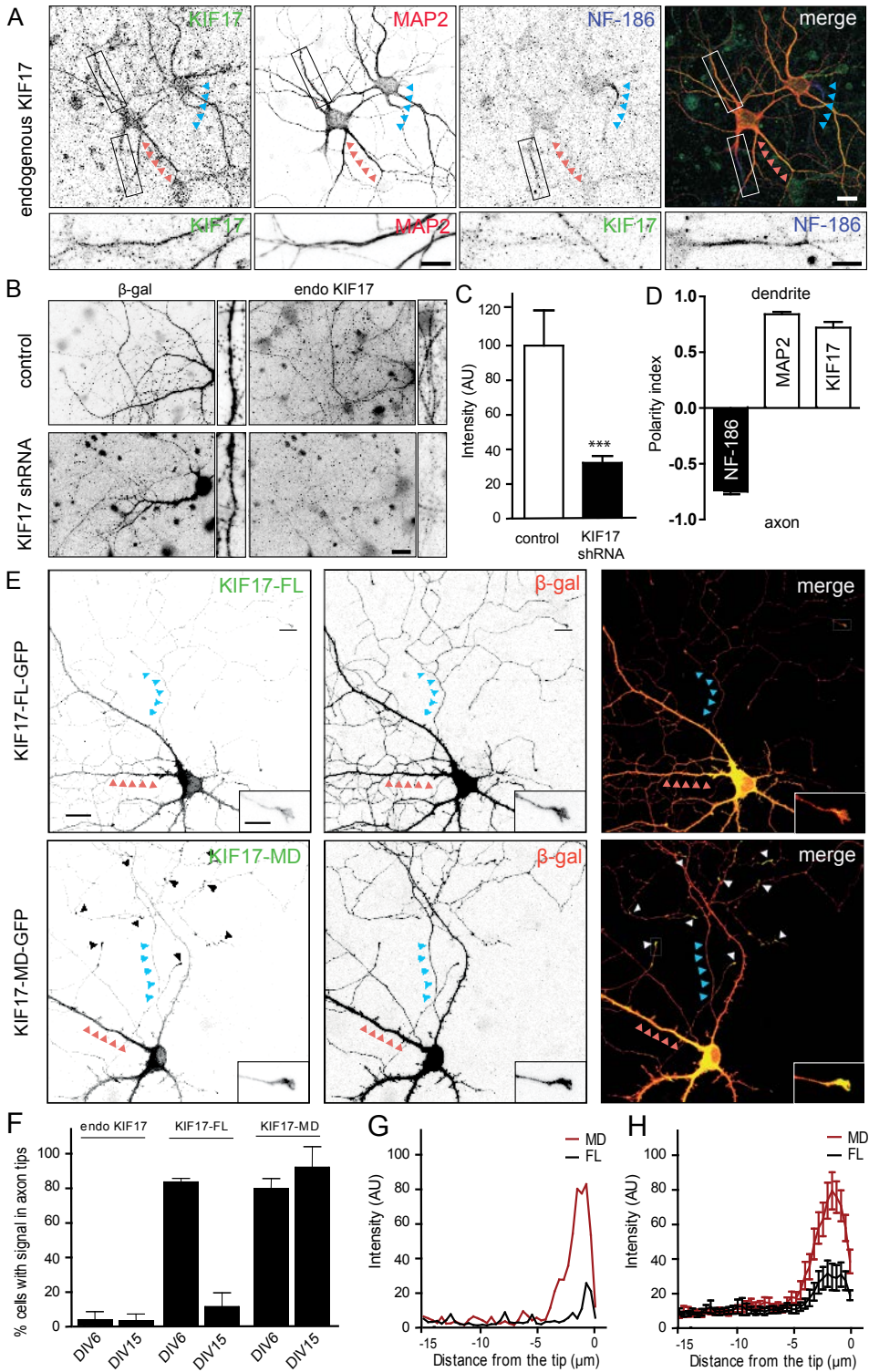
Full length KIF17 localizes to dendrites and tailless KIF17 targets the axon

Consistent with previous findings (Chu *et al.*, 2006; Guillaud *et al.*, 2003), we found that endogenous KIF17 and exogenously expressed full length KIF17 (KIF17-FL) localized to the dendritic compartment (MAP2 positive) of mature hippocampal neurons in culture (Figure 1A-E and S1A). Quantification revealed that endogenous KIF17 is localized to dendrites in developing (DIV6) and mature (DIV15) neurons; only ~5% of the cells show accumulations in axon tips and no AIS (NF-186 positive) enrichment is observed (Figure 1A,F). Interestingly, overexpressed KIF17-FL targeted the axon (~85%) in young neurons (DIV6), while in more mature neurons (DIV15) the localization of KIF17-FL was largely dendritic (~10% of neurons with axonal tip accumulation and no AIS accumulation) (Figure 1F and S1B,C). As reported (Huang and Banker, 2012; Kapitein *et al.*, 2010a; Nakata and Hirokawa, 2003; Song *et al.*, 2009), a truncated form of KIF17 containing the motor domain and dimerization region (amino acid 1-547) but lacking the tail domain, hereafter referred to as KIF17-MD, targeted the axon and accumulated in axon tips in both young and mature neurons (~80% and ~90%, respectively; Figure 1E-H). Together, these data demonstrate that the motor domain is selective for the axon and the tail region regulates the dendritic targeting of KIF17 in mature neurons.

Cargo binding relieves autoinhibition of full length KIF17

Autoinhibition is a well-described regulatory mechanism for kinesins, in which the tail domain interacts with the motor domain and prevents motor activity (Blasius *et al.*, 2007; Hackney and Stock, 2000; Hammond *et al.*, 2010; van der Vaart *et al.*, 2013; Yamada *et al.*, 2007). It has been suggested that cargo binding may unfold autoinhibited motors to initiate microtubule-based transport. *In vitro* studies have shown that binding kinesin to beads activates the motor (Coy *et al.*, 1999; Imanishi *et al.*, 2006). Expression of KIF17-FL in COS7 cells showed a diffuse cytoplasmic pattern without any microtubule labeling (Figure 2A). In contrast, both the KIF17-MD and coiled-coil 2 (CC2) mutant KIF17-G754E, which has no autoinhibition (Hammond *et al.*, 2010), showed a strong microtubule staining in the periphery of the cell (Figure 2A) and displayed fast motility towards the microtubule plus-ends (Figure 2B). The KIF17-G754E mutant showed very fast motility on microtubules with an instantaneous speed of 3.2 ± 0.1 $\mu\text{m/s}$ (Figure 2B). These data suggested that cargo-unbound KIF17-FL is autoinhibited in living cells.

To investigate if cargo binding can directly activate the motor in cells, we chemically induced the binding of KIF17 to peroxisomes using the FRB-FKBP dimerization system (Figure 2C) (Hoogenraad *et al.*, 2003; Kapitein *et al.*, 2010a). We expressed KIF17-GFP-FRB and PEX-RFP-FKBP in COS7 cells and addition of rapalog during live cell imaging induced KIF17 binding to the cargo (Kapitein *et al.*, 2010b). As shown by maximum projections, time-coded color plots and kymographs, rapalog treatment allowed KIF17-FL, KIF17-MD and KIF17-G754E to efficiently transport peroxisomes from the cell center to the cell periphery



◀ **Figure 1. Full length and truncated KIF17 constructs localize to different neuronal compartments**

A. Hippocampal neurons at DIV15 co-stained for endogenous KIF17, dendritic marker MAP2 and axon initial segment marker NF-186. **B.** Hippocampal neurons at DIV11+3 co-transfected with pSuper control or KIF17 shRNAs and β -galactosidase (β -gal) to highlight neuronal morphology and stained for endogenous KIF17 and β -gal. **C.** Quantification of KIF17 mean intensity in dendrites of neurons expressing pSuper control or KIF17 shRNAs (n = 34-38). **D.** Polarity index of NF-186, MAP2 and KIF17 in DIV15 neurons (n = 12). **E.** Hippocampal neurons at DIV19+2 co-transfected with β -gal and KIF17-FL-GFP or KIF17-MD-GFP. Inserts show zooms of axon tips. **F.** Percentage of cells with accumulations in at least 2 axon tips in young (DIV6) and mature (DIV15) neurons with endogenous KIF17 and overexpressed KIF17-FL-GFP and KIF17-MD-GFP (n = 22-30). **G.** Representative individual fluorescent intensity profile of KIF17-FL-GFP (black) and KIF17-MD-GFP (red) at the tip of the axon. **H.** Average normalized fluorescent intensity profiles of KIF17-FL-GFP (n = 20) and KIF17-MD-GFP (n = 20) at the tip of the axon. Blue arrowheads indicate axons and red arrowheads indicate dendrites. Scale bars: 20 μ m (A,B,E), 10 μ m (inset A) and 5 μ m (inset B,E). Error bars indicate SEM; ***p < 0.001 (Mann-Whitney test). See also Figure S1.

(Figure 2D-E and Video S1). The data suggested that the cargo binding relieves autoinhibition of KIF17-FL. Interestingly, analysis of displacement curves (Figure 2F,G and S2A-E) showed that the onset of motility of KIF17-FL is markedly slower ($t_{1/2} = 10.6 \pm 3.0$ min) compared to KIF17-G754E ($t_{1/2} = 5.5 \pm 2.9$ min) and KIF17-MD ($t_{1/2} = 4.7 \pm 2.2$ min). Next, we analyzed the speed of single peroxisomes (Figure 2H). Immobile peroxisomes were excluded from the analysis and only minimum track lengths of 1 μ m and 1 second were analyzed. All three KIF17 constructs showed similar single peroxisome behavior with an average velocity around 1 μ m/s (mean \pm SD: FL = 1.07 ± 0.50 ; MD = 0.91 ± 0.47 ; G754E = 1.09 ± 0.46 μ m/s) (Figure 2I). These velocities were comparable to previous reports of kinesin-mediated organelle transport in cells (0.5-2 μ m/s) (Guillaud *et al.*, 2003; Soppina *et al.*, 2009). These data indicate that the KIF17 motor domain alone and the non-autoinhibited KIF17 mutant quickly initiate cargo transport in living cells. These observations are consistent with the proposed role of the CC2 region in regulating KIF17 activity (Hammond *et al.*, 2010).

Full length KIF17 does not directly target dendrites but is anchored at AIS

To further study the role of the tail region on the dendritic targeting of KIF17, we used the cargo trafficking assay in cultured hippocampal neurons (Kapitein *et al.*, 2010a). Without rapalog-induced motor coupling, the peroxisomes are largely immobile in hippocampal neurons (Figure S3A). After coupling KIF17 to peroxisomes, we observed that KIF17-FL was able to transport peroxisomes but did not target the dendrites. Instead, it had a strong preference for the axon, where the peroxisomes anchored at the AIS (Figure 3A-C and Video S2). In contrast, KIF17-MD efficiently drove transport through the proximal axon. Earlier work established that the actin-rich AIS localized in the beginning of the axon functions as barrier for membrane-bound proteins (Winckler *et al.*, 1999), as well as transported cargoes (Al-Bassam *et al.*, 2012; Song *et al.*, 2009). It was observed that dendritic cargoes halt and reverse in the AIS, suggesting that the AIS barrier prevents 'unwanted' cargoes from entering the axon (Petersen *et al.*, 2014). Furthermore, it has been shown that the actin cytoskeleton is important for the function of the AIS cytosolic barrier (Al-Bassam *et al.*, 2012; Petersen *et al.*, 2014; Song *et al.*, 2009). Next,

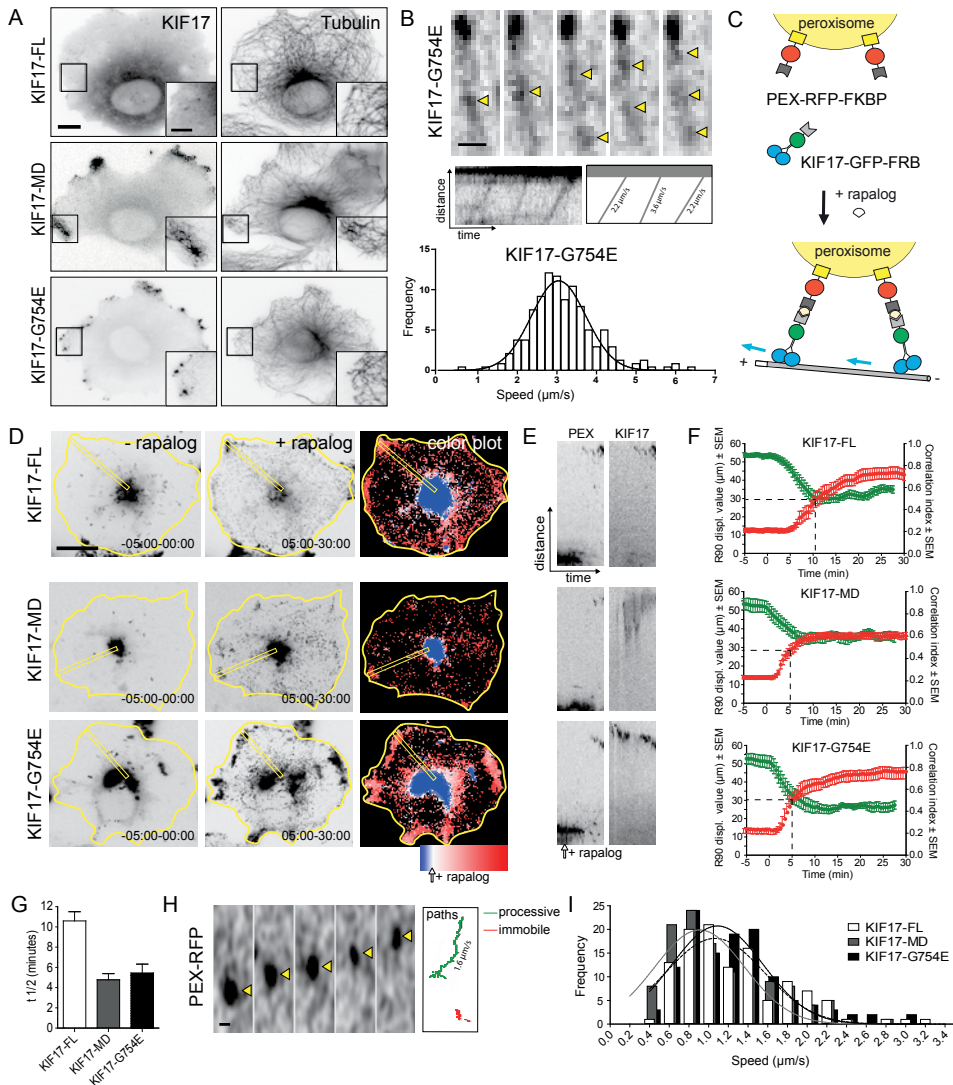


Figure 2. Cargo binding activates full length KIF17

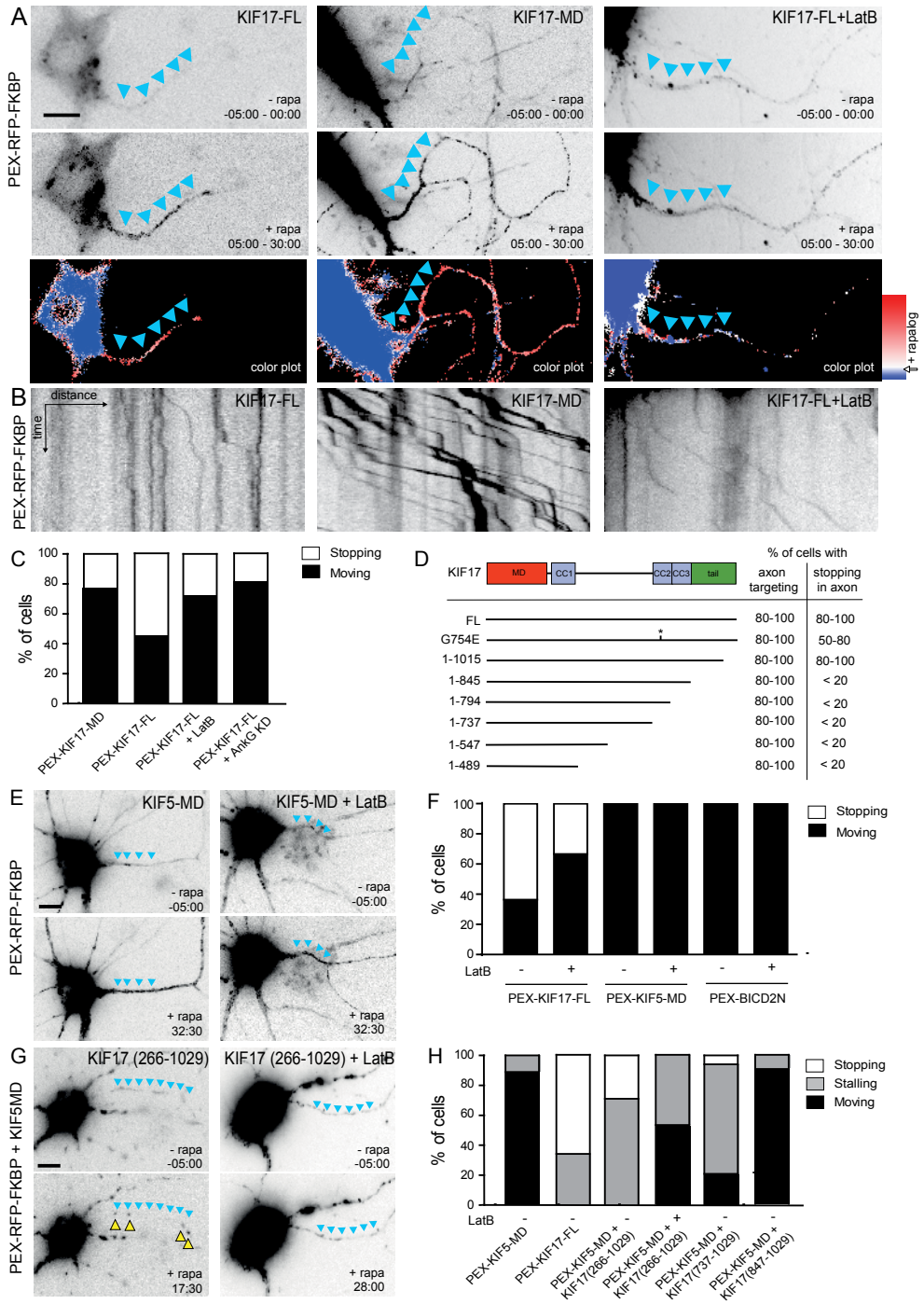
A. COS7 cells transfected with KIF17-FL-GFP, KIF17-MD-GFP or KIF17-G754E-GFP and stained with tubulin. **B.** Still frames and kymograph (3.2µm x 5s) of KIF17-G754E-GFP moving towards the tip of a microtubule. Histogram of average speeds of KIF17-G754E-GFP (n=31 tracks) was fitted with a Gaussian function. **C.** Schematic representation of rapalog-induced coupling of KIF17-GFP-FRB to PEX-RFP-FKBP. **D.** Cargo transport efficiency of indicated KIF17-GFP-FRB constructs. Left and middle panels show maximum projections of peroxisome motility before and after rapalog. Right panels are time-coded color plots. **E.** Kymographs (35µm x 30 min) of PEX-RFP-FKBP and KIF17-GFP as indicated in (D; yellow boxes). **F.** Graphs showing R90 displacement value (red) and correlation index (green) of peroxisomes over time (n=11-13). **G.** Graph showing t_{1/2} of indicated KIF17 constructs (n=11-13). **H.** Still frames of a single KIF17-FL coupled peroxisome in COS7 cells at 10 fps. Tracked path of a processive and an immobile peroxisome are indicated. **I.** Histograms showing the average speeds of processive peroxisomes coupled to KIF17-FL, KIF17-MD and KIF17-G754E (n=113-121 tracks) were fitted with a Gaussian fit. Scale bar: 20 µm (A,D), 5 µm (A, inset) and 0.5 µm (B,H). Error bars indicate SEM. See also Figure S2 and Video S1.

we treated neurons with Latrunculin B (LatB) to depolymerize actin or expressed Ankyrin G (AnkG) shRNA to disrupt the AIS (Figure S1D,E) and analyzed the behavior of KIF17-FL coupled peroxisomes. We observed that disrupting the actin cytoskeleton or the AIS increased cargo motility and allowed axon transport comparable to KIF17-MD (Figure 3C and Video S3). These data support the existence of an actin-based barrier at the AIS that regulates the entry of specific vesicles into the axon (Al-Bassam *et al.*, 2012; Song *et al.*, 2009). Since LatB treatment did not affect KIF5- or dynein-coupled peroxisome motility (Figure 3E,F), the actin cytoskeleton is responsible for the specific KIF17-FL-coupled cargo accumulations in the AIS. Next, we generated several truncated KIF17 constructs and found that the tail region (amino acid 846-1015) was required for anchoring at the AIS (Figure 3D). Consistently, the shortest KIF17 construct that anchored at the AIS - KIF17(1-1015) - did not strongly accumulate in axonal tips (Figure S2). Interestingly, rapalog-induced coupling of both truncated KIF5 motors (KIF5-MD-GFP-FRB) and the KIF17-tail region (KIF17(266-1029)-GFP-FRB) to peroxisomes induced cargo stalling in the proximal axon (Figure 3G,H). Moreover, the KIF17-tail region also stalls KIF5-MD-induced Rab3 positive vesicles at the AIS, which can be suppressed by actin depolymerization (Figure S3B-E). Furthermore, expression of the KIF17-tail region (as a dominant negative approach, without coupling to cargo) suppresses KIF17-FL-GFP-induced Rab3 stalling at the AIS (Figure S3F-G). These results indicate that the tail region of KIF17 is responsible for AIS anchoring.

One other possibility is that deactivation of KIF17 motor activity by back folding may cause cargo stalling at the AIS. However our data argue against this option: KIF17-G754E shows strong axonal tip accumulation when overexpressed in neurons but still anchors at the AIS (Figure 3D and S2). However, local deactivation of KIF17 may still be achieved via additional mechanisms, such as inhibiting microtubule binding or ATP hydrolysis of the kinesin motor via local activation of regulatory protein in the AIS.

KIF17 vesicles are redirected into dendrites by cytoplasmic dynein

Next we examined how KIF17 vesicles transported out of the proximal axon and into the dendrites and tested whether other motors present on the same cargo could redirect KIF17 transport. We first determined whether the retrograde motor dynein via recruitment of dynein adaptor BICD2 drives KIF17-bound vesicles out of the axon towards the soma. We expressed KIF17-FL-GFP-FRB, HA-BICD2N-FRB and PEX-RFP-FKBP in neurons. Addition of rapalog recruited both KIF17-FL and BICD2N to peroxisomes and increased retrograde movement of peroxisomes in the proximal axon (Figure 4A-C) from ~20% in neurons with KIF17-FL alone to ~50% in cells with KIF17-FL and BICD2N (Figure 4G). We next determined whether dynein also redirects KIF17 bound vesicles into dendrites. Addition of rapalog simultaneously recruited KIF17-FL and BICD2N to peroxisomes and quickly redistributed cargoes from the soma into the dendrites (Figure 4D-F and Video S4, S5). Under these conditions, all neurons showed dendrite localization of KIF17-FL, while in the absence of BICD2N dendrite targeting is rare (Figure 4H). These results demonstrate that KIF17 vesicles can be redirected into dendrites by



4

◀ Figure 3. The KIF17 tail region mediates cargo stalling at the AIS

A. Hippocampal neurons co-transfected with PEX-RFP-FKBP and KIF17-FL-GFP-FRB or KIF17-MD-GFP-FRB and live stained for AIS marker Neurofascin. Cells expressing KIF17-FL were treated with 10 μ M Latrunculin B (LatB) for 1-2 h before imaging. Maximum projections of peroxisomes motility before and after rapalog addition (top panels) and color plots of peroxisome distributions (bottom panels) are shown. **B.** Kymographs (31 μ m x 31sec) showing movement of peroxisomes in the proximal axon. **C.** Percentage of neurons with motile (moving) or non-motile (stopping) peroxisomes in the proximal axon expressing the indicated constructs (n=11-16). **D.** Behavior of the various KIF17 constructs after peroxisome coupling characterized as percentage of cells with axon targeting and non-motile (stopping) peroxisomes in the proximal axon. **E.** Hippocampal neurons co-transfected with PEX-RFP-FKBP and KIF5-MD-GFP-FRB before/after rapalog addition, with/without LatB treatment. Images show maximum projections. **F.** Percentage of neurons with moving or stopping peroxisomes in the proximal axon after rapalog-induced coupling with KIF17-FL-GFP-FRB, KIF5-MD-GFP-FRB or BICD2N-GFP-FRB, with/without LatB treatment (n=11-16). **G.** Hippocampal neurons co-transfected with PEX-RFP-FKBP, KIF5-MD-GFP-FRB and KIF17(266-1029)-GFP-FRB before and after rapalog addition, with/without LatB treatment. **H.** Percentage of neurons with moving, stalling or stopping peroxisomes in the proximal axon after rapalog-induced coupling of KIF5-MD-GFP-FRB together with indicated KIF17 constructs (n=12-30). Scale bars: 10 μ m (A,E,G). See also Figure S3 and Video S2 and S3.

dynein motor activity.

Previous studies have analyzed the movements of KIF17 bound vesicles in neurons and therefore concluded that KIF17 actively transports cargoes into dendrites (Guillaud *et al.*, 2003; Setou *et al.*, 2000). Since various motor types (dynein, kinesin and myosin) can simultaneously bind to cargo, it is challenging to interpret endogenous vesicle motility in neurons. Particularly in dendrites, where the microtubule cytoskeleton has opposite polarity orientations (Baas *et al.*, 1988). Moreover, motors attached to cargo can exist in active and inactive states and many regulators can influence their local motor activity (Fu and Holzbaur, 2014). By directly probing KIF17-mediated cargo movements, we found that full length KIF17 does not target dendrites but steers cargo into the axon, where it anchors at the AIS. We also demonstrate that dynein can drive KIF17-bound vesicles out of the axon and redirect them into the dendrites. These data fit well with the basic model for polarized transport where most kinesins are responsible for transport into axons and dynein motors are responsible for transport into dendrites (Kapitein and Hoogenraad, 2011; Rolls, 2011). Thus, the dendrite specific localization of KIF17 is not due to active KIF17 transport from the soma to the dendrite but to decreased axonal entry and the use of dynein activity to target dendrites. What is the role of KIF17 in dendrite specific cargo trafficking? First of all, in contrast to many other kinesin family members, KIF17 is a unique plus-end directed motor that prevents cargoes from entering the axon by AIS anchoring. The decreased axonal targeting emphasizes the importance of the actin-rich AIS in preventing 'unwanted' cargoes from entering the axon and setting up the polarized distribution of somatodendritic proteins. Second, dynein helps to bring KIF17 into dendrites. However, once the more distal dendrites are reached, KIF17 may take over from dynein and deliver cargo towards the more distal dendritic regions. This idea is consistent with the observed motility of KIF17-bound cargoes within dendritic branches (Kapitein *et al.*, 2010a; Yin *et al.*, 2012). Moreover, our data is in line with previous studies on polarized channel trafficking showing that KIF17 is required for K⁺ channel Kv4.2 transport in dendrites but does not, by itself,

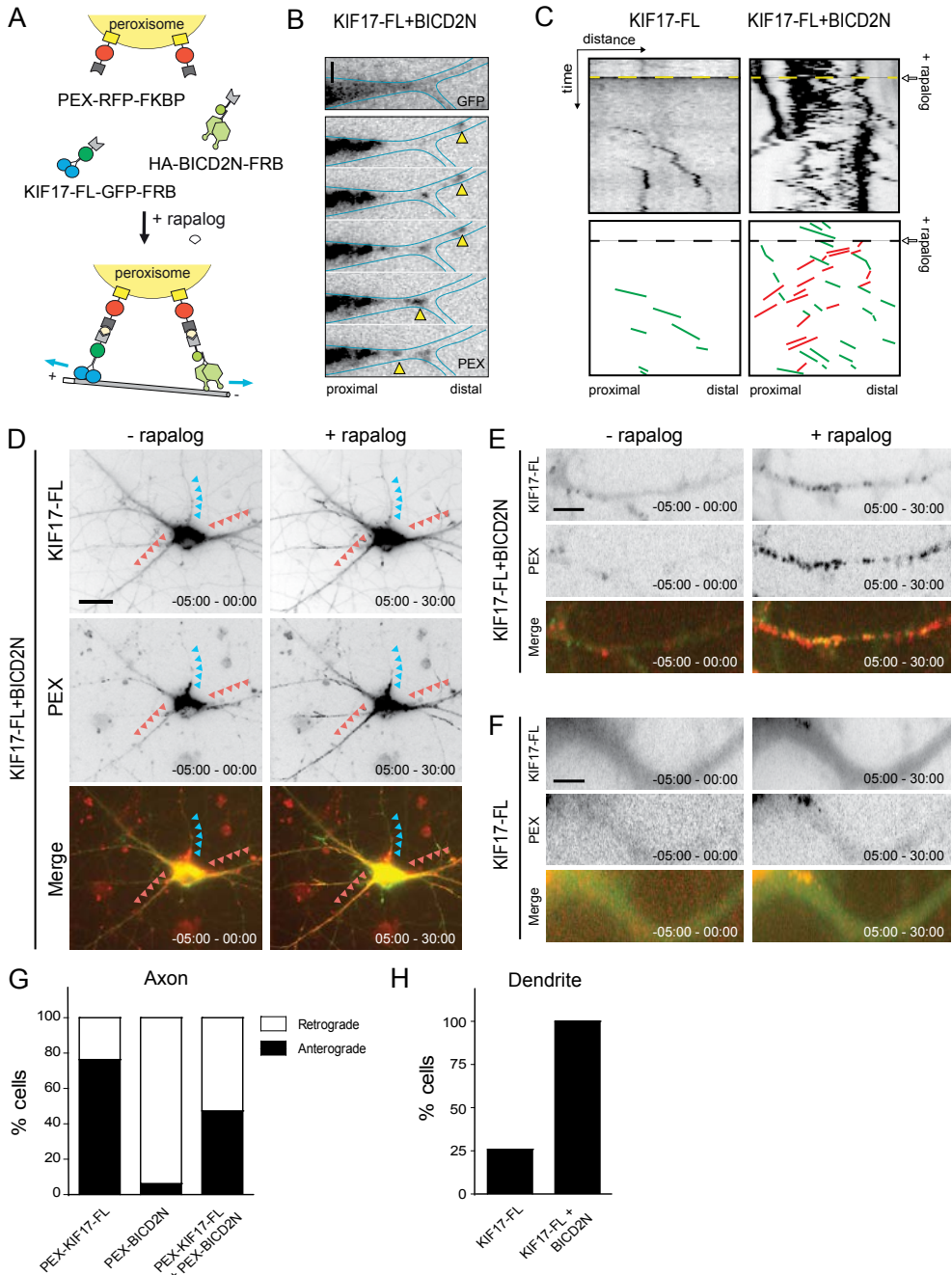


Figure 4. Dynein redirects KIF17 to dendrites

A. Schematic representation of rapalog-induced co-coupling of KIF17-FL-GFP-FRB and dynein adaptor HA-BICD2N-FRB to PEX-RFP-FKBP. **B.** Still frames of retrograde peroxisome movement in the proximal axon at 30s interval after simultaneous recruitment of HA-BICD2N-FRB and KIF17-FL-GFP-FRB. **C.** Kymographs (25 μm x

45 min) show increased retrograde movement of KIF17-FL-coupled peroxisomes in proximal axon in the presence of BICD2N-FRB. Illustrations of manually traced cargo displacements are indicated. **D.** Maximum projections of KIF17-FL-GFP and peroxisomes movements in neurons expressing PEX-RFP-FKBP, HA-BICD2N-FRB and KIF17-FL-GFP-FRB before and after rapalog addition. **E-F.** Maximum projections before and after rapalog of dendrites of neurons expressing PEX-RFP-FKBP and KIF17-FL-GFP-FRB with and without HA-BICD2N-FRB. **G.** Percentage of neurons with retrograde and anterograde movement in proximal axon expressing the indicated constructs. **H.** Percentage of neurons with KIF17-FL positive peroxisomes in dendrites expressing the indicated constructs. Scale bars: 20 μm (D), 5 μm (E,F) and 3 μm (B). See also Video S4 and S5.

specify dendritic localization of the channel (Chu *et al.*, 2006). However additional studies are needed to determine whether the transport kinetics of KIF17-attached peroxisomes can be compared to a bona fide KIF17 cargo. Within dendrites, KIF17 may play a role in the spatial and temporal fine-tuning of receptor and/or channel trafficking to synapses (Wong *et al.*, 2002; Yin *et al.*, 2012; Yin *et al.*, 2011). Together, the data suggest that cooperativity between different motors is an important part of the polarized sorting mechanism. However, it remains an open question how coupling between KIF17 and dynein is regulated. Several studies have shown that interaction between different motor types occurs via adaptor proteins, which act as a 'switch' between two motors to mediate trafficking (Fu and Holzbaur, 2014; Maeder *et al.*, 2014). Future research will have to clarify how KIF17 and dynein interact with adaptors and which regulators are involved to achieve targeted trafficking.

EXPERIMENTAL PROCEDURES

Animals and Ethics Statement

All animal experiments were performed in compliance with the guidelines for the welfare of experimental animals issued by the federal government of the Netherlands. All animal experiments were approved by the Animal Ethical Review Committee (DEC) of Utrecht University.

DNA Constructs, shRNA sequences and Antibodies

The KIF17 expression constructs were generated by a PCR-based strategy using the human KIF17 cDNA (accession NM_020816; IMAGE clone 6171598). The shRNA sequences used in this study are rat KIF17 shRNA1 (5'-GCCACCAAGATTAACCTGT-3'), rat KIF17 shRNA2 (5'-GACAGGACAAAGCTCAACA-3'), rat KIF17 shRNA3 (5'-CCATCAACATCGAGATCTA-3') and AnkyrinG shRNA (5'-GAGTTGTGCTGATGACAAG-3'). Details about the FRB/FKB constructs can be found in (Kapitein *et al.*, 2010a). The following antibodies were used: rabbit-anti-KIF17 (K3638, Sigma and H-280, Santa Cruz) and mouse-anti-AnkyrinG (Invitrogen). See the Supplemental Experimental Methods.

Cell culture, Transfections and Live Cell Imaging

Primary hippocampal neurons were harvested from rat E18 embryos, cultured on poly-

L-lysine (35 µg/ml) and laminin (5 µg/ml) coated coverslips in neurobasal medium (NB) supplemented with B27, 0.5 mM glutamine, 12.5 µM glutamate and Pen/Strep and transfected with Lipofectamine 2000 (Invitrogen). Imaging experiments were performed on Nikon Eclipse TE2000E microscope equipped with 40x oil objective, Coolsnap CCD camera (Photometrics), perfect-focus system and imaging chamber. Imaging chamber was maintained at 37°C and 5% CO₂ during acquisition. See the Supplemental Experimental Methods.

AUTHOR CONTRIBUTIONS

MAF, MEdS and RPT designed and performed the live cell imaging experiments and analyzed the results; ET performed ICC experiments and analysed the data; YC, CPF, AJ, PSW cloned constructs; LCK supervised the research; CCH supervised the research, coordinated the study and wrote the manuscript with input from all authors.

ACKNOWLEDGEMENTS

This work was supported by the Netherlands Organization for Scientific Research (NOW-ALW-VIDI: LCK, NWO-ALW-VICI: CCH), the Foundation for Fundamental Research on Matter ((FOM): LCK and CCH), which is part of the NWO, the Netherlands Organization for Health Research and Development (ZonMW-TOP: CCH), the European Research Council (ERC) (ERC-starting: LCK, ERC-consolidator: CCH). MEdS is supported by Fundação para a Ciência e Tecnologia (FCT-Portugal, grant SFRH/BD/68642/2010) and YC is part of the China Scholarship Council - Utrecht University (CSC-UU) PhD-program.

REFERENCES

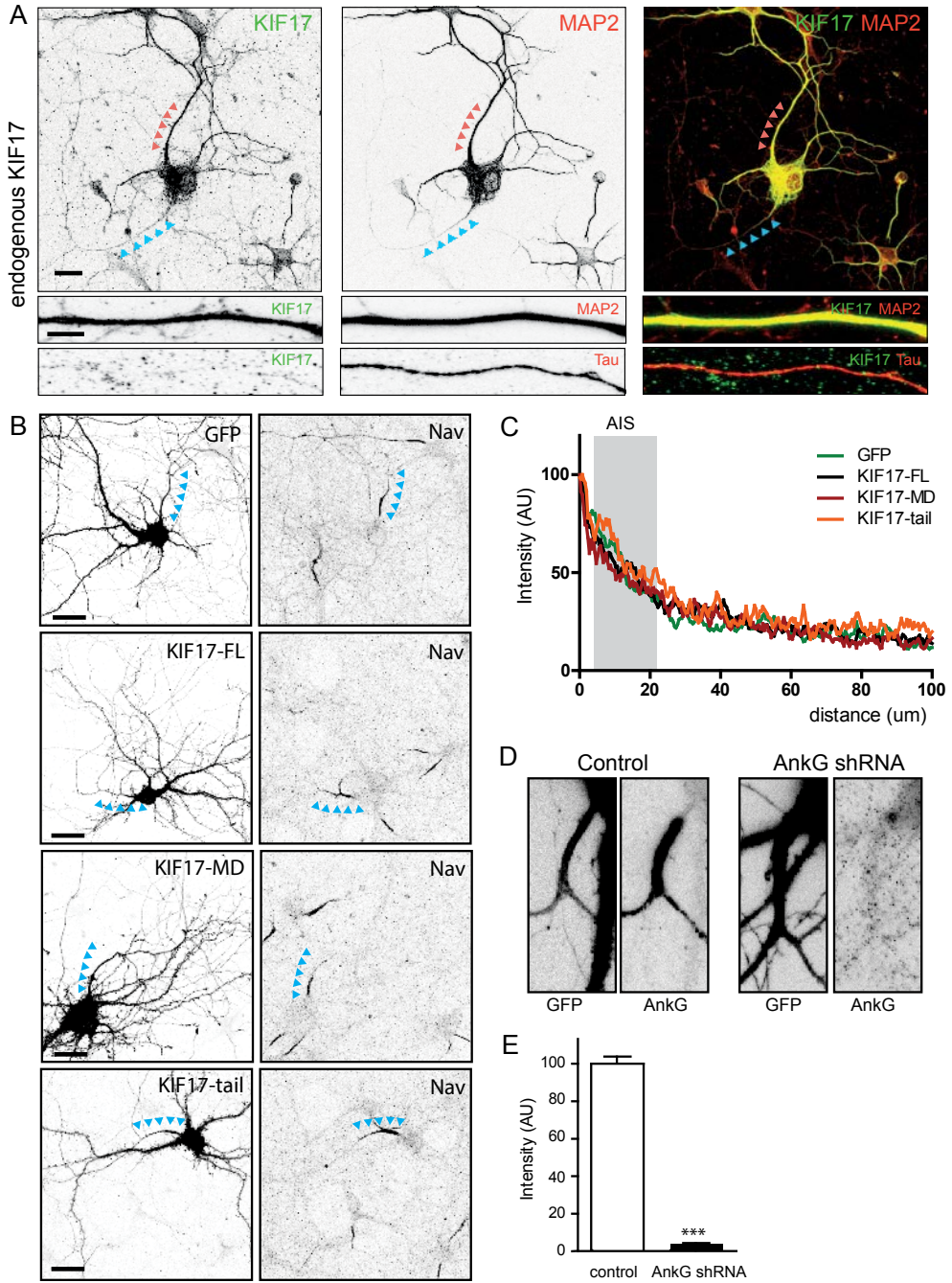
- Al-Bassam, S., Xu, M., Wandless, T.J., and Arnold, D.B. (2012). Differential trafficking of transport vesicles contributes to the localization of dendritic proteins. *Cell reports* 2, 89-100.
- Baas, P.W., Deitch, J.S., Black, M.M., and Banker, G.A. (1988). Polarity orientation of microtubules in hippocampal neurons: uniformity in the axon and nonuniformity in the dendrite. *Proceedings of the National Academy of Sciences of the United States of America* 85, 8335-8339.
- Blasius, T.L., Cai, D., Jih, G.T., Toret, C.P., and Verhey, K.J. (2007). Two binding partners cooperate to activate the molecular motor Kinesin-1. *The Journal of cell biology* 176, 11-17.
- Chu, P.J., Rivera, J.F., and Arnold, D.B. (2006). A role for Kif17 in transport of Kv4.2. *The Journal of biological chemistry* 281, 365-373.
- Coy, D.L., Hancock, W.O., Wagenbach, M., and Howard, J. (1999). Kinesin's tail domain is an inhibitory regulator of the motor domain. *Nature cell biology* 1, 288-292.
- Fu, M.M., and Holzbaur, E.L. (2014). Integrated regulation of motor-driven organelle transport by scaffolding proteins. *Trends in cell biology* 24, 564-574.
- Guillaud, L., Setou, M., and Hirokawa, N. (2003). KIF17 dynamics and regulation of NR2B trafficking in hippocampal neurons. *The Journal of neuroscience : the official journal of the Society for Neuroscience* 23, 131-140.
- Hackney, D.D., and Stock, M.F. (2000). Kinesin's IAK tail domain inhibits initial microtubule-stimulated ADP release. *Nature cell biology* 2, 257-260.
- Hammond, J.W., Blasius, T.L., Soppina, V., Cai, D., and Verhey, K.J. (2010). Autoinhibition of the kinesin-2 motor KIF17 via dual intramolecular mechanisms. *The Journal of cell biology* 189, 1013-1025.
- Hoogenraad, C.C., Wulf, P., Schiefermeier, N., Stepanova, T., Galjart, N., Small, J.V., Grosveld, F., de Zeeuw, C.I., and Akhmanova, A. (2003). Bicaudal D induces selective dynein-mediated microtubule minus end-directed transport. *The*

- EMBO journal 22, 6004-6015.
- Huang, C.F., and Banker, G. (2012). The translocation selectivity of the kinesins that mediate neuronal organelle transport. *Traffic (Copenhagen, Denmark)* 13, 549-564.
- Imanishi, M., Endres, N.F., Gennerich, A., and Vale, R.D. (2006). Autoinhibition regulates the motility of the *C. elegans* intraflagellar transport motor OSM-3. *The Journal of cell biology* 174, 931-937.
- Irla, M., Saade, M., Fernandez, C., Chasson, L., Victorero, G., Dahmane, N., Chazal, G., and Nguyen, C. (2007). Neuronal distribution of spatial in the developing cerebellum and hippocampus and its somatodendritic association with the kinesin motor KIF17. *Experimental cell research* 313, 4107-4119.
- Kapitein, L.C., and Hoogenraad, C.C. (2011). Which way to go? Cytoskeletal organization and polarized transport in neurons. *Molecular and cellular neurosciences* 46, 9-20.
- Kapitein, L.C., Schlager, M.A., Kuijpers, M., Wulf, P.S., van Spronsen, M., MacKintosh, F.C., and Hoogenraad, C.C. (2010a). Mixed microtubules steer dynein-driven cargo transport into dendrites. *Current biology : CB* 20, 290-299.
- Kapitein, L.C., Schlager, M.A., van der Zwan, W.A., Wulf, P.S., Keijzer, N., and Hoogenraad, C.C. (2010b). Probing intracellular motor protein activity using an inducible cargo trafficking assay. *Biophysical journal* 99, 2143-2152.
- Kayadjanian, N., Lee, H.S., Pina-Crespo, J., and Heinemann, S.F. (2007). Localization of glutamate receptors to distal dendrites depends on subunit composition and the kinesin motor protein KIF17. *Molecular and cellular neurosciences* 34, 219-230.
- Maeder, C.I., Shen, K., and Hoogenraad, C.C. (2014). Axon and dendritic trafficking. *Current opinion in neurobiology* 27, 165-170.
- Nakata, T., and Hirokawa, N. (2003). Microtubules provide directional cues for polarized axonal transport through interaction with kinesin motor head. *The Journal of cell biology* 162, 1045-1055.
- Petersen, J.D., Kaeck, S., and Banker, G. (2014). Selective microtubule-based transport of dendritic membrane proteins arises in concert with axon specification. *The Journal of neuroscience : the official journal of the Society for Neuroscience* 34, 4135-4147.
- Rolls, M.M. (2011). Neuronal polarity in *Drosophila*: sorting out axons and dendrites. *Developmental neurobiology* 71, 419-429.
- Setou, M., Nakagawa, T., Seog, D.H., and Hirokawa, N. (2000). Kinesin superfamily motor protein KIF17 and mLin-10 in NMDA receptor-containing vesicle transport. *Science (New York, NY)* 288, 1796-1802.
- Song, A.H., Wang, D., Chen, G., Li, Y., Luo, J., Duan, S., and Poo, M.M. (2009). A selective filter for cytoplasmic transport at the axon initial segment. *Cell* 136, 1148-1160.
- Soppina, V., Rai, A.K., Ramaiya, A.J., Barak, P., and Mallik, R. (2009). Tug-of-war between dissimilar teams of microtubule motors regulates transport and fission of endosomes. *Proceedings of the National Academy of Sciences of the United States of America* 106, 19381-19386.
- van der Vaart, B., van Riel, W.E., Doodhi, H., Kevenaar, J.T., Katrukha, E.A., Gumy, L., Bouchet, B.P., Grigoriev, I., Spangler, S.A., Yu, K.L., et al. (2013). CFEOM1-associated kinesin KIF21A is a cortical microtubule growth inhibitor. *Developmental cell* 27, 145-160.
- Winckler, B., Forscher, P., and Mellman, I. (1999). A diffusion barrier maintains distribution of membrane proteins in polarized neurons. *Nature* 397, 698-701.
- Wong, R.W., Setou, M., Teng, J., Takei, Y., and Hirokawa, N. (2002). Overexpression of motor protein KIF17 enhances spatial and working memory in transgenic mice. *Proceedings of the National Academy of Sciences of the United States of America* 99, 14500-14505.
- Yamada, K.H., Hanada, T., and Chishti, A.H. (2007). The effector domain of human Dlg tumor suppressor acts as a switch that relieves autoinhibition of kinesin-3 motor GAKIN/KIF13B. *Biochemistry* 46, 10039-10045.
- Yin, X., Feng, X., Takei, Y., and Hirokawa, N. (2012). Regulation of NMDA receptor transport: a KIF17-cargo binding/releasing underlies synaptic plasticity and memory *in vivo*. *The Journal of neuroscience : the official journal of the Society for Neuroscience* 32, 5486-5499.
- Yin, X., Takei, Y., Kido, M.A., and Hirokawa, N. (2011). Molecular motor KIF17 is fundamental for memory and learning via differential support of synaptic NR2A/2B levels. *Neuron* 70, 310-325.

SUPPLEMENTARY FIGURES

► **Figure S1, related to Figure 1. Exogenous KIF17 constructs (without inducible cargo attachment) do not accumulate at the AIS**

A. Cultured hippocampal neurons at DIV6 stained for endogenous KIF17 in combination with MAP2 and Tau. Axon is indicated with blue arrows, dendrite with red arrows. Bottom two panels show zooms of a MAP2 positive dendrite and Tau positive axon. Scale bars are 20 μm (top panels) and 5 μm (bottom two panels). **B.** DIV15 hippocampal neurons transfected with GFP, KIF17-FL-GFP, KIF17-MD-GFP and KIF17-tail and stained for voltage-gated Na⁺ channels (NaV), as marker for the axon initial segment. Axons are indicated with blue arrow. Scale bars are 20 μm . **C.** Average normalized fluorescent intensity profiles in the proximal axon of diffuse cytosolic GFP (n=21), KIF17-FL-GFP (n=23), KIF17-MD-GFP (n=22) and KIF17-tail (n=11). Grey area indicates the localization of the axon initial segment, calculated from an average of fluorescent intensity profiles of NaV staining (n=21). **D.** Zoom of the proximal axon of hippocampal neurons transfected with pSuper control or AnkG shRNA, together with GFP, and stained for AnkG. Scale bars are 5 μm . **E.** Quantification of AnkG mean intensity in proximal axons of neurons expressing pSuper control (n=27) or AnkG shRNA (n=27). Error bars indicate SEM; ***p < 0.001 (unpaired t-test).



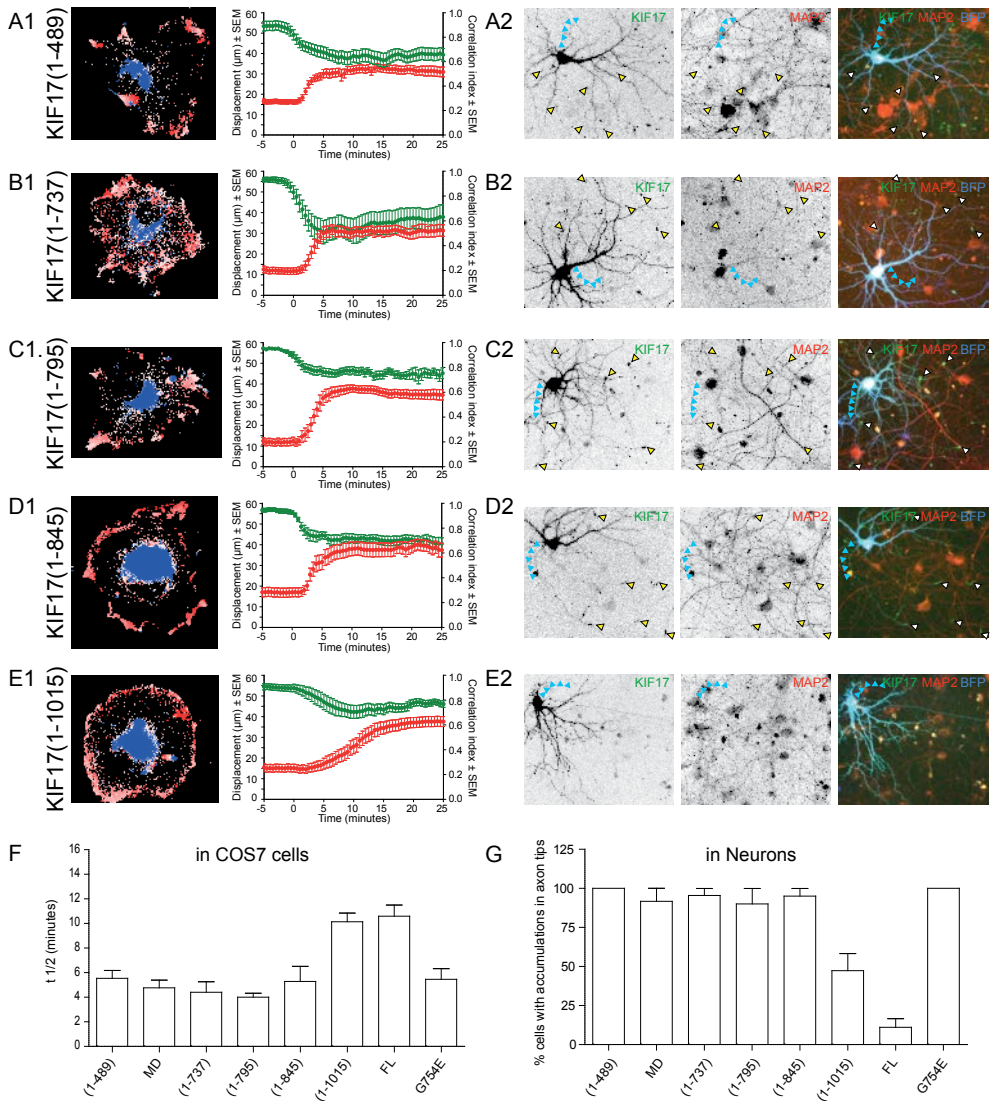


Figure S2, related to Figure 2. Behavior of KIF17 constructs in COS7 cells and neurons

A1-E1. Analysis of the inducible peroxisome trafficking assay in COS7 cells for full length KIF17 and various KIF17 deletion constructs. Color plots (left panel) show displacement of peroxisomes over time and graph (right panel) indicates peroxisome displacement (R90, red curve) and Correlative Index (CI analysis, green curve). **A2-E2.** Expression of various KIF17 constructs in hippocampal neurons and stained for MAP2. Blue arrows indicate axon, yellow arrows indicate accumulation of KIF17 in tips. **F.** $t_{1/2}$ as measured in COS7 cells (n=11-13 cells from 2 independent experiments). **G.** Percentage of cells with accumulations in axon tips in hippocampal neurons (n=18-23 cells from 2 independent experiments).

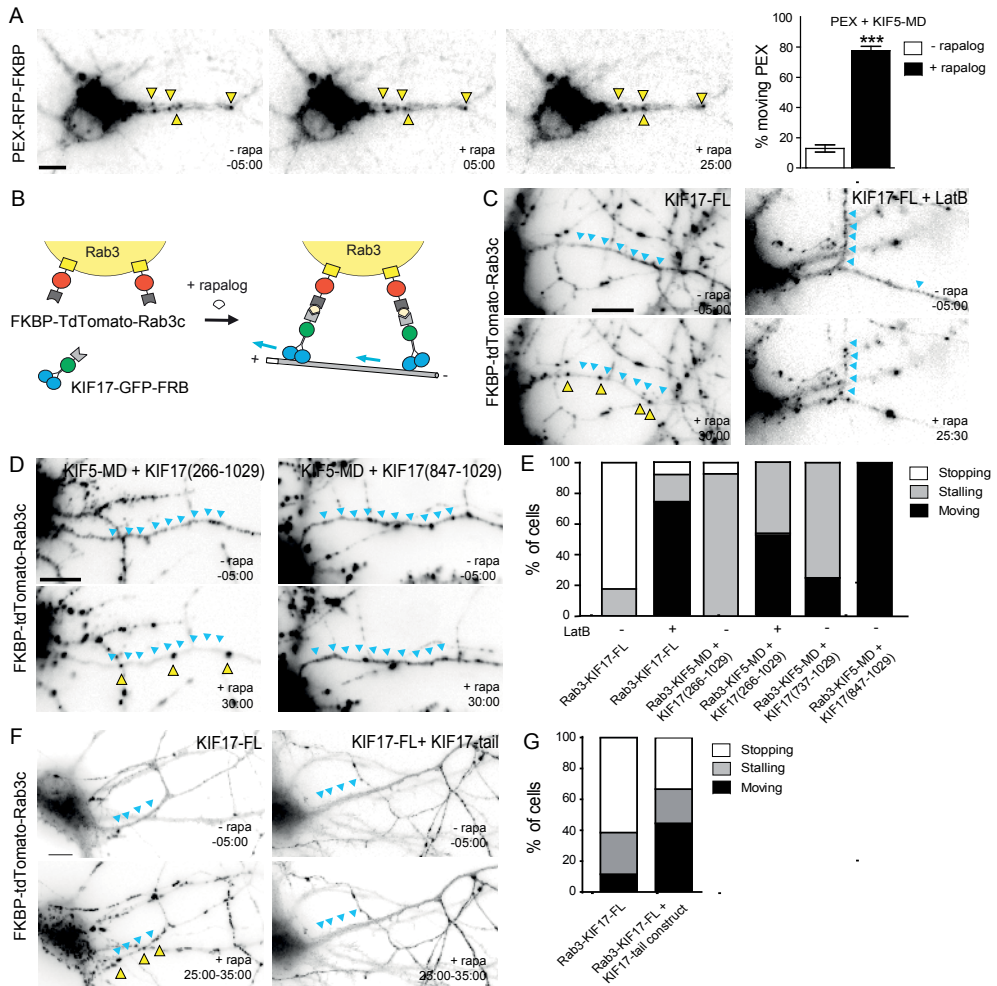


Figure S3, related to Figure 3. KIF17-tail region stalls KIF5-MD-induced Rab3 vesicles at the AIS

A. Left panels. Typical example of a cultured hippocampal neuron expressing PEX-RFP-FKBP (without exogenous motor constructs). Note that the peroxisome distribution before and after rapalog addition is very similar, indicating that peroxisomes are largely immobile in hippocampal neurons. Scale bar is 10µm. Right panel. Quantification of percentage of moving peroxisomes (PEX-RFP-FKBP) in the axon before and after recruitment of KIF5-MD (now with exogenous motor constructs) using rapalog (N=2, n=11 cells). 5 minute intervals were analyzed for each condition. Note that the peroxisome distribution after rapalog addition (KIF5-MD recruitments) is strongly increased (from ~15% to ~75% mobility). The results without rapalog again show that peroxisomes are largely immobile in hippocampal neurons without exogenous motor attachment. Graph represents mean ± SEM. Statistical significance was determined using an unpaired t-test with Mann-Whitney correction (***)p<0,001). **B.** Schematic diagram showing the coupling of KIF17-GFP-FRB to FKBP-TdTomato-Rab3c vesicles upon rapalog addition. **C.** Hippocampal neurons were transfected with KIF17-FL-GFP-FRB and FKBP-TdTomato-Rab3c and imaged and analyzed after 2 days. Images show stills from neurons expressing KIF17-FL-GFP-FRB and FKBP-TdTomato-Rab3c before and after rapalog addition. Most KIF17-FL-coupled cargos stop in the proximal axon (yellow arrowheads). In parallel experiments, neurons were treated with 10µM latrunculin B for 1-2 h before imaging. Depletion of actin

allows KIF17-FL-coupled cargos to move through the proximal axon. Scale bar is 10 μm . **D.** Images show stills from hippocampal neurons expressing KIF5-MD-GFP-FRB, KIF17 (266-1029)-GFP-FRB and FKBP-TdTomato-Rab3c before and after rapalog addition. Rapalog-induced coupling of Rab3c to KIF5-MD-GFP-FRB and KIF17(266-1029)-GFP-FRB induces stalling (also indicated as delayed KIF5-MD-induced cargo movements) of vesicles in the axon (top panel). Coupling of KIF17(847-1029)-GFP-FRB does not stall or stop KIF5-MD induced Rab3c vesicle movement. Scale bar is 10 μm . **E.** Percentage of neurons with moving, stalling or stopping Rab3c vesicles along the axon, when coupled to KIF5-MD-GFP-FRB and the indicated KIF17 truncations (n=11-17 cells from at least 2 independent experiments). **F.** Coupling of Rab3c vesicles to KIF17-FL-GFP-FRB in the presence or absence of KIF17 tail domain (KIF17(266-1029)-GFP; note that this construct contains the FRB domain). Images show maximum projections of the timelapse acquired for 10 minutes. The KIF17 tail domain acts as a dominant negative construct and prevents the accumulation and stopping of KIF17-FL-GFP-FRB coupled Rab3 vesicles in the proximal axon. Scale bar is 10 μm . **G.** Percentage of neurons with moving, stalling or stopping Rab3c vesicles along the axon in the presence or absence of the KIF17 tail domain (KIF17(266-1029)-GFP) after rapalog-induced coupling of KIF17-FL-GFP-FRB (n=26-27 neurons from at least 2 independent experiments).

SUPPLEMENTARY VIDEOS

Supplementary Video S1. KIF17-FL Transports Peroxisomes to the Periphery of COS7.

Cells after Rapalog Addition, Related to Figures 2D and 2E. mCOS7 cells were transfected with PEX-RFP-FKBP and KIF17-FL-GFP-FRB and imaged after 1 day overexpression. 100 nM rapalog was added during acquisition to induce coupling of KIF17-FL motors to peroxisomes. Images were taken at 30 s interval. Movie playback is 10 fps. Scale bar is 10 μm .

Supplementary Video S2. KIF17-FL Does Not Directly Target Dendrites but Is Anchored at AIS, Related to Figures 3A–3C.

Adult hippocampal neuron with zoom of the proximal axon. Neurons were transfected with PEX-RFP-FKBP (red) and KIF17-FL-GFP-FRB (green) and imaged after 2 day overexpression. 100 nM rapalog was added during acquisition. Images were taken at 30 s interval. Movie playback is 10 fps. Stalling peroxisomes are indicated with red arrows. Scale bars are 10 μm in full image and 5 μm in zoom.

Supplementary Video S3. Disrupting the AIS by AnkG KD Eliminates Stalling of KIF17-FL-Coupled Peroxisomes, Related to Figure 3C.

Zooms of the proximal axon of neurons transfected with PEX-RFP-FKBP and KIF17-MD-GFP-FRB or KIF17-FL-GFP-FRB with or without AnkG shRNA. Neurons were imaged after 2 day overexpression and 100 nM rapalog was added during acquisition. Images were taken at 30 s interval. Movie playback is 10 fps. Scale bar is 5 μm .

Supplementary Video S4. KIF17-FL Vesicles Are Redirected into Dendrites by Dynein, Related to Figures 4A, 4D, and 4E.

Neuron were transfected with PEX-RFP-FKBP (red), HA-BICD2N-FRB and KIF17-FL-GFP-FRB (green). Neurons were imaged after 2 day overexpression and 100 nM rapalog was added during acquisition to induce simultaneous coupling of KIF17-FL and dynein motors to peroxisomes. Images were taken at 30 s interval. Movie playback is 10 fps. Scale bar is 10 μm .

Supplementary Video S5. KIF17-FL Colocalizes with Peroxisomes in Dendrites after Coupling to BICD2N, Related to Figures 4A, 4D, and 4E.

Zoom of the proximal dendrite of a neurons transfected with PEX-RFP-FKBP (red), HA-BICD2N-FRB and KIF17-FL-GFP-FRB (green). Neurons were imaged after 2 day overexpression and 100 nM rapalog was added during acquisition. Images were taken at 30 s interval. Movie playback is 10 fps. Scale bar is 5 μm .

Videos available online

<http://dx.doi.org/10.1016/j.cub.2016.04.057>

**SUPPLEMENTARY METHODS*****DNA and shRNA constructs***

KIF17 constructs were generated by PCR-based strategy using human KIF17 cDNA sequence (accession NM_020816). PEX-RFP-FKBP construct contains human peroxisomes membrane-targeting sequence (accession NM_003630). HA-BICD2N-FRB construct was generated using BICD2N(1-594) from mouse cDNA (accession AJ250106). Further details about the motor constructs and the FRB/FKBP system can be found in [S1-S4]. KIF17tail(266-1029)-GFP-FRB, KIF17tail(737-1029)-GFP-FRB and KIF17(847-1029)-GFP-FRB were *AscI*/*SalI* subcloned into p β actin-GFP-FRB. FKBP-tdTomato-Rab3c was generated by insertion of PCR-amplified tdTomato in *Sal* and *SpeI* site, mouse Rab3c [S5] in *SpeI* and *NotI* sites and FKBP(1x) in *BamHI* and *SalI* sites of the p β actin-16-pl vector [S1]. The following shRNAs were cloned in pSuper [S6] and used in this study: rat KIF17 shRNA1 (5'-GCCACCAAGATTAACCTGT-3'), rat KIF17 shRNA2 (5'-GACAGACAAAGCTCAACA-3'), rat KIF17 shRNA3 (5'-CCATCAACATCGAGATCTA-3') and AnkG shRNA (5'-GAGTTGTGCTGATGACAAAG-3').

Antibodies and reagents

The following antibodies were used: mouse-anti-tubulin alpha (Sigma), mouse-anti- β -galactosidase (Promega), chicken anti- β -Galactosidase (BGL-1040, Aves Labs), mouse-anti-AnkyrinG (Invitrogen), mouse anti-pan-Nav (clone K58/35, S8809, Sigma), rabbit-anti-GFP (Sanbio), rabbit-anti-KIF17 (K3638, Sigma used in figure 1A-C), rabbit-anti-KIF17 (H-280, Santa Cruz used in Figure S1A) mouse-anti-MAP2 (Sigma), chicken anti-MAP2 (ab5392, Abcam), mouse-anti-Neurofascin-pan (NF-186, Neuromab) for fixed samples and mouse-anti-Neurofascin-pan Extracellular (Neuromab) for live experiments, mouse-anti-tau (Chemicon) and Alexa405-, Alexa488-, Alexa568- and Alexa647- conjugated secondary antibodies (Life Technologies).

Cell culture and transfections

Primary hippocampal neurons were harvested from rat E18 embryos and cultured on poly-L-lysine (35 μ g/ml) and laminin (5 μ g/ml) coated coverslips in neurobasal medium (NB) supplemented with B27, 0.5 mM glutamine, 12.5 μ M glutamate and Pen/Strep [S2]. Mature neurons (>DIV14) were used for all experiments unless otherwise indicated. Cells were transfected with Lipofectamine 2000 (Invitrogen) and fixed with 4% PFA+sucrose or ice-cold 100% methanol / 1 mM EGTA / 4% PFA+sucrose after 2-3 day expression. COS7 cells were cultured in DMEM/Ham's F10 medium (50/50%) with 10% FCS and 1% pen/strep. Cells were transfected with Fugene6 (Roche) and imaged after 1 day.

Immunofluorescence staining

After fixation, cells were washed three times for 5 min in PBS and incubated with primary antibodies in GDB buffer (0.2% BSA, 0.8 M NaCl, 0.5% Triton X-100, and 30 mM phosphate buffer, pH 7.4) overnight at 4°C [S1]. Neurons were then washed three times in PBS for 5 min at room temperature and incubated with secondary antibodies in GDB buffer for 1 h at room temperature. After three washes in PBS, coverslips were mounted in Vectashield (Vector Laboratories). Images were acquired using a wide-field fluorescence microscope (Eclipse 80i; Nikon) or a LSM510 confocal laser-scanning microscope (Zeiss) with 40x or 63x oil objectives. For fluorescence intensity comparison,

settings were kept the same for all conditions. Quantifications were performed using Image J.

Live cell imaging

Live cell imaging experiments were performed on Nikon Eclipse TE2000E microscope equipped with 40x oil objective, Coolsnap CCD camera (Photometrics), perfect focus system and imaging chamber [S2]. Imaging chamber was maintained at 37°C and 5% CO₂ during acquisition. Neurons were imaged in conditioned medium (NB + B27 + P/S) and COS7 were imaged in Ringer's medium. 100 nM rapalog was added during imaging at t = 00:00 (mm:ss). Cells were imaged at 30s intervals for 30-45 minutes. Movement of single peroxisomes and fast motility of KIF17-G754E were imaged at 10 fps and 20 fps respectively using total internal reflection (TIRF) on a Nikon Eclipse TE2000E microscope equipped with 100x oil objective and Evolve EMCCD camera (Photometrics).

Image processing and analyses

Where necessary, stage drift was corrected with FIJI plugin StackReg (translation) prior to analysis. Kymographs were made using FIJI plugin Multiple kymograph, line width = 3 pixels. Average values are stated in the text as mean ± SEM unless otherwise indicated.

Quantification of induced peroxisome transport in COS-7 cells. Image analysis of peroxisome trafficking assay has been described before [S4,S7]. Images of live cells were processed using MetaMorph (Molecular Devices) or LabVIEW (National Instruments) software. The R90 displacement value is calculated by measuring the diameter of a circle to enclose 90% of all intensity relative to the cell center. The average dispersion speed does not reflect the actual velocity of KIF17 but is the average speed with which KIF17 translocates cargo from cell center to cell periphery. $t_{1/2}$ is the time needed for the peroxisomes to reach halfway to the periphery of the cell. Correlation index shows the correlation between consecutive frames (CI ≈ 1: high correlation between frames; CI ≈ 0: low correlation between frames).

Quantification of induced peroxisome transport in neurons. Percentage of neurons with moving, stopping (non-motile) or stalling (irregular, slowly moving) peroxisomes in the proximal axon. Kymographs were drawn along the first 20-30 μm of the axon and peroxisome movement at 30s interval was analysed. We would like to emphasize that that not all KIF17-FL coupled peroxisomes accumulate at the AIS and stay in this axonal region. Some KIF17-coupled peroxisomes escape AIS stalling; they stop in the proximal axon and are released after some time, while others only slow down and move through the AIS. The peroxisomes that make it to the more distal axons are usually motile and are most likely driven by KIF17 motor activity.

Polarity index. Polarity index was calculated using the average dendrite intensity (Id) and average axonal intensity (Ia), using $PI = (Id - Ia) / (Id + Ia)$ [S7]. For non-polarized proteins $Id = Ia$ (PI=0), whereas $PI > 0$ or $PI < 0$ indicates polarization towards dendrites or axons, respectively.

Analysis of KIF17 and AnkG knockdown. DIV11 hippocampal neurons were transfected with either pSuper control or a mix of three shRNAs for KIF17 or AnkG shRNA, together with a fill (GFP or β-galactosidase). Neurons were fixed 72h after transfection and stained for KIF17 or AnkG. Mean intensities of KIF17 or AnkG signals were quantified in dendrites or the axon initial segment, respectively, of control and depleted neurons using ImageJ software.

Analysis of KIF17 distribution in neurons. Plot profiles were created from segmented lines traced in axonal tips or from the soma along the axon using Image J. Data processing and statistical analysis were done in Excel and GraphPad Prism (GraphPad Software).

SUPPLEMENTARY REFERENCES

- S1. Hoogenraad, C.C., Milstein, A.D., Ethell, I.M., Henkemeyer, M., and Sheng, M. (2005). GRIP1 controls dendrite morphogenesis by regulating EphB receptor trafficking. *Nature neuroscience* 8, 906-915.
- S2. Kapitein, L.C., Yau, K.W., and Hoogenraad, C.C. (2010). Microtubule dynamics in dendritic spines. *Methods in cell biology* 97, 111-132.
- S3. Kapitein, L.C., Schlager, M.A., Kuijpers, M., Wulf, P.S., van Spronsen, M., MacKintosh, F.C., and Hoogenraad, C.C. (2010). Mixed microtubules steer dynein-driven cargo transport into dendrites. *Current biology* 20, 290-299.
- S4. Kapitein, L.C., Schlager, M.A., van der Zwan, W.A., Wulf, P.S., Keijzer, N., and Hoogenraad, C.C. (2010). Probing intracellular motor protein

- activity using an inducible cargo trafficking assay. *Biophysical journal* 99, 2143-2152.
- S5. van Vlijmen, T., Vleugel, M., Evers, M., Mohammed, S., Wulf, P.S., Heck, A.J., Hoogenraad, C.C., and van der Sluijs, P. (2008). A unique residue in rab3c determines the interaction with novel binding protein Zwint-1. *FEBS letters* 582, 2838-2842.
- S6. Brummelkamp, T.R., Bernards, R., and Agami, R. (2002). A system for stable expression of short interfering RNAs in mammalian cells. *Science* 296, 550-553
- S7. Lipka J, Kapitein LC, Jaworski J, Hoogenraad CC. (2016). Microtubule-binding protein doublecortin-like kinase 1 (DCLK1) guides kinesin-3-mediated cargo transport to dendrites. *EMBO J.* 35, 302-18.

Spire proteins reorganize a pool of axonal actin and target cargo to the presynapse

Marta Esteves da Silva¹, Bram van Butselaar¹, Feline Lindhout¹, Rene van Dorland¹, Spiros Pachis¹, Riccardo Stucchi^{1,2,3}, Phebe S. Wulf¹, Anna Malik⁴, Jacek Jaworski⁴, Albert J. R. Heck^{2,3}, A. F. Maarten Altelaar^{2,3}, Norihiko Ohbayashi⁵, Mitsunori Fukuda⁵, and Casper C. Hoogenraad¹

¹Cell Biology, Department of Biology, Faculty of Science, Utrecht University, Utrecht, The Netherlands. ²Biomolecular Mass Spectrometry and Proteomics, Bijvoet Center for Biomolecular Research, Utrecht Institute for Pharmaceutical Sciences. ³The Netherlands Proteomics Centre, Utrecht University, Utrecht, The Netherlands. ⁴Laboratory of Molecular and Cellular Neurobiology, International Institute of Molecular and Cell Biology, Warsaw, Poland. ⁵Department of Developmental Biology and Neurosciences, Graduate School of Life Sciences, Tohoku University, Sendai, Japan.

ABSTRACT

The development of imaging techniques and novel probes for visualizing the actin cytoskeleton has been fruitful in the identification of new levels of actin organization in neuronal cells. However, the function of these newly identified structures is not yet elucidated. Spire proteins are actin nucleators, important for long-range actin-dependent transport of vesicles in mouse oocytes. Even though Spire proteins are known to be present in the mammalian brain, not much is known about the role of Spire in neuronal actin organization and function. Here, we study the distribution and function of Spire proteins in hippocampal neurons. Increased Spire levels induce the formation of actin clusters in the axon and affect cargo trafficking. Depletion of Spire causes rearrangement of endogenous actin structures and impairs the transport of synaptic vesicles precursors. Additionally, there is a decrease in the number of synaptic boutons and missorting of presynaptic components. A similar effect is observed when Myosin V function is impaired. These results point to a role of Spire proteins in actin organization and maintenance of the presynaptic terminals, suggesting an involvement of Spire and Myosin V in the delivering cargo to the presynapse.

INTRODUCTION

Eukaryotic cells are abundant in actin, which is involved in fundamental processes, such as cell motility, cell division, maintenance of shape and morphology, signaling and intracellular transport. In neuronal cells, actin is particularly involved in polarity and neurite outgrowth, transport of cargo, synaptogenesis and scaffolding of synaptic structures (Cingolani and Goda, 2008; Hotulainen and Hoogenraad, 2010). Actin is enriched in synapses and even though an extensive body of work has demonstrated the role of actin in synaptic transmission (Honkura *et al.*, 2008; Star *et al.*, 2002) and plasticity (Chen *et al.*, 2007; Fukazawa *et al.*, 2003; Okamoto *et al.*, 2004; Ramachandran and Frey, 2009), studies on the structural organization of actin in neuronal cells are only now coming to light. Recent work using super-resolution microscopy has demonstrated that actin is periodically organized in ring-like structures interspersed with spectrin in axons (Leterrier *et al.*, 2015; Xu *et al.*, 2013), dendrites and spines (Bar *et al.*, 2016; D'Este *et al.*, 2015; He *et al.*, 2016; Sidenstein *et al.*, 2016). In addition, other actin structures have been identified in neurons, such as actin patches (Korobova and Svitkina, 2010; Spillane *et al.*, 2011; Watanabe *et al.*, 2012) and the recently identified actin hotspots, from where actin trails can be generated (Ganguly *et al.*, 2015). Despite the advancements in the visualization of different levels of actin organization, little is known about the function of these structures in neuronal cells.

Another important aspect that has not been explored in detail is the role of actin in intracellular transport in neurons. As actin mostly accumulates in the presynaptic active zone and post-synaptic dendritic spines (Landis, 1988; Landis and Reese, 1983), Myosin motor proteins were shown to be involved in short-range transport of synaptic cargo (Bittins *et al.*, 2010). Previous work from mouse oocytes showed that Spire (or Spir) proteins cooperate with Formin-2 and that these actin nucleators generate an actin network important for asymmetric oocyte division (Pfender *et al.*, 2011). Additional work provided information regarding actin-dependent long range transport in oocytes (Schuh, 2011). The actin nucleators Spire1, Spire2 and Formin-2 are recruited to the membrane surface of Rab11-positive endosomes, generating an actin network that interconnects the vesicles and the plasma membrane. The endosomes are then transported along actin by Myosin Vb hence providing a mechanism of transport based on the actin cytoskeleton that can either be local or global along the cell.

Previous work in *Drosophila* oocytes shows that Spire acts together with Cappuccino in maintaining cell polarity during mid- oogenesis (Emmons *et al.*, 1995; Manseau and Schupbach, 1989; Wellington *et al.*, 1999). The coincident phenotype of *Drosophila* *spire* and *cappuccino* mutants provides solid indications of a common regulatory pathway. In fact, *Drosophila* Cappuccino has a very similar profile to the mammalian Formin-1 and Formin-2 proteins (Emmons *et al.*, 1995; Leader and Leder, 2000; Zeller *et al.*, 1999). Formin-2 is expressed in the mouse ovary oocyte and the brain, in the developing and mature central nervous system (Leader and Leder, 2000). Interestingly, Formin-2 deficient mice do not display abnormalities in the nervous system, but show hypofertility due to defective metaphase spindle positioning during meiosis I (Leader *et al.*, 2002). There are two mammalian homologues of the *Drosophila*

spire gene, *spir-1* and *spir-2* (Ciccarelli *et al.*, 2003; Kerkhoff *et al.*, 2001). *Spir-1* gene shares an overlapping expression pattern of the *formin-2* gene in the brain, enriched in the hippocampus, dentate gyrus and cerebellum (Schumacher *et al.*, 2004).

Spire actin nucleation is remarkably different from the other known nucleation factors, the Arp2/3 complex and the Formin superfamily of FH2 domain-containing nucleators (Chesarone and Goode, 2009) due to its ability to nucleate free G-actin monomers. Spire proteins identified so far – *Drosophila* dSpire, *Ciona savignyi* PEM-5 and the vertebrate Spire1 and Spire2 – contain four Wiskott-Aldrich syndrome protein (WASp) homology2 (WH2) domains that bind actin (Wellington *et al.*, 1999). The association of one actin monomer in each of the WH2 domains promotes actin nucleation by surpassing the kinetic barrier of spontaneous nucleation, without requiring additional factors (Quinlan *et al.*, 2005). The structure domain of Spire has been defined and it includes an N-terminal kinase noncatalytic C-lobe domain (KIND), four WH2 domains, a Spir-box and a C-terminal FYVE zinc finger (Fig.1A). The KIND domain interacts with Formin-1 and Formin-2 through a FSI motif (Formin-Spire interaction) adjacent to the FH2 domain on the C-terminus of Formin (Pechlivanis *et al.*, 2009). Structural studies demonstrated a 1:1 ratio of KIND/FSI complex formation (Vizcarra *et al.*, 2011; Zeth *et al.*, 2011) and that the Formin FH2 dimers bind two KIND domains, resulting in a heterotetrameric complex (Quinlan *et al.*, 2007). Interestingly, it was also demonstrated that interaction of Formin-2 with the KIND domain of Spire results in inhibition of actin nucleation by Formin (Quinlan *et al.*, 2007). The current model for Spire and Formin interaction proposes that the formation of the KIND/FSI complex induces dimerization of Spire protein. Spire dimers can then nucleate the two strands of the actin filament, by binding four actin monomers to each of the Spire-WH2 domains (Quinlan and Kerkhoff, 2008). After nucleation, the KIND/FSI dissociates and filament elongation occurs, as Formin polymerizes actin while associated with the barbed-end of the filament (Fig.1B). It is still unclear whether Spire proteins remain bound to the pointed- or to the barbed-end of actin during filament elongation or even if it dissociates after nucleation, as work from different independent groups show opposite results (Bosch *et al.*, 2007; Ito *et al.*, 2011; Quinlan *et al.*, 2005; Sitar *et al.*, 2011).

At the C-terminal of Spire there is a FYVE zinc-finger membrane-binding domain that is required for membrane localization (Kerkhoff, 2006; Otto *et al.*, 2000). FYVE domains are typically present in proteins targeted to lipid membranes by binding specifically to phosphatidylinositol-3-phosphate (PI3P) (Mari *et al.*, 2001; Ridley *et al.*, 2001; Sankaran *et al.*, 2001). The interplay between FYVE domains and Rab GTPases has been previously described. The FYVE domain of the early endosome antigen 1 (EEA1) is necessary to bind PI3P, while a short region directly adjacent to the FYVE domain binds to Rab5 (Simonsen *et al.*, 1998). Interestingly, the Spire FYVE domain lacks a basic pocket that specifically binds PI3P, which might affect its binding to membranes, or promote promiscuous interactions with negatively charged lipids (Otto *et al.*, 2000). The Spir-box is N-terminally adjacent to the FYVE domain. This highly conserved region is similar to a region flanking the FYVE domain of rabphilin-3A, involved in the interaction between rabphilin-3A and Rab3A (Kerkhoff *et al.*, 2001; Ostermeier

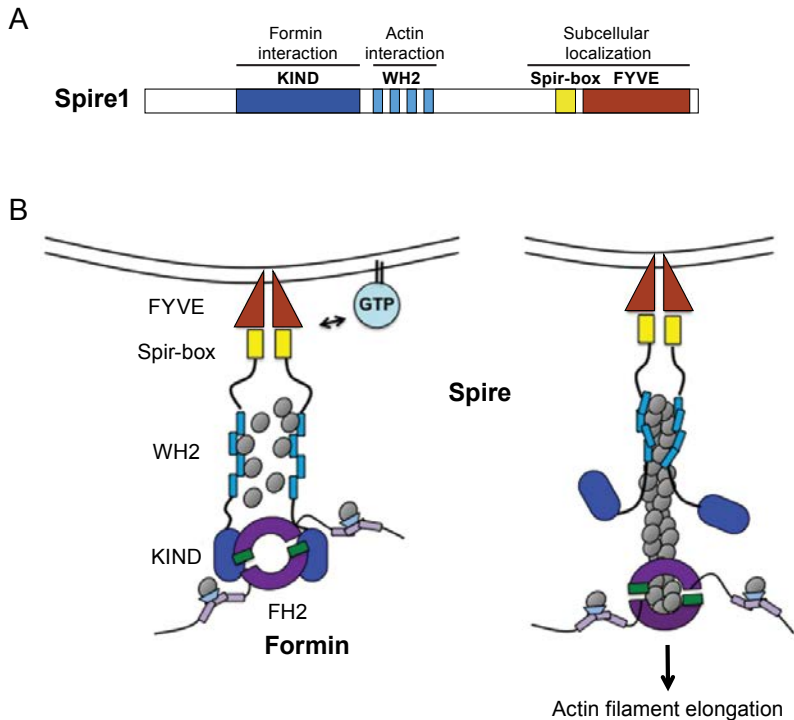


Figure 1. Spire protein structure and interaction with intracellular membranes and Formin

A. Schematic diagram of Spire1 domains and previously described interactions. **B.** Model of Spire/Formin cooperation in actin nucleation and elongation. Combined results from cell biology studies, protein interaction and *in vitro* nucleation assays propose that Spire proteins are targeted to intracellular membranes by the FYVE zinc finger domain. Specification of membrane localization is probably influenced by interaction between the Spir-box domain and GTP-bound proteins of the Ras superfamily. Spire binds to Formins via the KIND-FSI interaction, inducing Spire dimerization at the membrane. Each WH2 domain binds one actin monomer, promoting nucleation of the actin filament. Spire dimers nucleate the two strands of the actin filament. After nucleation, elongation is promoted by Formin coupled to the barbed-end of the new actin filament (adapted from Kerkhoff, 2011).

and Brunger, 1999), which suggests a role for Spir-box in the association of Spire proteins with Rab GTPases. In fact, Spire proteins colocalize with Rab11-endosomes in cells (Kerkhoff *et al.*, 2001), indicating a close functional relationship between the two proteins, even though a direct interaction has not been described so far. The proximity between Spir-box and FYVE might enhance the specificity of membrane targeting through interaction of Spire proteins with additional factors (Pylypenko *et al.*, 2016) (Fig.1B). Understanding the mechanism of Spire organization in membranes is still challenging, as over the years different models of action have been put forward. The most recent model proposes that the Spire FYVE domain interacts with the KIND domain in the N-terminal, thus generating a cytosolic backfolded monomer. As Spire binds to membranes, the KIND domain is released, allowing for Formin-2 recruitment, dimerization and actin nucleation (Tittel *et al.*, 2015).

In this preliminary study we investigate the function of Spire proteins in hippocampal neurons. Our results demonstrate that Spire proteins are involved in actin reorganization in the axon and may have an important role in the delivery of cargo to the presynapse.

RESULTS

Spire localizes in the axon and overlaps with actin clusters

Spire proteins are expressed in the developing and adult brain (Pleiser *et al.*, 2010; Schumacher *et al.*, 2004). Moreover, in a systematic proteomic profiling study in rat primary hippocampal cultures, it was shown that Spire1 is upregulated during differentiation (Frese *et al.*, 2017). To understand how Spire proteins are distributed in cultured hippocampal neurons, we expressed GFP- or mCherry-tagged Spire1 and Spire2 in DIV15 neurons (Fig.2A). Both Spire proteins show similar distribution patterns which overlap with actin rich structures in dendritic spines and cell body. Interestingly, Spire overexpression forms bright clusters distributed along the axon from the proximal region at the axon initial segment (AIS; Fig.2B) to more distal locations. These clusters clearly colocalize with actin and are only evident along the axon, indicating a specific distribution of overexpressed Spire in hippocampal axons.

To understand the function of Spire in axons, we performed knockdown experiments of Spire1 and Spire2. For this, we first generated 3 different short-hairpin RNAs (shRNAs) targeting Spire1 and Spire2. We next tested the knockdown efficiency in primary cortical neurons using RT-qPCR (Fig.2C). Spire1 shRNA#2 and Spire2 shRNA#2 showed more than 50% decrease in expression relative to GADPH. Additionally, we performed Western blot analysis with lysates from primary cortical neurons, and observed a significant decrease in Spire1 signal with Spire1 shRNA#2 and also with a combination of Spire1 #2 and Spire2 #2 shRNAs (Fig.2D). We could not perform the same experiment for Spire2 expression levels, as the commercially available Spire2 antibodies failed to detect endogenous levels of Spire2 in neuronal extracts. Additionally, the Spire1 antibody used for Western blot did not work efficiently in immunohistochemistry experiments. Considering the potential redundancy between Spire1 and Spire2 (Pfender *et al.*, 2011) we performed all knockdown experiments with a combination of the two shRNAs, from now on described as Spire 1+2 shRNA.

As Spire clusters cause actin accumulation along the axon including in the AIS, we tested whether expression or depletion of Spire would affect the structural organization of the AIS and axon outgrowth in developing neurons (4DIV; Fig.2E). Although the length of the AIS and the number of neurites positive for the AIS marker Neurofascin was not altered on Spire-depleted neurons (Fig.2F), there was a significant increase in AIS length in neurons expressing mCherry-Spire (Fig.2G,H). Axon morphology was also affected in Spire-expressing neurons, which had shorter and less branched axons compared to control neurons (Fig.2I-J).

Spire is involved in the maintenance of presynaptic boutons

Presynapses are actin-rich structures distributed along the axon, which contain the

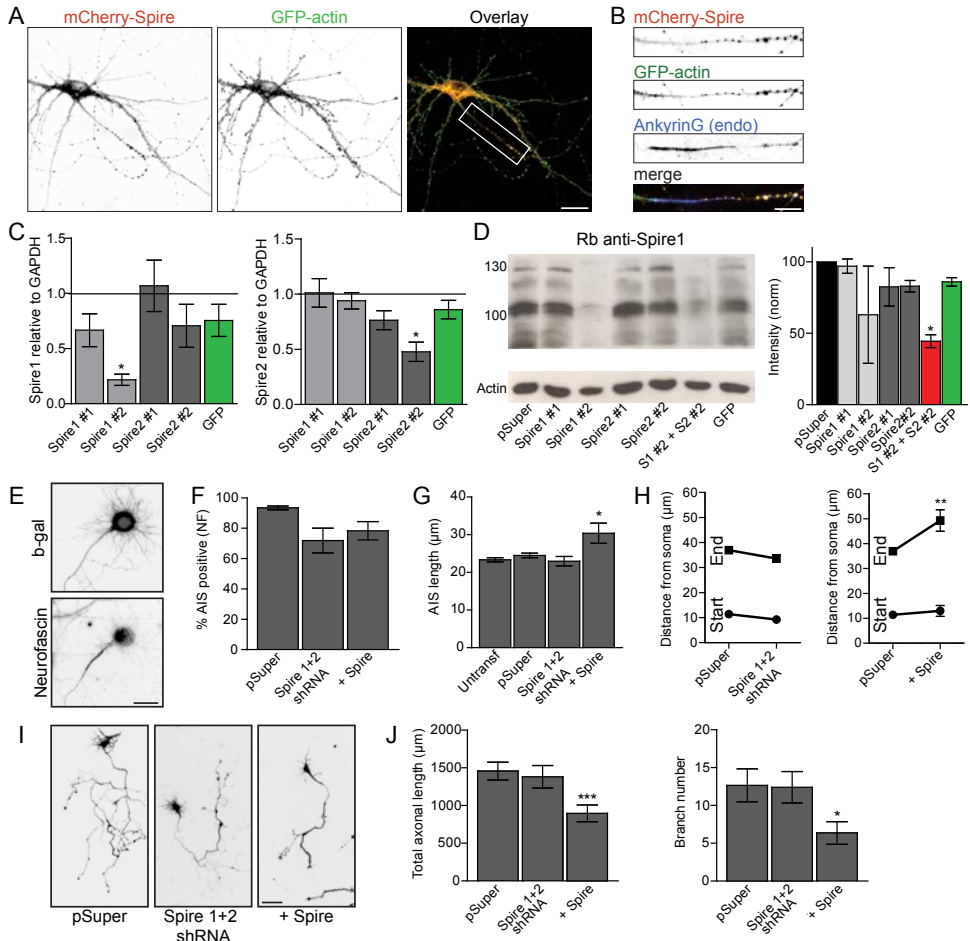


Figure 2. Spire distributes in clusters along the axon

A. Hippocampal neuron (DIV15) expressing mCherry-Spire (left) and GFP-actin (right). Spire distributes as clusters along the axon, which overlap with actin. Scale bar is 20 μm. **B.** (inset from **A**) Spire/actin clusters partially overlap with the AIS (visualized with AnkyrinG antibody). Scale bar is 10 μm. **C.** Validation of Spire1 and Spire2 shRNAs by RT-qPCR. Cortical neurons were electroporated with the described shRNAs. mRNA levels of Spire1 (left plot) and Spire2 (right plot) were quantified relatively to GAPDH levels and compared with GFP-expressing neurons. (N = 3 independent experiments). **D.** Western blot of cortical neuronal cultures expressing Spire1 and Spire2 shRNAs. Quantification of band intensities shows a strong decrease in Spire1 levels when Spire1 shRNA#1 and Spire2 shRNA#2 are combined (N = 2). **E.** Example of a DIV4 hippocampal neuron expressing β-galactosidase (top) and stained with AIS marker Neurofascin (bottom). Scale bar is 20 μm. **F.** Quantification of the fraction of neurons with AIS in the different conditions. **G.** Quantification of the length of AIS in the different conditions. Untransfected neurons were also quantified, showing no difference with control (pSuper) neurons (n = 25-125 neurons; N = 3-8 independent experiments). **H.** Distance from soma to the start of AIS and from soma to the end of AIS in control, Spire-depleted neurons (left) or Spire-expressing neurons (right). **I.** Examples of 4DIV neurons expressing β-galactosidase in the different conditions. Scale bar is 50 μm. **J.** Quantification of total axonal length (left) and branch number (right) in the different conditions (n = 22-35; N = 3). Graphs represent mean ± SEM. Statistical significance was determined using an unpaired t-test with Mann-Whitney correction (**C-D**), or one-way ANOVA using Kruskal-Wallis test and Dunnett's multiple comparison post hoc test (**F-H, J**) * p<0.05, ** p<0.01.

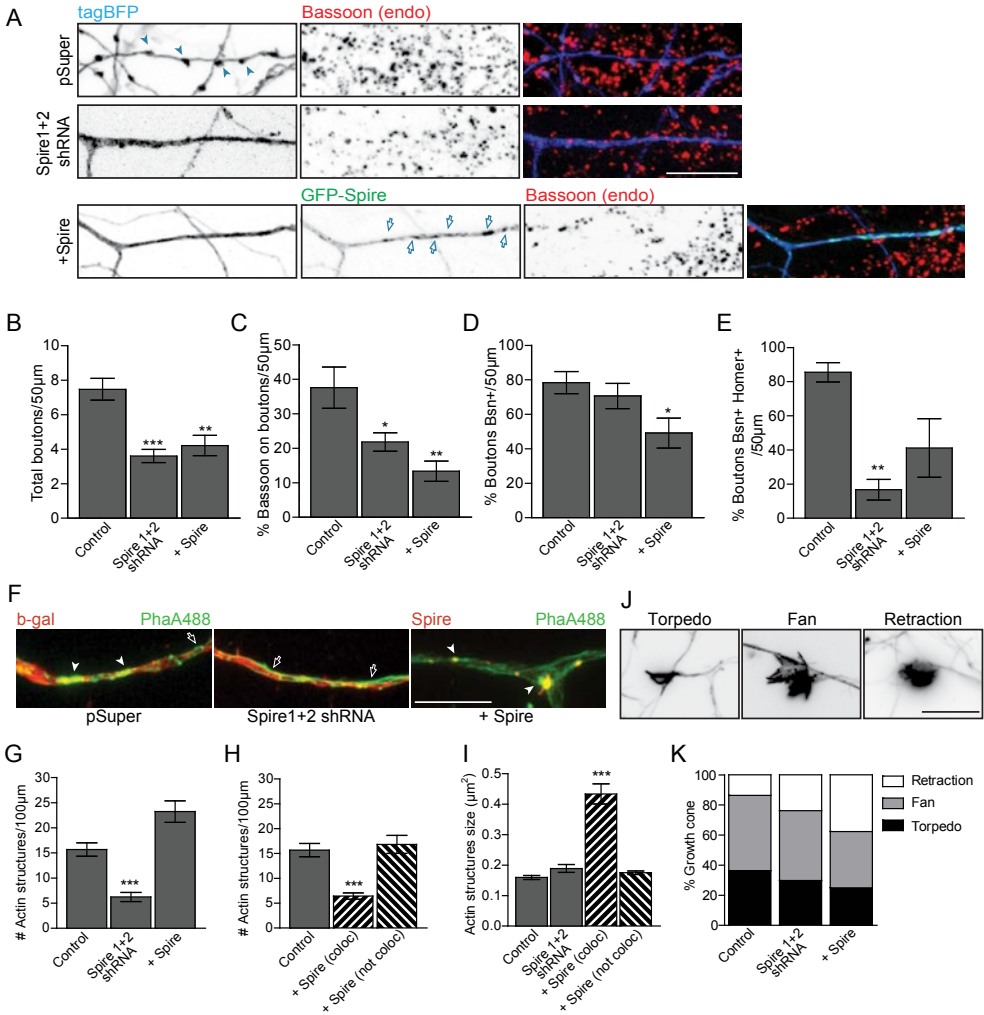


Figure 3. Spire regulates distribution of presynaptic components and reorganizes actin in the axon

A. Examples of axons co-expressing tagBFP and pSuper (control), Spire1+2 shRNA or GFP-Spire1 and further labeled with Bassoon. In control neurons synaptic boutons are clear (full arrows), but missing after Spire knockdown and in Spire-expressing neurons. GFP-Spire axonal clusters (open blue arrows) do not colocalize with boutons or Bassoon clusters. Scale bar is 10 μm .

B. Quantification of the number of synaptic boutons number per 50 μm of axon ($n = 20-35$; $N = 2$).

C. Quantification of the fraction of Bassoon clusters that are located in boutons.

D. Quantification of the fraction of boutons positive for Bassoon.

E. Quantification of the fraction of boutons that colocalize with pre- and postsynaptic markers (Bassoon and Homer, respectively).

F. Examples of neurons co-expressing β -galactosidase and pSuper (control), Spire1+2 shRNA, or mCherry-Spire and labeled with phalloidin Alexa488 to visualize endogenous actin structures. Arrow heads highlight actin clusters, and empty arrows indicate actin stretches along the axon. Scale bar is 10 μm .

G. Quantification of actin structures (clusters or stretches) in the different conditions. Quantification is based on phalloidin Alexa488 labelling.

H. Quantification of actin structures in Spire-expressing neurons. The increase in actin structures in Spire-expressing neurons corresponds to colocalization with Spire clusters.

I. Quantification of the size of actin structures. Actin structures that colocalize with Spire clusters are markedly bigger than the other conditions ($n = 30-40$; $N = 4$).

J. Examples of different classes of growth cones present in hippocampal neurons. Scale bar is 10 μm .

bar is 5 μm . **K.** Quantification of the different morphology of growth cones in the different conditions ($n = 19-21$; $N = 2$). Graphs represent mean \pm SEM. Statistical significance was determined using an unpaired t-test with Mann-Whitney correction (B-E), or one-way ANOVA using Kruskal-Wallis test and Dunnett's multiple comparison post hoc test (H-J) * $p < 0.05$, ** $p < 0.01$, *** $p < 0.001$.

presynaptic machinery and synaptic vesicles. They are often located in synaptic boutons, characterized by thickenings of the axon. We correlated Spire distribution with presynaptic bouton localization. In mature control neurons (21DIV), there are many synaptic boutons along the axon, which are positive for the presynaptic protein Bassoon (Fig.3A, blue arrowheads). When expressing Spire, we observed that Spire clusters do not colocalize with Bassoon (Fig.3A, open blue arrows), which suggested that Spire was excluded from presynaptic boutons. Additionally, the number of synaptic boutons was strongly decreased in Spire-expressing axons (Fig.3A,B), and the remaining boutons contained significantly less Bassoon clusters (Fig.3D), which indicates that most of the remaining Bassoon clusters are redistributed to the axonal shaft (Fig.3C). A similar phenotype was found in Spire-depleted neurons, in which the number of presynaptic boutons was also markedly decreased (Fig.3B). Moreover, the fraction of Bassoon puncta on boutons (Fig.3C) and the fraction of boutons colocalizing with Bassoon and Homer (a postsynaptic marker; Fig.3E) were strongly decreased. These results indicate that even though Spire itself is not localized at the presynapse, its presence is required for the maintenance of the presynaptic structure and proper localization of components to the presynapse.

Spire regulates proper actin organization along the axon

As Spire clusters accumulate actin, it is important to understand how Spire could affect the axonal actin cytoskeleton. Using fluorescently labeled phalloidin that binds to actin filaments we examined endogenous actin structures in more detail. In control neurons we observed small actin structures along the axon (Fig.3F, pSuper). Considering the axonal actin structures that have recently been described, it is tempting to speculate that these actin structures correspond to previously described 'hotspots' found in axons (Ganguly *et al.*, 2015; Ladt *et al.*, 2016). However, actin hotspots were observed in live-imaging experiments with overexpression of actin-bound peptides (Utr-CH), which could influence the stability of these structures. Further work is clearly needed to fully understand the nature and dynamics of phalloidin-labeled structures. Upon Spire knockdown the number of actin structures significantly decreased (Fig.3G). In addition, the remaining actin clusters were morphologically distinct, as they became slightly more elongated in the absence of Spire (Fig.3F, open arrows). In contrast, when mCherry-Spire was overexpressed, the clusters become enlarged and show strong F-actin accumulation (Fig.3F,I, white arrowheads). When analyzing the images, we split the actin patches according to their overlapping distribution with Spire clusters, and observed that the actin structures colocalizing with Spire account for an additional fraction of actin structures compared to control (Fig.3H) and are larger in size than control and non-colocalizing structures (Fig.3I). The axonal growth cone is also highly enriched in actin and its function is dependent on actin dynamics (Bradke

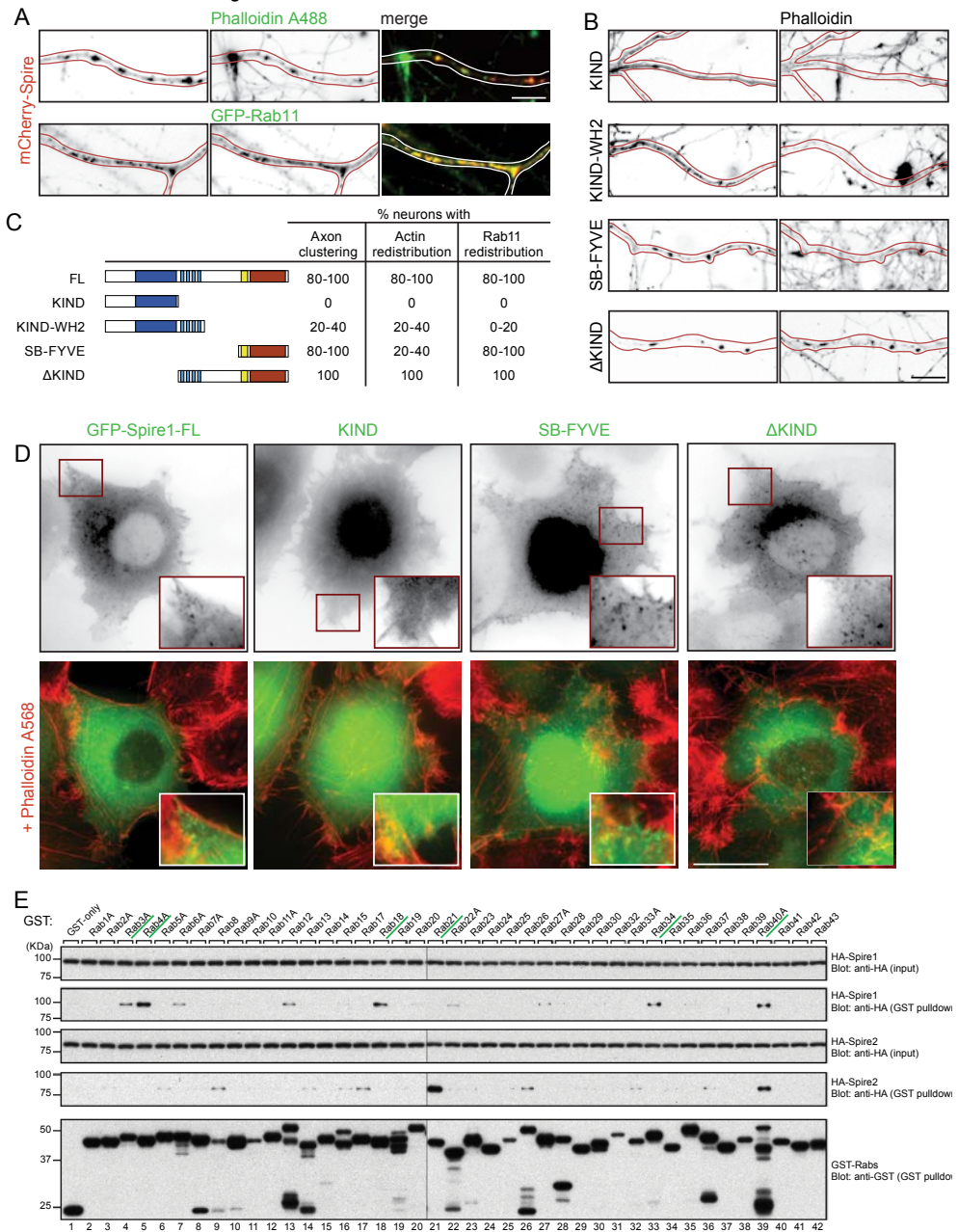


Figure 4. Interplay between the KIND and WH2 domains determines Spire clustering in the axon and redistribution of actin and cargo

A. Expression of full-length Spire1 (Spire1-FL) clusters endogenous actin (top panel) and expressed Rab11 (bottom panel) in the axon. Scale bar is 10 μ m. **B.** Examples of axons expressing Spire1-FL and Spire1 truncations (left) and labeled with phalloidin Alexa568 (right). Scale bar is 10 μ m. **C.** Summary of the effect of overexpression of Spire1 truncations in the formation of axonal clusters, reorganization of axonal actin and distribution of Rab11 endosomes

in the axon ($n = 5-35$; $N = 2-3$). **D.** Expression of full-length and truncated Spire1 in HeLa cells. Insets show that Spire1-KIND is cytoplasmic and that Spire1-FL, SB-FYVE and Δ KIND form clusters close to the periphery of the cell (top panel), where endogenous actin is also localized (bottom panel). Scale bars are 20 μm and 5 μm (inset). **E.** GST pull-down assay with GST-Rabs (Rab1–43) and lysates of COS-7 cells expressing HA-Spire1 or HA-Spire2. The positions of the molecular mass markers (in kDa) are shown on the left. Rab-GTPases that show a interaction with Spire-1 or Spire-2 are underlined in green.

and Dotti, 1999; Lowery and Van Vactor, 2009). We analyzed the morphology of growth cones according to previous studies. Growth cones were classified as follows: a retraction bulb when the growth cone is shrinking, a fan which is the most exploratory behavior, and a torpedo when the growth cone is in clear expansion (van der Vaart *et al.*, 2013) (Fig.3J,K). While there is no major change in growth cone morphology after Spire depletion, overexpression of Spire strongly affects growth cone shape by increasing the fraction of retraction bulbs.

The WH2-SB-FYVE domains of Spire are necessary for actin and endosome redistribution in neurons

Previous work demonstrated that Spire nucleates actin from cellular membranes, particularly from Rab11-positive recycling endosomes (Schuh, 2011). Indeed, expressing Spire in hippocampal neurons showed accumulation of Rab11-positive endosomes at the actin-positive Spire clusters in the axon (Fig.4A). To further investigate the relation between Spire and Rab11, we generated several Spire truncation constructs (Fig.4C), according to Spire1 previously identified structural domains (Kerckhoff, 2006). Spire1 truncations were co-expressed with Rab11 in neuronal cultures and labeled with phalloidin to visualize endogenous F-actin. The Formin-interacting KIND domain is diffusive and does not form actin-rich clusters or rearranges Rab11-endosome distributions (Fig.4B,C and Supp. Fig.S1). The KIND-WH2 is mostly diffusive, forming only few clusters in the axon that colocalize with endogenous actin (Fig.4B). Spire1-Spir-box-FYVE (SB-FYVE) forms clusters in the axon, that cause Rab11 redistribution (Supp. Fig.S1) but very little actin reorganization (Fig.4B-C). Similar to the full length Spire, the C-terminal fragment containing the WH2-SB-FYVE domains (Δ KIND) formed large actin- and Rab11-positive clusters in the axon (Fig.4B,C, Supp. Fig.S1), indicating that the KIND domain is not critically involved in cluster formation, and in fact it even seems to reduce clustering. In contrast to what was observed in neurons, in HeLa cells full-length Spire was largely diffuse and formed only a few actin-rich clusters (Fig.4D). Expression of the Spire1-SB-FYVE and Spire1- Δ KIND revealed a punctate pattern throughout cells which colocalizes with both endogenous Rab11 and tdTomato-Rab11 (Fig.4D, Supp. Fig.S2A,B). Spire1- Δ KIND clusters also accumulated endogenous actin. Interestingly, the distribution of endogenous Rab11-endosomes and F-actin was not altered by Spire clusters, but instead the clusters accumulated where endosomes and F-actin are typically localized in cells. Additionally, when co-expressing Spire1 with Rab11, the Spire1 clusters were redistributed to Rab11-endosomes in the periphery and not the opposite, as happens in neurons (Supp. Fig.S2).

Several studies have shown the interplay between Rab proteins and Spire. For example,

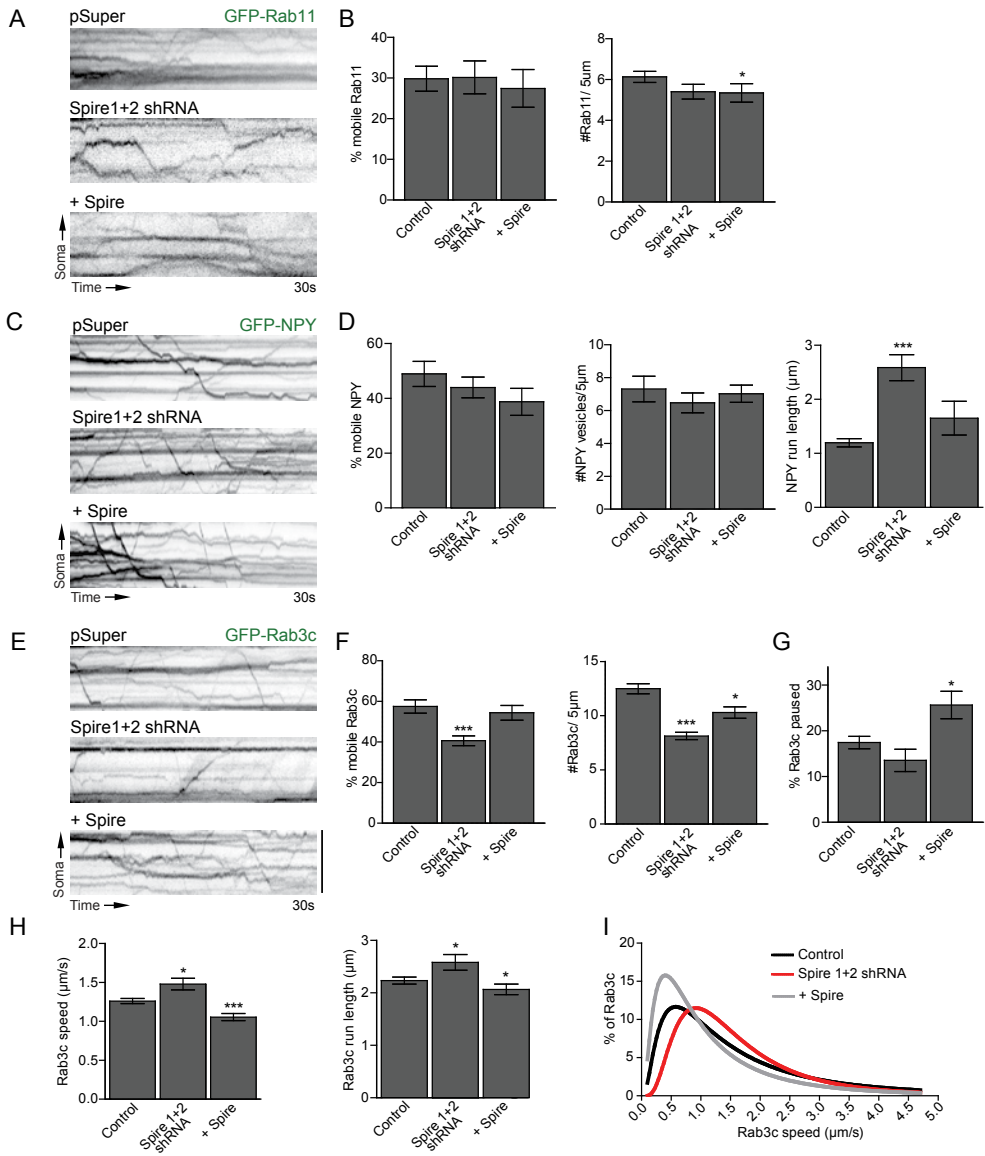


Figure 5. Spire clusters affect cargo trafficking in the axon

A. Kymographs of Rab11-transport, co-expressed with pSuper (control), Spire 1+2 shRNA or mCherry-Spire1. **B.** Quantification of the fraction of mobile Rab11-transport in the different conditions (left) and the number of Rab11-transport per 5 μm of axon, in the different conditions (right) (n = 13-21, N = 3). **C.** Kymographs of NPY-transport, co-expressed with pSuper (control), Spire 1+2 shRNA or mCherry-Spire1. **D.** Quantification of the fraction of mobile NPY-transport in the different conditions (left), number of NPY-transport per 5 μm of axon (middle), and the run length of transport in the different conditions (right) (n = 14-17, N = 4). **E.** Kymographs of Rab3c-transport, co-expressed with pSuper (control), Spire 1+2 shRNA or mCherry-Spire1. Scale bar is 5 μm. **F.** Quantification of the fraction of mobile Rab3c-transport in the different conditions (left) and the number of Rab3c-transport per 5 μm of axon, in the different conditions (right). **G.**

Quantification of the fraction of paused Rab3c vesicles in the different conditions, corresponding to vesicles that were previously moving and pause during the acquisition time. **H.** Quantification of Rab3c speeds along the axon (left), the average run length of Rab3c vesicles (right). **I.** Lognormal fits of the (non-Gaussian) distribution Rab3c speeds quantified in **H** (n = 10-14; N = 3). Graphs represent mean \pm SEM. Statistical significance was determined by using Kruskal-Wallis test or one-way ANOVA and Dunnett's multiple comparison post hoc test, respectively; *p<0.05, **p<0.01, ***p<0.001. Scale bar is 5 μ m.

Spire colocalizes with Rab11 endosomes (Kerkhoff *et al.*, 2001) and Spire1 interacts with Rab3A GTPase in cancer cell models (Lagal *et al.*, 2014). Therefore we tested whether Spire interacts with other members of the family of Rab GTPases. To do this, we performed a GST-pull down assay with a library of GST-Rabs (1-43) and lysates of COS7 cells expressing HA-Spire1 or HA-Spire2. HA-tagged proteins and GST-Rabs were detected by immunoblotting with the antibodies indicated (Fig.4E). We found no evident binding between Spire proteins to Rab11 in this assay. Nevertheless, Spire1 was pulled down by Rab3A, Rab4A, Rab18 and several other Rabs, while Spire2 was pelleted by e.g. Rab21 and Rab40. Our data support a partnership between Spire proteins and Rab GTPase and indicate a wider interplay between Spire and Rab proteins than previously anticipated.

Spire is involved in cargo trafficking in the axon

The observed interplay of Spire with Rab GTPases and the actin cytoskeleton suggests that Spire proteins may be involved in axonal cargo trafficking. Therefore, we performed live-imaging of different axonal cargos such as Rab11-positive recycling endosomes, NPY-vesicles and Rab3-vesicles, which are precursors of synaptic vesicles. By performing kymograph analysis we quantified the number and mobility of cargo. We did not observe differences in the total number or mobility of Rab11-endosomes or NPY in Spire-depleted or Spire-expressing neurons (Fig.5A-D). However, there was a clear increase in the distance travelled by NPY-vesicles in the axon when Spire was depleted (Fig.5D, right graph). In contrast to Rab11 and NPY cargo, we found a significant decrease in mobile Rab3c vesicles along the axon in Spire-depleted neurons (Fig.5E-F), which indicates that Spire might be involved in the transport of Rab3c-vesicles along the axon. To study this in more detail we measured the speed of single vesicles in the axon and observed that Rab3c-vesicles move faster and for longer distances when Spire is depleted. In contrast, in Spire-expressing neurons Rab3c-vesicles move significantly slower and for shorter distances (Fig.5H), and the fraction of Rab3c-vesicles pausing along the axon is increased (Fig.5G). Previous work suggested that the actin cytoskeleton can oppose microtubule-based cargo trafficking (Kapitein *et al.*, 2013). This data suggests that Spire might be required for stalling synaptic vesicles in axons, which is further evidenced by plotting the distribution of Rab3c-vesicles speeds (Fig.5I). We observed a marked shift in the speed of Rab3c-vesicles transport in Spire-silenced neurons to speeds above 1 μ m/s, whereas in the case of Spire overexpression, more vesicles move with speeds below 1 μ m/s (Fig.5I). These results indicate that Spire is required for proper Rab3 vesicle trafficking in axons.

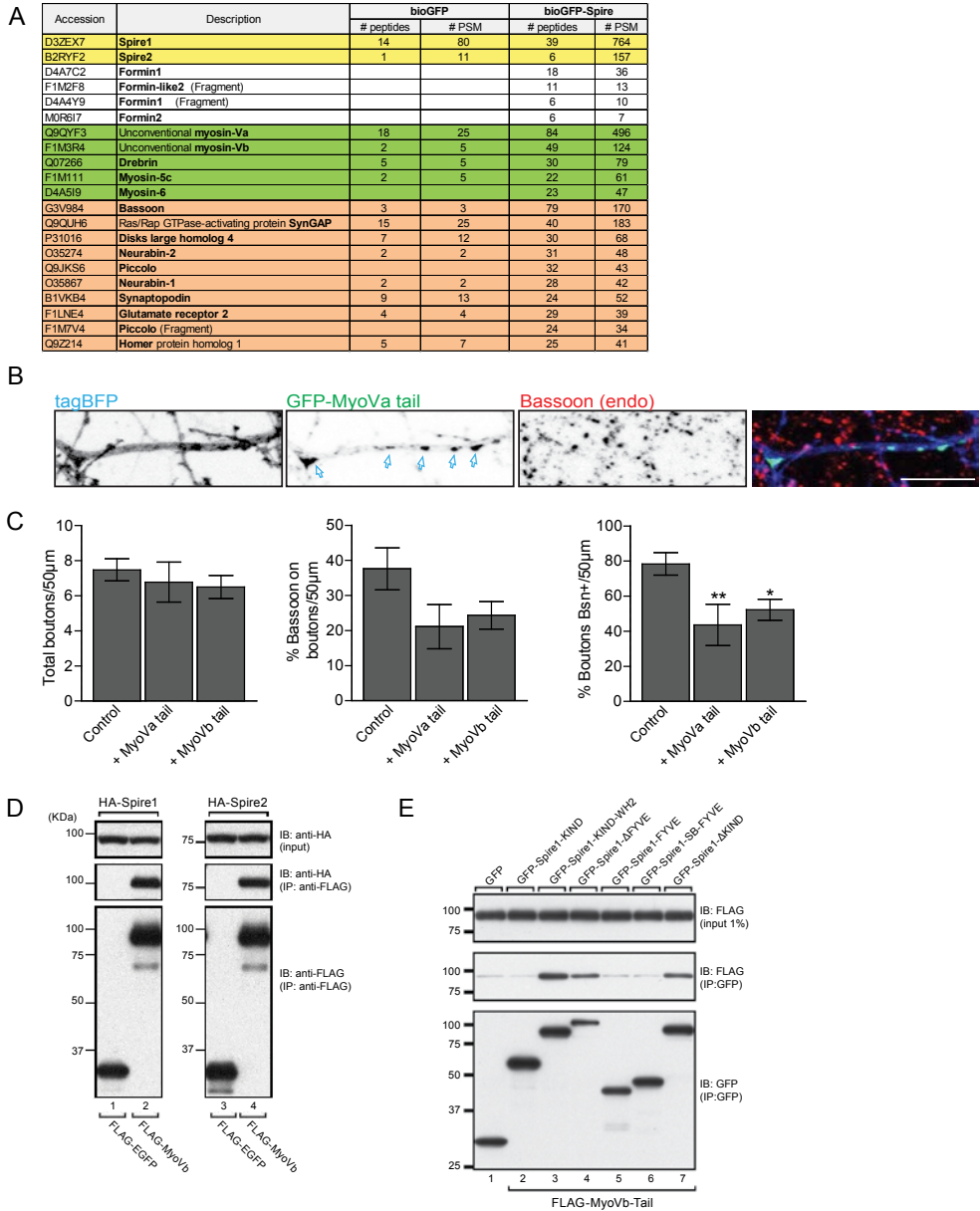


Figure 6. Spire interacts with Myosin V and presynaptic components

A. Binding partners of Bio-GFP-Spire1 in HEK293 cells loaded with brain extracts and identified by mass spectrometry. White: Formins; Green: actin-related proteins; Orange: synaptic markers. **B.** Example of axon co-expressing tagBFP and GFP-Myosin Va tail and labeled with Bassoon. GFP-Myosin Va tail forms cluster similar to Spire along the axon (open blue arrows) that do not colocalize with boutons or Basson clusters. Scale bar is 10 μ m. **C.** Quantification of bouton number along 50 μ m axon in the specified conditions (left), the fraction of Bassoon clusters that colocalize with boutons (middle) and the fraction of boutons positive for Bassoon ($n = 9$; $N = 2$). **D.** Co-immunoprecipitation assays in COS7 cells show interaction between HA-Spire1 and HA-Spire2 and with Myosin

Vb-tail. **E.** Co-immunoprecipitation assays in COS7 cells show that Myosin Vb-tail interacts with the WH2 domain of Spire1. Graphs represent mean \pm SEM. Statistical significance was determined using an unpaired t-test with Mann-Whitney correction (C) * $p < 0.05$, ** $p < 0.01$.

Spire interacts with Myosin V and regulates the distribution of presynaptic components in the axon

To investigate the mechanism by which Spire anchors cargos to actin-rich structures in the axon, we searched for Spire interactors using a pull-down approach. Here, lysates of HEK293T expressing Bio-GFP-Spire1 and the protein-biotin ligase BirA were incubated with adult rat brain extracts, and isolated proteins were analyzed by mass spectrometry. We verified binding of Bio-GFP-Spire1 to the previously identified partner Formin-2 (but also Formin-1; Fig.6A, yellow). Potential Spire1 binding partners were identified, including actin-based motors Myosin V and Myosin VI and other actin-related proteins (Fig.6A, green), and pre- and postsynaptic proteins Bassoon, SynGAP, Neurabin, Piccollo and Homer (Fig.6A, orange). To validate the pull down data we performed co-immunoprecipitation assays and confirmed the interaction between Spire1 and Spire2 and Myosin Vb-tail (Fig.6D). Additional experiments using the truncated forms of Spire showed that Spire1 and Myosin Vb tail interact via the WH2 domain (Fig.6E). Given the nature of this domain, we hypothesized this interaction happens via actin. When expressed in hippocampal neurons, GFP-Myosin Va-tail and Myosin Vb-tail had a very similar distribution pattern as Spire, forming enlarged clusters along the axon (Fig.6B). Similar to Spire expression (Fig.3A-D), the fraction of Bassoon clusters on boutons is decreased in myosin-V-tails-expressing axons and the fraction of synaptic boutons that contain Bassoon clusters was reduced (Fig.6C). These results suggest an uncharacterized interaction between Spire and the actin motor protein Myosin V, which may regulate the distribution of presynaptic cargo along the axon.

DISCUSSION

The neuronal actin cytoskeleton is very dynamic and provides structure for intracellular transport in a more flexible, tunable way than the microtubule network. The development of new tools to label and visualize actin structure and dynamics has revealed new actin structures in neurons, whose function needs to be studied in detail (Ganguly *et al.*, 2015; Xu *et al.*, 2013). Recent published work highlights the functional links between actin and actin regulators, myosins and cargo, that synergistically cooperate to specify transport (Cheng *et al.*, 2012; Schuh, 2011; Sirotkin *et al.*, 2005; Sun *et al.*, 2006). Spire proteins are a family of actin nucleators, which are involved in a previously unidentified mode of transport of cargo, which is actin-dependent and allows the movement of vesicles in oocyte cells over long distances (Schuh, 2011). The work described in this chapter shows the distribution of Spire proteins in primary hippocampal cultures and suggests that presynaptic proteins are transported along the axon in a Spire-dependent way. As more work needs to be performed to corroborate our findings, in this

discussion I present ideas for future experiments.

Spire involvement in axonal actin reorganization

Expression of fluorescently tagged-Spire1 and Spire2 constructs in primary hippocampal neurons showed a clear distribution of Spire in actin-rich structures, including dendritic spines and soma. Most strikingly, Spire was present in the axon, forming clusters that span from proximal to the distal axon. Even though Spire1 and Spire2 are both expressed in the developing and adult mammalian brain, their expression pattern is not overlapping. Spire1 is mostly expressed in the hippocampus, dentate gyrus and Purkinje cells of the cerebellum (Schumacher *et al.*, 2004), while Spire2 is present in the thalamus, the external and central nucleus of the inferior colliculus and the cerebral cortex (Pleiser *et al.*, 2010). However, due to high structural homology in the conserved domains between the two proteins and the fact that both are expressed in neuronal cells hints for a similar and redundant function in these cells. In fact, previous studies in mouse oocytes highlighted the need to knockdown both mammalian Spire proteins for the effective inhibition of the formation of the cytoplasmic actin meshwork (Pfender *et al.*, 2011). We generated different shRNAs against Spire1 and Spire2 to deplete Spire expression in neurons, which were validated and used in a combination of one shRNA of each Spire protein in all the knockdown experiments.

As mentioned before, actin organizes in different structures along the axon and has an important role in AIS structure (Watanabe *et al.*, 2012). As Spire clusters were also distributed in the AIS we examined this structure in conditions of enhanced or reduced levels of Spire. The AIS seemed unaffected in all conditions, although the AIS (determined by labeling of the cell adhesion molecule Neurofascin) extended slightly further in the axon in Spire-expressing neurons. This could be an indication of a reorganization of Neurofascin distribution in the distal AIS, possibly due to rearrangement of actin. We also analyzed the axon morphology of young neurons and observed that the length of the axon and the number of axonal branches was decreased when Spire was overexpressed. Additionally, growth cone morphology was slightly affected in Spire-expressing neurons, with an increased fraction of retracted growth cones relative to fan- or torpedo-like growth cones. This suggests that a loss of growth cone dynamics may underlie the decreased axonal growth phenotype. Taken together, these results suggest that Spire levels affect axonal growth and AIS maintenance. We hypothesize that when Spire is overexpressed, actin is trapped in Spire clusters and not available at the growing tips of neurites for proper expansion and elongation. Indeed, arrested actin was observed in our experiments where endogenous actin was labeled. Spire clusters caused the accumulation of additional actin in the axonal shaft, which will not be available at the growing tips. Future work should focus on examining growth dynamics and actin distribution at the growth cone in live-cell experiments. Interestingly, upon Spire depletion we observed a significant decrease in the number of actin structures identified by phalloidin staining. The remaining structures had altered morphology, forming more elongated stretches than in control. These observations point towards a role of Spire proteins in the formation or maintenance of these axonal actin structures.

Recent work has described actin ‘hotspots’, stationary structures along the axon from where actin is polymerized in actin trails in a Formin-2-dependent fashion (Ganguly *et al.*, 2015). Yet, it is not known how actin hotspots are generated. Spire and Formin proteins are known to work in synergy in other model systems, binding to membranes to promote actin nucleation and polymerization (Schuh, 2011), so one could hypothesize the actin structures observed by phalloidin labelling correspond to actin hotspots. We are currently performing high-resolution live-cell imaging microscopy to better understand the nature and dynamics of these structures. Our first approach is to use currently available actin tools for live-cell imaging, fluorescently-labeled Lifeact and UtrCH. Preferably we would like to image endogenous F-actin structures, which will be tested with labeling using SiR-actin. We propose to image actin structures in control and Spire-depleted axons, as well as in Spire clusters. When polymerization of actin filaments from the actin structures is observed, we will manipulate actin dynamics by the Formin-2 inhibitor SMiFH2 or after Formin-2 knockdown with shRNAs. Collectively, we are hopeful that ongoing experiments will give us a better insight on the nature of these axonal actin structures and the involvement of Spire proteins in their formation and maintenance.

Spire in the maintenance of the presynapse

As presynaptic terminals are actin-rich locations along the axonal shaft, it is tempting to propose a putative role for Spire proteins in the presynapse. Interestingly, when performing a proteomic screen to identify novel Spire1 interactors we identified many synaptic proteins as strong hits. We examined a possible role for Spire in maintaining presynaptic terminals of mature neurons, focusing on presynaptic boutons and the distribution of the presynaptic marker Bassoon. We observed that the number of synaptic boutons was decreased upon Spire depletion and in Spire-expressing neurons. The remaining boutons had significantly less Bassoon puncta, which were redistributed to the axonal shaft. Spire clusters did not colocalize with Bassoon or with synaptic boutons, indicating that Spire is not localized in the presynapse but its presence is of importance for maintenance and/or targeting of presynaptic cargo to the correct location. We are currently testing new commercial Spire antibodies in our primary hippocampal cultures to examine if endogenous Spire is also absent from the presynapse. Future experiments include validation of other candidates from the proteomic screen, to understand if this is a general phenotype affecting the entire presynaptic complex or if it is possible to identify specific interactions. As Spire clusters do not localize with the presynapse, it would be interesting to also examine the relative distance of these clusters from the presynapse, as there could be a spatial correlation between the two.

Spire in vesicle redistribution and cargo transport

Previous work described that Spire proteins are recruited to membranes, particularly to the membrane of Rab11-recycling endosomes, where they play a role in actin organization and transport (Pfender *et al.*, 2011; Schuh, 2011). Even though an interplay between the Spire-box domain and Rab11 has been proposed (Pfender *et al.*, 2011), a direct interaction between Spire

and Rab11 has not been identified. We used different truncations of Spire1 to understand which domains are involved in the formation of Spire clusters and targeting to Rab11-endosomes. In agreement with previous results, the C-terminal domains Spir-box and FYVE are important for Rab11 redistribution, and the WH2 domain for actin redistribution. The KIND domain has a cytoplasmic distribution without affecting actin or Rab11-endosome distribution. Interestingly, when expressed in HeLa cells, Spire was distributed to Rab11-endosomes. As the C-terminal FYVE domain can interact with different negatively charged lipids (Tittel *et al.*, 2015), the interaction between Spire and membrane vesicles may not be exclusive to Rab11 endosomes. Indeed, when we expressed HA-Spire1 or HA-Spire2 in COS7 cells and performed a GST-pull down assay with a library of GST-Rabs, we did not detect an interaction with Rab11, even though we found interactions with other Rabs in the library. Additionally, further immunoprecipitation assays showed a strong interaction of Spire with Myosin Vb tail via the WH2 domain. This data is in agreement with very recently published work that reveals a tripartite complex where Myosin V interacts with both Spire and Rab11 to promote membrane recruitment of actin nucleation and polymerization machineries and motor activity (Pylypenko *et al.*, 2016). It is then clear that additional factors are involved in the specific recruitment of Spire to the membrane of vesicles and opens the possibility for other vesicles to be targeted by Spire proteins. Future work should focus in understanding the interactions revealed in our pull-down data.

Given its distribution along the axon and the ability of Spire to bind vesicle membranes, we next tested whether Spire is involved in transport processes. Transport of Rab11-endosomes was not altered in Spire-depleted or Spire-expressing neurons, and NPY-vesicles mobility was only slightly affected. However, Rab3c vesicles moved faster and over longer distances when Spire was depleted. Interestingly, our pull-down data showed an interaction with Spire1 and Rab3. This could be an indication that Spire clusters are involved in anchoring cargo along the axon, as its depletion would allow for longer transport along the microtubule tracks. However, the fact that fewer vesicles are present along the axon and the ones present are less motile when Spire is depleted is an indication that Spire might be involved in actin-based transport of these vesicles.

Spire-dependent actin reorganization in the axon is required for delivery of presynaptic components to the presynapse

We hypothesized whether the identified interaction with Myosin V tail and Spire has a role in targeting cargo to the presynapse. We expressed Myosin Va and Vb tail constructs, which are dominant negative forms of the actin-based motor Myosin V and observed that, much like observed in Spire depletion, both the number of synaptic boutons and the number of Bassoon puncta at the presynapse were decreased. This provides a first indication of a coincident involvement of Spire and Myosin V in the delivery of cargo to the presynapse. Previous work demonstrated that Myosin V transports cargo along the axon (Bittins *et al.*, 2010; Lewis *et al.*, 2009) and interacts with presynaptic components (Prekeris and Terrian, 1997). We propose

to examine the transport of cargo, either Rab3-vesicles or other synaptic components, from Spire clusters to the presynapse, in Spire-depleted conditions and upon Myosin V inhibition or knockdown. As there will be many vesicles simultaneously being transported along the axon, we propose to visualize a subset of vesicles using Dendra2-Syn1, which is the C-terminus of Synaptophysin I fused with the photoswitchable fluorophore Dendra2 (Staras *et al.*, 2010). This protein can be quickly and locally photoswitched from green to red emission following exposure to 488nm light, allowing for fine-tuned visualization of a small fraction of vesicles over time. We propose to label the vesicles on a Spire cluster and follow their redistribution along the axon in the different conditions.

Our data demonstrate that Spire proteins have a role in the organization of actin structures, maintenance of presynaptic terminals and transport of axonal cargo. Spire proteins are distributed along the axon, where they may generate actin structures from membranes of vesicles, and in synergy with Formin-2 polymerize new actin filaments to transport cargo to presynapses via Myosin V. This would represent a slower, differentially-regulated, actin-based mechanism for delivering cargo to the presynapse.

AUTHOR CONTRIBUTIONS

MEdS, BvB, FL, RvD, and SP performed experiments in neurons. MEdS, BvB and SP designed and cloned the Spire constructs and shRNAs. RvD tested Spire antibodies in neurons. MEdS, BvB and FL performed live-cell imaging experiments and analysed the data. RS performed mass spectrometry. PSW performed pull-down experiments in HEK cells. AM and JJ designed and performed experiments in cortical neurons and RT-qPCR. NO and MF performed the pull-down experiments with GST-Rab library and with Myosin V tail. CJW and CCH supervised the research and coordinated the study.

ACKNOWLEDGEMENTS

The authors would like to thank Dr Schuh for the Spire 1 and Spire2 constructs and Dr Kerkhoff for the Spire1-KIND antibody. This work was supported by the Netherlands Organization for Scientific Research (NWO-ALW-VICI, CCH; NWO ZonMW-VIDI, CJW and HYH), the Foundation for Fundamental Research on Matter (FOM, CCH), which is part of the NWO, the Netherlands Organization for Health Research and Development (ZonMW-TOP: CCH), the European Research Council (ERC-consolidator: CCH). MEdS is supported by Fundação para a Ciência e Tecnologia (FCT-Portugal, grant SFRH/BD/68642/2010).

EXPERIMENTAL METHODS

Ethics Statement

All animal experiments were performed in compliance with the guidelines for the welfare of experimental animals issued by the Government of The Netherlands. All animal experiments were approved by the Animal Ethical Review Committee (DEC) of Utrecht University.

Expression constructs

The following mammalian expression plasmids have been described previously: HA- β -Galactosidase (Jaworski *et al.*, 2009), pSuper vector (Brummelkamp *et al.*, 2002), GFP-Rab11a (Hoogenraad *et al.*, 2010), TdTomato-Rab11a, MyosinVa and MyosinVb tails (Esteves da Silva *et al.*, 2015), GFP-Rab3c (van Vlijmen *et al.*, 2008), NPY-GFP (Schlager *et al.*, 2010), tag-BFP (van Bergeijk *et al.*, 2015). All other constructs were created using PCR based strategies. GW2-GFP/mCherry/HA-Spire1 and Spire2 and pEGFP-Bio-GFP-Spire1 were cloned from pGEM-HE-mEGFP-Spire1 and Spire2. The following GW2-GFP truncated forms of Spire1 were generated from GW2-GFP-Spire1: KIND (aa1-236), KIND-WH2 (aa1-746), Spir-box-FYVE (aa542-742), Δ KIND (aa237-742).

The following shRNA sequences were designed according to literature or using the selection program at the Whitehead Institute (<http://sirna.wi.mit.edu/>): Spire1 shRNA#1 (5'-AAACCATGGAAGTGCATACGTT-3'), Spire1 shRNA#2 (5'-AATCAGATGAAGAAGTCCAGTTT-3'), Spire2 shRNA#1 (5'-AAATCAAACAGGAGCGGAGGCTT-3'), Spire2 shRNA#2 (5'-TTCCTGTAGCGTAAAGATGAA-3') (Pfender *et al.*, 2011). The complementary oligonucleotides were annealed and inserted into pSuper vector.

Hippocampal neuron and cortical cultures and transfections

Primary hippocampal and cortical cultures were prepared from embryonic day 18 (E18) rat brains (Goslin and Banker, 1989; Kapitein *et al.*, 2010). Hippocampal neurons were plated on coverslips coated with poly-L-lysine (37.5 μ g/ml) and laminin (1.25 μ g/ml) at a density of 100,000/well. Hippocampal cultures were grown in Neurobasal medium (NB) supplemented with B27, 0.5 mM glutamine, 15.6 μ M glutamate and 1% penicillin/streptomycin. Hippocampal neurons at 14-21 DIV were transfected using Lipofectamine 2000 (Invitrogen). Briefly, DNA (3.6 μ g/well) was mixed with 3 μ l Lipofectamine 2000 in 200 μ l NB, incubated for 30 minutes and then added to the neurons in NB with 0.5 mM glutamine at 37°C in 5% CO₂ for 45 min to 1 hour. Next, neurons were washed with NB and transferred in the original medium at 37°C in 5% CO₂ for 2-4 days. Cortical neurons (1 x 10⁶ cells/well) were transfected using the Amaxa Rat Neuron Nucleofector Kit (Lonza) with 3 μ g of plasmid DNA and plated in 6-well plates (5 x 10⁵ cells/well) coated with poly-L-lysine (37.5 μ g/ml) and laminin (1.25 μ g/ml) containing DMEM supplemented with 10% FCS. Cells were allowed to recover and adhere to the surface at 37°C in 5% CO₂, and after 4 hours the medium was replaced with Neurobasal medium (NB) supplemented with B27, 0.5 mM glutamine, 15.6 μ M glutamate and 1% penicillin/streptomycin. Cells were grown at 37°C in 5% CO₂ prior to lysis and Western blot analysis.

Cortical neuron cultures, electroporation and RT-qPCR

Primary cortical cultures were prepared from embryonic day 19 (E19) rat brains and transfected using the Amaxa nucleofection procedure as described before (Swiech *et al.*, 2011). RNA from cultured neurons was isolated with the RNeasy Protect minikit (Qiagen). cDNA was prepared with High Capacity RNA-to-cDNA Master Mix (Applied Biosystems) according to the manufacturer's protocol. qPCR was performed using a 7900HT real-time PCR system and TaqMan gene expression assays (Applied Biosystems) with the following TaqMan rat probes: GAPDH (Rn99999916_s1). The results were analyzed by the comparative Ct method for relative quantification. SDS version 2.4 and RQ Manager version 1.2.1 programs were used for data acquisition and preliminary analysis.

Antibodies and reagents

The following antibodies were used: rabbit anti-HA (Santa-Cruz), mouse anti-Neurofascin pan (NeuroMab), mouse anti-Neurofascin pan extracellular (NeuroMab), mouse anti-AnkyrinG (Life Technologies), mouse anti-Bassoon (Stressgen), rabbit anti-Homer1 (Synaptic Systems, catalog number 160 002), rabbit anti-Rab11 (Invitrogen, catalog number 71-5300), homemade rabbit anti-Spire1-KIND and Alexa 488-, Alexa 568- and Alexa 633- conjugated secondary antibodies (Life Technologies). Phalloidin-Alexa488 and -568 (Life Technologies) was used to stain F-actin.

Immunohistochemistry

For immunohistochemistry, neurons were fixed for 10 min with 4% paraformaldehyde (PFA)/4% sucrose in PBS at room temperature. After fixation cells were washed 3 times for 5 minutes in PBS at room temperature and incubated with the primary-antibody mix in GDB buffer (0.2% BSA, 0.8M NaCl, 0.5% Triton X-100, 30mM phosphate buffer, pH 7.4) overnight at 4°C. Next the neurons were washed 3 times for 5 minutes in PBS at room temperature and incubated with the secondary-antibody mix in GDB buffer for at most 1 hour at room temperature. Neurons were then washed 3 times for 5 min in PBS at room temperature and subsequently mounted on slides in Vectashield

mounting medium (Vector Laboratories).

Imaging acquisition and analysis

Axon initial segment, axon outgrowth, and morphology of endogenous actin. Neurons were stained for Neurofascin or AnkyrinG to visualize AIS. Images were acquired with a Nikon Eclipse 80i upright fluorescent microscope, using a Nikon Plan Fluor 40x/NA 1.30 oil objective and a Coolsnap HQ2 camera (Photometrics), a Mercury lamp and appropriate filters. The software used for acquisition was NIS Elements BR software. The length and position of the axon initial segment was determined by analyzing intensity plots generated by ImageJ in Matlab. A macro determined the distance from the start of the intensity plot (Soma) to the start of the AIS and to the end of the AIS.

For axon outgrowth, neurons were stained with against HA-tagged β -galactosidase and images were acquired using a Nikon Eclipse 80i upright fluorescent microscope and a Nikon Plan Fluor 10x/NA 0.30 dry objective. Axonal length was measured using NeuronJ plug-in of ImageJ.

To visualize endogenous F-actin and growth cone morphology, neurons were labeled with Phalloidin Alexa488. Images were acquired using a Nikon Eclipse 80i upright fluorescent microscope and a Nikon Plan Fluor 40x/NA 1.40. Growth cone morphology and counting of actin structures was performed manually using ImageJ.

Spire-truncations, actin and Rab11 redistribution. Neurons expressing truncated versions of Spire1 were labelled with phalloidin-Alexa568 or co-expressed with TdTomato-Rab11. Images were acquired with a Nikon Eclipse 80i upright fluorescent microscope, using a Nikon Plan Fluor 40x/NA 1.30 oil objective and a Coolsnap HQ2 camera (Photometrics), a Mercury lamp and appropriate filters. The software used for acquisition was NIS Elements BR software. Redistribution of actin and Rab11-endosomes was determined manually using ImageJ.

Spire clusters, synaptic boutons and Bassoon clusters. Old neurons were stained for Bassoon and/or Homer to label pre- and postsynapses. Confocal images were acquired using LSM700 (Zeiss) with a 63x/1.40 Oil DIC objective and additional 1.3 zoom using 488nm, 555nm and 633 nm laser lines. A total thickness of 5 μ m was scanned for each position and maximum intensity projections were generated for analysis. Imaging settings were kept the same when pictures were compared for fluorescence intensity. Morphology of synaptic boutons was measured manually in ImageJ. Bassoon clusters were manually counted along 50 μ m of the axon using ImageJ.

Live cell imaging microscopy

All imaging was performed in full conditioned medium at 37°C and 5% CO₂. Live-cell imaging was performed using a two-color Total Internal Reflection Fluorescence (TIRF) microscope (Nikon Eclipse TE2000E) equipped with an incubation chamber (Tokai Hit; INUG2-ZILCS-H2) mounted on a motorized stage (Prior). Neurons were imaged every 100ms for 30s using CFI Apo TIRF 100x 1.49 N.A. oil objective (Nikon) and an Evolve 512 EMCCD camera (Photometrics). Kymographs were created in ImageJ. Quantification of vesicle mobility and speeds was performed using ImageJ.

Cell culture experiments

HeLa cells were cultured in DMEM medium (Life Technologies) supplemented with 10% with 10% FCS and 1% pen/strep. Cells were transfected with Fugene6 (Roche) and imaged after 1 day. Following fixation with 4% paraformaldehyde (PFA) and labeling of F-actin with phalloidin or Rab11 antibody, confocal images were acquired using LSM700 (Zeiss) with a 40x/1.40 Oil DIC objective and using 488nm, 555nm and 633 nm laser lines. A total thickness of 5 μ m was scanned for each position and maximum intensity projections were generated for analysis. Imaging settings were kept the same when pictures were compared for fluorescence intensity.

Biotin-streptavidin pull-down experiments, mass spectrometry and Western blot analysis

Streptavidin bead pull-down assays were performed as previously described (Jaworski *et al.*, 2009). HEK293 cells were transfected with BirA and bio-GFP-Spire1 or bio-GFP using Fugene transfection reagent according to the manufacturer's instructions. Cells were lysed 16 h later in 20 mM Tris-HCl, pH 8.0, 150 mM KCl, 1% Triton X-100, and protease inhibitors (Roche). Cell lysates were centrifuged at 13,000 rpm for 10 min and the supernatants were incubated with Dynabeads M-280 streptavidin (blocked in chicken egg albumin, Life Technologies) for 30 min at 4°C. Beads were separated by using a magnet (Invitrogen) and washed two times in low salt wash buffer (20 mM Tris-HCl, pH 7.4, 100 mM KCl, and 0.1% Triton X-100), two times in high salt wash buffer (20 mM Tris-HCl, pH 7.4, 500 mM KCl, and 0.1% Triton X-100), and two more times in low salt wash buffer to remove binding proteins

from HEK cells. Brains were obtained from female adult rats and homogenized in 10x volume/weight in tissue lysis buffer (50 mM TrisHCL, 150 mM NaCl, 0.1% SDS, 0.2% NP-40 and protease inhibitors (Roche)). Brain lysates were centrifuged at 16,000 g for 15 min at 4°C. The resulting supernatant was incubated with the Dynabeads containing bio-GFP-Spire1 or bio-GFP for 2 h at 4°C and washed with low salt wash buffer three times. Mass spectrometry was performed as described before (Frese *et al.*, 2017).

For Western blot, cortical neurons were lysed in SDS-PAGE sample buffer containing DTT and loaded on a Tris-Glycine SDS-polyacrylamide gel and blotted on PVDF membranes. Blots were blocked in 2% BSA in PBS-T (0.05% Tween20) followed by primary and secondary incubation (in 1% BSA in PBS-T) prior to ECL (homemade), film exposure and development.

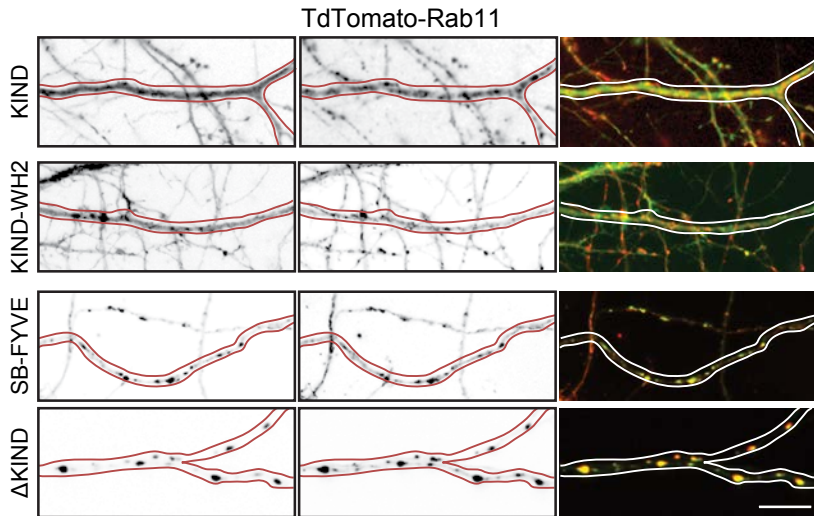
GST pull-down assays

COS-7 cells (1 x 10⁶ cells/10-cm dish) were transfected with HA-Spire1 or HA-Spire2 by using Lipofectamine-LTX Plus (Invitrogen) according to the manufacturer's instructions. 36 hours after the transfection, the cells were harvested and lysed with the cell lysis buffer (50 mM HEPES-KOH pH7.2, 150 mM NaCl, 1 mM MgCl₂, and 1% Triton X-100 supplemented with complete EDTA-free protease inhibitor cocktail (Roche)). Glutathione-Sepharose beads (wet vol., 10 ml; GE Healthcare) coupled with GST-Rabs (3 mg for each Rab except Rab40A; 9 mg for Rab40A because it contained a large amount of degradation products) (Itoh *et al.*, 2008; Kanno *et al.*, 2010) were treated with the cell lysis buffer containing 0.5 mM GTPγS and 2.5 mM EDTA on ice for 15 min, treated with 10 mM MgCl₂ on ice for 15 min, and then incubated with COS-7 cell lysates expressing HA-Spire1 or HA-Spire2 at 4°C for 2 hours. The beads were washed three times with the washing buffer (50 mM HEPES-KOH, pH7.2, 150 mM NaCl, 1 mM MgCl₂, 0.2% Triton X-100) and HA-Spire1/2 proteins bound to the beads were analyzed by 10% SDS-PAGE followed by immunoblotting with HRP-conjugated anti-HA tag antibody (1/10,000 dilution; 3F10; Roche) and HRP-conjugated anti-GST antibody (1/5000 dilution; Santa Cruz).

Co-immunoprecipitation assays

COS-7 cells (4 x 10⁵ cells/6-cm dish) were transfected with pEF-FLAG-MyoVb-tail, pEGFP-C1 (Clontech-Takara Bio Inc, Japan), or plasmids encoding each truncated form of GFP-Spire1 by using Lipofectamine-LTX Plus (Invitrogen). 36 hours after transfection the cells were harvested and lysed with the cell lysis buffer (50 mM HEPES-KOH pH 7.2, 150 mM NaCl, 1 mM MgCl₂, 1% Triton X-100, and complete EDTA-free protease inhibitor cocktail (Roche)). Co-immunoprecipitation assays were performed as described previously (Fukuda and Kanno, 2005). In brief, anti-GFP antibody-conjugated Sepharose beads (MBL, Japan) were coupled with each of truncated GFP-Spire1 proteins and then incubated with FLAG-MyoVb-tail-expressing COS-7 cells lysates. Proteins bound to the beads were analyzed by 10% SDS-PAGE followed by immunoblotting with HRP-conjugated anti-FLAG tag antibody (1/20,000; M2; SIGMA) and HRP-conjugated anti-GFP antibody (1/10,000; MBL, Japan).

SUPPLEMENTARY FIGURES

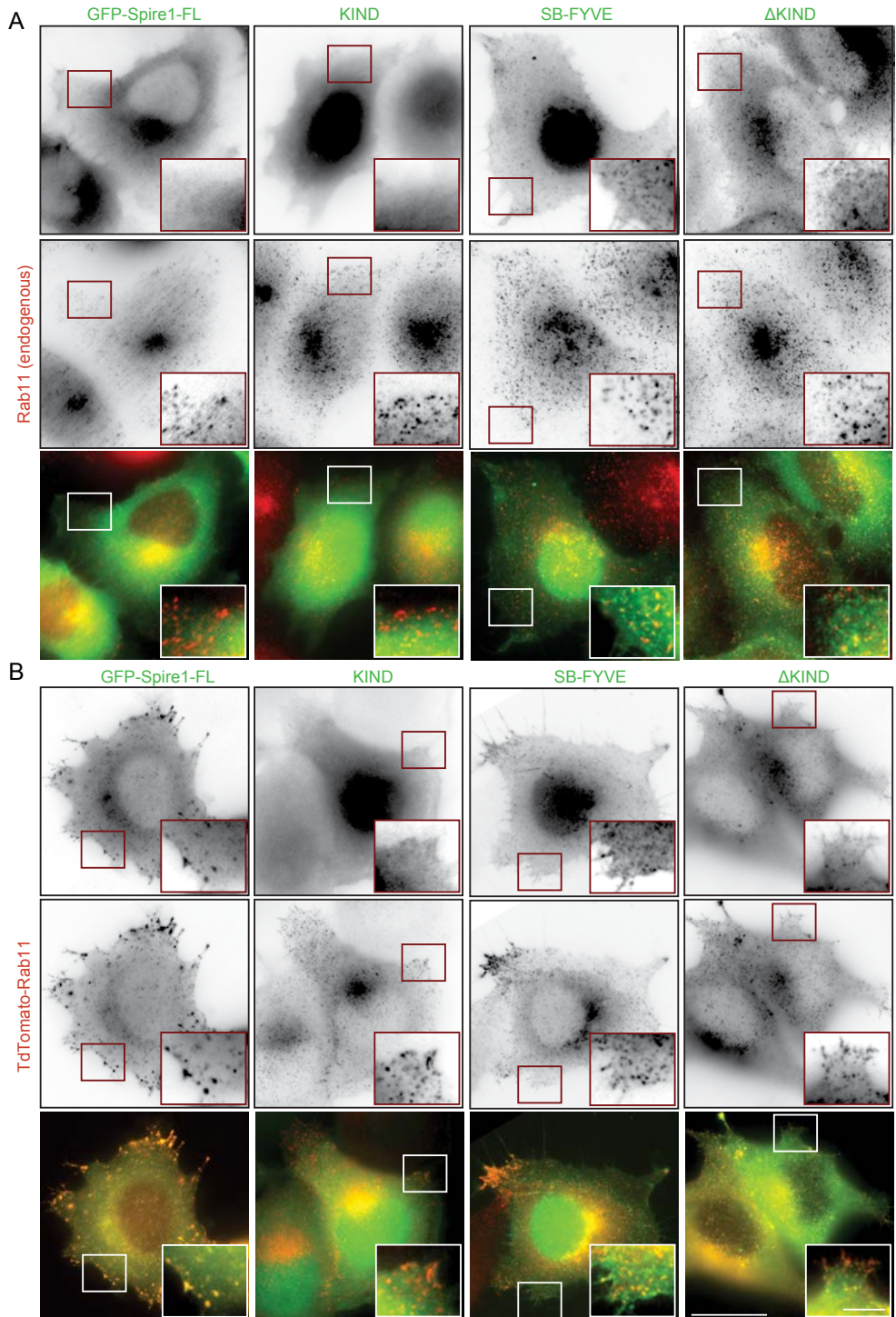


Supplementary Figure S1 (relative to Figure 4.B,C)

Examples of axons co-expressing Spire1-FL or Spire1 truncations (left) and Tdtomato-Rab11 (right). Scale bar is 10 μ m.

► **Supplementary Figure S2 (relative to Figure 4.D)**

A. Expression of full-length and truncated Spire1 in HeLa cells (top panel) and labelling with a Rab11 antibody (middle panel). Scale bars are 20 μm and 5 μm (inset). **B.** Co-expression of full-length or truncated Spire1 in HeLa cells (top panel) with TdTomato-Rab11 (middle panel). Scale bars are 20 μm and 5 μm (inset).



5

REFERENCES

- Bar, J., Kobler, O., van Bommel, B., and Mikhaylova, M. (2016). Periodic F-actin structures shape the neck of dendritic spines. *Scientific reports* 6, 37136.
- Bittins, C.M., Eichler, T.W., Hammer, J.A., 3rd, and Gerdes, H.H. (2010). Dominant-negative myosin Va impairs retrograde but not anterograde axonal transport of large dense core vesicles. *Cellular and molecular neurobiology* 30, 369-379.
- Bosch, M., Le, K.H., Bugyi, B., Correia, J.J., Renault, L., and Carlier, M.F. (2007). Analysis of the function of Spire in actin assembly and its synergy with formin and profilin. *Molecular cell* 28, 555-568.
- Bradke, F., and Dotti, C.G. (1999). The role of local actin instability in axon formation. *Science* 283, 1931-1934.
- Brummelkamp, T.R., Bernards, R., and Agami, R. (2002). A system for stable expression of short interfering RNAs in mammalian cells. *Science* 296, 550-553.
- Chen, L.Y., Rex, C.S., Casale, M.S., Gall, C.M., and Lynch, G. (2007). Changes in synaptic morphology accompany actin signaling during LTP. *The Journal of neuroscience : the official journal of the Society for Neuroscience* 27, 5363-5372.
- Cheng, J., Grassart, A., and Drubin, D.G. (2012). Myosin 1E coordinates actin assembly and cargo trafficking during clathrin-mediated endocytosis. *Molecular biology of the cell* 23, 2891-2904.
- Chesarone, M.A., and Goode, B.L. (2009). Actin nucleation and elongation factors: mechanisms and interplay. *Current opinion in cell biology* 21, 28-37.
- Ciccarelli, F.D., Bork, P., and Kerkhoff, E. (2003). The KIND module: a putative signalling domain evolved from the C lobe of the protein kinase fold. *Trends in biochemical sciences* 28, 349-352.
- Cingolani, L.A., and Goda, Y. (2008). Actin in action: the interplay between the actin cytoskeleton and synaptic efficacy. *Nature reviews Neuroscience* 9, 344-356.
- D'Este, E., Kamin, D., Gottfert, F., El-Hady, A., and Hell, S.W. (2015). STED nanoscopy reveals the ubiquity of subcortical cytoskeleton periodicity in living neurons. *Cell reports* 10, 1246-1251.
- Emmons, S., Phan, H., Calley, J., Chen, W., James, B., and Manseau, L. (1995). *Cappuccino*, a *Drosophila* maternal effect gene required for polarity of the egg and embryo, is related to the vertebrate limb deformity locus. *Genes & development* 9, 2482-2494.
- Esteves da Silva, M., Adrian, M., Scharzle, P., Lipka, J., Watanabe, T., Cho, S., Futai, K., Wierenga, C.J., Kapitein, L.C., and Hoogenraad, C.C. (2015). Positioning of AMPA Receptor-Containing Endosomes Regulates Synapse Architecture. *Cell reports* 13, 933-943.
- Frese, C.K., Mikhaylova, M., Stucchi, R., Gautier, V., Liu, Q., Mohammed, S., Heck, A.J., Altelaar, A.F., and Hoogenraad, C.C. (2017). Quantitative Map of Proteome Dynamics during Neuronal Differentiation. *Cell reports* 18, 1527-1542.
- Fukazawa, Y., Saitoh, Y., Ozawa, F., Ohta, Y., Mizuno, K., and Inokuchi, K. (2003). Hippocampal LTP is accompanied by enhanced F-actin content within the dendritic spine that is essential for late LTP maintenance *in vivo*. *Neuron* 38, 447-460.
- Ganguly, A., Tang, Y., Wang, L., Ladt, K., Loi, J., Dargent, B., Leterrier, C., and Roy, S. (2015). A dynamic formin-dependent deep F-actin network in axons. *The Journal of cell biology* 210, 401-417.
- Goslin, K., and Banker, G. (1989). Experimental observations on the development of polarity by hippocampal neurons in culture. *J Cell Biol* 108, 1507-1516.
- He, J., Zhou, R., Wu, Z., Carrasco, M.A., Kurshan, P.T., Farley, J.E., Simon, D.J., Wang, G., Han, B., Hao, J., et al. (2016). Prevalent presence of periodic actin-spectrin-based membrane skeleton in a broad range of neuronal cell types and animal species. *Proceedings of the National Academy of Sciences of the United States of America* 113, 6029-6034.
- Honkura, N., Matsuzaki, M., Noguchi, J., Ellis-Davies, G.C., and Kasai, H. (2008). The subspine organization of actin fibers regulates the structure and plasticity of dendritic spines. *Neuron* 57, 719-729.
- Hoogenraad, C.C., Popa, I., Futai, K., Martinez-Sanchez, E., Wulf, P.S., van Vlijmen, T., Dortland, B.R., Oorschot, V., Govers, R., Monti, M., et al. (2010). Neuron specific Rab4 effector GRASP-1 coordinates membrane specialization and maturation of recycling endosomes. *PLoS biology* 8, e1000283.
- Hotulainen, P., and Hoogenraad, C.C. (2010). Actin in dendritic spines: connecting dynamics to function. *The Journal of cell biology* 189, 619-629.
- Ito, T., Narita, A., Hirayama, T., Taki, M., Iyoshi, S., Yamamoto, Y., Maeda, Y., and Oda, T. (2011). Human spire interacts with the barbed end of the

- actin filament. *Journal of molecular biology* 408, 18-25.
- Itoh, T., Fujita, N., Kanno, E., Yamamoto, A., Yoshimori, T., and Fukuda, M. (2008). Golgi-resident small GTPase Rab33B interacts with Atg16L and modulates autophagosome formation. *Molecular biology of the cell* 19, 2916-2925.
- Jaworski, J., Kapitein, L.C., Gouveia, S.M., Dortland, B.R., Wulf, P.S., Grigoriev, I., Camera, P., Spangler, S.A., Di Stefano, P., Demmers, J., et al. (2009). Dynamic microtubules regulate dendritic spine morphology and synaptic plasticity. *Neuron* 61, 85-100.
- Kanno, E., Ishibashi, K., Kobayashi, H., Matsui, T., Ohbayashi, N., and Fukuda, M. (2010). Comprehensive screening for novel rab-binding proteins by GST pull-down assay using 60 different mammalian Rabs. *Traffic* 11, 491-507.
- Kapitein, L.C., Schlager, M.A., Kuijpers, M., Wulf, P.S., van Spronsen, M., MacKintosh, F.C., and Hoogenraad, C.C. (2010). Mixed microtubules steer dynein-driven cargo transport into dendrites. *Curr Biol* 20, 290-299.
- Kapitein, L.C., van Bergeijk, P., Lipka, J., Keijzer, N., Wulf, P.S., Katrukha, E.A., Akhmanova, A., and Hoogenraad, C.C. (2013). Myosin-V opposes microtubule-based cargo transport and drives directional motility on cortical actin. *Current biology* : CB 23, 828-834.
- Kerkhoff, E. (2006). Cellular functions of the Spir actin-nucleation factors. *Trends in cell biology* 16, 477-483.
- Kerkhoff, E., Simpson, J.C., Leberfinger, C.B., Otto, I.M., Doerks, T., Bork, P., Rapp, U.R., Raabe, T., and Pepperkok, R. (2001). The Spir actin organizers are involved in vesicle transport processes. *Current biology* : CB 11, 1963-1968.
- Korobova, F., and Svitkina, T. (2010). Molecular architecture of synaptic actin cytoskeleton in hippocampal neurons reveals a mechanism of dendritic spine morphogenesis. *Molecular biology of the cell* 21, 165-176.
- Ladt, K., Ganguly, A., and Roy, S. (2016). Axonal actin in action: Imaging actin dynamics in neurons. *Methods in cell biology* 131, 91-106.
- Lagal, V., Abrivard, M., Gonzalez, V., Perazzi, A., Popli, S., Verzeroli, E., and Tardieux, I. (2014). Spire-1 contributes to the invadosome and its associated invasive properties. *Journal of cell science* 127, 328-340.
- Landis, D.M. (1988). Membrane and cytoplasmic structure at synaptic junctions in the mammalian central nervous system. *Journal of electron microscopy technique* 10, 129-151.
- Landis, D.M., and Reese, T.S. (1983). Cytoplasmic organization in cerebellar dendritic spines. *The Journal of cell biology* 97, 1169-1178.
- Leader, B., and Leder, P. (2000). Formin-2, a novel formin homology protein of the cappuccino subfamily, is highly expressed in the developing and adult central nervous system. *Mechanisms of development* 93, 221-231.
- Leader, B., Lim, H., Carabatsos, M.J., Harrington, A., Ecsedy, J., Pellman, D., Maas, R., and Leder, P. (2002). Formin-2, polyploidy, hypofertility and positioning of the meiotic spindle in mouse oocytes. *Nature cell biology* 4, 921-928.
- Letierrier, C., Potier, J., Caillol, G., Debarnot, C., Rueda Boroni, F., and Dargent, B. (2015). Nanoscale Architecture of the Axon Initial Segment Reveals an Organized and Robust Scaffold. *Cell reports* 13, 2781-2793.
- Lewis, T.L., Jr., Mao, T., Svoboda, K., and Arnold, D.B. (2009). Myosin-dependent targeting of transmembrane proteins to neuronal dendrites. *Nature neuroscience* 12, 568-576.
- Lowery, L.A., and Van Vactor, D. (2009). The trip of the tip: understanding the growth cone machinery. *Nature reviews Molecular cell biology* 10, 332-343.
- Manseau, L.J., and Schupbach, T. (1989). cappuccino and spire: two unique maternal-effect loci required for both the anteroposterior and dorsoventral patterns of the *Drosophila* embryo. *Genes & development* 3, 1437-1452.
- Mari, M., Macia, E., Le Marchand-Brustel, Y., and Cormont, M. (2001). Role of the FYVE finger and the RUN domain for the subcellular localization of Rabip4. *The Journal of biological chemistry* 276, 42501-42508.
- Okamoto, K., Nagai, T., Miyawaki, A., and Hayashi, Y. (2004). Rapid and persistent modulation of actin dynamics regulates postsynaptic reorganization underlying bidirectional plasticity. *Nature neuroscience* 7, 1104-1112.
- Ostermeier, C., and Brunger, A.T. (1999). Structural basis of Rab effector specificity: crystal structure of the small G protein Rab3A complexed with the effector domain of rabphilin-3A. *Cell* 96, 363-374.
- Otto, I.M., Raabe, T., Rennefahrt, U.E., Bork, P., Rapp, U.R., and Kerkhoff, E. (2000). The p150-Spir protein provides a link between c-Jun N-terminal kinase function and actin reorganization. *Current biology* : CB 10, 345-348.
- Pechlivanis, M., Samol, A., and Kerkhoff, E. (2009).

- Identification of a short Spir interaction sequence at the C-terminal end of formin subgroup proteins. *The Journal of biological chemistry* 284, 25324-25333.
- Pfender, S., Kuznetsov, V., Pleiser, S., Kerkhoff, E., and Schuh, M. (2011). Spire-type actin nucleators cooperate with Formin-2 to drive asymmetric oocyte division. *Current biology : CB* 21, 955-960.
- Pleiser, S., Rock, R., Wellmann, J., Gessler, M., and Kerkhoff, E. (2010). Expression patterns of the mouse Spir-2 actin nucleator. *Gene expression patterns : GEP* 10, 345-350.
- Prekeris, R., and Terrian, D.M. (1997). Brain myosin V is a synaptic vesicle-associated motor protein: evidence for a Ca²⁺-dependent interaction with the synaptobrevin-synaptophysin complex. *The Journal of cell biology* 137, 1589-1601.
- Pylypenko, O., Welz, T., Tittel, J., Kollmar, M., Chardon, F., Malherbe, G., Weiss, S., Michel, C.I., Samol-Wolf, A., Grasskamp, A.T., et al. (2016). Coordinated recruitment of Spir actin nucleators and myosin V motors to Rab11 vesicle membranes. *eLife* 5.
- Quinlan, M.E., Heuser, J.E., Kerkhoff, E., and Mullins, R.D. (2005). *Drosophila* Spire is an actin nucleation factor. *Nature* 433, 382-388.
- Quinlan, M.E., Hilgert, S., Bedrossian, A., Mullins, R.D., and Kerkhoff, E. (2007). Regulatory interactions between two actin nucleators, Spire and Cappuccino. *The Journal of cell biology* 179, 117-128.
- Quinlan, M.E., and Kerkhoff, E. (2008). Actin nucleation: bacteria get in-Spired. *Nature cell biology* 10, 13-15.
- Ramachandran, B., and Frey, J.U. (2009). Interfering with the actin network and its effect on long-term potentiation and synaptic tagging in hippocampal CA1 neurons in slices *in vitro*. *The Journal of neuroscience : the official journal of the Society for Neuroscience* 29, 12167-12173.
- Ridley, S.H., Ktistakis, N., Davidson, K., Anderson, K.E., Manifava, M., Ellison, C.D., Lipp, P., Bootman, M., Coadwell, J., Nazarian, A., et al. (2001). FENS-1 and DFPC1 are FYVE domain-containing proteins with distinct functions in the endosomal and Golgi compartments. *Journal of cell science* 114, 3991-4000.
- Sankaran, V.G., Klein, D.E., Sachdeva, M.M., and Lemmon, M.A. (2001). High-affinity binding of a FYVE domain to phosphatidylinositol 3-phosphate requires intact phospholipid but not FYVE domain oligomerization. *Biochemistry* 40, 8581-8587.
- Schlager, M.A., Kapitein, L.C., Grigoriev, I., Burzynski, G.M., Wulf, P.S., Keijzer, N., de Graaff, E., Fukuda, M., Shepherd, I.T., Akhmanova, A., et al. (2010). Pericentrosomal targeting of Rab6 secretory vesicles by Bicaudal-D-related protein 1 (BICDR-1) regulates neuritogenesis. *The EMBO journal* 29, 1637-1651.
- Schuh, M. (2011). An actin-dependent mechanism for long-range vesicle transport. *Nature cell biology* 13, 1431-1436.
- Schumacher, N., Borawski, J.M., Leberfinger, C.B., Gessler, M., and Kerkhoff, E. (2004). Overlapping expression pattern of the actin organizers Spir-1 and formin-2 in the developing mouse nervous system and the adult brain. *Gene expression patterns : GEP* 4, 249-255.
- Sidenstein, S.C., D'Este, E., Bohm, M.J., Danzl, J.G., Below, V.N., and Hell, S.W. (2016). Multicolour Multilevel STED nanoscopy of Actin/Spectrin Organization at Synapses. *Scientific reports* 6, 26725.
- Simonsen, A., Lippe, R., Christoforidis, S., Gaullier, J.M., Brech, A., Callaghan, J., Toh, B.H., Murphy, C., Zerial, M., and Stenmark, H. (1998). EEA1 links PI(3)K function to Rab5 regulation of endosome fusion. *Nature* 394, 494-498.
- Sirotkin, V., Beltzner, C.C., Marchand, J.B., and Pollard, T.D. (2005). Interactions of WASp, myosin-I, and verprolin with Arp2/3 complex during actin patch assembly in fission yeast. *The Journal of cell biology* 170, 637-648.
- Sitar, T., Gallinger, J., Ducka, A.M., Ikonen, T.P., Wohlhoefer, M., Schmoller, K.M., Bausch, A.R., Joel, P., Trybus, K.M., Noegel, A.A., et al. (2011). Molecular architecture of the Spire-actin nucleus and its implication for actin filament assembly. *Proceedings of the National Academy of Sciences of the United States of America* 108, 19575-19580.
- Spillane, M., Ketschek, A., Jones, S.L., Korobova, F., Marsick, B., Lanier, L., Svitkina, T., and Gallo, G. (2011). The actin nucleating Arp2/3 complex contributes to the formation of axonal filopodia and branches through the regulation of actin patch precursors to filopodia. *Developmental neurobiology* 71, 747-758.
- Star, E.N., Kwiatkowski, D.J., and Murthy, V.N. (2002). Rapid turnover of actin in dendritic spines and its regulation by activity. *Nature neuroscience* 5, 239-246.
- Staras, K., Branco, T., Burden, J.J., Pozo, K., Darcy, K., Marra, V., Ratnayaka, A., and Goda, Y. (2010). A vesicle superpool spans multiple presynaptic

- terminals in hippocampal neurons. *Neuron* 66, 37-44.
- Sun, Y., Martin, A.C., and Drubin, D.G. (2006). Endocytic internalization in budding yeast requires coordinated actin nucleation and myosin motor activity. *Developmental cell* 11, 33-46.
- Swiech, L., Blazejczyk, M., Urbanska, M., Pietruszka, P., Dortland, B.R., Malik, A.R., Wulf, P.S., Hoogenraad, C.C., and Jaworski, J. (2011). CLIP-170 and IQGAP1 cooperatively regulate dendrite morphology. *The Journal of neuroscience : the official journal of the Society for Neuroscience* 31, 4555-4568.
- Tittel, J., Welz, T., Czogalla, A., Dietrich, S., Samol-Wolf, A., Schulte, M., Schwille, P., Weidemann, T., and Kerkhoff, E. (2015). Membrane targeting of the Spir.formin actin nucleator complex requires a sequential handshake of polar interactions. *The Journal of biological chemistry* 290, 6428-6444.
- van Bergeijk, P., Adrian, M., Hoogenraad, C.C., and Kapitein, L.C. (2015). Optogenetic control of organelle transport and positioning. *Nature* 518, 111-114.
- van der Vaart, B., van Riel, W.E., Doodhi, H., Kevenaer, J.T., Katrukha, E.A., Gumy, L., Bouchet, B.P., Grigoriev, I., Spangler, S.A., Yu, K.L., et al. (2013). CFEOM1-associated kinesin KIF21A is a cortical microtubule growth inhibitor. *Developmental cell* 27, 145-160.
- van Vlijmen, T., Vleugel, M., Evers, M., Mohammed, S., Wulf, P.S., Heck, A.J., Hoogenraad, C.C., and van der Sluijs, P. (2008). A unique residue in rab3c determines the interaction with novel binding protein Zwint-1. *FEBS letters* 582, 2838-2842.
- Vizcarra, C.L., Kreutz, B., Rodal, A.A., Toms, A.V., Lu, J., Zheng, W., Quinlan, M.E., and Eck, M.J. (2011). Structure and function of the interacting domains of Spire and Fmn-family formins. *Proceedings of the National Academy of Sciences of the United States of America* 108, 11884-11889.
- Watanabe, K., Al-Bassam, S., Miyazaki, Y., Wandless, T.J., Webster, P., and Arnold, D.B. (2012). Networks of polarized actin filaments in the axon initial segment provide a mechanism for sorting axonal and dendritic proteins. *Cell reports* 2, 1546-1553.
- Wellington, A., Emmons, S., James, B., Calley, J., Grover, M., Tolia, P., and Manseau, L. (1999). Spire contains actin binding domains and is related to ascidian posterior end mark-5. *Development* 126, 5267-5274.
- Xu, K., Zhong, G., and Zhuang, X. (2013). Actin, spectrin, and associated proteins form a periodic cytoskeletal structure in axons. *Science* 339, 452-456.
- Zeller, R., Haramis, A.G., Zuniga, A., McGuigan, C., Dono, R., Davidson, G., Chabanis, S., and Gibson, T. (1999). Formin defines a large family of morphoregulatory genes and functions in establishment of the polarising region. *Cell and tissue research* 296, 85-93.
- Zeth, K., Pechlivanis, M., Samol, A., Pleiser, S., Vonrhein, C., and Kerkhoff, E. (2011). Molecular basis of actin nucleation factor cooperativity: crystal structure of the Spir-1 kinase non-catalytic C-lobe domain (KIND)*formin-2 formin SPIR interaction motif (FSI) complex. *The Journal of biological chemistry* 286, 30732-30739.

DeActs: genetically encoded tools for perturbing the actin cytoskeleton in single cells

Martin Harterink^{1,*}, **Marta Esteves da Silva**^{1,*}, Lena Will¹, Julia Turan², Adiljan Ibrahim², Alexander E. Lang³, Eljo Y. van Battum⁴, R. Jeroen Pasterkamp⁴, Lukas C. Kapitein¹, Dmitri Kudryashov⁵, Ben A. Barres², Casper C. Hoogenraad¹, and J. Bradley Zuchero^{2,6}

Nature Methods, May 2017 [Epub ahead of print]

¹Cell Biology, Department of Biology, Faculty of Science, Utrecht University, Utrecht, The Netherlands. ²Department of Neurobiology, Stanford University School of Medicine, Stanford, California, USA. ³Institute for Experimental and Clinical Pharmacology and Toxicology, Albert-Ludwigs University of Freiburg, Freiburg, Germany. ⁴Department of Translational Neuroscience, Brain Center Rudolf Magnus, University Medical Center Utrecht, The Netherlands. ⁵Department of Chemistry and Biochemistry, The Ohio State University, Columbus, Ohio, USA. ⁶Department of Neurosurgery, Stanford University School of Medicine, Stanford, California, USA. *These authors contributed equally to this work.

ABSTRACT

The actin cytoskeleton is essential for many fundamental biological processes, but tools to directly manipulate actin dynamics are limited to cell-permeable drugs precluding single cell perturbations. Here we describe DeActs, genetically encoded actin-modifying polypeptides, which effectively induce actin disassembly in eukaryotic cells. We demonstrate that DeActs are universal tools for studying the actin cytoskeleton in single cells in culture, tissues, and multicellular organisms, including various neurodevelopmental model systems.

INTRODUCTION

Studying the role of the actin cytoskeleton is important for understanding many cell biological processes such as motility and cellular morphogenesis. Perturbation of the actin cytoskeleton is typically achieved using cell-permeable drugs, such as latrunculin or cytochalasin to promote actin disassembly (MacLean-Fletcher and Pollard, 1980; Spector *et al.*, 1983). However, these pharmacological approaches do not allow for cell-type specific perturbation, and therefore cannot be used to manipulate a subset of cells within complex multicellular model systems. Neuronal development is one example where the role of actin dynamics has been debated (Vitriol and Zheng, 2012), in part due to the lack of proper tools to manipulate actin in single neurons in culture, tissues or multicellular organisms. The ideal tool to manipulate the actin cytoskeleton would (1) trigger disassembly of actin filaments, similar to latrunculin, (2) directly interact with actin, rather than inducing cytoskeletal changes indirectly through upstream signaling pathways, (3) be genetically encoded and not rely on the addition of ectopic cofactors (Wu *et al.*, 2009), and (4) allow cellular visualization (e.g., as a GFP-fusion). Since actin is one of the most highly conserved proteins throughout eukaryotes this tool would also permit broad use in different experimental model systems.

To develop genetic tools that directly target the actin cytoskeleton (Disassembly-promoting, encodable Actin tools; DeActs), we screened both endogenous actin-binding domains that constitutively interact with actin and bacterial toxins that directly modify actin by transiently transfecting HeLa cells with candidate peptides (Fig.1A and Supplementary Fig. S1). Gelsolin segment 1 (GS1) is a ~120 amino acid domain that sequesters actin monomers *in vitro* but lacks the severing activity and calcium-sensitivity of full-length gelsolin (McLaughlin *et al.*, 1993; Way *et al.*, 1990). A GFP-GS1 (DeAct-GS1) fusion dramatically disrupted actin filaments when expressed in primary rat embryonic fibroblasts and HeLa cells, in contrast to GFP alone (Fig.1B and Supplementary Fig.S1). Actin is a common target of pathogenic bacteria, and numerous species produce toxins that are specific to actin and either covalently modify it or bind directly (Aktories *et al.*, 2011). *Salmonella enterica* SpvB is an ADP-ribosyltransferase that ADP-ribosylates actin monomers on a conserved arginine (Supplementary Fig.S2) to render them unable to polymerize (Margarit *et al.*, 2006), leading to net disassembly of all dynamic actin filaments. A GFP-fusion with the mono(ADP-ribosyl)transferase domain (DeAct-SpvB) caused complete loss of detectable actin filaments in cells (Fig.1B). As expected, disrupting actin with both DeAct constructs caused defects in cellular actin filament levels and distribution (Fig.1C-E), cell morphology, proliferation, and focal adhesions (Supplementary Fig.S3). Furthermore, live imaging revealed that DeActs caused profound defects in cell motility and loss of filopodia dynamics (Fig.1F, Supplementary Fig.S3, and Supplementary Video S1). In all cases DeAct-SpvB caused more dramatic effects, which is consistent with DeAct-SpvB being an enzyme, while DeAct-GS1 binds stoichiometrically to actin (Way *et al.*, 1990) and thus requires higher expression to induce actin disassembly. Consistently, cell motility was only inhibited at high expression of DeAct-GS1 (Fig.1F and Supplementary Video S2), whereas low levels of DeAct-SpvB expression were sufficient to cause efficient actin disassembly (Fig.1D) and inhibit

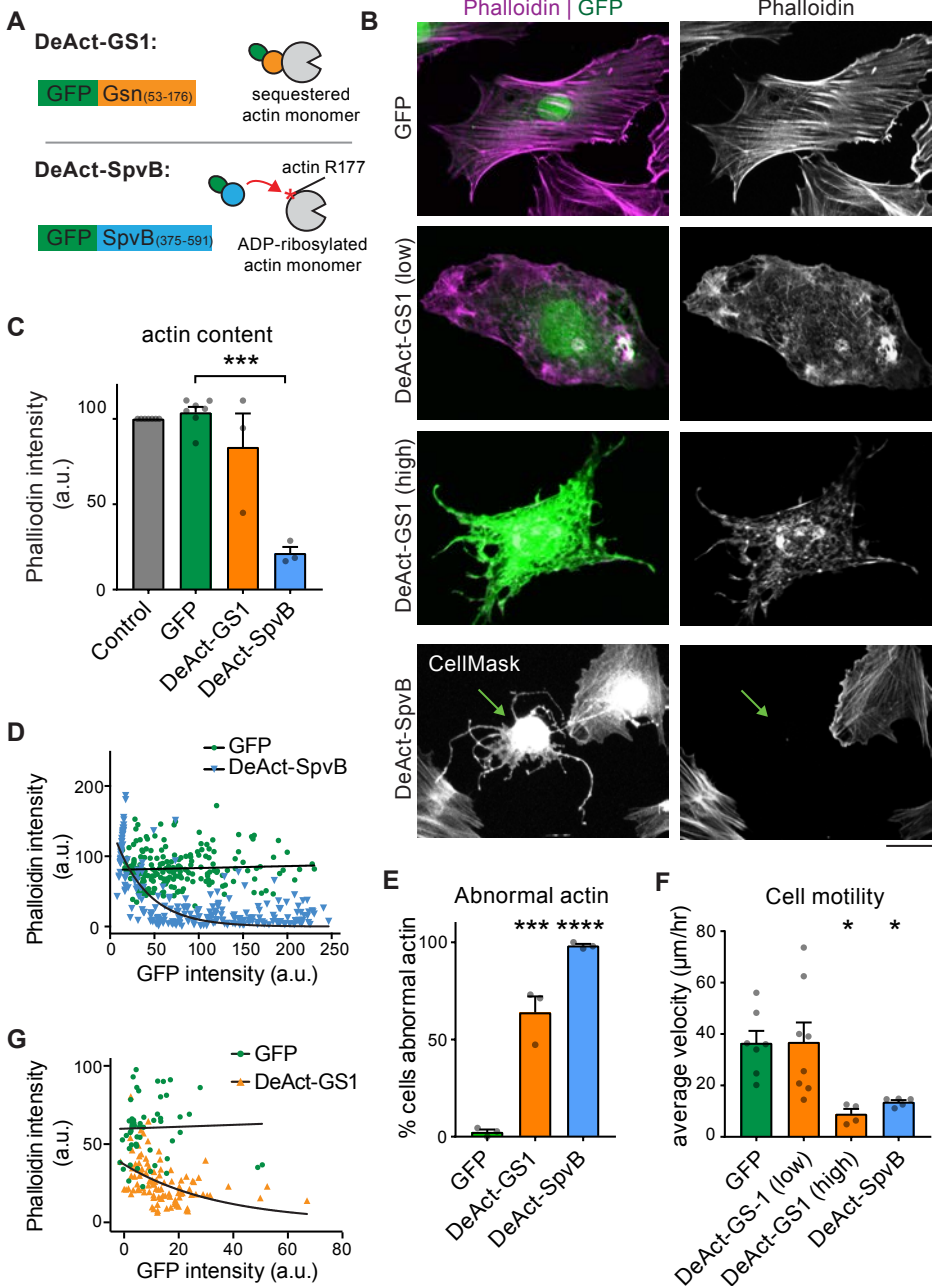


Figure 1. Construction and characterization of DeActs.

A. Schematic of DeAct constructs and mechanism of action. **B.** Expression of DeActs in rat embryonic fibroblasts, visualized with Alexa Fluor 594-phalloidin. CellMask Blue was used to reveal full cell morphology upon DeAct-SpvB expression. Note the expression level-dependent disruption of actin cytoskeleton and cell morphology in cell expressing DeAct-GS1, and complete loss of actin filaments in cell expressing DeAct-SpvB. Scale, 20 μm .

Representative micrographs from N = 4 independent experiments. **C-E.** Quantification of DeAct effect on actin in rat embryonic fibroblasts showing **(C)** average phalloidin intensities (N = 7, 7, 3, 3 independent experiments, left to right), **(D)** phalloidin intensity relative to the DeAct-SpvB level (n = 207 GFP or 240 DeAct-SpvB cells), and **(E)** percent of cells with abnormal actin filament distribution (N = 3 independent experiments; see Supplementary Methods). **F.** Velocities of single cell motility of rat embryonic fibroblasts transfected with DeActs or GFP control (see also Supplementary Video S2). n = 7, 8, 4, or 5 expressing cells per condition, left to right. **G.** Oligodendrocyte-specific expression of GFP or DeAct-GS1 in primary rat oligodendrocytes using the OL-specific myelin basic protein promoter, quantifying phalloidin intensity relative to the DeAct-GS1 level (fluorescence intensities not directly comparable to panel **D**). n = 55 GFP or 103 DeAct-GS1 cells. Graphs show mean \pm SEM. Trend lines in **D** and **G** show nonlinear (exponential) fit; each data point is one cell. Statistical significance: one-way ANOVA followed by Dunnett's multiple comparison test, ****p<0.0001, ***p<0.001, *p<0.05.

cell motility (Fig.1F and Supplementary Fig.S3). To look more closely at the dose-dependence of DeAct-GS1, we made use of the observation that *in vitro* differentiated rat oligodendrocyte cells (OLs) do not require an intact actin cytoskeleton to maintain a flattened cell morphology (Zuchero *et al.*, 2015). Expressing DeAct-GS1 in these cells under control of a mature OL promoter (Gow *et al.*, 1992) induced a dose-dependent loss of actin filaments without causing cell retraction (Fig.1G and Supplementary Fig.S3). Finally, to allow inducible DeAct expression we made use of the TetOn-3G system (Clontech), which resulted in rapid DeAct expression, efficient actin disruption, and inhibition of cell motility following addition of doxycycline (Supplementary Fig.S4). By adding a constitutively expressed mCherry to the same DNA construct in the opposite direction, we also allowed visualization of transfected cells prior to induction of DeAct expression (Supplementary Fig.S5). To suppress background expression of SpvB in the absence of doxycycline, we fused a DHFRdd destabilization domain (Iwamoto *et al.*, 2010) to SpvB to attenuate its expression (Supplementary Fig.S5). Together, these DeAct constructs represent a toolkit for rapid and tunable perturbation of the actin cytoskeleton in cells and their simultaneous visualization.

We next tested whether DeActs could be used to study the role of actin dynamics in other cellular model systems, such as developing neurons in culture. Primary hippocampal neurons expressing DeAct-GS1 or DeAct-SpvB revealed a robust cell-specific decrease in actin filaments in the axonal growth cone, highly similar to latrunculin-treated neurons (Fig.2A-C). Growth cone morphology was severely altered with DeAct expression or after latrunculin treatment, with a marked shift from fan- or torpedo-like shape (exploratory and elongating growth cones) to bulb and collapsed shape (stationary or eliminating growth cones) (van der Vaart *et al.*, 2013) (Fig.2A,D). Whereas in control conditions more than 40% of axonal tips were dynamic, subsequent treatment with latrunculin markedly decreased dynamics as expected (Fig.2E and Supplementary Fig.S6E,F). Consistently, DeAct expression inhibited axonal growth cone dynamics to a similar extent as latrunculin (Fig.2E and Supplementary Video S3). Thus, DeActs disrupt the actin cytoskeleton in a cell-specific manner and cause neuronal morphology defects.

A major advantage of genetically encoded DeActs is the ability to use them in multicellular organisms where cytoskeletal drugs may have broader effects and/or are more

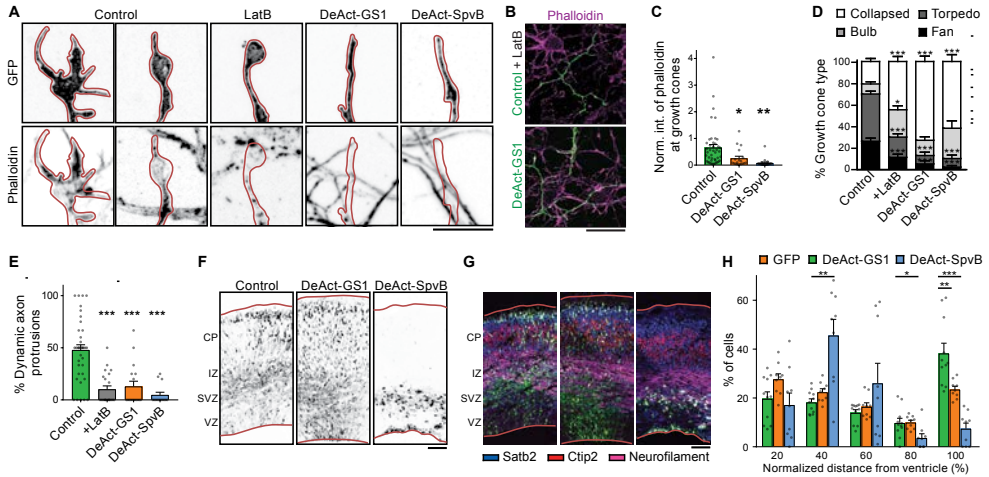


Figure 2. DeActs markedly affect growth cones and neuronal migration.

A. Growth cones of DIV4 rat embryonic hippocampal neurons expressing MARCKS-eGFP +/- latrunculin B (LatB) or DeAct-GS1 or DeAct-SpvB and stained with Alexa Fluor 568-phalloidin to visualize actin filaments. Scale, 10 μ m. **B.** Overview of actin filament staining (magenta) in neuronal cultures expressing MARCKS-eGFP and treated with LatB (affects the whole culture), or expressing DeAct-GS1 (cell-specific). Scale, 40 μ m. **C.** Quantification of actin filament intensity in growth cones normalized to untransfected neighboring neurons; LatB affects all growth cones, therefore cannot be included (N = 4, 2, 2 independent experiments, n = 44, 19, 22 neurons, left to right). **D.** Quantification of growth cone morphology upon MARCKS-eGFP or DeAct expression compared to LatB (N = 4, 2, 2, 2 independent experiments, n = 44, 23, 19, 22 neurons, left to right). **E.** Dynamics of axonal branches are lost after addition of LatB or in neurons expressing DeAct constructs. (N = 4, 2, 2, 2 independent experiments, n = 37, 22, 17, 14 neurons, left to right). See also Supplementary Fig.S6 and Supplementary Video S3. **F-G.** Cortical neuronal migration after *in utero* electroporation with GFP (control), DeAct-GS1, or DeAct-SpvB. **(F)** Same slice as **(G)** combined with immunostaining against Satb2 (cortical layer II-IV), Ctip2 (cortical layer IV-V) and Neurofilament (axons in the IZ). CP, Cortical plate; IZ, intermediate zone; SVZ, subventricular zone; VZ, ventricular zone. Scale, 100 μ m. **H.** Quantification of cortical neuronal migration described in **(F)**. (N = 3 embryos from 3 different litters, n = 3412, 2143, 847 cells GFP, DeAct-GS1 or DeAct-SpvB). Graphs show mean \pm SEM. Statistical significance: one-way ANOVA and Dunnett's multiple comparison post hoc test, and Wilcoxon test for paired data, ***p<0.001, **p<0.01, *p<0.05.

difficult to administer. The first *in vivo* system we used was the developing embryonic mouse neocortex, where newly born neurons polarize and migrate from the ventricular zone towards the cortical plate (Barnes and Polleux, 2009). We electroporated CMV-promoter-driven DeAct DNA constructs into the brains (motor cortices) of E14.5 mouse embryos *in utero* to target neuronal precursor cells, then allowed them to develop for 3 days prior to sacrificing and analyzing cortical migration. In control animals, GFP-positive neurons migrated efficiently to the upper layers of the cortical plate (Fig.2F-H). In contrast, expression of DeAct-GS1 led to a marked decrease in the number of neurons that reached the upper cortical layers, although no clear morphological differences were observed (Supplementary Fig.S6), Consistent with our culture studies, neurons expressing DeAct-SpvB failed to become bipolar and did not migrate

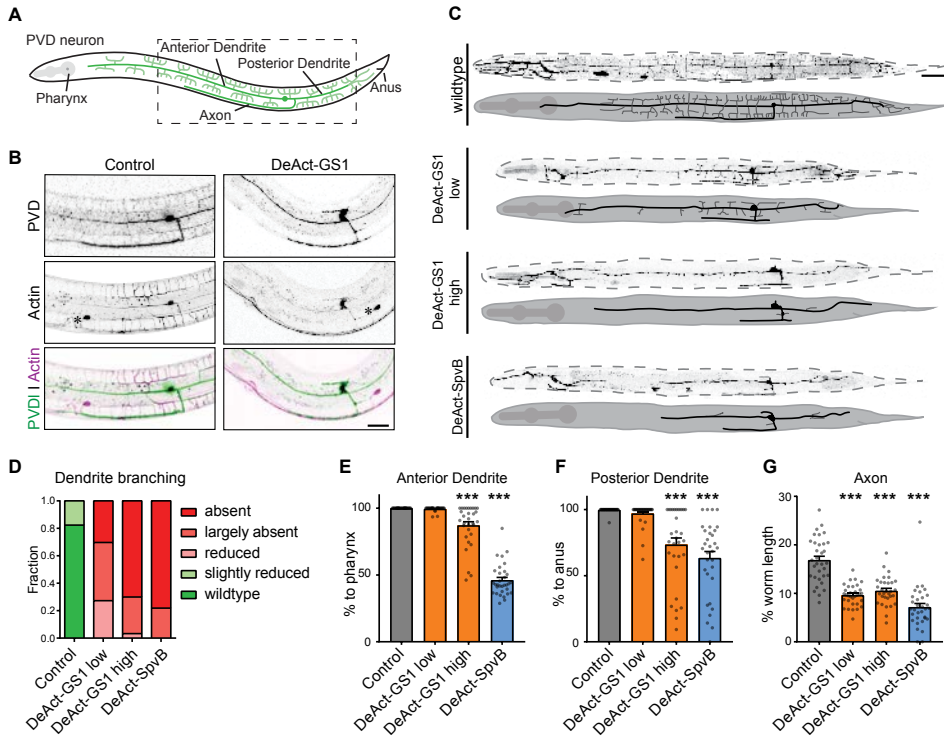


Figure 3. DeActs efficiently inhibit PVD neuron development in *C. elegans*

A. Schematic representation of the *C. elegans* highly branched PVD neuron. **B.** Co-expression of the moesinABD actin marker with GFP (control) or DeAct-GS1 in the PVD neuron. Other neurons expressing the actin marker are marked by *. Scale, 20 μ m. **C.** Representative images and schematic representation of the PVD neuron morphology upon cell specific DeAct expression. Scale, 50 μ m. **D-G.** Quantification of the DeAct-induced branching defects (**D**) and primary neurite outgrowth defects (**E-G**). Controls are siblings which lost the DeAct constructs. N = 34 for controls and N = 32 for DeAct animals (for DeAct-GS1 64 animals were analyzed and split in low and high DeAct expressing animals). Graphs show mean \pm SEM. Statistical significance: one-way ANOVA and Dunnett's multiple comparison post hoc test. Micrographs are representative, ***p<0.001.

towards the cortical plate, but instead accumulated in the subventricular zone (Fig.2F-H). Thus, DeActs cause strong developmental defects during neuronal migration *in vivo*.

As a second *in vivo* model we used the nematode *C. elegans*, for which conventional drugs are hard to use due to its impermeable exoskeleton. The PVD sensory neuron possesses a stereotyped morphology with two highly branched dendrites (anterior and posterior) and an axon that extends first ventrally and then anteriorly into the ventral nerve cord (Fig.3A). We first found that the moesin-based actin marker moeABD (Chia *et al.*, 2014) was enriched in the many dendritic side branches (Fig.3B). We expressed DeActs using a specific PVD neuron promoter that is activated early during neurite extension (Maniar *et al.*, 2011). Consistent with a role for actin assembly, PVD neuron-specific DeAct expression led to severe loss of dendrite

branching (Fig.3B-D). In addition to branching, primary neurite outgrowth was largely blocked upon DeAct-SpvB expression or high expression of DeAct-GS1 (Fig.3E-G). Thus, DeAct-SpvB led to strong neuronal phenotypes *in vivo* whereas the severity of the DeAct-GS1 induced phenotypes was dose-dependent.

In conclusion, by repurposing the actin binding domain of gelsolin (DeAct-GS1) and the actin-modifying enzymatic activity of SpvB (DeAct-SpvB), we created tools that allow for cell-specific perturbation of the actin cytoskeleton both in cultured cells and multicellular *in vivo* model systems. Having genetically encoded tools allows for control of actin dynamics using cell type-specific and inducible promoters, and opens up possibilities for elucidating the role of actin dynamics in fundamental and disease relevant cellular processes.

DATA AVAILABILITY

The data that support the findings of this study and detailed protocols for all methods are available from the corresponding authors upon request. The following plasmids have been deposited at Addgene: pCMV-DeAct-GS1 (Addgene plasmid 89445), pCMV-DeAct-SpvB (Addgene plasmid 89446), pTetON-EGFP (Addgene plasmid 89453), pTetON-DeAct-GS1 (Addgene plasmid 89454), and pTetON-DHFRdd-SpvB; CMV-mCherry (Addgene plasmid 89463). Other plasmids are available upon request.

ACKNOWLEDGMENTS

We thank C. Bargmann (Rockefeller) for the CX11480 strain, K. Shen (Stanford) for the moesin actin marker, K. Satchell (Northwestern) for MARTXVC, K. Aktories (Albert-Ludwigs University of Freiburg) for TccC3 and C2I, D. Mullins (UCSF) for cofilin(S3A), T. Wandless and L.-c. Chen (Stanford) for DHFRdd; L. Spector, E. Vitriol, and M.Z. Lin for helpful discussions; Wormbase; and Stanford Neuroscience Microscopy Service, supported by NIH NS069375. We gratefully acknowledge funding from the Netherlands Organization for Scientific Research (NWO) (NWO-ALW-VENI to M.H., NWO-ALW-VICI to C.C.H., NWO-ALW-VICI to R.J.P., the European Research Council (ERC Consolidator Grant; C.C.H.), the Deutsche Forschungsgemeinschaft (Germany) project AK6/22-2 (A.E.L.), NIH R01 GM114666 (D.K.), the National Multiple Sclerosis Society (J.B.Z and B.A.B), NIH R01 EY10257 (B.A.B.), and the Dr. Miriam and Sheldon G. Adelson Medical Research Foundation (B.A.B). M.E.d.S. is supported by Fundação para a Ciência e Tecnologia (FCT, Portugal; grant SFRH/BD/68642/2010). J.B.Z. is a Career Transition Award Fellow of the National Multiple Sclerosis Society.

AUTHOR CONTRIBUTIONS

M.H., M.E.d.S., C.C.H., D.K., and J.B.Z. conceived the project. M.H., M.E.d.S., L.W., J.T., A.I., E.v.B., R.J.P., L.C.K., C.C.H., and J.B.Z. planned and/or executed experiments. A.E.L., D.K., and B.A.B. contributed essential reagents and expertise. M.H., M.E.d.S., C.C.H., and J.B.Z. wrote the paper with input from all authors. C.C.H. and J.B.Z. supervised all aspects of

the work.

SUPPLEMENTARY METHODS

Ethics Statement

All animal experiments were performed in compliance with the guidelines for the welfare of experimental animals issued by the Government of The Netherlands. All animal experiments were approved by the Animal Ethical Review Committee (DEC) of Utrecht University or were approved by Stanford University's Administrative Panel on Laboratory Animal Care.

Molecular biology and design of DeActs

We used published biochemical data to determine the minimal actin binding or modifying domains of Gelsolin (Gelsolin segment 1, GS1) (Finidori *et al.*, 1992; McLaughlin *et al.*, 1993; Way *et al.*, 1990; Way *et al.*, 1992), *Salmonella enterica* SpvB (mono(ADP-ribosyl)transferase domain) (Hochmann *et al.*, 2006; Margarit *et al.*, 2006; Tezcan-Merdol *et al.*, 2001), *Vibrio cholerae* MARTXVC (actin crosslinking domain) (Kudryashov *et al.*, 2008; Sheahan *et al.*, 2004), *Salmonella* SipA (actin crosslinking minimal domain) (Lilic *et al.*, 2003), *Photobacterium luminescens* TccC3 (mono(ADP-ribosyl)transferase domain) (Lang *et al.*, 2010), and *Clostridium botulinum* C2I (mono(ADP-ribosyl)transferase domain) (Schleberger *et al.*, 2006; Vandekerckhove *et al.*, 1988). Despite extensive biochemical data on the mechanisms, specificity, and minimal functional domains of these peptides (Aktories *et al.*, 2011; Finidori *et al.*, 1992; Hochmann *et al.*, 2006; Margarit *et al.*, 2006; McLaughlin *et al.*, 1993; Tezcan-Merdol *et al.*, 2001; Way *et al.*, 1990; Way *et al.*, 1992) they have not previously been developed as cell biological tools. DNA sequences encoding candidate peptides were cloned into pEGFP-C1 (Clontech) by standard procedures. To create constitutively active cofilin (GFP-P2A-cofilin(S3A) (Agnew *et al.*, 1995)) we first inserted a P2A self-cleavable peptide sequence in the multicloning site of pEGFP-C1, then inserted DNA encoding full-length human cofilin(S3A) (kind gift of Brittany Belin) in frame on the C-terminal side. In the case of DeAct-GS1 and DeAct-SpvB we truncated proteins within regions predicted to be disordered (Li *et al.*, 1999).

The following mammalian expression plasmids have been described previously: pGW2-MARCKS-eGFP (Schatzle *et al.*, 2011), pSuper vector (Brummelkamp *et al.*, 2002), p β actin-GFP (Kapitein *et al.*, 2010a), tagRFP-Paxillin (Bouchet *et al.*, 2016), *E. coli* dihydrofolate reductase destabilization domain (DHFRdd) with R12Y, G67S, Y100I mutations (Iwamoto *et al.*, 2010) was a gift of Tom Wandless and Ling-chun Chen (Stanford). pGW2-MARCKS-TagRFP-T was generated by introducing Tag-RFP-T to GW2-MARCKS by PCR strategy. For the *in utero* experiments, DeAct-GS1 and DeAct-SpvB were cloned in a pGW2-GFP vector. For the *C. elegans* experiments the *Pdes-2::mKate2::GS1* and *Pdes-2::mKate2::SpvB* were cloned using multisite Gateway cloning. The *des-2* promoter sequence was based on Maniar *et al.* (2011) (Maniar *et al.*, 2011) and cloned into pDONR4-1, the mKate2 sequence (kind gift from Henrik Bringmann (Redemann *et al.*, 2011)) was cloned into pDONR221 and the DeAct-GS1 or DeAct-SpvB sequences were cloned into pDONR2-3. pKN146 was used as destination vector which is the pCFJ201 vector supplemented with the *unc-54* UTR (kind gift from H.C. Korswagen). The cytoplasmic mKate2 was cloned into the pCFJ150 (Frokjaer-Jensen *et al.*, 2008) using the pCM1.36 *tbb-2* UTR (Addgene #17249). All constructs were validated by sequencing. Gelsolin and SpvB sequences used for in DeAct constructs can be found in Supplementary Data S1.

Cell culture experiments

HeLa cells (American Type Culture Collection) were cultured in DMEM medium (Life Technologies) supplemented with 10% FBS, 2 mM L-glutamine, nonessential amino acids, and penicillin/streptomycin (all from Gibco) at 37°C with 5% CO₂. We used cells from ATCC for <5 passages so did not authenticate or test for mycoplasma contamination in-house. HeLa Tet-On 3G stable cell line (Clontech #631186) were cultured in the same media, but with Tet System Approved FCS that is guaranteed to have no contaminating tet/dox (Clontech). Expression from the TetON promoter was induced with doxycycline (1-100 ng/mL as noted; Sigma D9891). Primary rat embryonic fibroblasts (REFs) were isolated as previously described (Vierbuchen *et al.*, 2010) and plated in the same growth media. Briefly, we surgically isolated limbs from E13.5-E14.5 mixed-sex Sprague-Dawley (Charles River) rat embryos,

dissociated cells mechanically and with trypsin, then allowed REFs to proliferate in growth media for at least 3 passages. For transfection, cells were seeded onto glass coverslips one day prior and transfected using XtremeGENE HP DNA Transfection Reagent (Roche) or Eugene (Roche) according to the manufacturer's protocol, or treated with latrunculin A (EMD Millipore) to induce actin disassembly. OPCs were purified from enzymatically dissociated mixed sex P7-P8 Sprague-Dawley (Charles River) rat brains by immunopanning and grown in serum-free defined medium, as described previously (Dugas *et al.*, 2006). PDGF (10 ng/ml, PeproTech) and NT-3 (1 ng/ml, PeproTech) were added to the media to induce OPC proliferation. OPCs were transfected as described previously (Dugas *et al.*, 2006) using a Lonza/Amaya nucleofector kit, with $2\text{--}3 \times 10^6$ OPCs per transfection, then differentiated into mature OLs by removal of PDGF and NT-3 and addition of thyroid hormone (triiodothyronine, T3; 40 ng/ml; Sigma) as described (Dugas *et al.*, 2006). We used the myelin basic protein promoter (MBPp) (Gow *et al.*, 1992) for expression of DeActs in mature OLs.

Cells were fixed in 4% formaldehyde (prepared from paraformaldehyde) for 15 min, permeabilized with 0.1% Triton X-100 for 3 min, then blocked in 3% BSA in PBS. Native GFP fluorescence was visualized to detect DeAct expression. Cells were stained with Alexa Fluor 594-phalloidin (Invitrogen) to visualize actin filaments, DAPI to visualize nuclei, HCS CellMask Blue (Invitrogen) to reveal cellular morphology, or immunostained for myelin basic protein (MBP) to detect oligodendrocytes (Abcam ab7349, used at 1:100). Cells were visualized by epifluorescence using a Zeiss Axio Imager M1 and Axiovision software, most frequently with a 20x 0.8 NA Plan Apo objective, or by confocal using an LSM510 scan head on an Axio Observer Z1 with either a 63x 1.4 NA objective (all of the above, Carl Zeiss Microscopy). Identical illumination and acquisition conditions were used for each experiment. Confocal images of HeLa cells for focal adhesion quantification were acquired using LSM700 (Zeiss) with a 40x/1.30 Oil DIC objective using 488nm and 555nm laser lines. A total thickness of 5 μm was scanned for each position and maximum intensity projections were generated for analysis.

Hippocampal neuron cultures, transfections and drug treatments

Primary hippocampal cultures were prepared from mixed sex embryonic day 18 (E18) rat brains by mechanical and enzymatic dissociation (Goslin and Banker, 1989; Kapitein *et al.*, 2010b). Cells were plated on coverslips coated with poly-L-lysine (37.5 $\mu\text{g}/\text{ml}$) and laminin (1.25 $\mu\text{g}/\text{ml}$) at a density of 100,000/well. Hippocampal cultures were grown in Neurobasal medium (NB) supplemented with B27, 0.5 mM glutamine, 15.6 μM glutamate and penicillin/streptomycin. Hippocampal neurons at DIV2 were transfected using Lipofectamine 2000 (Invitrogen). Briefly, DNA (3.6 $\mu\text{g}/\text{well}$) was mixed with 3 μl Lipofectamine 2000 in 200 μl NB, incubated for 30 minutes and then added to the neurons in NB with 0.5 mM glutamine at 37°C in 5% CO₂ for 45 min to 1 hour. Next, neurons were washed with NB and transferred in the original medium at 37°C in 5% CO₂ for 36–48 hours. Neurons were co-transfected with GFP-tagged MARCKS (control), GS1 or SpvB together with empty pSuper vector. Whenever indicated 10 μM latrunculin B (Sigma) was added to the neuron cultures and either imaged 1 min and up to 30 minutes after addition or fixed after 30 minutes.

Neuron immunocytochemistry, growth cone morphology and phalloidin intensity analysis

For immunocytochemistry, neurons were fixed for 10 min with 4% formaldehyde/4% sucrose in PBS at room temperature. After fixation cells were washed 3 times for 5 minutes in PBS at room temperature and incubated with Alexa Fluor 568-phalloidin (Life Technologies A12380) for 1 hour at room temperature. Neurons were then washed 3 times for 5 minutes in PBS at room temperature and subsequently mounted on slides in Vectashield mounting medium (Vector Laboratories). Confocal images were acquired using LSM700 (Zeiss) with a 63x/1.40 Oil or 40x/1.30 Oil DIC objective using 488nm and 555nm laser lines. A total thickness of 5 μm was scanned for each position and maximum intensity projections were generated for analysis. Imaging settings were kept the same when pictures were compared for fluorescence intensity. Growth cone morphology was classified manually and phalloidin intensity was measured in ImageJ. The entire growth cone areas were considered and normalized to growth cones of untransfected neighboring neurons.

To be able to identify the axon in the live cell imaging experiments, neuronal cultures were incubated with extracellular Neurofascin-pan mouse primary antibody (NeuroMab, clone number A12/18) in conditioned Neurobasal medium, for 10 minutes at 37°C. After this, neurons were washed 3 times in warm Neurobasal medium and anti-mouse Alexa405 antibody (Life Technologies, catalogue number A31553) in conditioned Neurobasal medium was added for 10 minutes at 37°C. Neurons were then washed 3 times in warm Neurobasal medium and returned to the

conditioned medium.

Live cell imaging microscopy

All imaging was performed in full conditioned medium at 37°C and 5% CO₂ unless otherwise indicated. For live imaging of REF cell motility, cells were plated on PDL-coated plastic bottom ImageLock plates (Essen Bioscience) and imaged in an IncuCyte ZOOM Live Cell Imaging System (Essen Bioscience) with 10% CO₂. For wound healing assays, cells were plated on 5 µg/mL fibronectin, grown until confluent, then mechanically scratch-wounded with a sterile p2 pipette tip. Non-adhered cells were washed off with fresh growth media and imaged once per hour. Live cell imaging of hippocampal neurons was performed by laser confocal spinning disk microscopy, using a Nikon Eclipse-Ti (Nikon) microscope with Plan Apo 40x N.A. 1.30 oil objective (Nikon). The microscope is equipped with a motorized stage (ASI; MS-2000), a Perfect Focus System (Nikon), an incubation chamber (Tokai Hit; INUBG2E-ZILCS) and uses MetaMorph 7.7.6 software (Molecular Devices) to control the camera and all motorized parts. Confocal excitation and detection is achieved using 100 mW Cobolt Calypso 491nm and 100mW Cobolt Jive 561nm lasers and a Yokogawa spinning disk confocal scanning unit (CSU-X1-A1; Yokogawa) equipped with a triple-band dichroic mirror (z405/488/568trans-pc; Chroma) and a filter wheel (CSU-X1-FW-06P-01; Yokogawa) containing BFP (ET-BFP 49021), GFP (ET-GFP (49002)), mCherry (ET-mCherry (49008)) and mCherry/GFP (ET-mCherry/GFP (59022)) emission filters (all Chroma). Confocal images were acquired with a Evolve 512 EMCCD camera (Photometrics) at a final magnification of 67 nm/pixel, including the additional 2.0x magnification introduced by an additional lens mounted between scanning unit and camera (Edmund Optics). For quantifying single cell motility of fibroblasts, we first imaged the GFP channel to identify GFP- or DeAct-expressing cells, then subsequently imaged with phase microscopy to limit phototoxicity until the final frame of the video, with 15 minute intervals. To classify DeAct-GS1 expressing cells as high or low expressers, we quantified average cellular GFP intensity from initial fluorescence images (background subtracted, ImageJ), and defined high expressers as those cells with GFP signals above the median value. Cell motility was measured in ImageJ by first aligning images with the StackReg plugin, then measuring displacement of the nucleus using the MTrackJ plugin.

Axonal branches were imaged in time lapses of 5 minutes, with 5 seconds interval between acquisition and a z-stack stream at every time point, to guarantee the entire axonal branch complexity is imaged. In control conditions (MARCKS-eGFP), 5-6 neurons were first imaged in Neurobasal medium. After that 10 µM latrunculin B (Sigma) was added to the imaging chamber and the same cells were imaged from 1 to 30 minutes. The dynamics of axonal branches was quantified manually using ImageJ.

Time-lapse live-cell imaging of filopodia dynamics in HeLa cells was performed using a TIRF microscope (Nikon Eclipse TE2000E) equipped with an incubation chamber (Tokai Hit; INUG2-ZILCS-H2) mounted on a motorized stage (Prior). Cells were imaged in full medium at 37°C and 5% CO₂ every 5 seconds for 5 minutes using a 100x objective (Apo TIRF 100x/NA 1.49, Nikon) and an Evolve 512 EMCCD camera (Photometrics) (Kapitein *et al.*, 2013). Excitation was achieved using a 488 nm LuxX488-100 diode laser and a 561 nm Cobolt Jive laser, fiber-coupled to the Nikon TIRF module. GFP-expressing cells treated with Latrunculin B were first imaged without the drug and then imaged again after 5 to 30 minutes upon addition of 10 µM of Latrunculin. Quantification of total and dynamic filopodia numbers was performed using ImageJ.

In utero electroporation and immunohistochemistry

Pregnant C57Bl/6 mice at E14.5 were deeply anaesthetized with Isoflurane (induction: 3-4%, surgery, 1.5-2%), injected with 0.05mg/kg buprenorphinhydrochloride in saline, and hereafter the abdominal cavity was opened under sterile surgical conditions. Uterine horns were exposed and 1.7µl DNA mixture containing pGW2-GFP alone or together with DeAct-GS1 or DeAct-SpvB dissolved in MilliQ water with 0.05% Fast Green (Sigma) was injected in the lateral ventricles of the embryo's using glass micropipettes (Harvard Apparatus) and a PLI-200 Pico-injector (Harvard Apparatus). Brains (motor cortex) were electroporated with gold plated tweezer-electrodes (Fischer Scientific) using and ECM 830 Electro-Square-Porator (Harvard Apparatus) set to three unipolar pulses at 30V (100ms interval and pulse length). Embryos were placed back into the abdomen, and abdominal muscles and skin were sutured separately. The mother mice were awakened by releasing them from Isoflurane. Embryos were collected at E17.5 and brains were fixed in 4% formaldehyde and submerged in 30% sucrose. 12µm coronal brain cryosections were made and were blocked and permeabilized in 10% Normal Horse Serum + 0.2% Triton X-100 in PBS prior to staining with first antibody (anti-GFP, MBL-Sanbio, anti-Ctip2, Abcam, anti-Neurofilament heavy chain, Abcam

and anti-Satb2, Abcam) in blocking solution overnight and fluorescent secondary antibody staining (Alexa 488, Alexa 568 and Alexa 647, Life technologies) and mounting with Vectashield mounting medium (Vectorlabs). Confocal images were acquired using LSM700 (Zeiss) with a 20x/ 0.8 objective using 405nm, 488nm, 555nm and 633nm laser lines. A total thickness of 15 μm in 1 μm steps was scanned for each position and maximum intensity projections were generated for analysis. To cover the entire brain slice, 4 images were taken side-by-side and image stitching was performed using ZEN 2011 Software.

C. elegans strains, transgenes and imaging

Strains were cultured using standard conditions (Brenner, 1974) at 15 °C and imaged at room temperature at the L4 or young adult stage. For the PVD morphology experiments the DeAct-GS1 and DeAct-SpVB constructs were injected in either NCI1686 (*wdlIs51*), which expressed GFP in the PVD, or in STR58 (*hrtIs3[Pdes-2::myristoylGFP;unc-122::DsRed]*), which is an integrant of CX11480 (*kyEx3017*) (Maniar *et al.*, 2011), generating: STR198 *hrtIs3;hrtEx52[Pdes-2::mKate2::GS1(20ng/ μl);Pmyo-2::tdTom]*, STR199 *wdlIs51;hrtEx53[Pdes-2::mKate2::GS1(4ng/ μl);Pmyo-2::tdTom]*, STR200 *hrtIs3;hrtEx54[Pdes-2::mKate2::SpvB(4ng/ μl);Pmyo-2::tdTom]*. The Actin marker strains were generated using a construct expressing the moesin actin binding domain (kind gift from Kang Shen, Stanford (Chia *et al.*, 2012)), generating: STR213 *hrtEx60[Punc-86::GFP::moeABD;Pdes-2::mKate2;Pmyo-2::tdTom]*; STR232 *hrtEx68[Pdes-2::mKate2::GS1(20ng/ μl);Punc-86::GFP::moeABD;Pmyo-2::tdTom]*. Worms were anesthetized with 10 mM tetramisole, imaged by confocal microscopy and maximum intensity projections of acquired Z stacks (1 μm steps) and straightening of the animal was done using ImageJ software (Universal Imaging Corporation).

Data analysis and statistics

All data acquisition and analysis were performed blinded to the experimental condition. We used nested analysis to first average technical replicates (e.g., three coverslips). In all cases N refers to number of independent experiments, or number of mice or worms for *in vivo* experiments (while n refers to technical replicates). Sample sizes used were similar to those generally employed in the field. Animals were allocated randomly to each experimental group. Data shown are from all animals tested; none were treated as outliers. Micrographs and blots were analyzed using NIH ImageJ and linearly contrast adjusted for display using Adobe Photoshop, with identical settings for each experiment. For quantification of fluorescent and phase micrographs, ROIs were drawn by hand or by thresholding multichannel images using ImageJ (NIH). Mean gray value (average intensity) of each individual channel was measured, and background (outside of cell area) was subtracted for each micrograph. Qualitative scoring of abnormal actin in cells was performed by an investigator blinded to experimental condition. In our hands untransfected rat embryonic fibroblasts had stereotyped phalloidin staining with similar filament intensities and distribution (e.g. stress fibers and cortical actin). GFP+ cells were considered abnormal if they had dim phalloidin staining or disorganized actin filaments (lacking stress fibers and/or presence of actin filament foci as in latrunculin-treated cells), excluding mitotic cells. Data were analyzed and plotted using Excel (Microsoft) and Prism (GraphPad Software). Unless otherwise stated, error bars are SEM, and p values were calculated using Student's t test for single comparisons or ANOVA followed by Dunnett's multiple comparison test, assuming equal variance.

SUPPLEMENTARY FIGURES

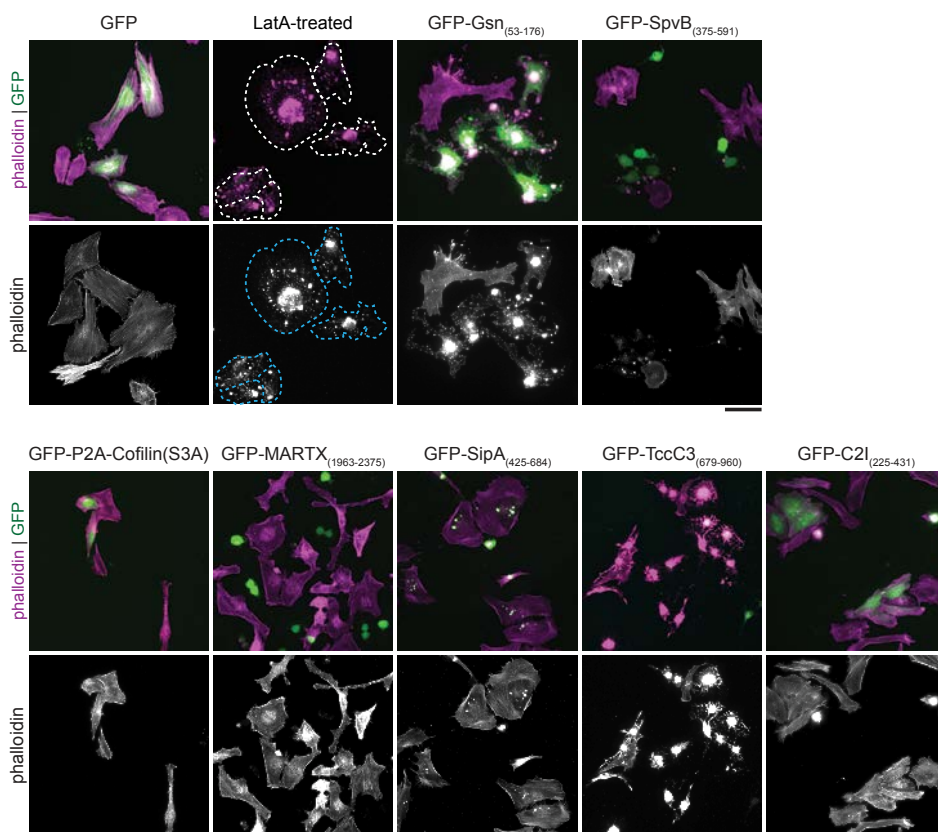
► Supplementary Figure S1. Screen for polypeptides that affect cellular actin filaments

A. Table summarizing results from all polypeptides tested. Source shows organism, gene, and amino acid numbers used. Effect on F-actin is qualitative analysis of gross changes in cellular phalloidin intensity and distribution. In addition to human Gelsolin-GS1 and *Salmonella* SpvB described in this paper candidate proteins included: GFP-P2A (self-cleavable peptide) tagged constitutively active human Cofilin(S3A) (Agnew *et al.*, 1995), *Vibrio cholerae* MARTXVC actin crosslinking domain (Kudryashov *et al.*, 2008; Sheahan *et al.*, 2004), *Salmonella* SipA actin crosslinking minimal domain (Lilic *et al.*, 2003), *Photobacterium luminescens* TccC3 actin stabilizing ADP ribosylation domain (Lang *et al.*, 2010), and *Clostridium botulinum* C2I ADP ribosylation domain (Schleberger *et al.*, 2006; Vandekerckhove *et al.*, 1988). **B.** Representative micrographs from the screen. HeLa cells were transiently transfected with GFP-tagged constructs or latrunculin A then fixed and stained for actin filaments (594-phalloidin, red) and nuclei (DAPI, blue). Due to these being transient transfections, expression levels varied from cell to cell. N = 1 (cofilin, MARTXVC), 2 (SipA), or 4 (TccC3, C2I) independent experiments. Scale, 50 μm .

A

Construct	Source	Effect on F-actin	Construct notes
GFP-Gsn actin monomer-binding	human Gelsolin (AA#53-176)	+++	Dose-dependent loss of actin filaments; phenocopies LatA
GFP-SpvB ADP-ribosylation domain	<i>Salmonella enterica</i> SpvB (AA#375-591)	++++	Dramatic loss of actin filaments and cell rounding
GFP-P2A-Cofilin(S3A) constitutively active	human Cofilin-1(S3A) (full length)	-	No gross effect on cellular actin filaments
MARTXvc Actin Crosslinking Domain - GFP	<i>Vibrio cholerae</i> MARTXvc (AA#1963-2375)	++++	Dramatic loss of actin filaments and cell rounding
GFP-SipA "Actin staple" minimal domain	<i>Salmonella typhimurium</i> SipA (AA#425-684)	+	Few bright F-actin foci colocalizing with GFP-SipA; most of cytoskeleton unaffected
GFP-TccC3 ADP-ribosylation domain	<i>Photobacterium luminescens</i> (AA#679-960)	+++	Bright phalloidin staining in TccC3+ cells
GFP-C2I ADP-ribosylation domain	<i>Clostridium botulinum</i> C2-I (AA#225-431)	-	No gross effect on cellular actin filaments

B



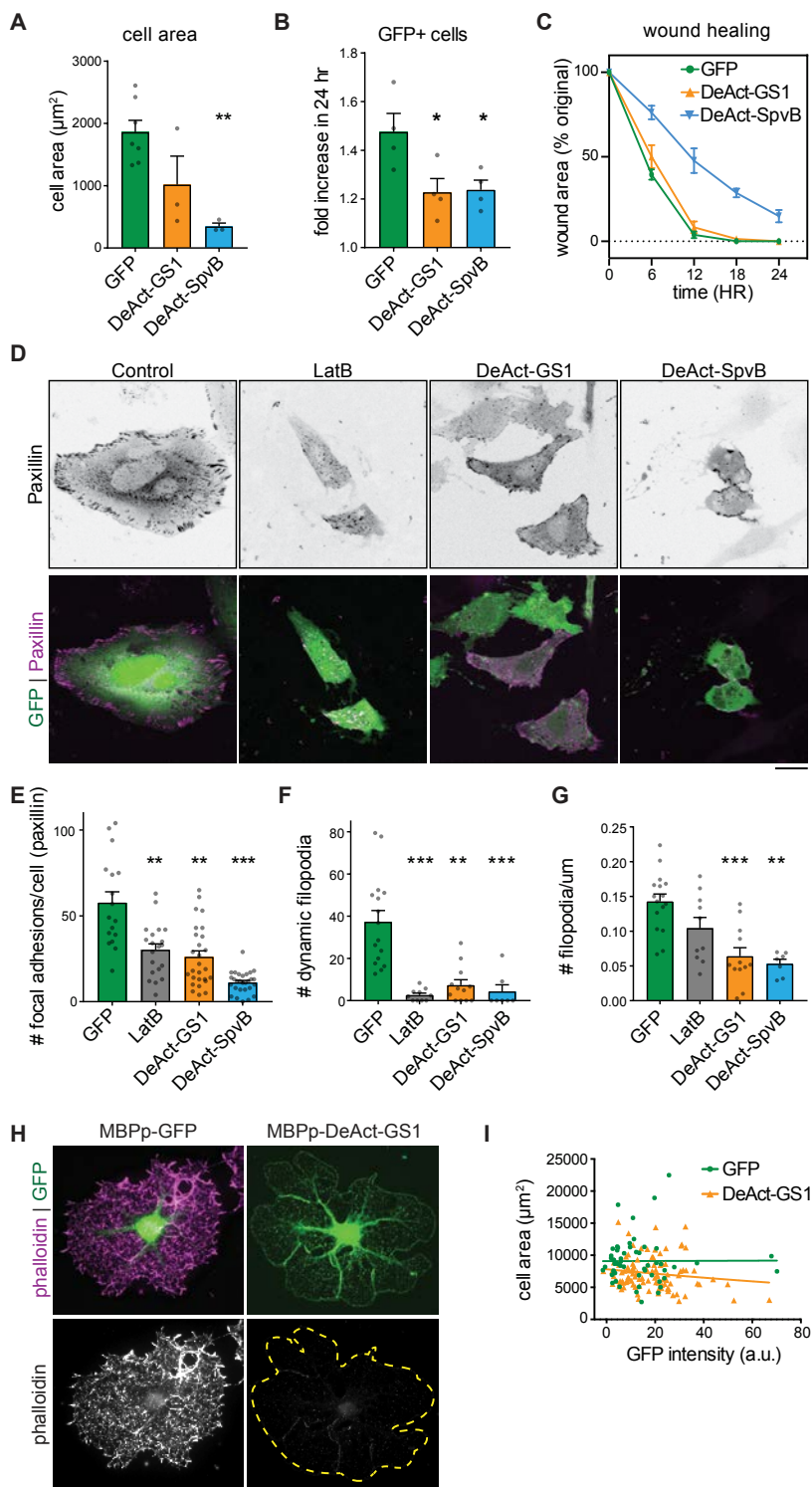
Human beta actin (AKI70837)	...DGVTHTVPIYEGYALPHA I L R LDLAGRDLDYLMKILTERG...
Human gamma actin (NP_001186883)	...DGVTHTVPIYEGYALPHA I L R LDLAGRDLDYLMKILTERG...
Human alpha cardiac actin (P68032)	...DGVTHNVPIYEGYALPHA I M R LDLAGRDLDYLMKILTERG...
Human aortic smooth muscle actin (NP_001135417)	...DGVTHNVPIYEGYALPHA I M R LDLAGRDLDYLMKILTERG...
Human gamma enteric smooth muscle actin (NP_001606)	...DGVTHNVPIYEGYALPHA I M R LDLAGRDLDYLMKILTERG...
Mouse beta actin (EDL19081)	...DGVTHTVPIYEGYALPHA I L R LDLAGRDLDYLMKILTERG...
Mouse gamma actin (AAH99371)	...DGVTHTVPIYEGYALPHA I L R LDLAGRDLDYLMKILTERG...
Mouse alpha skeletal muscle actin (P68134)	...DGVTHNVPIYEGYALPHA I M R LDLAGRDLDYLMKILTERG...
<i>C. elegans</i> ACT-5 (CAB05817)	...DGVTHTVPIYEGYALPHA I Q R LDLAGRDLDYMMKILTERG...
<i>D. melanogaster</i> Act5C (NP_0012849 15)	...DGVSHTVPIYEGYALPHA I L R LDLAGRDLDYLMKILTERG...
<i>D. melanogaster</i> Act42A (NP_523625)	...DGVSHTVPIYEGYALPHA I L R LDLAGRDLDYLMKILTERG...
<i>Acanthamoeba castellanii</i> actin (CAA23399)	...DGVTHTVPIYEGYALPHA I L R LDLAGRDLDYLMKILTERG...
<i>S. cerevisiae</i> actin (AAA34391)	...DGVTHVVPYIYAGFSLPHA I L R IDLAGRDLDYLMKILSERG...

Supplementary Figure S2. SpvB targets a conserved residue on actin

SpvB ADP-ribosylates a conserved arginine on actin monomers (R177 in human beta actin) (Margarit *et al.*, 2006). Lineup shows cytoplasmic and muscle actins from diverse eukaryotes, with this residue (highlighted in yellow) conserved in all actin homologs. Accordingly, DeAct-SpvB functions in all eukaryotes we have tested thus far. NCBI Reference sequence numbers are shown in parentheses.

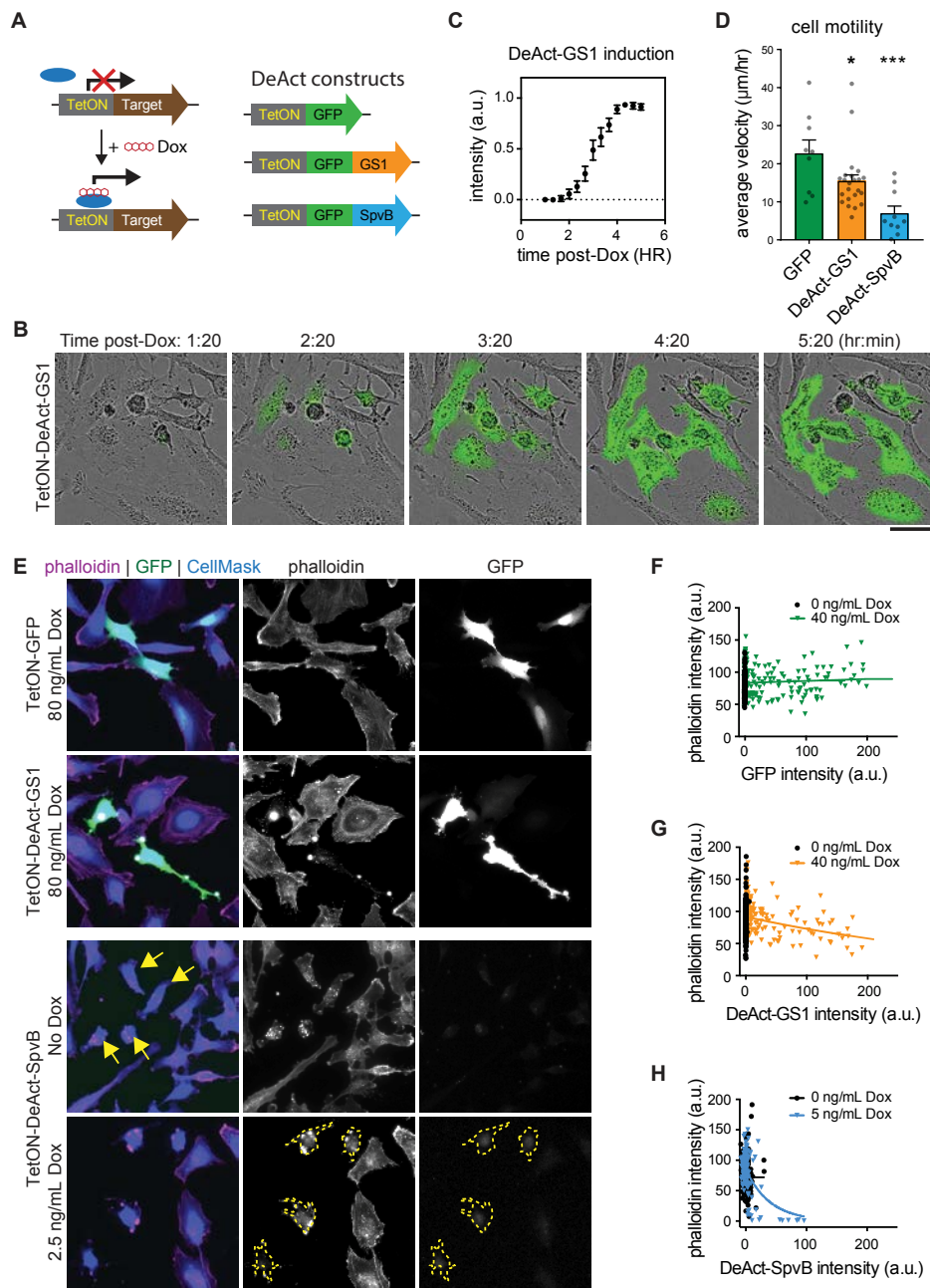
► Supplementary Figure S3. Expression of DeActs in cultured cells

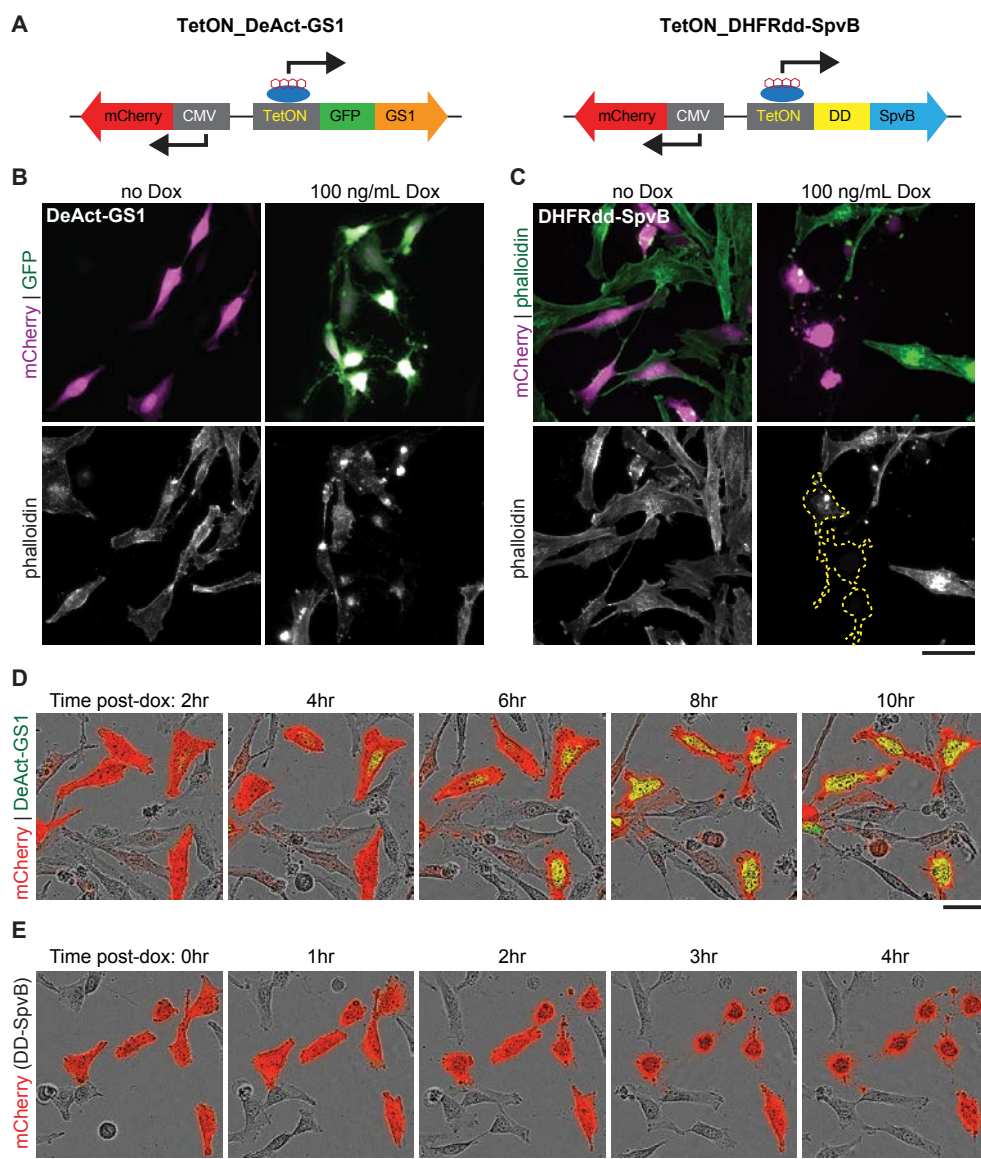
A. DeActs decrease average cell surface area in HeLa cells. Graphs shows mean \pm SEM. Statistical significance: one-way ANOVA and Dunn's multiple comparison post hoc test, $**p < 0.01$; $N = 3$ independent experiments. **B.** Live cell imaging to count HeLa cells expressing GFP, DeAct-GS1 or DeAct-SpvB at 24hr and 48hr post-transfection. Fold increase in GFP+ cells reflects the combination of proliferation and new expression minus cell death. $*p < 0.05$, $N = 4$, $n = 150$ -200 GFP+ cells per experiment. **C.** Wound healing of rat embryonic fibroblasts transiently transfected with DeActs or GFP control and scratch-wounded at time zero. Note that no defect in wound healing is observed upon DeAct-GS1 transfection, most probably due to the fraction of untransfected and low DeAct-GS1 expressing cells. $N = 2$ independent experiments. **D.** HeLa cells co-expressing the focal adhesion marker tagRFP-paxillin (red) (Bouchet *et al.*, 2016) and GFP, DeAct-GS1 or DeAct-SpvB (green). GFP expressing cells were treated with 10 μ M latrunculin B for 30 minutes. Scale, 20 μ m. **E.** DeActs decrease the number of focal adhesions per cell, visualized by paxillin overexpression. Treatment with latrunculin B has the same effect. Graphs show mean \pm SEM. Statistical significance: one-way ANOVA and Dunn's multiple comparison post hoc test, $***p < 0.001$, $**p < 0.01$ ($N = 2$ independent experiments for all conditions, $n = 17, 20, 27, 28$ cells, left to right). **F-G.** Live-imaging of HeLa cells co-expressing GFP, DeAct-GS1 or DeAct-SpvB and MARCKS-tagRFP-T shows that DeActs decrease the number of dynamic filopodia (**F**) and the total number of filopodia per cell (**G**). Graphs show mean \pm SEM. Statistical significance: one-way ANOVA and Dunn's multiple comparison post hoc test, $***p < 0.001$, $**p < 0.01$, ($N = 3, 2, 2, 2$ independent experiments, $n = 16, 10, 12, 7$ cells, left to right). (see also Supplementary Video S1). **H-I.** DeAct-GS1 induced loss of actin filaments in mature OLS does not affect cell area. Trend lines in I shows nonlinear (exponential) fit; each data point is one cell. Data are from a single experiment representative of $N = 3$ independent experiments.



► **Supplementary Figure S4. Rapid induction of DeActs with third-generation TetON promoter**

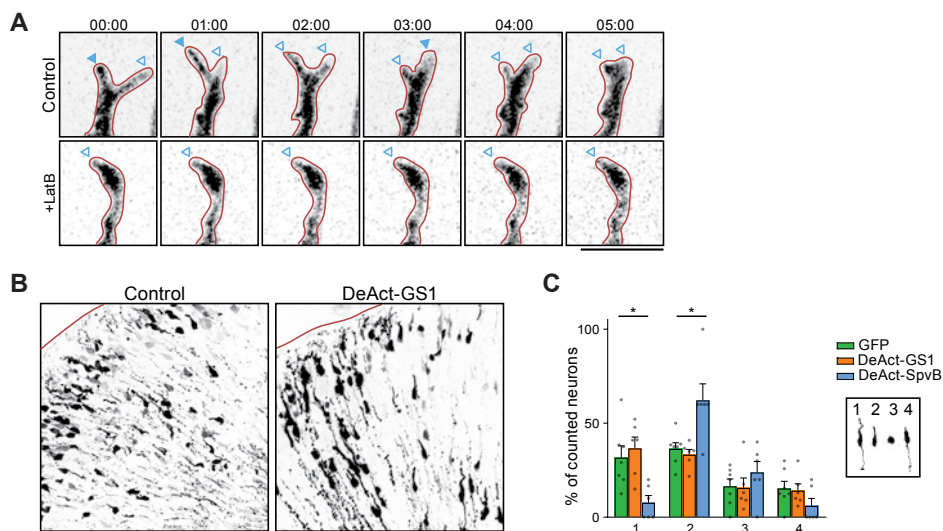
A. Mechanism of action and construct design for doxycycline/tet-inducible DeActs using Clontech Tet-On 3G inducible expression vector. In presence of the tetracycline-regulated transactivator (Tet-On 3G, blue), doxycycline (Dox) induces dose-dependent expression from the TetON 3G promoter. Tet-On 3G HeLa cells (stably expressing Tet-On 3G transactivator; Clontech) were transfected with Tet-ON_GFP, TetON_DeAct-GS1, or TetON_DeAct-SpvB in **(B-H)**. **B-C.** Rapid induction of DeAct-Gsn expression. 24 hr post transfection, expression of TetON_DeAct-GS1 was induced by addition of 100 ng/mL Dox, and cells were imaged every 20 minutes. **(B)** shows frames from live cell imaging. **(C)** shows normalized GFP fluorescence following addition of Dox at time 0; average of 10 cells from one representative experiment of $N = 3$ independent experiments. **D.** Live cell imaging of HeLa cells expressing TetON DeActs. Rate of single cell motility was measured after detection of GFP expression, imaging every 20 min for at least 3 hr. Graph shows mean \pm SEM. Statistical significance: one-way ANOVA and Dunn's multiple comparison post hoc test, *** $p < 0.001$, * $p < 0.05$, $n = 9, 23, 10$ GFP+ cells, left to right. **E.** Representative micrographs of cells expressing TetON DeActs. 24 hr post transfection, cells were treated with or without Dox as noted for 6 hr, then fixed and stained with Alexa 594-phalloidin and CellMask Blue to visualize cell morphology. **F-H.** Cells were transfected with TetON_GFP **(F)**, TetON_DeAct-Gsn **(G)** or TetON_DeAct-SpvB **(H)** as above and treated with or without Dox as noted overnight, then fixed and stained with Alexa 594-phalloidin. Scatter plots show actin filament level (phalloidin) as a function of DeAct expression; each data point is a single cell from one representative experiment of $N = 2$ independent experiments. Note that DeAct-SpvB expression intensities **(H)** are not comparable to GFP and DeAct-GS1 **(F,G)** due to low expression induced by 5 ng/mL Dox. Graphs in C,D show mean \pm SEM. All scale bars, 50 μm .





Supplementary Figure S5. Identification of transfected cells with dual-promoter, inducible DeActs

A. Construct design for dual-promoter constructs with constitutive mCherry expression (CMV promoter) and inducible DeAct expression on the opposite strand. Left, dual-promoter TetON_DeAct-GS1; right, TetON_SpvB tagged with *Escherichia coli* dihydrofolate reductase destabilization domain (DHFRdd) with R12Y, G67S, Y100I mutations (Iwamoto *et al.*, 2010). **B-C.** HeLa TetON 3G cells (stably expressing Tet transactivator protein) were transfected with dual-promoter CMV_mCherry/TetON_DeAct-GS1 (**B**) or CMV_mCherry/TetON_DHFRdd-SpvB constructs (**C**). After 24 hours DeAct expression was induced with 100 ng/mL Dox, then cells were fixed after 18 hr and stained for actin filaments with Alexa 647-phalloidin. **D-E.** HeLa Tet-On 3G transfected as above were imaged every hour after addition of Dox. Note rapid induction of DeAct-GS1 visualized by GFP expression (**D**), and induction of attenuated (DHFRdd-tagged) SpvB demonstrated by rapid cell rounding (**E**). All scale bars, 50 μ m. B-E are representative micrographs from N = 3 independent experiments.



Supplementary Figure S6. Expression of DeActs in neurons

A. A representative example of dynamic axonal branches from a 5 minute time lapse acquisition. Closed arrow heads indicate growth and open arrow heads represent no growth or retraction (see also Supplementary Video S3). Scale, 10 μ m. **B-C.** Cortical neuronal migration after *in utero* electroporation with GFP, DeAct-GS1, or DeAct-SpvB. Scale, 50 μ m. **(C)** Quantification of neuronal morphologies of GFP-positive neurons which migrated past the IZ. 1, leading and trailing process; 2, leading process only; 3, no processes; 4, trailing process only (N = 3 embryos from 3 different litters, n = 104, 135, 38 cells GFP, DeAct-GS1, or DeAct-SpvB). Graphs show mean \pm SEM. Statistical significance: one-way ANOVA and Dunnett's multiple comparison post hoc test, *p<0.05.

SUPPLEMENTARY VIDEOS

Supplementary Video S1

This video corresponds to Supp. Fig.S3F-G. Live-imaging of HeLa cells co-expressing MARCKS-TagRFP-T and GFP, DeAct-GS1 or DeAct-SpvB. DeActs inhibit filopodia dynamics. Total time: 5 minutes. Acquisition was performed at 5 seconds per frame. 20x sped up. (AVI 1.9 Mb). Scale, 5 μ m.

Supplementary Video S2

This video corresponds to Fig.1F. Cell motility of rat embryonic fibroblasts expressing GFP or GFP-GS1. Total time: 24 hr. Acquisition was performed at 1 hr per frame. 25,200x sped up. (AVI, 1.7 Mb).

Supplementary Video S3

This video corresponds to Fig.2E and Supp. Fig.S6A. Dynamics of axonal growth cones is lost after addition of latrunculin B or in neurons expressing DeAct constructs. Total time: 5 minutes. Acquisition was performed at 5 seconds per frame. 10x sped up. (AVI, 1.1 Mb).

Videos available online

<http://dx.doi.org/10.1038/nmeth.4257>



SUPPLEMENTARY DATA

Supplementary Data S1. Sequences of DeAct constructs

Full DNA sequences, Genbank accession numbers, and corresponding amino acid numbers of DeAct-GS1 and DeAct-SpvB are as follows:

DeAct-GS1

(human GSN; Genbank NM_000177.4; sequence encoding amino acids #53-176):

```
GTGGTGGAAACACCCCGAGTTCCCTCAAGGCAGGGAAGGAGCCTGGCCCTGCAGATCTGGCGT
GTGGAGAAGTTCGATCTGGTGCCCGTGCCACCAACCTTTATGGGAGACTTCTTCACGGGC
GACGCCTACGTATCCTGAAGACAGTGCAGCTGAGGAACGGAAATCTGCAGTATGACCTC
CACTACTGGCTGGGCAATGAGTGCAGCCAGGATGAGAGCGGGCGGCCCATCTTTACC
GTGCAGCTGGATGACTACCTGAACGGCCGGCCGTGCAGCACCGTGAGGTCCAGGGCTTC
GAGTCGGCCACCTTCCCTAGGCTACTTCAAGTCTGGCCTGAAGTACAAGAAAGGAGGTGTG
GCATCAGGATTC
```

DeAct-SpvB

(*Salmonella enterica* spvB; Genbank D14490.1; sequence encoding amino acids #375-591):

```
GGAGGTAATTCATCTCGACCAAAATCAAAATGGGCGATTGTAGAGGCATCAAAGCAGAT
TCAAGCTCTGAGGTAATTCAGCTCAAGGGTACAGTGTGATTAATAAATATTTACGTGGG
GATGATTATCCTGAAACACAGGCAAAGAACTCTGCTCTCCAGAGACTATCTTTCCACAAAT
GAACCCAGTGATGAGGAGTTTAAAAATGCCATGTCAGTTTATATAAATGATATTGCGGAGGGAT
TAAGTTCACTTCCCGAAACAGATCACAGAGTCGTATACCGGGGCCTGAAGCTTGATAAGCCCCG
```


CATTATCGGATGTGCTGAAGGAATACACTACTATAGGTAATATAATAATAGATAAAAGCTTTTATGAG
 TACATCGCCAGATAAGGCATGGATAAATGACACTATTCTCAACATATACCTAGAAAAAGGACATAAA
 GGTAGAATACTCGGAGATGTTGCACATTTTAAGGGAGAGGCAGAGATGCTTTTCCCTCCAAAT
 ACTAAACTCAAAATCGAAAGCATTGTAAATTTGTGGATCCCAAGACTTTGCAAGCCAGCTTAG
 TAAGCTGAGATTAAGTGATGATGCAACTGCTGACACAAACAGGATAAAAAAGAATAATAAACATGAG
 GGTACTCAACTCA

REFERENCES

- Agnew, B.J., Minamide, L.S., and Bamburg, J.R. (1995). Reactivation of phosphorylated actin depolymerizing factor and identification of the regulatory site. *The Journal of biological chemistry* 270, 17582-17587.
- Aktories, K., Lang, A.E., Schwan, C., and Mannherz, H.G. (2011). Actin as target for modification by bacterial protein toxins. *The FEBS journal* 278, 4526-4543.
- Barnes, A.P., and Polleux, F. (2009). Establishment of axon-dendrite polarity in developing neurons. *Annual review of neuroscience* 32, 347-381.
- Bouchet, B.P., Gough, R.E., Ammon, Y.C., van de Willige, D., Post, H., Jacquemet, G., Altelaar, A.M., Heck, A.J., Goult, B.T., and Akhmanova, A. (2016). Talin-KANK1 interaction controls the recruitment of cortical microtubule stabilizing complexes to focal adhesions. *eLife* 5.
- Brenner, S. (1974). The genetics of *Caenorhabditis elegans*. *Genetics* 77, 71-94.
- Brummelkamp, T.R., Bernards, R., and Agami, R. (2002). A system for stable expression of short interfering RNAs in mammalian cells. *Science* 296, 550-553.
- Chia, P.H., Chen, B., Li, P., Rosen, M.K., and Shen, K. (2014). Local F-actin network links synapse formation and axon branching. *Cell* 156, 208-220.
- Chia, P.H., Patel, M.R., and Shen, K. (2012). NAB-1 instructs synapse assembly by linking adhesion molecules and F-actin to active zone proteins. *Nature neuroscience* 15, 234-242.
- Dugas, J.C., Tai, Y.C., Speed, T.P., Ngai, J., and Barres, B.A. (2006). Functional genomic analysis of oligodendrocyte differentiation. *The Journal of neuroscience : the official journal of the Society for Neuroscience* 26, 10967-10983.
- Finidori, J., Friederich, E., Kwiatkowski, D.J., and Louvard, D. (1992). In vivo analysis of functional domains from villin and gelsolin. *The Journal of cell biology* 116, 1145-1155.
- Frokaer-Jensen, C., Davis, M.W., Hopkins, C.E., Newman, B.J., Thummel, J.M., Olesen, S.P., Grunnet, M., and Jorgensen, E.M. (2008). Single-copy insertion of transgenes in *Caenorhabditis elegans*. *Nature genetics* 40, 1375-1383.
- Goslin, K., and Banker, G. (1989). Experimental observations on the development of polarity by hippocampal neurons in culture. *The Journal of cell biology* 108, 1507-1516.
- Gow, A., Friedrich, V.L., Jr., and Lazzarini, R.A. (1992). Myelin basic protein gene contains separate enhancers for oligodendrocyte and Schwann cell expression. *The Journal of cell biology* 119, 605-616.
- Hochmann, H., Pust, S., von Figura, G., Aktories, K., and Barth, H. (2006). *Salmonella enterica* SpvB ADP-ribosylates actin at position arginine-177-characterization of the catalytic domain within the SpvB protein and a comparison to binary clostridial actin-ADP-ribosylating toxins. *Biochemistry* 45, 1271-1277.
- Iwamoto, M., Bjorklund, T., Lundberg, C., Kirik, D., and Wandless, T.J. (2010). A general chemical method to regulate protein stability in the mammalian central nervous system. *Chemistry & biology* 17, 981-988.
- Kapitein, L.C., Schlager, M.A., van der Zwan, W.A., Wulf, P.S., Keijzer, N., and Hoogenraad, C.C. (2010a). Probing intracellular motor protein activity using an inducible cargo trafficking assay. *Biophysical journal* 99, 2143-2152.
- Kapitein, L.C., van Bergeijk, P., Lipka, J., Keijzer, N., Wulf, P.S., Katrukha, E.A., Akhmanova, A., and Hoogenraad, C.C. (2013). Myosin-V opposes microtubule-based cargo transport and drives directional motility on cortical actin. *Current biology : CB* 23, 828-834.
- Kapitein, L.C., Yau, K.W., and Hoogenraad, C.C. (2010b). Microtubule dynamics in dendritic spines. *Methods in cell biology* 97, 111-132.
- Kudryashov, D.S., Durer, Z.A., Ytterberg, A.J., Sawaya, M.R., Pashkov, I., Prochazkova, K., Yeates, T.O., Loo, R.R., Loo, J.A., Satchell, K.J., et al. (2008). Connecting actin monomers by iso-peptide bond is a toxicity mechanism of the *Vibrio cholerae* MARTX

- toxin. Proceedings of the National Academy of Sciences of the United States of America 105, 18537-18542.
- Lang, A.E., Schmidt, G., Schlosser, A., Hey, T.D., Larrinua, I.M., Sheets, J.J., Mannherz, H.G., and Aktories, K. (2010). Photorhabdus luminescens toxins ADP-ribosylate actin and RhoA to force actin clustering. Science 327, 1139-1142.
- Li, X., Romero, P., Rani, M., Dunker, A.K., and Obradovic, Z. (1999). Predicting Protein Disorder for N-, C-, and Internal Regions. Genome informatics Workshop on Genome Informatics 10, 30-40.
- Lilic, M., Galkin, V.E., Orlova, A., VanLoock, M.S., Egelman, E.H., and Stebbins, C.E. (2003). Salmonella SipA polymerizes actin by stapling filaments with nonglobular protein arms. Science 301, 1918-1921.
- MacLean-Fletcher, S., and Pollard, T.D. (1980). Mechanism of action of cytochalasin B on actin. Cell 20, 329-341.
- Maniar, T.A., Kaplan, M., Wang, G.J., Shen, K., Wei, L., Shaw, J.E., Koushika, S.P., and Bargmann, C.I. (2011). UNC-33 (CRMP) and ankyrin organize microtubules and localize kinesin to polarize axon-dendrite sorting. Nature neuroscience 15, 48-56.
- Margarit, S.M., Davidson, W., Frego, L., and Stebbins, C.E. (2006). A steric antagonism of actin polymerization by a salmonella virulence protein. Structure 14, 1219-1229.
- McLaughlin, P.J., Gooch, J.T., Mannherz, H.G., and Weeds, A.G. (1993). Structure of gelsolin segment 1-actin complex and the mechanism of filament severing. Nature 364, 685-692.
- Redemann, S., Schloissnig, S., Ernst, S., Pozniakowsky, A., Ayloo, S., Hyman, A.A., and Bringmann, H. (2011). Codon adaptation-based control of protein expression in *C. elegans*. Nature methods 8, 250-252.
- Schatzle, P., Ster, J., Verbich, D., McKinney, R.A., Gerber, U., Sonderegger, P., and Mateos, J.M. (2011). Rapid and reversible formation of spine head filopodia in response to muscarinic receptor activation in CA1 pyramidal cells. The Journal of physiology 589, 4353-4364.
- Schleberger, C., Hochmann, H., Barth, H., Aktories, K., and Schulz, G.E. (2006). Structure and action of the binary C2 toxin from Clostridium botulinum. Journal of molecular biology 364, 705-715.
- Sheahan, K.L., Cordero, C.L., and Satchell, K.J. (2004). Identification of a domain within the multifunctional *Vibrio cholerae* RTX toxin that covalently cross-links actin. Proceedings of the National Academy of Sciences of the United States of America 101, 9798-9803.
- Spector, I., Shochet, N.R., Kashman, Y., and Groweiss, A. (1983). Latrunculins: novel marine toxins that disrupt microfilament organization in cultured cells. Science 219, 493-495.
- Tezcan-Merdol, D., Nyman, T., Lindberg, U., Haag, F., Koch-Nolte, F., and Rhen, M. (2001). Actin is ADP-ribosylated by the *Salmonella enterica* virulence-associated protein SpvB. Molecular microbiology 39, 606-619.
- van der Vaart, B., van Riel, W.E., Doodhi, H., Kevenaar, J.T., Katrukha, E.A., Gumy, L., Bouchet, B.P., Grigoriev, I., Spangler, S.A., Yu, K.L., et al. (2013). CFEOM1-associated kinesin KIF21A is a cortical microtubule growth inhibitor. Developmental cell 27, 145-160.
- Vandekerckhove, J., Schering, B., Barmann, M., and Aktories, K. (1988). Botulinum C2 toxin ADP-ribosylates cytoplasmic beta/gamma-actin in arginine 177. The Journal of biological chemistry 263, 696-700.
- Vierbuchen, T., Ostermeier, A., Pang, Z.P., Kokubu, Y., Sudhof, T.C., and Wernig, M. (2010). Direct conversion of fibroblasts to functional neurons by defined factors. Nature 463, 1035-1041.
- Vitriol, E.A., and Zheng, J.Q. (2012). Growth cone travel in space and time: the cellular ensemble of cytoskeleton, adhesion, and membrane. Neuron 73, 1068-1081.
- Way, M., Pope, B., Gooch, J., Hawkins, M., and Weeds, A.G. (1990). Identification of a region in segment 1 of gelsolin critical for actin binding. The EMBO journal 9, 4103-4109.
- Way, M., Pope, B., and Weeds, A.G. (1992). Are the conserved sequences in segment 1 of gelsolin important for binding actin? The Journal of cell biology 116, 1135-1143.
- Wu, Y.I., Frey, D., Lungu, O.I., Jaehrig, A., Schlichting, I., Kuhlman, B., and Hahn, K.M. (2009). A genetically encoded photoactivatable Rac controls the motility of living cells. Nature 461, 104-108.
- Zuchero, J.B., Fu, M.M., Sloan, S.A., Ibrahim, A., Olson, A., Zaremba, A., Dugas, J.C., Wienbar, S., Capriariello, A.V., Kantor, C., et al. (2015). CNS myelin wrapping is driven by actin disassembly. Developmental cell 34, 152-167.

General Discussion

Marta Esteves da Silva

Cell Biology, Faculty of Science, Utrecht University, Utrecht, The Netherlands

In this thesis, several aspects of synaptic cargo transport have been described. To allow for proper synaptic organization and function, synaptic molecules need to be correctly sorted in a precise and regulated fashion. However, how synaptic cargo is targeted to precise locations is incompletely understood. The work described in this thesis aimed at understanding how synaptic cargo is correctly delivered to the synapse by the actin and the microtubule cytoskeleton. In **Chapters 2 and 3** we explored dendritic sorting and the fine-tuning in transport of postsynaptic cargo to dendritic spines. In **Chapter 4** we focused on different regulation mechanisms for the dendritic kinesin KIF17 and their functional consequences. In **Chapter 5** we turned to axonal and presynaptic cargo trafficking by investigating the role of a novel family of actin nucleators in the delivery of cargo to the presynapse. Finally, in **Chapter 6** we characterized novel tools to manipulate the actin cytoskeleton. These will be useful in the future to unravel new aspects of actin structure and function not only in neuronal cells, but in many other biological systems.

NOVEL INSIGHTS ON THE INTRACELLULAR TRAFFICKING OF POSTSYNAPTIC RECEPTORS

As major components of the excitatory postsynapse, AMPA receptors play an essential role in fast excitatory signaling, in basal conditions and during synaptic plasticity (Huganir and Nicoll, 2013). AMPA receptors frequently alternate from synaptic and extra-synaptic locations (Ashby *et al.*, 2006; Heine *et al.*, 2008; Sharma *et al.*, 2006), and their delivery to the postsynaptic membrane must be tightly regulated. This process occurs through lateral diffusion or intracellular trafficking via the endosomal pathway (reviewed in (Newpher and Ehlers, 2008). Previous work has shown that AMPA receptors are transported on endosomes (Ehlers, 2000; Lee *et al.*, 2004) and that specifically recycling endosomes provide a pool of AMPA receptors to the postsynapse upon LTP (Park *et al.*, 2004). The transport of these AMPA receptor-containing endosomes and how their presence or absence from spines affects the postsynapse has not been addressed. In Chapter 2 we explored in detail the intracellular transport of AMPA receptors via recycling endosomes to and from excitatory synapses located in dendritic spines of hippocampal neurons. We observed that AMPA receptor-containing recycling endosomes are highly dynamic structures, able to move over long distances along dendrites and targeting multiple spines. Recycling endosomes are transported along the dendritic shaft exclusively by microtubules, whereas both the microtubule and the actin cytoskeleton are involved in targeting these vesicles to spines.

To collect further information about the motor-based transport of cargo to dendritic spines we used a chemically-induced recruitment assay (FRB-FKBP system) (Kapitein *et al.*, 2010b) to specifically recruit microtubule or actin motors to recycling endosomes. With this assay we were able to recruit recycling endosomes to the postsynapse in and out of the postsynapse. Our data show that specific microtubule- and actin-based motors work in different directions to insert or remove cargo from the postsynapse. Induced removal of AMPA-receptor containing recycling endosomes decreases the number of AMPA receptors along the surface

of the postsynapse and PSD95 levels at the postsynapse (Figure 1). These results indicate that the correct positioning of endosomes determines the maintenance and turnover of important synaptic components that ultimately may affect synaptic function and organization.

The work described in Chapter 2 focuses in recycling endosomes as simplified carriers of synaptic cargo. However, if one considers the different functions already ascribed to these vesicles, it is possible that their presence and dynamics at the synapse provide additional levels of regulation of cargo transport and delivery. For instance, the endocytic pathway is strongly entangled with signaling mechanisms, which are important for compartmentalization of the endocytic membrane (Miaczynska *et al.*, 2004; Sadowski *et al.*, 2009). Precise spatial and temporal targeting of endosomes to the synapse can contribute to the correct propagation or abrogation of signaling events crucial for proper synaptic function in basal conditions or upon synaptic plasticity.

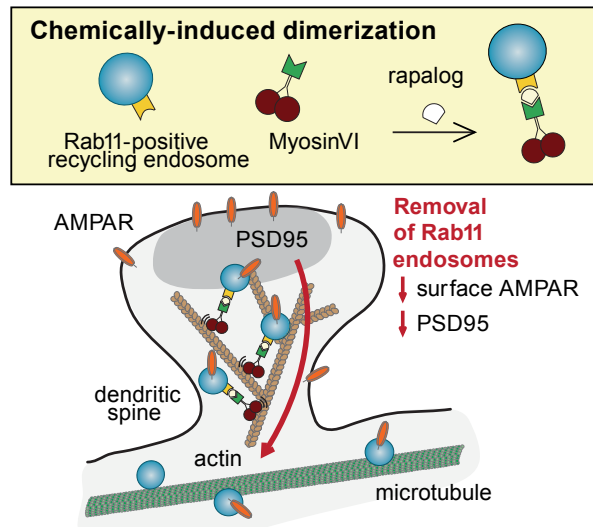


Figure 1. Positioning of AMPA-receptor containing endosomes regulates synapse architecture

AMPA receptors are targeted to the postsynapse either by lateral diffusion or intracellular transport. In Chapter 2 we report the transport of AMPA receptors inside recycling endosomes in dendrites and spines and the involvement of microtubule and actin in these trafficking process. Application of the FRB-FKBP induced-dimerization system allows for temporal control of endosomal trafficking in dendritic spines. Recycling endosomes can be inserted in spines by coupling to Myosin V and removed from spines by Myosin VI. Using this approach we observed that induced removal of AMPAR-containing endosomes by Myosin VI decreases surface AMPA receptor expression and PSD-95 clusters at the postsynapse, suggesting that endosome positioning is an important factor in controlling synapse architecture (adapted from Esteves da Silva *et al.*, 2015).

REGULATORY MECHANISMS OF SPINE MICROTUBULE INVASIONS

In hippocampal neurons, most excitatory synapses are located on dendritic spines. Even though spine heads are enriched in actin, previous work has revealed that microtubules can enter

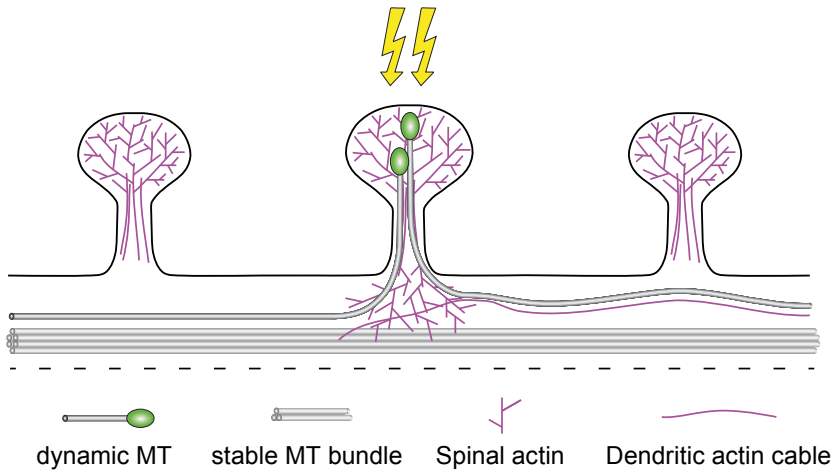


Figure 2. Model illustrating potential mechanisms of microtubule entries in spines

The work described in Chapter 3 shows that dynamic microtubules entering dendritic spines can interact with bundles of stable microtubule and/or dendritic actin cables. Synaptic stimulation enhances actin structures at the base of the spine, thereby connecting to stable microtubules and/or actin cables and leading to increased chances of microtubule targeting to spines.

dendritic spines in basal conditions or after cLTP, resulting in spine enlargement and increase in PSD95 content (Hu *et al.*, 2008; Jaworski *et al.*, 2009; Merriam *et al.*, 2011). Nevertheless, the regulation of microtubule entry into spines still remains to be elucidated. In Chapter 3 we performed high-resolution live-cell imaging in dissociated neuronal cultures and in slice cultures to elucidate the mechanisms underlying microtubule targeting to spines.

We first observed that microtubules enter spines in different stages of neuronal development. Interestingly, and opposite to other studies (Merriam *et al.*, 2013) we observed microtubules travelling long distances (up to 50 μm) before entering a spine. Moreover, we found that a large fraction of microtubule catastrophes occurs inside spines, which could be an indication that microtubule translocation to spines is a mechanism for stopping dendritic microtubule growth. By applying cLTP protocols we found preferential targeting of microtubules to spines that underwent calcium-influx mediated by NMDA receptor activation. As these protocols also cause alterations in spine actin dynamics, we manipulated actin dynamics and observed that microtubule entries in spines are increased when actin is stabilized but decreased upon destabilization of the actin cytoskeleton. Even though these results show that actin dynamics is essential for microtubule entry to spines, additional experiments showed that this is not due to protein-protein interactions at the microtubule growing tip, suggesting that microtubules are steered into spines through mechanical or sterical action of actin. Indeed, we observed that structural remodeling of actin dynamics at the base of the spines directly affects microtubule targeting after synaptic activation (Figure 2). Additionally, cortactin knockdown decreases microtubule entry in spines and decreases actin dynamics at the spine base after

stimulation, which is in agreement with previous work that shows activity-dependent cortactin redistribution (Hering and Sheng, 2003; Iki *et al.*, 2005; Seese *et al.*, 2012). Our work indicates that microtubule entry in spines is activity-regulated and dependent on actin reorganization inside and at the base of dendritic spines (Figure 2). Previous studies showed that microtubule-based motors can deliver cargo to the postsynapse (Esteves da Silva *et al.*, 2015; McVicker *et al.*, 2016). Nevertheless, the importance of this transport route is not elucidated yet, as microtubule invasions of spines is not a frequent event, and actin-based transport can also deliver or remove cargo from the postsynapse. Future work should clarify the role of microtubule inside dendritic spines in basal or activity-induced conditions.

REGULATION OF MICROTUBULE MOTOR-BASED TRANSPORT: LESSONS FROM KIF17

Over the last decades several studies highlighted the sorting of cargo on neuronal cells. Neurons are compartmentalized in axons and dendrites with defined organization of the cytoskeleton and cytoskeletal motor proteins transport cargo in specific directions. The nature of the motor itself is of major importance. KIF17, a member of the kinesin-2 family, is a dendrite-specific motor protein. Previous studies have shown that KIF17 mediates the transport of NMDA and kainate receptor subunits (Guillaud *et al.*, 2003; Kayadjanian *et al.*, 2007; Setou *et al.*, 2000). Overexpression of KIF17 causes upregulation of the NMDA receptor subunit NR2B and enhances memory and learning in mice (Wong *et al.*, 2002). The KIF17 knockout mice show a reduced number of synaptic NMDA receptors and impaired neuronal plasticity and spatial memory (Yin *et al.*, 2012; Yin *et al.*, 2011). However, it remains unclear why this kinesin is specifically targeted to the dendrites. The study of individual motor protein function and regulation in cells is challenging, as many different motors may attach to endogenous cargo and be redundant in their transport. To tackle this, in Chapter 4 we made use of the FRB-FKBP recruitment assay to understand the motor behavior of KIF17 in living neurons. This way, we largely surpassed possible interference by other motor proteins. Furthermore, we were able to manipulate the system to study either the full-length KIF17, or truncated and mutated forms of this kinesin. The work described in Chapter 4 shows that KIF17 targeting to dendrites is regulated in three distinct steps, requiring other cytoskeletal components and motor proteins. Firstly, the tail domain inhibits the motor activity of full length KIF17 (KIF17-FL), which can be relieved by recruitment of cargo to the motor protein. Interestingly, upon activation of KIF17, transport preferentially targeted the axon and not dendrites. Secondly, KIF17-MD transported cargo along the axons, whereas cargo coupled to KIF17-FL are anchored at the AIS. Further experiments showed that this anchoring was dependent on the dynamic actin cytoskeleton present in the AIS and the tail domain region of KIF17. Auto-inhibition of the motor protein by the tail domain is not important here, as KIF17-G754E, a mutated form that does not allow auto-inhibition, still anchors at the AIS.

As KIF17 exhibits axon-targeting behavior but is stalled in the AIS, how is cargo transported by KIF17 ultimately targeted to dendrites? It has been previously shown that

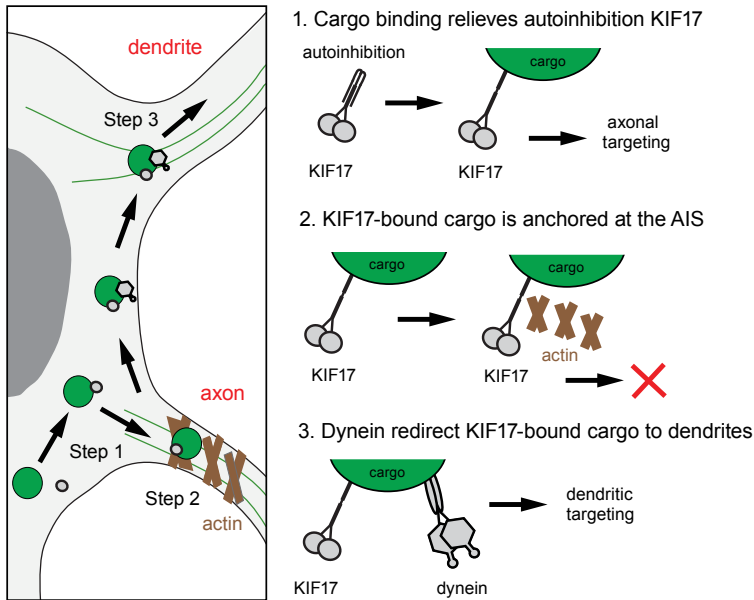


Figure 3. Three-step model for polarized sorting of KIF17 into dendrites

In neurons, the kinesin-2 family protein KIF17 is a dendrite-specific motor protein and interacts with several dendritic cargos. In Chapter 4, we explored the regulation of polarized sorting of this kinesin. Using the FRB-FKBP dimerization system we observed that 1) Binding of KIF17 to cargo relieves auto-inhibition by its tail domain in living cells; 2) KIF17-bound cargo does not target dendrites autonomously. Instead KIF17-bound cargo enter the axon and is anchored in the AIS; 3) KIF17-bound cargo is redirected to dendrites by dynein (adapted from Franker et al, 2016).

dynein selectively distributes cargo to dendrites via recruitment of the dynein adaptor BICD2 (Hoogenraad *et al.*, 2003; Kapitein *et al.*, 2010a), so we hypothesized that recruitment of BICD2 would remove KIF17-bound cargo from the AIS to dendrites. Using the chemically-induced assay, we simultaneously recruited both motor proteins to cargo and observed an increase in dendrite targeting, a rare event in the absence of BICD2. Thus, the third mechanism of KIF17 cargo transport to dendrites requires the involvement of the minus-end directed motor protein, dynein (Figure 3). The work described in Chapter 4 highlights a previously undocumented mechanism where KIF17 and dynein cooperate in sorting cargo to dendrites by preventing the entry of dendritic cargo in the AIS by KIF17 followed by transport of KIF17-bound cargo to dendrites via interaction with dynein. Using the chemically-induced dimerization assay, targeting of NMDA receptors or other known KIF17 cargo to the dendrites should be explored in the future, to understand the importance of KIF17-based transport in response to synaptic activity. It would be interesting to understand if and where KIF17 actively transports cargo in dendrites. This could be achieved by local and reversible instantaneous coupling of KIF17 to cargo. Such is possible due to recently developed techniques that allow for recruitment of motors to cargo by light (van Bergeijk *et al.*, 2015). Using this system, KIF17 could be coupled to cargo along the dendrite, to understand if motor function is preferentially activated either

proximally or distally, and if such transport contributes to targeting of NMDA receptors to the postsynapse and influences synaptic plasticity.

SPIRE PROTEINS: A NEW MODEL FOR ACTIN-BASED DELIVERY OF CARGO TO THE PRESYNAPSE

The actin cytoskeleton is remarkably enriched at the presynapse, and its dynamics are instrumental for synaptic function (Sankaranarayanan *et al.*, 2003). However, the precise role for actin at the presynapse is still debated. It was suggested that it has a role in recruitment and clustering of synaptic vesicles or in the transport of vesicles via actin-motor proteins (Cingolani and Goda, 2008; Dillon and Goda, 2005; Rust and Maritzen, 2015; Wolf *et al.*, 2015). With the development of new tools and techniques, novel actin structures were identified along the axon (Ganguly *et al.*, 2015; Xu *et al.*, 2013). It is now important to understand the role of such structures, particularly in trafficking of presynaptic cargo or in structural organization of the presynapse. Recent work described the involvement of Spire proteins in long-range, actin-dependent transport of cargo in cells (Schuh, 2011). The study demonstrates that in oocytes Spire proteins and Formin-2 bind to vesicle membranes to generate and polymerize actin filaments that are used as tracks by Myosin V to transport cargo along the cell. In this manner, a network of newly-polymerized actin filaments is generated locally from the vesicle membranes allowing the transport of such vesicles to the periphery along the actin cytoskeleton. In Chapter 5 we described for the first time how Spire proteins are distributed in primary hippocampal neurons and their involvement on the delivery of cargo to the presynapse.

In primary hippocampal neurons, overexpressed Spire appears as clear clusters, enriched in actin and distributed along the axon. Previous work showed that Spire nucleates actin but is also able to bind to the plasma membrane or other vesicular membranes, through the SpireBox-FYVE C-terminal domains (Kerkhoff *et al.*, 2001), where it is able to generate new actin filaments (Schuh, 2011). Our work shows that Spire overexpression causes accumulation of Rab11-positive endosomes in axonal Spire clusters. Using different truncated versions of Spire we identified that the C-terminal domains WH2-SB-FYVE are critical for redistributing actin of Rab11-positive endosomes, while the KIND domain, where Formins are known to bind (Pechlivanis *et al.*, 2009) does not play a role in this process. As the interaction between Spire and Rab GTPases is not completely elucidated, we performed a GST pull-down assay using a library of GST-Rabs and found no clear binding between Spire proteins to Rab11. However, other Rab proteins were immunoprecipitated with Spire. This could either be an indication of an indirect interaction between Rab11 and Spire proteins or that Spire proteins might in fact bind to other Rab proteins in the membrane of vesicles. Interestingly, we observed that Rab3, known to be present in the membrane of precursors of synaptic vesicles (Fischer von Mollard *et al.*, 1991), interacts with Spire1. Live-cell imaging experiments of Rab11-positive endosomes and NPY-positive vesicles upon Spire depletion shows that the transport of Rab11-cargo along the axon is not affected compared with controls. As most of the transport along the axonal shaft is microtubule-based it is possible that Spire clusters would have a minimal participation in

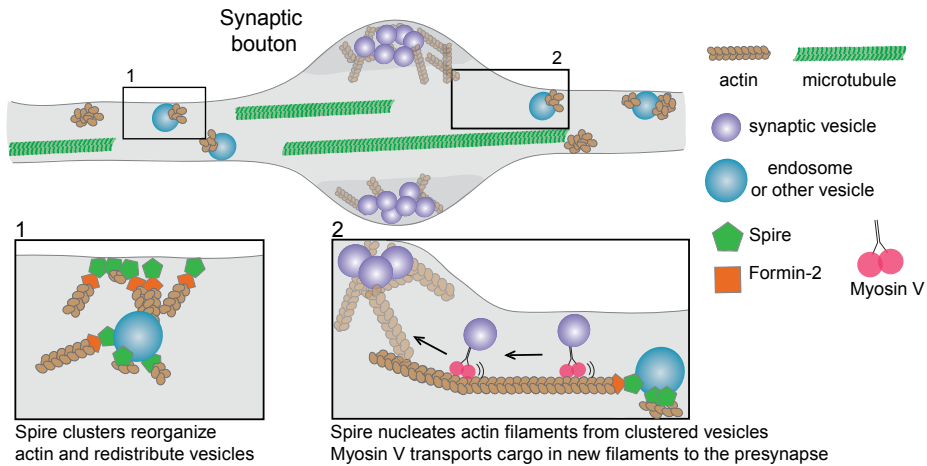


Figure 4. Model illustrating the role of Spire proteins in actin reorganization and delivery of cargo to the presynapse

Different actin structures have been identified in the axon. The results described in Chapter 5 demonstrate that: 1) Spire expression creates clusters in the axon that cause actin reorganization and vesicle redistribution; upon Spire depletion, there is impairment of the transport of Rab3-vesicles, decreased number of synaptic boutons and synaptic components. The same is observed with Myosin V tail. From these preliminary results we proposed a model where 2) Spire proteins are recruited to vesicles, generating and elongating new actin filaments (probably with the involvement of Formin-2), that are used by Myosin V to deliver cargo to the presynapse.

the transport of these vesicles. After Spire depletion there are fewer Rab3-positive vesicles but the mobile ones move faster, which indicates that Spire proteins are possibly involved in the motility or anchoring of these vesicles along the axon. As Rab3-positive vesicles transport cargo to the presynapse we hypothesized whether Spire clusters would be involved in this process. Our current data shows that even though Spire does not colocalize with presynaptic boutons, depletion of Spire causes a decrease on presynapse number along the axons and also a decrease in the number of Bassoon-positive presynaptic boutons, which suggests that Spire has a role in delivering presynaptic cargo to the presynapse. Keeping in mind that more work needs to be done, our current hypothetical model places Spire clusters close to the presynapse as a starting point for the delivery of cargo to the presynapse.

Previous work described actin hotspots along the axon, from where actin trails are polymerized. Even though it has been shown that actin trail formation is dependent on Formin, generation of actin hotspots is Formin-independent (Ganguly *et al.*, 2015). Interestingly, we observed that upon Spire depletion there are less actin clusters along the axons and the ones remaining are more elongated. This could be an indication that the clusters formed by Spire correspond to actin hotspots and that their generation is Spire-dependent, which should be further validated. We also confirmed the previously described interaction of Spire1 to Myosin V (Pylypenko *et al.*, 2016; Schuh, 2011). Additionally, expression of Myosin V dominant negative

phenocopied Spire overexpression, with the formation of large clusters along the axons and a decrease in the Bassoon-positive puncta. It is possible that Bassoon clusters are transported by actin based-motors in actin filaments that protrude from the actin clusters. If so, these data indicate that Myosin V plays a role in the delivery of cargo from Spire clusters. Another possibility is that Spire clusters are important for the delivery of other presynaptic cargo and that failure in this transport affects presynaptic organization, thus resulting in the altered distribution of Bassoon puncta and ultimately in the organization of the presynapse. Our efforts are now focused in understanding how the actin clusters relate to transport of presynaptic cargo. To do so, we propose to study the dynamics of these actin clusters and their relation with Spire proteins by imaging actin dynamics in living neurons. We propose a model where Spire proteins are nucleators of actin along the axon, generating actin hotspots from where actin trails can be polymerized in a Formin-2-dependent manner. In this model, Myosin V transports presynaptic cargo to the presynapse, thereby creating a slow, tunable mechanism to deliver cargo to the presynapse (Figure 4). If verified, the work described on Chapter 5 suggests a new mechanism of delivering cargo to the presynapse that relies on actin structures in the axon.

DEVELOPMENT AND CHARACTERIZATION OF NEW TOOLS TO STUDY ACTIN

Intracellular transport of cargo relies heavily on the cytoskeletal tracks and so it is important to understand the building and organization of the cytoskeleton inside cells. As described in Chapter 1, actin has several important functions in cell types and is particularly important in neurons. In recent years, new tools have been developed to image and label and the development of super-resolution microscopy allowed for visualization of actin with increased quality and resolution. For example, the development of Lifeact and Utr-CH, small domains of ABPs able to bind to F-actin with minimal disturbance to actin structure and dynamics, allowed for fine imaging of actin filaments in living cells (Burkel *et al.*, 2007; Riedl *et al.*, 2008). Another example is Silicon-rhodamine actin (SiR-actin), a recently developed fluorogenic probe for labelling endogenous actin with minimal influence on actin polymerization or cytotoxicity, which allows the visualization of actin structures with great resolution in living cells (D'Este *et al.*, 2015; Lukinavicius *et al.*, 2014). Nevertheless, disturbing the actin cytoskeleton to study either the structure itself or the consequences arising from perturbation is still rather limiting, as it relies on the application of drugs or toxins that affect either F- or G-actin (reviewed in Dillon and Goda, 2005). While several findings in the field have resulted from the application of these tools, serious methodological limitations arise from their use. For instance, these toxins are not applicable in all model systems, as it hinders single-cell or cell-type specific perturbations, which is particularly important in multicellular systems or even whole organisms.

In Chapter 6 we described two novel genetically encoded tools to manipulate the actin cytoskeleton. The starting point was a screen where different actin-binding domains from endogenous proteins and bacterial toxins known to change the actin cytoskeleton were transfected in cells. This highlighted two peptides that cause actin destabilization by acting

differently on its structure: GS1, which is an actin-sequestering domain of Gelsolin (McLaughlin *et al.*, 1993; Way *et al.*, 1990) and SpvB, a bacterial toxin that ADP-ribosylates actin monomers inhibiting their polymerization into actin filaments (Margarit *et al.*, 2006). Overexpression of GFP-tagged DeActs (DeAct-GS1 and DeAct-SpvB) caused major disruption of actin filaments in expressing cells resulting in severe morphological defects. Further characterization of GS1 and SpvB as actin-destabilizing tools showed that motility in these cells is severely affected and that actin-rich and actin-dependent cellular structures, such as filopodia and focal adhesions were strongly impaired. One of the great advantages of DeActs is the possibility to be used in different experimental model systems. In primary hippocampal cultures expression of DeActs caused a severe reduction in the levels of endogenous actin and impaired growth cone dynamics. We further validated the successful application of DeActs *in vivo*, by targeting the neocortex of mouse developing embryos using an *in utero* strategy and looking at neurons of live *C. elegans*. We observed that DeAct expression affects the migration of newly-differentiated neurons along the cortical plate, and impaired dendritic branching in the worm PVD neuron.

The work in Chapter 6 demonstrates that DeActs are simple and reliable tools for perturbing the actin cytoskeleton in single cells, or in specific cell-types. Furthermore, its expression can be controlled by inducible promoters and applied to many different model systems. We are optimistic that these tools will have widespread use in different applications allowing for detailed understanding of actin related processes in a wide range of model organisms and cell types. In the context of this thesis, DeActs could be used in future experiments using aimed at better understanding the role of actin dynamics either in synapse structure and organization or in the actin-dependent delivery of cargo to synapse. In addition, expressing DeActs in primary hippocampal neurons would permit the study of the stability and dynamics of actin clusters and actin trails in individual axons without disturbing the entire culture system. Using the inducible promoters, one could have temporal control of the destabilization of the actin cytoskeleton. This would provide further information on the role of actin clusters in the formation and/or maintenance of the neighboring presynapse, and the involvement of Spire proteins in these events.

CONCLUDING REMARKS

A great body of work has contributed to what is currently known about the function of neuronal cytoskeleton. Nevertheless, there is still much to elucidate. The cytoskeletal involvement on the recruitment and delivery of synaptic components has been a particularly challenging endeavor to tackle, as there are several layers of regulation involved. Intracellular transport to synapses involves the complex interplay of microtubules and the actin cytoskeleton. Microtubules are important for sorting of synaptic cargo from the soma to dendrites or axon and long-range transport along the neurites, whereas actin is important for the recruitment and anchoring of cargo at the synapse. Even though this view is not completely incorrect, it is presumably incomplete. The actin and the microtubule cytoskeleton are extensively interconnected, and different mechanisms are in place to regulate the affinity of motors to the cytoskeletal

tracks. Motor proteins are differentially regulated, as we further understand mechanisms of activation or inhibition by the motor itself or by adaptor proteins. The nature of the cargo to be transported is also fundamental in determining its final destination, as interactions between cargo, motors and the cytoskeleton are in place. Different aspects of synaptic cargo transport by the cytoskeleton have been described in this thesis and collectively provide a better insight into the transport of synaptic cargo by the neuronal cytoskeleton.

Why is it important to elucidate the mechanisms of intracellular synaptic cargo transport? Synaptic function is fundamental for proper information processing in the brain. As we advance our understanding on neuropathologic mechanisms, it becomes evident that synaptic dysfunction is a hallmark of different neurological disorders. Moreover, different aspects of synaptic cargo transport are affected in some of these disorders (Kevenaar *et al.*, 2016; Millecamps and Julien, 2013; van Spronsen *et al.*, 2013). Understanding how the cytoskeleton, adaptors, regulatory proteins and the synaptic cargo itself come together for proper recruitment and delivery of components to the pre- and postsynapse is urgent and crucial to increase our understanding of synaptic function in health and disease. We are witnessing an exciting period in neuroscience, with the development of innovative techniques and the involvement of other scientific disciplines. Hopefully, it will result in the development of novel approaches and significantly increase our understanding of synapse assembly, maintenance and function, and ultimately contribute to develop strategies and therapies to tackle neurological disorders.

REFERENCES

- Ashby, M.C., Maier, S.R., Nishimune, A., and Henley, J.M. (2006). Lateral diffusion drives constitutive exchange of AMPA receptors at dendritic spines and is regulated by spine morphology. *The Journal of neuroscience : the official journal of the Society for Neuroscience* 26, 7046-7055.
- Burkel, B.M., von Dassow, G., and Bement, W.M. (2007). Versatile fluorescent probes for actin filaments based on the actin-binding domain of utrophin. *Cell motility and the cytoskeleton* 64, 822-832.
- Cingolani, L.A., and Goda, Y. (2008). Actin in action: the interplay between the actin cytoskeleton and synaptic efficacy. *Nature reviews Neuroscience* 9, 344-356.
- D'Este, E., Kamin, D., Gottfert, F., El-Hady, A., and Hell, S.W. (2015). STED nanoscopy reveals the ubiquity of subcortical cytoskeleton periodicity in living neurons. *Cell reports* 10, 1246-1251.
- Dillon, C., and Goda, Y. (2005). The actin cytoskeleton: integrating form and function at the synapse. *Annual review of neuroscience* 28, 25-55.
- Ehlers, M.D. (2000). Reinsertion or degradation of AMPA receptors determined by activity-dependent endocytic sorting. *Neuron* 28, 511-525.
- Esteves da Silva, M., Adrian, M., Schatzle, P., Lipka, J., Watanabe, T., Cho, S., Futai, K., Wierenga, C.J., Kapitein, L.C., and Hoogenraad, C.C. (2015). Positioning of AMPA Receptor-Containing Endosomes Regulates Synapse Architecture. *Cell reports* 13, 933-943.
- Fischer von Mollard, G., Sudhof, T.C., and Jahn, R. (1991). A small GTP-binding protein dissociates from synaptic vesicles during exocytosis. *Nature* 349, 79-81.
- Ganguly, A., Tang, Y., Wang, L., Ladt, K., Loi, J., Dargent, B., Leterrier, C., and Roy, S. (2015). A dynamic formin-dependent deep F-actin network in axons. *The Journal of cell biology* 210, 401-417.
- Guillaud, L., Setou, M., and Hirokawa, N. (2003). KIF17 dynamics and regulation of NR2B trafficking in hippocampal neurons. *The Journal of neuroscience : the official journal of the Society for Neuroscience* 23, 131-140.
- Heine, M., Groc, L., Frischknecht, R., Beique, J.C., Lounis, B., Rumbaugh, G., Huganir, R.L., Cognet,

- L., and Choquet, D. (2008). Surface mobility of postsynaptic AMPARs tunes synaptic transmission. *Science* 320, 201-205.
- Hering, H., and Sheng, M. (2003). Activity-dependent redistribution and essential role of cortactin in dendritic spine morphogenesis. *The Journal of neuroscience : the official journal of the Society for Neuroscience* 23, 11759-11769.
- Hoogenraad, C.C., Wulf, P., Schiefermeier, N., Stepanova, T., Galjart, N., Small, J.V., Grosveld, F., de Zeeuw, C.I., and Akhmanova, A. (2003). Bicaudal D induces selective dynein-mediated microtubule minus end-directed transport. *The EMBO journal* 22, 6004-6015.
- Huganir, R.L., and Nicoll, R.A. (2013). AMPARs and synaptic plasticity: the last 25 years. *Neuron* 80, 704-717.
- Iki, J., Inoue, A., Bito, H., and Okabe, S. (2005). Bi-directional regulation of postsynaptic cortactin distribution by BDNF and NMDA receptor activity. *The European journal of neuroscience* 22, 2985-2994.
- Kapitein, L.C., Schlager, M.A., Kuijpers, M., Wulf, P.S., van Spronsen, M., MacKintosh, F.C., and Hoogenraad, C.C. (2010a). Mixed microtubules steer dynein-driven cargo transport into dendrites. *Current biology : CB* 20, 290-299.
- Kapitein, L.C., Schlager, M.A., van der Zwan, W.A., Wulf, P.S., Keijzer, N., and Hoogenraad, C.C. (2010b). Probing intracellular motor protein activity using an inducible cargo trafficking assay. *Biophysical journal* 99, 2143-2152.
- Kayadjanian, N., Lee, H.S., Pina-Crespo, J., and Heinemann, S.F. (2007). Localization of glutamate receptors to distal dendrites depends on subunit composition and the kinesin motor protein KIF17. *Molecular and cellular neurosciences* 34, 219-230.
- Kerckhoff, E., Simpson, J.C., Leberfinger, C.B., Otto, I.M., Doerks, T., Bork, P., Rapp, U.R., Raabe, T., and Pepperkok, R. (2001). The Spir actin organizers are involved in vesicle transport processes. *Current biology : CB* 11, 1963-1968.
- Kevenaar, J.T., Bianchi, S., van Spronsen, M., Olieric, N., Lipka, J., Frias, C.P., Mikhaylova, M., Harterink, M., Keijzer, N., Wulf, P.S., et al. (2016). Kinesin-Binding Protein Controls Microtubule Dynamics and Cargo Trafficking by Regulating Kinesin Motor Activity. *Current biology : CB* 26, 849-861.
- Lee, S.H., Simonetta, A., and Sheng, M. (2004). Subunit rules governing the sorting of internalized AMPA receptors in hippocampal neurons. *Neuron* 43, 221-236.
- Lukinavicius, G., Reymond, L., D'Este, E., Masharina, A., Gottfert, F., Ta, H., Guther, A., Fournier, M., Rizzo, S., Waldmann, H., et al. (2014). Fluorogenic probes for live-cell imaging of the cytoskeleton. *Nature methods* 11, 731-733.
- Margarit, S.M., Davidson, W., Frego, L., and Stebbins, C.E. (2006). A steric antagonism of actin polymerization by a salmonella virulence protein. *Structure* 14, 1219-1229.
- McLaughlin, P.J., Gooch, J.T., Mannherz, H.G., and Weeds, A.G. (1993). Structure of gelsolin segment 1-actin complex and the mechanism of filament severing. *Nature* 364, 685-692.
- McVicker, D.P., Awe, A.M., Richters, K.E., Wilson, R.L., Cowdrey, D.A., Hu, X., Chapman, E.R., and Dent, E.W. (2016). Transport of a kinesin-cargo pair along microtubules into dendritic spines undergoing synaptic plasticity. *Nature communications* 7, 12741.
- Merriam, E.B., Millette, M., Lumbard, D.C., Saengsawang, W., Fothergill, T., Hu, X., Ferhat, L., and Dent, E.W. (2013). Synaptic regulation of microtubule dynamics in dendritic spines by calcium, F-actin, and drebrin. *The Journal of neuroscience : the official journal of the Society for Neuroscience* 33, 16471-16482.
- Miaczynska, M., Pelkmans, L., and Zerial, M. (2004). Not just a sink: endosomes in control of signal transduction. *Current opinion in cell biology* 16, 400-406.
- Millecamps, S., and Julien, J.P. (2013). Axonal transport deficits and neurodegenerative diseases. *Nature reviews Neuroscience* 14, 161-176.
- Newpher, T.M., and Ehlers, M.D. (2008). Glutamate receptor dynamics in dendritic microdomains. *Neuron* 58, 472-497.
- Park, M., Penick, E.C., Edwards, J.G., Kauer, J.A., and Ehlers, M.D. (2004). Recycling endosomes supply AMPA receptors for LTP. *Science* 305, 1972-1975.
- Pechlivanis, M., Samol, A., and Kerckhoff, E. (2009). Identification of a short Spir interaction sequence at the C-terminal end of formin subgroup proteins. *The Journal of biological chemistry* 284, 25324-25333.
- Pylypenko, O., Welz, T., Tittel, J., Kollmar, M., Chardon, F., Malherbe, G., Weiss, S., Michel, C.I., Samol-Wolf, A., Grasskamp, A.T., et al. (2016). Coordinated recruitment of Spir actin nucleators and myosin V motors to Rab11 vesicle membranes. *eLife* 5.
- Riedl, J., Crevenna, A.H., Kessenbrock, K., Yu, J.H.,

- Neukirchen, D., Bista, M., Bradke, F., Jenne, D., Holak, T.A., Werb, Z., et al. (2008). Lifeact: a versatile marker to visualize F-actin. *Nature methods* 5, 605-607.
- Rust, M.B., and Maritzen, T. (2015). Relevance of presynaptic actin dynamics for synapse function and mouse behavior. *Experimental cell research* 335, 165-171.
- Sadowski, L., Pilecka, I., and Miaczynska, M. (2009). Signaling from endosomes: location makes a difference. *Experimental cell research* 315, 1601-1609.
- Sankaranarayanan, S., Atluri, P.P., and Ryan, T.A. (2003). Actin has a molecular scaffolding, not propulsive, role in presynaptic function. *Nature neuroscience* 6, 127-135.
- Schuh, M. (2011). An actin-dependent mechanism for long-range vesicle transport. *Nature cell biology* 13, 1431-1436.
- Seese, R.R., Babayan, A.H., Katz, A.M., Cox, C.D., Lauterborn, J.C., Lynch, G., and Gall, C.M. (2012). LTP induction translocates cortactin at distant synapses in wild-type but not Fmr1 knock-out mice. *The Journal of neuroscience : the official journal of the Society for Neuroscience* 32, 7403-7413.
- Setou, M., Nakagawa, T., Seog, D.H., and Hirokawa, N. (2000). Kinesin superfamily motor protein KIF17 and mLin-10 in NMDA receptor-containing vesicle transport. *Science* 288, 1796-1802.
- Sharma, K., Fong, D.K., and Craig, A.M. (2006). Postsynaptic protein mobility in dendritic spines: long-term regulation by synaptic NMDA receptor activation. *Molecular and cellular neurosciences* 31, 702-712.
- van Bergeijk, P., Adrian, M., Hoogenraad, C.C., and Kapitein, L.C. (2015). Optogenetic control of organelle transport and positioning. *Nature* 518, 111-114.
- van Spronsen, M., Mikhaylova, M., Lipka, J., Schlager, M.A., van den Heuvel, D.J., Kuijpers, M., Wulf, P.S., Keijzer, N., Demmers, J., Kapitein, L.C., et al. (2013). TRAK/Milton motor-adaptor proteins steer mitochondrial trafficking to axons and dendrites. *Neuron* 77, 485-502.
- Way, M., Pope, B., Gooch, J., Hawkins, M., and Weeds, A.G. (1990). Identification of a region in segment 1 of gelsolin critical for actin binding. *The EMBO journal* 9, 4103-4109.
- Wolf, M., Zimmermann, A.M., Gorlich, A., Gurniak, C.B., Sassoe-Pognetto, M., Friauf, E., Witke, W., and Rust, M.B. (2015). ADF/Cofilin Controls Synaptic Actin Dynamics and Regulates Synaptic Vesicle Mobilization and Exocytosis. *Cereb Cortex* 25, 2863-2875.
- Wong, R.W., Setou, M., Teng, J., Takei, Y., and Hirokawa, N. (2002). Overexpression of motor protein KIF17 enhances spatial and working memory in transgenic mice. *Proceedings of the National Academy of Sciences of the United States of America* 99, 14500-14505.
- Xu, K., Zhong, G., and Zhuang, X. (2013). Actin, spectrin, and associated proteins form a periodic cytoskeletal structure in axons. *Science* 339, 452-456.
- Yin, X., Feng, X., Takei, Y., and Hirokawa, N. (2012). Regulation of NMDA receptor transport: a KIF17-cargo binding/releasing underlies synaptic plasticity and memory *in vivo*. *The Journal of neuroscience : the official journal of the Society for Neuroscience* 32, 5486-5499.
- Yin, X., Takei, Y., Kido, M.A., and Hirokawa, N. (2011). Molecular motor KIF17 is fundamental for memory and learning via differential support of synaptic NR2A/2B levels. *Neuron* 70, 310-325.



Addendum

Summary
Samenvatting
Sumário

Curriculum vitae
Publications

Acknowledgements



SUMMARY

The brain is a very complex organ, responsible for the most important tasks performed by humans and animals. What makes it so unique? It is organized in an extraordinary way that allows for external information to be received, decoded and resolved in a fast and accurate way. Out of all the types of cells that make up the brain, neurons are particularly special. Their particular shape, with dendrites and axons that extend over long distances, allows one neuron to communicate with a neighboring neuron or with neurons that are far apart.

Communication between neurons occurs through synapses. To ensure that communication is faithful between neurons, synapses must be correctly located and assembled. For that to happen, specific proteins and other molecules need to be delivered to the pre- and the post-synapses. Trafficking of cargo to synapses is a complex and highly regulated event, which is currently not completely understood. The cytoskeleton, made of microtubule and actin polymers, provides the roads for motor proteins to walk and deliver synaptic cargo to its final destination. How is the cytoskeleton organized along the neuron? What activates or inhibits motor proteins to transport cargo? Which cargo is targeted for transport and where is this determined? Even though these are not simple questions to be answered, with the use of different approaches and methodologies this thesis describes our effort in advancing the understanding of synaptic cargo trafficking in hippocampal neurons.

Chapters 2 and 3 focus on the postsynapse. In hippocampal neurons, most excitatory synapses are located in dendritic spines, which are small subcompartments that protrude from the dendrite on which the postsynapse is localized. At the surface of the postsynapse, the signal from the presynaptic axon is received by membrane receptors, such as AMPA receptors. In chapter 2 we describe the visualization of trafficking of AMPA receptors to dendritic spines inside recycling endosomes via the microtubule and the actin cytoskeleton. After coupling these vesicles to specific motor proteins it was possible to control the insertion or removal of AMPA receptors from the postsynapse with consequences to the organization and functionality of the postsynapse.

In chapter 3, our studies in the postsynapse focused on microtubule invasions of dendritic spines. Microtubules are typically located along the dendritic shaft and microtubule entries in spines are not a frequent and well understood event. These events were studied in great detail, as well as its functional implications in basal conditions or upon synaptic plasticity.

Motor proteins are fundamental for transport inside cells, including correct delivering of cargo to the synapse. In chapter 4, the regulation of the dendritic kinesin KIF17 was studied, and by coupling KIF17 to specific cargo we provided novel insights on how this motor protein is distinctly regulated by its own tail domain and by binding to cargo.

In chapter 5, the axonal actin cytoskeleton and its role in presynaptic cargo trafficking was explored. This chapter provides evidence that Spire proteins are distributed along the axonal shaft, where they contribute to the organization and maintenance of actin structures. Moreover, our preliminary results indicate that Spire proteins are important in the targeting of cargo to the presynapse.



Finally, chapter 6 describes the development and characterization of novel tools to manipulate the actin cytoskeleton. DeActs (Disassembly-promoting encodable Actin tools) were studied in different model systems, highlighting their robustness and wide applicability. It is my expectation that DeActs will be a widely used approach in different experiment setups and will help to further understand the role of actin dynamics in health and disease. Together, the results described in this thesis advance our knowledge on many aspects of synaptic cargo trafficking and I am hopeful they will open doors for further studies and methodologies to be used in this field.

SAMENVATTING

Het brein is een zeer complex orgaan, dat verantwoordelijk is voor de belangrijkste dingen die mensen en dieren uitvoeren. Wat maakt het brein zo uniek? Hersenen zijn zo georganiseerd, dat externe informatie snel en nauwkeurig kan worden ontvangen, ontcijferd en verwerkt. Van alle verschillende soorten cellen waaruit hersenen bestaan, zijn hersencellen (de zogenaamde neuronen) met name speciaal. Hun bijzondere celvorm, waarbij dendrietten en axonen ver weg reiken, stelt een neuron in staat om te communiceren met andere neuronen over korte en lange afstanden.

Communicatie tussen twee neuronen verloopt via contactpunten die synapsen worden genoemd. Goede communicatie vereist de juiste plaatsing en opbouw van synapsen, waarvoor specifieke eiwitten en andere moleculen moeten worden getransporteerd naar de pre- en postsynapsen. Transport van moleculaire vrachten naar synapsen is een complex en sterk gereguleerd proces, dat momenteel niet volledig begrepen wordt. Het cytoskelet, bestaande uit actine- en microtubulepolymeren, vormt de wegen waarover motoreiwitten bewegen om hun moleculaire vrachten naar de synapsen te brengen. Hoe is het cytoskelet georganiseerd in neuronen? Wat activeert of inhibeert motoreiwitten om transport te beginnen of beëindigen? Welke moleculaire vrachten worden geselecteerd voor transport, en waar wordt dit besloten? Hoewel deze vragen niet eenvoudig te beantwoorden zijn, beschrijft dit proefschrift onze inzet om met verschillende aanpakken en methodes het transport van synaptische vrachten in hippocampale neuronen beter te begrijpen.

Hoofdstuk 2 en 3 richten zich op de postsynaps. In het geval van hippocampale neuronen worden de meeste exciterende synapsen gevonden in kleine subcompartimenten die uit de dendrietten steken, de zogenaamde dendritische spines. Aan het oppervlak van de postsynaps wordt het signaal van de presynaptische axon opgevangen door membraanreceptoren zoals AMPA-receptoren. In hoofdstuk 2 beschrijven we de visualisering van het transport van AMPA-receptoren naar dendritische spines, in 'recyclende' endosomen via het microtubule- en actinecytoskelet. Door deze endosomen aan specifieke motoreiwitten te koppelen, was het mogelijk om AMPA-receptoren aan de postsynaps toe te voegen of te verwijderen, wat consequenties had voor de organisatie en functionaliteit van de postsynaps.

In hoofdstuk 3 richten we onze aandacht op de invasies van microtubuli in dendritische spines. Microtubuli bevinden zich doorgaans in de dendritische schacht, en het binnendringen van spines is een infrequente en slecht begrepen gebeurtenis. We hebben dit fenomeen en de functie ervan in detail bestudeerd, in zowel onbehandelde hippocampale neuronen als in neuronen waarbij synaptische plasticiteit geïnduceerd werd.

Motoreiwitten zijn onmisbaar voor transport binnen cellen, waaronder het leveren van moleculaire vrachten aan synapsen. Hoofdstuk 4 beschrijft onderzoek naar de regulering van een dendritisch motoreiwit, de kinesine KIF17. Door KIF17 aan specifieke vrachten te koppelen, verkregen we nieuwe inzichten in hoe de activiteit van dit motoreiwit gereguleerd wordt door zijn eigen staartdomein en de koppeling van moleculaire vrachten.

Hoofdstuk 5 onderzoekt de rol van het axonale actinecytoskelet in het transport van

presynaptische cargo. Dit hoofdstuk levert bewijs dat Spire-eiwitten langs de axonale schacht lokaliseren, waar ze een bijdrage leveren aan de organisatie en het onderhoud van actinestructuren. Onze preliminaire resultaten suggereren bovendien dat Spire-eiwitten belangrijk zijn voor het sturen van moleculaire vrachten naar de presynaps.

Tenslotte beschrijft hoofdstuk 6 de ontwikkeling en karakterisering van nieuwe moleculaire gereedschappen om het actinecytoskelet mee te manipuleren. We bestudeerden 'DeActs' (Disassembly-promoting encodable Actin tools) in verschillende modelsystemen en onderstrepen daarmee hun robuustheid en brede inzetbaarheid. Ik verwacht dat DeActs een veelgekozen strategie zullen worden in verschillende soorten experimenten, en dat ze zullen bijdragen aan het begrijpen van de rol van het actinecytoskelet in gezondheid en ziekte.

Alles bij elkaar, beschrijven de resultaten in dit proefschrift onze nieuwe inzichten over het transport van synaptische, moleculaire vrachten. Ik ben optimistisch dat deze kennis deuren opent naar verdere onderzoeken en nieuwe methodieken binnen dit veld.

SUMÁRIO

O cérebro é um órgão extremamente complexo, ao qual se deve as tarefas mais importantes desempenhadas por humanos e animais. O que o torna tão especial? A sua elaborada organização permite que informação externa seja recebida, decodificada e resolvida de forma rápida e precisa. De todos os tipos de células que formam o cérebro, os neurónios destacam-se particularmente. A sua morfologia única, com dendrites e axónios que se estendem ao longo de grandes distâncias, permite que um neurónio comunique quer com neurónios na sua periferia, quer com outros muito afastados.

A comunicação entre neurónios ocorre através de sinapses. Para que esta comunicação se processe adequadamente, é imperativo que a localização e formação de sinapses ocorra de forma precisa. Para isso, proteínas e outras moléculas precisam ser especificamente enviadas para a pré- ou para a pós-sinapse. Actualmente, sabemos que o transporte de carga para as sinapses é um evento complexo e altamente regulado, para o qual existe pouca informação disponível. O citosqueleto, formado por polímeros de microtubulos e actina, fornece as vias nas quais as proteínas motoras se movimentam para entregar a sua carga no destino final. Como é o citosqueleto organizado ao longo do neurónio? O que activa ou inibe as proteínas motoras para que estas transportem a carga? O que determina qual a carga e para onde esta deve ser transportada? Ainda que sejam questões de difícil resposta, o trabalho delineado nesta tese representa um esforço para responder a estas perguntas e uma contribuição para o avanço do conhecimento relativamente ao transporte de carga sináptica em neurónios de hipocampo, através do uso de diferentes abordagens e metodologias.

Nos capítulos 2 e 3, a abordagem foca-se na pós-sinapse. Nos neurónios do hipocampo, a maioria das sinapses excitatórias localiza-se em espículas dendriticas, pequenos subcompartimentos que se destacam ao longo da dendrite e onde se encontra a maquinaria pós-sináptica. Na superfície da pós-sinapse, é recebido o sinal vindo do axónio pré-sináptico por receptores membranares, tais como os receptores AMPA. No capítulo 2, é descrita a visualização do transporte de receptores AMPA para as espículas dendriticas no interior de endossomas de reciclagem, feito através do citosqueleto de microtubulos e actina. Após a conjugação destes endossomas com proteínas motoras específicas, foi possível manipular a inserção ou remoção de receptores AMPA de espículas, bem como analisar os efeitos consequentes na organização e funcionalidade da pós-sinapse.

No capítulo 3, os estudos conduzidos na pós-sinapse focam-se na invasão dos microtubulos nas espículas dendriticas. Habitualmente, os microtubulos situam-se ao longo do eixo da dendrite e a entrada de microtubulos em espículas é um evento pouco frequente, do qual temos pouco conhecimento. Estes eventos, bem como as suas implicações funcionais em condições basais e no caso de plasticidade sináptica, foram estudados em profundidade.

As proteínas motoras são fundamentais para o transporte intracelular e desempenham um papel importante na distribuição correcta de carga na sinapse. No capítulo 4, estudou-se a regulação da cinesina KIF17, uma proteína motora dendritica e através da sua conjugação com carga específica, foi possível decifrar e perceber como esta proteína motora é distintamente

regulada pela sua própria cauda e pela sua ligação à carga.

No capítulo 5, aborda-se o citosqueleto de actina presente no axónio, assim como o seu papel no transporte de carga pré-sináptica. Neste capítulo apresentam-se evidências de que as proteínas Spire se distribuem ao longo do eixo de axónio, onde contribuem para a organização e manutenção de estruturas formadas por actina. Adicionalmente, os nossos resultados preliminares mostram que as proteínas Spire são importantes no direccionamento de carga até à pré-sinapse.

Por último, o capítulo 6 descreve o desenvolvimento e a caracterização de novas ferramentas usadas para manipular o citosqueleto de actina. As DeActs (do inglês, Disassembly-promoting encodable Actin tools) foram estudadas em diferentes sistemas-modelo, destacando a sua robustez e amplo potencial de aplicabilidade. Acredito que as DeActs serão amplamente utilizadas em diferentes condições experimentais e que ajudarão a compreender melhor o papel da dinâmica de actina na saúde e na doença. Os resultados descritos nesta tese representam um significativo aumento do nosso conhecimento sobre vários aspectos relativos ao transporte de carga sináptica e espero que o trabalho aqui descrito possa abrir portas a novos estudos e metodologias neste tópico.

CURRICULUM VITAE

Marta Santos Esteves da Silva was born on the 3rd of May 1986 in Almada, Portugal. In 2004 she enrolled in the Bachelor of Cell and Molecular Biology at Universidade Nova de Lisboa and in 2008 she continued her studies in the Masters of Cell and Molecular Biology at Universidade de Coimbra, where she first became interested in Neurobiology. Marta went to Belgium under the ERASMUS mobility program for a Master's internship at the Department of Neuroscience of Janssen Pharmaceutica, part of the Johnson & Johnson Family of Pharmaceutical Companies. During this time she was in close contact with primary hippocampal neuron cultures and learned a lot about neuronal development and organization. In 2010, driven by her interest in fundamental research in Neurobiology, Marta joins the Laboratory of Protein Trafficking and Synapse Function of Dr Casper Hoogenraad at the Department of Neuroscience of the Erasmus Medical Center, in Rotterdam, where she becomes familiar with many different cellular and molecular biology techniques, and advanced microscopy methodologies. In 2011, she was awarded with a full PhD scholarship from Fundação para a Ciência e Tecnologia (FCT, Portugal) to pursue her PhD studies at the laboratory of Molecular Neuroscience of Prof. Casper Hoogenraad at the University of Utrecht. During her time as a PhD, Marta was engaged in training and supervising MSc and BSc Life Sciences students and participated in several courses and workshops. She also presented and discussed her work in diverse national and international conferences. The results of her PhD research are described in this thesis. Marta continues to pursue her scientific career, currently working as a Scientist at Charles River Laboratories.



PUBLICATIONS

DeActs: genetically encoded tools for perturbing the actin cytoskeleton in single cells

Martin Harterink*, [Marta Esteves da Silva](#)*, Lena Will, Julia Turan, Adiljan Ibrahim, Alexander E. Lang, Eljo Y van Battum, R. Jeroen Pasterkamp, Lukas C. Kapitein, Dmitri Kudryashov, Ben A. Barres, Casper C. Hoogenraad, J. Bradley Zuchero
Nature Methods (2017) Epub ahead of print. *equal contribution

Three-step model for polarized sorting of KIF17 into dendrites.

Mariella A. Franker*, [Marta Esteves da Silva](#)*, Roderick P. Tas*, Elena Tortosa, Yujie Cao, Cátia P. Frias, Anne F. Janssen, Phebe S. Wulf, Lukas C. Kapitein, Casper C. Hoogenraad
Curr Biol (2016). 26, 1705-1712. *equal contribution

Positioning of AMPA receptor-containing endosomes regulates synapse architecture

[Marta Esteves da Silva](#), Max Adrian, Philipp Schätzle, Joanna Lipka, Takuya Watanabe, Sukhee Cho, Kensuke Futai, Corette J. Wierenga, Lukas C. Kapitein, Casper C. Hoogenraad
Cell Rep (2015) 13, 933-943

Bicaudal D family adaptor proteins control the velocity of dynein-based movements

Max Schlager, Andrea Serra-Marques, Ilya Grigoriev, Laura F. Gumy, [Marta Esteves da Silva](#), Phebe S. Wulf, Anna Akhmanova, Casper C. Hoogenraad
Cell Rep (2014) 8, 1248-1256

Activity-dependent actin remodeling at the base of dendritic spines promotes microtubule entry

Philipp Schätzle, [Marta Esteves da Silva](#), Roderick Tas, Eugene A. Katrukha, Hai Yin Hu, Corette J. Wierenga, Lukas C. Kapitein and Casper C. Hoogenraad
[in preparation]

Spire proteins reorganize a pool of axonal actin and target cargo to the presynapse

[Marta Esteves da Silva](#), Bram van Butselaar, Feline Lindhout, Rene van Dorland, Spiros Pachis, Riccardo Stucchi, Phebe S. Wulf, Anna Malik, Jacek Jaworski, Albert J. R. Heck, A. F. Maarten Altaar, Norihiko Ohbayashi, Mitsunori Fukuda and Casper C. Hoogenraad
[in preparation]

ACKNOWLEDGMENTS

Well, I am reaching the end of the book. I started my PhD full of hopes and dreams and now I leave with a bag full of emotions, great friendships, intense experiences and awesome memories. It has in fact been quite the adventure, at times frustrating and difficult, many times rewarding and fulfilling. It's about time I show the proper appreciation to all of those involved in the rollercoaster ride that was my PhD!

First of all I have to thank **Casper**, my supervisor and promotor. I have always been thankful for the opportunity to join your lab and grow, not only professionally but most of all personally. I remember my first interview and our discussions regarding the grant proposal even before I joined your group. I appreciated that you gave me the freedom to think and elaborate my own project, from which I ended up being awarded with the grant. It gave me a sense of confidence that was very important in the beginning of my project. I will also always remember the endless drawings of spines and motor proteins you have made to explain my data and your ideas for the projects. Those drawings kept always showing up, to the last meeting we had! In fact, as I was cleaning out my desk I found some of the first drawings ever made in these meetings (and did our ideas change in the meantime!). I have had the opportunity to learn immensely with you, either in our regular meetings or in the different social events we were together. I appreciate the relaxed and informal atmosphere created in our meetings that made me feel comfortable to come up with new ideas and to pose problems with confidence. And of course to talk about my professional and personal ups and downs. Even when things got tough, with crazy revision requests and frustrating results, your glass half-full perspective injected hope in me to carry on and reach the finish line. And so I did! After all this time, I still do not know how you cope with all your responsibilities and how you always manage to find time to answer mails or talk on your office. Now that I am finished you can show me where you keep the Casper clones hidden! I sincerely thank you for everything and wish you the best of luck in your new adventure in California and that the lab continues to flourish as it has been over the last years!

Secondly I have to thank my co-promotor **Corette**. When you joined our department I was super happy to have a 'true Neuroscientist' with us! I always appreciated our discussions and your participation at the lab meetings, the way you think about the projects is unique and fresh, not to mention the neuro-expertise you brought with you which proved so beneficial in many cases! My work has gained immensely from your input and my monthly meetings greatly benefited from your presence and inquisitive mind! You provided great input to the AMPA/Rab11, the DeActs and most of all to the Spire project. I was really happy when you joined as a co-promotor, and in the end your support and to-the-point comments as I was writing the thesis made this book much more rich and interesting! Thank you so much, I wish you the greatest success for you and your (expanding) lab!

I would also like to thank the other group leaders of the Cell Biology department. **Lukas**, thanks for the first data of the Rab11 project and for all the fruitful discussions over the project. Our shared monthly meetings were always entertaining and useful in getting new ideas

or troubleshooting difficult problems. I wish you the best of luck and many success for you and your group. **Anna**, your knowledge of pretty much everything cell-related is impressive. I have always been astonished by your ability to remember old or new experiments and papers discussed during the meetings and I always felt lucky when you shared background Science stories that I would never hear about otherwise. Your feedback during the lab meetings was always extremely pertinent and useful, and I would always leave with a handful of new experiments to try, many of them providing good insight into the projects. I wish you a very successful time in the Cell Biology department and hope your lab continues with the fantastic work! **Esther**, we met at Erasmus and I have always appreciated your hard working spirit, always with a smile on your face! Our bench collaboration worked perfectly and I am happy we got to share great moments both in and outside the lab over the years. I sincerely wish you all the best and that you get all better soon and come to dance at my party! **Paul**, it has been a pleasure to meet you and your nanobody work and thanks for the great moments during the lunch breaks. Good luck for you and your lab! **Sabrina**, it was so nice to meet you and see you become a PI. Thanks for all the inspirational conversations. Many success to you and your lab! **Harold**, you have been a great addition to our department, and I have always enjoyed our discussions on postsynaptic stuff and more. Congratulations on becoming a PI, I wish lots of success to the MacGillavry lab! And finally **Fons**, your happy face has always been the joy of the department. The passion with which you coordinate and take care of the Life Science students is noble and highly appreciated by everyone. Keep on smiling and motivating the young scientific minds! Even though not a part of the Cell Biology crew, our neighbors of the 5th floor have always been great colleagues. **Sander, Mike and Inge**, thanks for the great discussions in seminars and good times during our shared social events! Good luck with your labs, keep up the fantastic work with the cool worms!

To **Antoinette Killian, Elly Hol, Catherine Rabouille, Maarten Kole, Jeroen Pasterkamp** and **Paul Lucassen**, thank you for being a member of my reading committee and assessing my thesis. I look forward to discuss my PhD work with you soon.

I would like to thank all the people that contributed to the projects I have been involved during my PhD. Here goes a big thank you to the external collaborators involved. To **Kensuke Futai, Takuya Watanabe** and **Sukhee Cho**, many thanks for the electrophysiology experiments in the Rab11 project. To **Mitsunori Fukuda, Norihiko Ohbayashi Jacek Jaworski, Anna Malik, Albert Heck** and **Maarten Altelaar**, thank you for your important contributions to the Spire project, I am hopeful this project will result in a nice publication soon. To **Brad Zuchero, Julia Turan, Adiljan Ibrahim, Alexander Lang, Eljo van Battum, Jeroen Pasterkamp, Dmitri Kudryashov** and **Ben Barres**, many thanks for your efforts in the DeActs work!

My time as a PhD student has been amazing, in great part due to the fantastic colleagues I got to meet and interact with. I will always remember my time at office N503 with a big smile, mostly because of the awesome roomies I shared it with! **Robert**, we were the settlers and got the nice desks by the window. I had a wonderful time sharing the office with you, learning about your love for Astronomy, Statistics and coding. Even though you tried really hard to

recruit me into the wonderful world of R and failed, I have to say you captivated my interest and after this is done I might give it another try! Also, I will always remember the contrast of your impeccably organized desk with mine. I really hope you're enjoying being a doctor and wish all the best to you and your loving family! **Petra**, it was great to have you as an office roomie and bench buddy. Your energy and good attitude always impressed me, and we shared some great moments and conversations over the years. I hope you're having an amazing time in the US and wish you all the best! **Joanna**, we had some really good laughs in the office and lots of fun canoeing and over drinks. I hope we get to stay in touch and best of luck for you and Jan in sunny California! **Elena**, the quietest Spanish lady I ever met, it was wonderful to have you around, for a laugh or a talk at any time of the day, or to just randomly complain about the Dutch weather. I wish you the best of success and have fun in your California adventure! **Dieudonné**, you came to Robert's old desk and I could tell we would get along just by the way your desk looked after some months. It's clear we both appreciate the organized-chaos style! Little did I know that you would have so much to share, and how many good times would there be to remember. Including a day with your super cute pet dinosaur! I want to thank you for the many great conversations and laughs and the motivational boosts you would inject me when I most needed. Also, a big thanks for the Dutch translation of the summary. I am sure you will do great in finishing up your PhD and wish the best for the future! **Feline**, I appreciate your motivation and proactiveness. Also, you're great fun to chat at the office or at lunch time. I had a wonderful time with you in Coimbra! And many thanks for the tips on San Diego. Best of luck with your PhD, hope you have fun with the Spires! **Xingxiu**, thanks for the big smiles and good talks about Chinese culture. Wish you lots of success in the continuation of your PhD! **Jessica**, welcome to N503, I hope you have as much fun there as I did!

To the neuron culture team: **Marijn**, **Josta**, **Elena**, **Dieudonné**, **Xingxiu**, **Bart**, **Amélie**, **Ginny**, thanks for the fun Monday mornings and the not-so-pleasant periods of contaminations. Together we were able to tackle the problems and provide great cells for all the colleagues to work. **Marijn**, it was great fun to get to know you in Erasmus and to move to Utrecht University with you. Your lively mood and tendency to miss things will be remembered. Wish you all the best for your career! **Josta**, your organizational skills and working method are impressive! Lucky for us, you also used them to organize awesome social events for the department, thanks! I had a great time at the Gordon Conference with you and wish you the best for the future! **Bart**, the funny man, always making me smile even when I did not feel like it. Thanks for all the moments shared, I do miss Bart's jokes quite a lot! **Amélie**, it was a real pleasure to have you around, I wish you lots of success, both here and in the US! **Ginny**, even though our neuronal culture duties did not overlap much it was really nice to meet you and wish you the best in your career. **Elia**, when I left the lab you were about to join the culture team. I hope you're enjoying it as much as I did. Good luck for your project and all the best!

To all my other colleagues in Casper lab, thank you! **Gabi**, our lunch times were also great fun, and I really enjoyed our shared appreciation for the Daily Show. Good luck with your project! **René**, my last bench partner, I wish you all the best and good luck with the Spire

project. **Olga**, it was great having you around and wish you all the best in your return to the US! **Robin**, it was really nice to meet you as a master student and even more when you joined the lab for your PhD. Best of luck with it! **Lena**, many thanks for our great conversations and for your precious help with the slice work. I wish you lots of success in your career! **Riccardo**, thanks for your help with the mass spectrometry and many excuses for spending so much time in your office...Good luck with finishing your PhD! **Yujie**, your cloning skills are super impressive! Always keep your smile up and good luck with the continuation of your PhD! **Sybren** and **Nicky**, you are both very motivated and driven and I am sure you will do great in the continuation of your work. Best of luck! **Michael**, even though you were only briefly in the lab, I had a great time with you and wish all the best. **Martin**, thanks so much for everything. For all the discussions, the troubleshooting, the good times over some drinks and of course for the opportunity to collaborate in the DeActs paper. It has been a real pleasure and I am very, very happy it got to see the light of day! I'll keep in my memory all the laughs and fun we've had over the years. Wish you a very successful career doing what you love so much!

To all the great colleagues that have left before me to other adventures, thanks! **Phil**, working with you was awesome...and fast. You would make me run around as quickly as you do and at times you talked so fast that it became difficult to follow. But I figured that out and we had an amazing time working together in the microtubule invasions work. I had decided that I would not image one more spine and only you could convince me other way. It was a very fruitful time and I learned immensely over our work discussions. It became a really good manuscript that I sincerely hope to be published soon. In the meantime, there were really fun moments to remember, especially when you got upset with the Portuguese girls chatting in your office. I hope you're having a great time in Switzerland and wish all the best to you, Sylvia and your lovely family! **Sam**, I may not have liked you very much when I met you but time showed me you're a really awesome guy and I cherish all the good times we have shared in the lab and elsewhere! Also, many thanks for showing me how to work with InDesign. Let's plan that BBQ! Wish you all the best for your career and your life! **Kah Wai**, I have many good moments to remember with you. Thanks for being a great housemate and helping me (well, not so much...) with Dutch homework and buying my first bike. You would kill my patience every time you answered my question with another question and always made me go through a huge interrogatory when I wanted to use something from the shed, but mostly I remember how much I laughed when you were around. Wish you the best for you and your loving family! **Mariella**, we started almost at the same time at Erasmus and I always liked to have you around. Your gentle and strong personality is lovely and I always enjoyed our conversations and the many good times together. I am happy we get to stay in touch and wish only the best for your life and career! **Marleen**, getting to know you and have you around in the lab was awesome. I enjoyed our conversations, the singing moments and sharing of frustrations in the dark room of the confocal. We see the light, girl! Good luck with wrapping up and many success for your future! **Max**, it was really nice to share the monthly meetings with you and many good times in and outside the lab. Also, many thanks for your contribution to the Rab11 work. Good

luck finishing up and wish you lots of success in California! **Bas**, thanks for all the good times and contagious sense of humor. Wish you the best! **Marina**, your time with us was intense and very productive, and super, super fun! You have the best laughter! Lots of success in your career! **Margriet**, your time in the Casper lab was great fun, especially at lunch times! I hope your smile continues to shine and that you're really happy in the new job! **Karin**, thanks for the great times shared either in Erasmus or at the Cell Bio in Utrecht. I predict that more fun times together will follow soon. All the best! **Laura**, we've had some really nice moments that I'll always remember. Hope you're enjoying your new job, wish you the best! To the people I met back at Erasmus MC, I want to thank you for all the help in the first months of my time in Casper lab. **Nanda, Max and Myrrhe** it was awesome to start in the lab with you at Erasmus. Wish you all the best! **Chris**, we met in my first weeks in the Netherlands and you were one of the first to teach me some Dutch words. Everytime I meet you I immediately think: lekker ding! Thanks for all the great moments at parties. Wish you all the best!

The 5th floor of the Kruyt is filled with great people from many different groups and I want to send a big thank you to all of them! **Hai Yin**, your relaxed nature and constant smile are a joy to be around. Your strong, optimistic attitude will get you anywhere. Good luck with the rest of your PhD! **Dennis**, what a nice addition to the group! You can keep up with my sense of humor more than anyone else and our lunch breaks would always be great fun! I am sure you miss me already, right? Best of luck and enjoy your PhD! **Anaël**, your energy and ability to put a smile in people's faces is priceless. Cheers to the penguin dance! All the best for your career and your family. **Eugene**, we have shared many good moments together and I always enjoyed talking to you about this, that and everything else. Many thanks for taking your time to discuss analysis stuff with me. Keep up the great work and all the best for your life. **Helma and Qingyang**, you've been great colleagues over the years and I will keep in my memory the fun chats and good moments we shared in your office. Wish you lots of happiness and success! **Ilya**, your atypical sense of humor was always entertaining and I want to thank you for all the times you help me with microscope problems and analysis. **João**, always keep your great sense of humor and drive to do good Science. Thanks for the good time! To **Anne and Roderick**, thanks for the great lunch breaks and good luck with your PhD! To **Ivar, Amol, York, Chao, Chiung-Yi, Peter-Jan, Fangrui, Elske, Jian, Lars, Suzanne, Vincent, Janine, Ruben, Katherina, Vida, Irati, Sara and Hui**, thanks for all the good times together as PhD students. Keep up the good work and enjoy your PhD time! To **Jingchao, Hari, Renu, Ben, Kai, Shasha, Ankit, Maud, Ruddi, Dušan, Wilco, Desirée, Mithila, Helena, Selma, Thijs, Marta, Bram and Raimond**, a big thanks for being great colleagues and the good conversations we have shared over the years. May you have great success in your life! To **Rachid and Sofia**, thanks for all the laughs over the years! To **Bram and Spiros**, whom I supervised while in their Masters internships, thanks for being great students, for making me learn how to supervise people and manage projects, for the good science you have performed and for the enjoyable time together. I wish you lots of success in your careers! **Miriam and Maartje**, thank you for the patience and kindness to help me sending constructs on a weekly basis. Keep up the good work!



Andrea, this adventure would not have been the same without you. We have lived and grown so much together! The good memories are endless and ever since you left it has not been the same. It makes me really happy to see you motivated in your new adventure in San Francisco and I know you are on the right path to become what you always dreamed to be. I will for sure always be around to watch it all happen. Obrigada por tudo, miúda!

Cátia, my extraordinary Catipedia! You have been an amazing colleague and a friend beyond words. Until this day you amaze me with your knowledge of pretty much anything, especially Science and Eurovision-related! Most of all I admire your big, big heart and warm hugs when I most needed them! You are meant for great things and I know for sure that you will be very successful in anything you set your mind to. I am happy we don't have to set apart now that I am done, and be sure to know I am always here for you!

Phebe, you have been part of this PhD from beginning to the end. We have many stories and delighting moments to remember and I am super happy we've become good friends and I will finish this chapter with you by my side. You are the pulling force of our lab and I admire your energy and work ethics. I am sure we'll be meeting often in the future and continue growing our book of memories together! I wish you all the best for your life. Thanks for everything Mama Wulf!

Inês, I left you for the end of the lab people because I knew this one was going to get emotional. Our friendship has grown over the years and I can't imagine concluding this chapter without you. You've become an essential part of my life and I know I can always count on you for anything. And rest assure that nothing will change now that I left the lab. I'll have you by my side on the Defense and I am taking you for life regardless of where we go, you have no choice! May the future bring you all the smiles in the world, you deserve it!

During the years I have been doing my PhD I met many people that had a big role in my life outside the lab. **Roland**, thanks for being a good friend and always having a motivational word for me. I wish you all the happiness of the world! **Reinier**, it has been great to meet you and share so many fun and energetic moments together. Let's keep doing that! Good luck with your PhD! **Iris**, you were a great housemate and our time together at Potterstraat was really fun! All the best for you! **Saskia, Serge, Doenja, Elisa** and **Vuza**, our dancing lessons at Touchee were a magical stress-relief at the end of a difficult day, and your energy and good spirits sure helped with that! **Hashim** and **Manarti**, it was great to have you as my neighbors and share fun meals together. **Jim**, we had a really good time making Kah Wai's movie, and your directing and editing skills are superb! **Ida, Ricardo** and **Luisa** I really enjoyed our weekend gatherings in Amsterdam! **João** and **Lisette**, our moments together are always so much fun and I am really looking forward to that Windsurf lesson in the Summer! Thank you all and wish you all the best!

I also want to thank my friends back in Portugal. **Marta**, minha Martinha, our friendship goes beyond time and I have shared with you some of the best experiences of my life. Thanks for always being around and being immensely supportive. I only wish the best for you and your wonderful family! **Sofia, Miguel, Andreia** e **Pedro**, we have been friends for almost a

lifetime! Thanks for the visits, for always finding time to meet me in my short stays back home and for always believing in me!

To all my good friends in different parts of the world, you show me distance does not matter when one truly cares. Thanks! **Lia** and **Hugo**, thanks for the nice chats and support, I wish you all the best in your future! **Raquel**, **Geert**, **Christelle**, **Rita**, **Jorge** and baby **Duarte** we have shared some wonderful moments together and it always feels great to meet you and continue to expand our good memories! Wish you all lots of happiness and smiles! And finally, **Soraia** and **André**. So many good moments, so many conversations and laughs, so many glasses of Port, so many fantastic experiences! **Soraia**, you have been amazing throughout the years, pulling me forward and always picking me up when I was down. You believed in me when I didn't and you are truly an example of how dedication and perseverance come a long way. You are an extraordinary scientist and mostly an out-of-this-world friend and I know that no matter how far you choose to go, you are always by my side, no matter what. I wish you both the best this world has to give you, and I am always, always here for you!

To my **Estarolas**, 'expertos' em tudo e mais alguma coisa. You guys have been the greatest friends I could have ever asked for. Our group chats, Christmas gatherings, city trips and Skype meetings have fueled my spirit more than you can ever imagine. **Ana**, **Joana**, **Kaare**, **Giuseppe** and baby **Matilda**, our weekend gatherings in Amsterdam or Utrecht made me forget the problems and worked as therapy to start the week with a smile in my face. I will never forget your support and care for me. I am immensely thankful for having such good friends close by! **Ana**, a big thanks for the Sumário, you worked wonders on my rusty Portuguese writing skills! **Raquel**, **Carolina**, **Filipa**, **Frederico**, **David**, **Vasco**, **Giorgio**, **Juliana** and **Mariana** thank you so much for all the chaotic and exhilarating moments together, you have filled my days with so much joy! We have great memories to share and many, many more to come! **Raquel**, good luck with finishing your PhD, you will do great and have a bright future ahead of you. Thanks for everything guys and let's keep on collecting awesome memories together!

Quero também agradecer a toda a minha **Família** pelo apoio e preocupação que demonstraram ao longo destes anos. Embora o tempo fosse sempre pouco, os momentos partilhados no Verão ou no Natal foram sempre recheados de alegria e diversão. Estão sempre no meu pensamento! À Rosa, ao Manuel e ao Artur agradeço todo o apoio e interesse demonstrados e pelos bons momentos que partilhamos quando vamos a casa. Muito obrigada por tudo!

À minha mana **Joana**, tenho de agradecer este mundo e o outro. És a melhor mana do mundo, e se já o sabia quando parti nesta aventura, agora ainda tenho mais certezas. Apoiaste-me, encorajaste-me e deste-me muitas vezes a força para seguir em frente. Tenho imenso orgulho em ti, no que te tornaste e na Família que estás a criar. Embora me parta o coração que não possas cá estar para o grande dia, enche-me de felicidade que a nossa **Vitória** venha a caminho para se juntar ao nosso clã! **Bruno**, obrigada pelo teu apoio incondicional e por todos os bons momentos que passamos juntos. **Vicente**, embora ainda sejas muito pequenino para perceberes, enches-me o coração de alegria quando mais preciso. Obrigada a todos vós!

Tia Bé, quero agradecer-te imenso que tenhas vindo ao meu grande dia! E também todo

o apoio que sempre me deste e o orgulho que sei que tens por mim. Mais orgulho sinto eu por ti, és uma verdadeira guerreira e nada conseguirá alguma vez abalar a energia que tens dentro de ti. Obrigada por todos estes anos de carinho!

Mamazita e Papazito, esta tese é dedicada a vós. É difícil descrever o que sinto quando escrevo estas palavras, mas quero que saibam que me sinto uma privilegiada por ter uns pais como os meus, que tão bem me educaram e se esforçaram para me inculcar valores para que me tornasse no melhor ser possível. Espero sinceramente que estejam orgulhosos de mim. Eu tenho imenso orgulho em vocês! E espero que no futuro também possa ser tão bom exemplo para alguém como vocês são para mim. O vosso apoio foi incondicional do princípio ao fim e nunca duvidaram que poderia levar este desafio a bom porto. Acreditem que a distância continua a ser complicada de gerir, mas saibam que estão sempre, sempre no meu coração, tal como eu sei que estou nos vossos. Adoro-vos!

Ficaste para o fim, **Daniel**. Porque és sem dúvida a personagem mais importante na minha vida. Porque estiveste comigo desde o início até ao fim desta aventura e até muito antes disto. És contigo que cresço e me torno um ser melhor todos os dias. Foste incansável ao longo de todos estes anos e estiveste sempre lá para me apoiar quando eu precisei. Partilhámos os bons e os maus momentos, sempre juntos, mesmo que a distância por vezes não o permitisse. Este PhD é teu também e não me imagino a fazê-lo sem ti a meu lado! Tenho tanto para te agradecer, e quero aqui destacar o excelente trabalho que fizeste na formatação deste livro, que belo que ficou graças à tua preciosa dedicação! Que tenhamos toda uma vida em conjunto pela frente, talvez aí te consiga agradecer da forma que mereces. Obrigada amor!

That's it.
PhDONE!

Marta

